DISSERTATION

POSTCRANIAL ESTIMATORS OF BODY MASS IN PECORANS WITH EMPHASIS ON *CAPROMERYX* (MAMMALIA:ARTIODACTYLA)

Submitted by

Janice Elaine Saysette

Department of Biology

In partial fulfillment of the requirements

for the degree of Doctor of Philosophy

Colorado State University

Fort Collins, Colorado

Spring 1999

COLORADO STATE UNIVERSITY

March 26, 1999

WE HEREBY RECOMMEND THAT THE DISSERTATION PREPARED UNDER OUR SUPERVISION BY JANICE ELAINE SAYSETTE ENTITLED POSTCRANIAL ESTIMATORS OF BODY MASS IN PECORANS WITH EMPHASIS ON *CAPROMERYX* (MAMMALIA:ARTIODACTYLA) BE ACCEPTED AS FULFILLING IN PART REQUIREMENTS FOR THE DEGREE OF DOCTOR OF PHILOSOPY.

Committee on Graduate Work

Advisor

Department Head/Director

ABSTRACT OF DISSERTATION

POSTCRANIAL ESTIMATORS OF BODY MASS IN PECORANS WITH EMPHASIS ON *CAPROMERYX* (MAMMALIA:ARTIODACTYLA)

Mammalian body mass is correlated to a variety of ecological and physiological parameters. Reconstruction of the masses of extinct species is of interest because of the information obtained that can elucidate past ecologies. The most common method of mass estimation has generally been from tooth measurements, as teeth are most commonly preserved in the fossil record. Postcranial estimators have been less frequently used, and have been primarily confined to measures of width and length. Some notable exceptions have used a geometric shape to model the surface area and volume of the femoral head. In an attempt to expand on this concept, a number of postcranial articulations were modeled on different geometric shapes in order to evaluate the effectiveness of such models in predicting body mass of extant pecoran artiodactyls. Predictive least squares regression equations were developed from the modern sample and applied to the extinct antilocaprid *Capromeryx*. In addition to body mass estimation the phylogeny of *Capromeryx* was evaluated, resulting in species synonymies that decreased the number of species within the genus from five to three.

Janice Elaine Saysette
Biology Department
Colorado State University
Fort Collins, Colorado 80523
Spring 1999

ACKNOWLEDGEMENTS

Most of all, I would like to thank my sons, Grant and Ian, for their patience and good humor putting up with mom sitting at the computer for all of these months. Their hugs, laughter and loving concern kept me going. I also appreciate the herd of teenagers that so often descend upon my household, providing laughter and silliness, and reminding me that life is not always so serious. It is a joy to watch you all grow into fine young men: Chris Anderson, Justin Christian, Joel Haddorf, Tom Metz, Tyson Riffe-Smith, Jake Smeester, and John Carroll Smith.

I would especially like to thank my advisor Bruce Wunder, for his long standing faith in me despite innumerable odds over the years. Many thanks also to my committee Cal Jennings, Danny Walker, and Elaine Anderson for their encouragement and help during this process. My sincere appreciation goes to Charles Repenning and Dave Webb for reading drafts and providing helpful comments. For the exceptional artwork, I would like to thank Dave Daitch.

A project like this is never completed without the support of good friends who took the time to remind me that there was a light at the end of the tunnel. Special thanks to Judy Allen, Kathy Rehm-Paul, and Sara Tutt. To the following people I owe thanks for much needed laughs and supportive conversations; Jim Chase, Bobbie Cook, Janelle Corn, Warren Eastland, Pilar Flores, Sandy Jackson, Wini Kessler, Alana Macdonald, Sue McGinley, Mary Painter and Ivy Pike. Although some of you have moved and we have lost touch, I will never forget your unselfish support during stormy times.

In particular, I would like to thank John Damuth for his help with statistics and numerous other issues that arose during the writing of this thesis. His patience and good humor was much appreciated. For help with the resolution of periodic paleontological crises, many thanks goes to the following patient souls : Audrone Biknevicius, Christine Janis, Jay Lilligraven, Malcolm McKenna, Jim Morgan, Charles Repenning, and Dave Webb. For long productive discussions in the areas of physics and biomechanics, my sincere appreciation goes to Paul Worden.

Finally, I would like to thank the many colleagues who provided friendship, information, encouragement and laughs during visits to their institutions. I am especially indebted to the following people for allowing me to examine and borrow specimens in their care:

AMNH: American Museum of Natural History, New York; Richard Tedford, Malcolm McKenna, and John Alexander; MSU: Midwestern State University, Wichita Falls, Walt Dalquest; UM: University of Michigan, Ann Arbor, Gregg Gunnell; UNSM: University of Nebraska State Museum, Lincoln, George Corner; USNM: United States National Museum, Washington D.C., Robert D. Fisher; LACM: Natural History Museum of Los Angeles County, George C. Page Museum, Chris Shaw; KU: University of Kansas Natural History Museum, Lawrence, Bob Timm, John Chorn, Thor Holmes, Desui Miao; FMNH: Florida Museum of Natural History, Gainesville, Dave Webb and Marc Frank; UAHMP: Universidad Autónoma del Estado de Hidalgo, Museo de Paleontología, Joaquin Arroyo; UCMP: University of California at Berkeley Museum of Paleontology, Berkeley, Mark Goodwin and Pat Holroyd; TMM: Texas Memorial Museum, University

of Texas at Austin, Melissa Winans and Ernest Lundelius; UTEP: University of Texas at El Paso, Art Harris; UWBM: University of Washington, Burke Museum; John Rensberger and Jim Morgan; UW: University of Wyoming Department of Anthropology Comparative Osteological Collection, Danny Walker.

TABLE OF CONTENTS

Signature Page ii
Abstract iii
Acknowledgments iv
Table of Contents vii
List of Tables viii
List of Figures ix

CHAPTER I. GENERAL INTRODUCTION 1

CHAPTER II. HISTORY OF THE ANTILOCAPRIDAE AND SYSTEMATIC REVIEW OF *CAPROMERYX* 6

Introduction 6
Materials and Methods 25
Institutional Abbreviations 27
Systematic Paleontology 27
Results 43
Discussion 49
Conclusions 61
References 63

CHAPTER III. MULTIVARIATE MORPHOMETRIC ANALYSES OF SKELETAL VARIABLES IN MODERN AND FOSSIL PECORANS 70

Introduction 6
Materials and Methods 88
Results 94
Discussion 153
Modern Sample 162
Fossil Sample 167
Conclusions 169
References 170

APPENDIX I 178

APPENDIX II 181

LIST OF TABLES

2.1 Mean Body Mass Estimates for Teeth and Postcrania 50

2.2 Summary of Horn-core Measurements by Species 59

3.1 Definitions of Variables and Accompanying Forumlae 95

3.2 Mean Predicted Body Masses for Each Variable and Species 99

3.3 Summary of Predictive Equations 105

3.4 Fossil Localities 154

3.5 Body Mass Predictions for *Capromeryx* 155

3.6 Variables Providing Best Mass Estimates 166

LIST OF FIGURES

2.1 Composite ruminant toothrow showing *Palaeomeryx* fold 13

2.2 Classification of the Ruminantia 15

2.3 *Cosoryx* showing merycodontine "pseudo antlers" with burrs 18

2.4A Horn-core of *Plioceros* showing antero-posterior flattening 21

2.4B Sagittal section of horn-core of *Antilocapra* 21

2.5 Measurements of the *Capromeryx* horn-core 28

2.6 Holotype of *Capromeryx mexicanus* sensu Furlong 1925 32

2.7A Horn-core of *Capromeryx furcifer* 35

2.7B Horn-core of *Capromeryx minor* sensu Taylor 1911 35

2.7C Horn-core of *Capromeryx mexicanus* sensu Furlong 1925 35

2.8 Horn-core of *Capromeryx arizonensis* sensu Skinner 1942 39

2.9 Holotype of *Capromeryx tauntonensis* 40

2.10A Right p4; *Capromeryx tauntonensis* 42

2.10B Left p4; *Capromeryx arizonensis* sensu Skinner 1942 42

2.10C Right p4; *Capromeryx tauntonensis* showing metaconid-entoconid closure 42

2.11 Log-log plot of body mass against M2 length 45

2.12 Log-log plot of body mass against m1 length 47

2.13 Log-log plot of body mass against m2 length 48

2.14 Log-log quadratic plots of tooth variables 52

3.1 Load-deformation curve 75

3.2A Bending forces in a loaded beam 77

3.2B Compression and tension in a loaded beam 77

3.3 Cross section of a long bone showing axes and second moments of area 80

3.4 Ungulate forelimb showing scapular orientation 109

3.5 Measurements of the scapula 107

3.6 Log-log plot of body mass against surface area glenoid fossa 109

3.7 Measurements of the humerus 110

3.8A Log-log plot of body mass against length of the humerus 111

3.8B Log-log plot of body mass against cross-sectional area of humerus 111

3.9A Hyperboloid of revolution; distal humerus 113

3.9B Obliquely cut right circular cylinder; distal humerus 113

3.9C Frustrum of right circular cone; distal humerus 113

3.10A Log-log plot of body mass against HM3 115

3.10B Log-log plot of body mass against HM4 115

3.10C Log-log plot of body mass against HM5 115

3.11 Surface area of the proximal radius articulation 116

3.12A Log-log plot of body mass against length of radius 117

3.12B Log-log plot of body mass against surface area of proximal radius 117

3-13 Measurements of the ulna 119

3.14A Log-log plot of body mass against length of the olecranon 120

3.14B Log-log plot of body mass against surface area of trochlear notch 120

3.15 Measurements of the magnum 122

3.16 Log-log plot of body mass against volume of magnum 123

3.17A Greatest length of metacarpal 125

3.17B Proximal surface area metacarpal modeled on a trapezium 125

3.17C Distal articulation metacarpal modeled on a barrel 125

3.18A Log-log plot of body mass against length of metacarpal 126

3.18B Log-log plot of body mass against proximal surface area of metacarpal 126

3.18C Log-log plot of body mass against distal articulation of metacarpal 126

3.19 Measurements of the femur 129

3.20A Log-log plot of body mass against greatest length of femur 130

3.20B Log-log plot of body mass against cross-sectional area of femur 130

3.21A Log-log plot of body mass against volume of femoral head 131

3.21B Log-log plot of body mass against surface area of femoral head 131

3.22 Measurements of the tibia 133

3.23A Log-log plot of body mass plotted against greatest length of tibia 134

3.23B Log-log plot of body mass plotted against distal breadth of tibia 134

3.24A Log-log plot of body mass plotted against medial condyle tibia as a trapezium 136

3.24B Log-log plot of body mass plotted against medial condyle tibia as a rectangle 136

3.24C Log-log plot of body mass plotted against surface area distal tibia 136

3.25 Measurements of the astragalus 138

3.26A Log-log plot of body mass against greatest length astragalus 139

3.26B Log-log plot of body mass against greatest width astragalus 139

3.27A Log-log plot of body mass against volume distal astragalus 141

3.27B Log-log plot of body mass against area posterior articulation astragalus 141

3.28 Measurements of the calcaneum 143

3.29A Log-log plot of body mass against length of calcaneum 144

3.29B Log-log plot of body mass against width sustentaculum 144

3.30A Log-log plot of body mass against proximal calcaneum 145

3.30B Log-log plot of body mass against distal calcaneum 145

3.31 Measurements of the cubonavicular 147

3.32 Log-log plot of body mass against ventral surface cubonavicular 148

3.33 Measurements of the metatarsal 149

3.34A Log-log plot of body mass against greatest length metatarsal 150

3.34B Log-log plot of body mass against proximal surface metatarsal 150

3.34C Log-log plot of body mass against distal articulation metatarsal 150

CHAPTER I. GENERAL INTRODUCTION

The objective of paleontology is the analysis and reconstruction of biological patterns within the history of lineages over time (Wing et al. 1992). These patterns or biological processes, can partially be defined as the paleoecology of an organism; the relationships between an organism and its environment and its community (Wing et al. 1992). The reconstruction of the paleoecology of an organism necessitates the utilization of different methodologies and the collection of different data than are the norm for modern ecologists (Gifford 1981). The use of methods such as taphonomy, analysis of pollen and phytoliths, correlation of faunal associations, radiometric dating and geological information are all of use when one cannot actually observe the organism or its community.

Other methods for reconstructing paleoecology are more subtle. Much can be learned, for example, by the reconstruction of the body mass of an organism. Body mass has been correlated to a variety of physiological and ecological variables, all of which can provide insight into the biology of an extinct organism (Eisenberg 1981; Damuth 1981; McNab 1990). Reconstruction of body mass of extinct species is dependent upon studies of related extant organisms as a basis for the development of accurate predictive regression equations, if such related species are available (Scott 1985; Gingerich 1990).

The extinctions which took place at the end of the last glaciation, approximately 10,000 ybp are of interest not only due to the relative recentness of the event, but also because of the disproportionate number of grazing and browsing herbivores that were lost (Graham and Lundelius 1984). There are a number of theories attempting to explain the extinctions, and most focus on environmental deterioration and loss of plant diversity (Graham and Lundelius 1984; Guthrie 1984). Many of these herbivores were very large as compared to species today, and were the end result of thousands of years of increases in body size . Examples of the largest species are most prevalent among the carnivores and the browsing and grazing perissodactyls and artiodactyls (Webb 1984; Graham and Lundelius 1984). Of the herbivores, four genera of antilocaprids were alive during the late Pleistocene. One of these, *Capromeryx*, was very small in mass (10 kg), having dwarfed over time since its appearance during the mid-Blancan (3.09 Ma). Interestingly, *Capromeryx* became extinct, while the much larger *Antilocapra* survived the extinction event.

Pronghorn are a uniquely North American pecoran artiodactyl family, having evolved and diversified here over the last 21 million years, only to succumb to the extinction pressures at the end of the last glaciation. The one remaining species, *Antilocapra americana*, is now widespread throughout the West, having experienced a population rebound due to conservation efforts initiated in 1920 (Cadieux 1987). The Antilocapridae is divided into two sub-families, the Merycodontinae and the Antilocaprinae. The merycodonts were present in the fossil record from the late Arikareean (21Ma) to the late Clarendonian (9 Ma) (Tedford et al. 1987). The later

antilocaprines appeared during the late Clarendonian (9 Ma), and persisted until the late Rancholabrean when only *A. americana* survived the late Pleistocene extinction event (Tedford et al. 1987; Lundelius et al. 1987).

The focus of this study is twofold; 1) To re-examine the phylogeny of *Capromeryx*, and 2) To develop postcranial measurements of articulations for prediction of body mass in modern pecoran artiodactyls with application to fossil forms such as *Capromeryx*.

REFERENCES

Cadieux, C. L. 1987. Pronghorn antelope: Great Plains rebound; pp. 132-143 *in* H. Kallman (ed.), Restoring America's Wildlife. U.S. Fish and Wildlife Service, Washington, D. C.

Damuth, J. 1981. Population density and body size in animals. Nature 290:699-700.

Eisenberg, J. F. 1981. The Mammalian Radiations. University of Chicago Press, Chicago, 610 pp.

Gifford, D. P. 1981. Taphonomy and Paleoecology: A critical review of archaeology's sister disciplines. Advances in Archaeological Method and Theory 4:365-438.

Gingerich, P. D. 1990. Prediction of body mass in mammalian species from long bone lengths and diameters. Contributions from the Museum of Paleontology, University of Michigan 28(4):79-92.

Graham, R. W. and E. L. Lundelius. 1984. Coevolutionary disequilibrium and Pleistocene extinctions; pp.223-249 *in* P. S. Martin and R. G. Klein (eds.), Quaternary Extinctions: A Prehistoric Revolution. University of Arizona Press, Tucson.

Guthrie, R. D. 1984. Mosaics, allelochemics and nutrients: An ecological theory of late Pleistocene megafaunal extinctions; pp.259-298 *in* P. S. Martin and R. G. Klein (eds.), Quaternary Extinctions: A Prehistoric Revolution. University of Arizona Press, Tucson.

Lundelius, E. L., T. Downs, E. H. Lindsay, H. A. Semken, R. J. Zakrzewski, C. S. Churcher, C. R. Harington, G. E. Schultz, and S. D. Webb. The North American Quaternary Sequence; pp. 211-235 *in* M. O. Woodburne (ed.), Cenozoic Mammals of North America: Geochronology and Biostratigraphy. University of California Press, Berkeley.

McNab, B. 1990. The physiological significance of body size; pp.11-23 *in* J. Damuth and B. J. MacFadden (eds.), Body Size in Mammalian Paleobiology: Estimation and Biological Implications. Cambridge University Press, Cambridge.

Scott, K. M. 1985. Allometric trends and locomotor adaptations in the Bovidae. Bulletin of the American Museum of Natural History, 179(2):197-288.

Tedford, R. H., M. F. Skinner, R. W. Fields, J. M. Rensberger, D. P. Whistler, T. Galusha, B. E. Taylor, J. R. Macdonald, and S. D. Webb. 1987. Faunal succession and biochronology of the Arikareean (Late Oligocene through earliest Pliocene epochs) in North America; pp. 153-210 *in* M. O. Woodburne (ed.), Cenozoic Mammals of North America: Geochronology and Biostratigraphy. University of California Press, Berkeley.

Webb, S. D. 1984. Ten million years of mammal extinctions in North America; pp.189-210 *in* P. S. Martin and R. G. Klein (eds.), Quaternary Extinctions: A Prehistoric Revolution. University of Arizona Press, Tucson.

Wing, S. L., H-D. Sues, R. Potts, W. A. DiMichele, and A. K. Berensmeyer. Evolutionary Paleoecology; pp.1-13 *in* A. K. Berensmeyer, J. D. Damuth, W. A. DiMichele, R. Potts, H-D. Sues, and S. L. Wing (eds.), Terrestrial Ecosystems through Time: Evolutionary Paleoecology of Terrestrial Plants and Animals. University of Chicago Press, Chicago.

CHAPTER II: HISTORY OF THE ANTILOCAPRIDAE AND SYSTEMATIC REVIEW OF *CAPROMERYX*

INTRODUCTION

The Antilocapridae consists of 21 genera contained within two subfamilies, the Merycodontinae and the Antilocaprinae. Merycodontinae will be used as a valid taxon, even though Janis et al. (1998) considers the group to be paraphyletic. There has been some controversy surrounding this family, revolving around not only the relationship between the two subfamilies, but also whether or not the Antilocapridae are more closely aligned with the cervids rather than with the bovids as has been traditionally thought (Scott and Janis 1987). The earlier appearing Merycodontinae possess only generalized antilocaprid features (see later discussion), and there is a considerable difference in the appearance of the cranial appendages between the two subfamilies (Janis et al. 1998). The merycodont "antler" is reminiscent of the cervids, whereas the antilocaprine horn-core is more similar in appearance to that of the bovids. At least two of the merycodontine genera, *Meryceros* and *Submeryceros*, are now thought to be invalid, and are probably the same as *Merycodus* (McKenna and Bell 1997; Janis et al. 1998).

There are also some controversial generic designations within the Antilocaprinae. In a recent paper, Janis et al. (1998) gave *Ottoceros* and *Ceratomeryx* only tentative

placement within their revised cladogram, as it was thought that the two genera were too poorly known to include with certainty. The entire group is badly in need of revision, but this awaits a detailed study of the large number of antilocaprid fossils currently housed at the American Museum of Natural History, the United States National Museum, and other facilities, and is beyond the scope of this dissertation.

The Plio-Pleistocene antilocaprine *Capromeryx* is of interest for a number of reasons. First, the genus is present in the fossil record for approximately 3 Ma, longer than that of any other Plio-Pleistocene antilocaprid. Second, *Capromeryx* experienced a dwarfing trend over time, with the two oldest species, *C. tauntonensis* and *C. gidleyi* also being the largest. This trend was in contrast to other antilocaprid genera of the time, which were all larger than *Capromeryx*. Finally, the genus was extremely widespread geographically, suggesting a highly adaptive lifestyle.

Capromeryx will be examined here, with a revision of the species contained within that one genus. Because there is a suite of osteological characters that define artiodactyls in general, and antilocaprids in particular, a brief review of those characters through the systematic levels that pertain to the Antilocapridae will be provided. The primary objective of this study is to examine problems within the genus and to redefine the species of *Capromeryx* .

Characters Relating to the Antilocapridae

Artiodactyla — The mammalian order Artiodactyla first appeared during the early Eocene, and is represented by the oldest known genus *Diacodexis*, rabbit-sized animals

known from North America, Europe, and Asia (Rose 1982; Krishtalka and Stucky 1986; Carroll 1988). Artiodactyls evolved from primitive condylarths, which were small, primarily herbivorous placental mammals (Carroll 1988). In addition to the artiodactyls, condylarths are also thought to have given rise to such diverse groups as proboscideans, perissodactyls, cetaceans, and the South American ungulates (Carroll 1988).

Artiodactyls are characterized by two unique osteological features of the foot; paraxonic symmetry, in which the plane of symmetry passes between the third and fourth digits and a "double pulley" arrangement of the articular surfaces of the astragalus (Scott and Janis 1987; Vaughn 1986). The first digit appears in only a few fossil artiodactyls and the second and fifth digits are often reduced or absent in more derived groups (Nowak 1991). *Diacodexis* is allied with the artiodactyls on the basis of the shape of the astragalus alone (Rose 1982; Carroll 1988). The structure of the astragalus limits movement of the limb to the vertical plane, allowing for a much more efficient distribution of force across the joints, and thereby enhancing the efficiency of cursorial locomotion (Carroll 1988).

Other osteological features of this group include the absence of a third trochanter on the femur, elongated metacarpals and metatarsals in the form of a fused "cannon" bone (except in the Suiformes), a markedly reduced fibula, molars more complex than pre-molars, and nasal bones not expanded posteriorly (Carroll 1988; Nowak 1991). With the exception of suids, many artiodactyls have frontal appendages in the form of horns or antlers (Nowak 1991).

By the late Eocene, three sub-orders of artiodactyls are recognizable: Suiformes (pigs, peccaries and hippopotami); Tylopoda (camels, llamas, and the extinct oreodonts,

xiphodonts, and protoceratids); and Ruminantia (tragulids, deer, antelopes, cattle, sheep, goats, antilocaprids, and giraffes) (Janis and Scott 1987; Carroll 1988; Nowak 1991). Suids retain the primitive bunodont dentition that arose in the earliest groups such as the dichobunid condylarths (Gazin 1955; Carroll 1988). The more derived selenodont dentition, consisting of crescent shaped cusps, exists in the other two other suborders of higher artiodactyls, the tylopods and the ruminants (Carroll 1988).

Ruminantia — The basal ruminant osteological character suite includes fusion of the cuboid and navicular bones in the tarsus, forming the cubonavicular; an incisiform lower canine (in those forms that retain a canine); and loss of the upper incisors; which in living species are replaced by a horny pad (Colbert 1941; Webb and Taylor 1980; Janis and Scott 1987). There are a number of other features that unite the Ruminantia above the level of the most primitive members, the Hypertragulidae. In addition to some minor cranial features, they include the loss of the trapezium and the fusion of the magnum and trapezoid in the manus, loss of metacarpal I, reduction of the fibula to a malleolar bone (or lateral malleolus), loss of upper P1, and a variety of tooth features including the presence of an internal cingulum on the upper molars and the presence of an ectostylid on the lower molars (Webb and Taylor 1980; Janis and Scott 1987).

The Ruminantia may be further subdivided into two infraorders, Tragulina and Pecora. Tragulina is more primitive, and is composed of living chevrotains, or mouse deer, and the extinct leptomerycids and hypertragulids. Tragulines are characterized by absence of cranial appendages, small body size (average about 10 kg), well developed upper canines, and an elongated astragalus with nonparallel sides (Webb and Taylor 1980;

Janis and Scott 1987). Wide ranging through Europe, Africa, Asia and North America during the Miocene through the Pleistocene, the remaining four living species are restricted to West and Central Africa and southeast Asia (Nowak 1991). Higher ruminants (Pecora) are united by features including the loss of the trapezium in the manus, a compact parallel sided astragalus, postorbital bar formed from the frontal bone, and an anterior cingulum on the lower molars (Janis and Scott 1987).

There are some physiological variables that limit body size in ruminants. In living ruminants, plant material is rapidly ingested and then later regurgitated into the mouth for further chewing and mechanical breakdown as "cud." The cud is then swallowed for further processing and fermentation in the rumen with the aid of cellulose digesting bacteria, after which it proceeds into other parts of the stomach and finally into the intestine (Schmidt-Nielsen 1990). This process allows ingestion of more fibrous and nutritionally poor plant material. Ruminants therefore can afford to be less selective in their diet than many other herbivores, as long as the nutritional content is sufficient (Janis 1976; Guthrie 1984).

It has been shown that in a wide variety of animals, including birds, marsupials, and placental mammals, basal metabolic rate scales to body mass (M) at approximately the 3/4 power ($M^{0.75}$) (Kleiber 1961; Calder 1984). This suggests that as animals get larger, the energy requirement per unit of mass decreases with increasing body size, and that larger animals have lower metabolic rates per unit of mass than do small animals, although the overall total metabolic rate is still greater (Calder 1984). Consequently, the total caloric intake of a large animal is still considerably greater than that of a small animal,

necessitating an overall larger ingestion of food for maintenance. Therefore, in very large herbivores, rate of intake and rate of passage become more of an issue than the ability to totally breakdown cellular walls (Demment and Van Soest 1985; Owen-Smith 1988).

Demment and Van Soest (1985) found that rumination is most advantageous for medium sized herbivores. As body size increases, the rate of passage of ingesta decreases, resulting in greater digestibility of the cell wall portion of plant material, and allowing medium sized ruminants to ingest lower quality plant material high in fiber content. Rumination thus allows these medium sized species to take advantage of habitats with poor quality forage (Janis 1976; Demment and Van Soest 1985). However, the advantage of rumination decreases with increasing body size because of the increase in total energy requirements for an animal with a very large body mass (Demment and Van Soest 1985). A very large ruminant would require increasingly longer retention times in order to break down high fiber winter or dry season grasses since the availability of more digestible spring leaves and stems decreases seasonally (Owen-Smith 1988). Because the process of rumination requires by definition, a longer period of time for rate of passage, very large ruminants would be unable to obtain enough caloric intake from low quality forage to sustain the total energy requirements necessary for such a large animal.

Demment and Van Soest (1985) found that high fiber forages with slow digestion rates need an animal of greater than 1200 kg in order to accomplish maximal digestion of the material. The large amount of plant material needed to maintain a large herbivore means that they must be less selective in their diet and ingest high fiber material. At the same time, because of the decrease in metabolic needs per unit of mass, large herbivores

do not need to retain the ingesta for prolonged periods of time (Demment and Van Soest 1985). The upper limit to body size in ruminants is therefore correlated closely to retention time. The largest herbivores are nonruminants because they have a faster rate of passage of ingesta than do ruminants, and the fact that their metabolic needs per unit of mass are less than that of smaller species. The only exception to this general rule are the Equidae, which are comparable to medium sized ruminants in body size, who use caecal digestion similar to that found in very large herbivores. The Equidae apparently achieved ecological separation from other North American perissodactyls during the Eocene by adapting to a high fiber diet (Janis 1976). This is evidenced by the increasing molarization of the premolars, increasing hypsodonty, and increasing complexity of the grinding surface of the teeth over time, indicating a greater food intake than other medium sized herbivores of the time (Janis 1976; MacFadden 1992).

Pecora — The Pecoran character suite includes an enlarged fossa for stapedial muscle on the petrosal, multiple tooth characteristics including presence of "*Palaeomeryx*" fold on molars of brachydont species and a bilobate lower canine, fusion of the metapodials, and a posterior tuberosity on the metatarsus (Vaughn 1986; Janis and Scott 1987; Carroll 1988; Webb and Taylor 1980). The *Palaeomeryx* fold is actually an extension of the postprotocristid, and is lost in hypsodont species such as the antilocaprids (Fig.2-1). Possession of cranial appendages has been thought of as a synapomorphy uniting Pecora, but Janis and Scott (1987) cite fossil and ontogenetic evidence (horn-core tissue transplants) that suggests that cranial appendages have evolved at least twice within the ruminants. Pecora includes Moshidae, Antilocapridae, Cervidae, Giraffidae, and Bovidae.

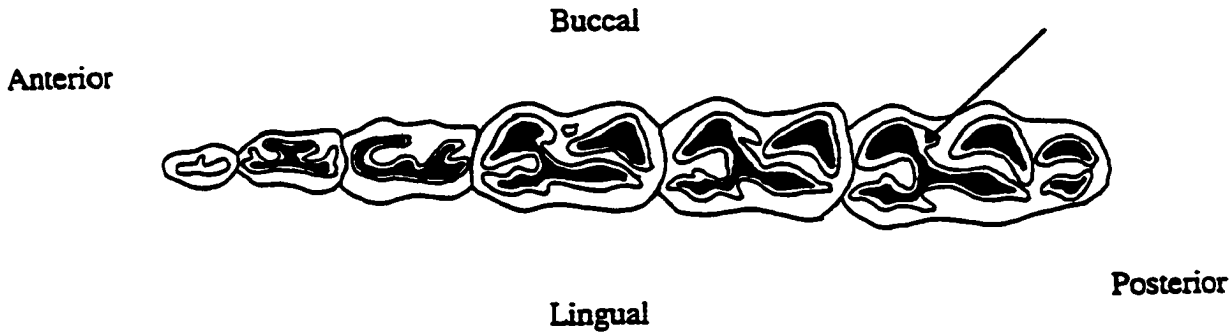

Fig. 2-1. Diagram of composite ruminant teeth; right lower toothrow; derived pecoran condition. Arrow points to *Palaeomeryx* fold. Modified from Janis and Scott 1987.

The Cervoidea, Bovoidea, and Giraffoidea are often accorded superfamily status within Pecora (Simpson 1945; Webb and Taylor 1980; McKenna and Bell 1997). In older classifications, the tragulids are included within Pecora as Traguloidea (Stirton 1944; Romer 1966). More recently, the tragulids and their extinct relatives have been left out of Pecora and placed into their own infraorder Tragulina, as previously mentioned (Webb and Taylor 1980; Leinders and Heintz 1980; Scott and Janis 1987).

Some of the most recent classifications (Leinders and Heintz 1980; Scott and Janis 1987), recognize only two superfamilies, Cervoidea and Bovoidea, and place the Antilocapridae within Cervoidea and the giraffes within Bovoidea (Fig. 2-2). McKenna and Bell (1997) retain Giraffoidea as a third superfamily of the Pecora, but as there is no accompanying text, it is difficult to evaluate their rationale. The traditional inclusion of the antilocaprids within Bovidea was based upon rather vague features such as the loss of side toes and hypsodont dentition (Matthew 1904; Simpson 1945), and the apparent but not real similarity of bovid horn exfoliation with antilocaprid shedding of a deciduous keratin sheath (O'Gara and Matsen 1975).

The inclusion of the antilocaprines within the Cervoidea is based upon two osteological features; a closed metatarsal gully and double lacrimal orifice. These are typical of cervids except for *Moschus*, which has a closed metatarsal gully and a single lacrimal orifice, despite possessing other cervoid features (Leinders and Heintz 1980). Scott and Janis (1987) conclude that the double lacrimal orifice evolved more than once and is present in the Suidae, and two tribes of Bovidae, the Bovini and Tragelaphini.

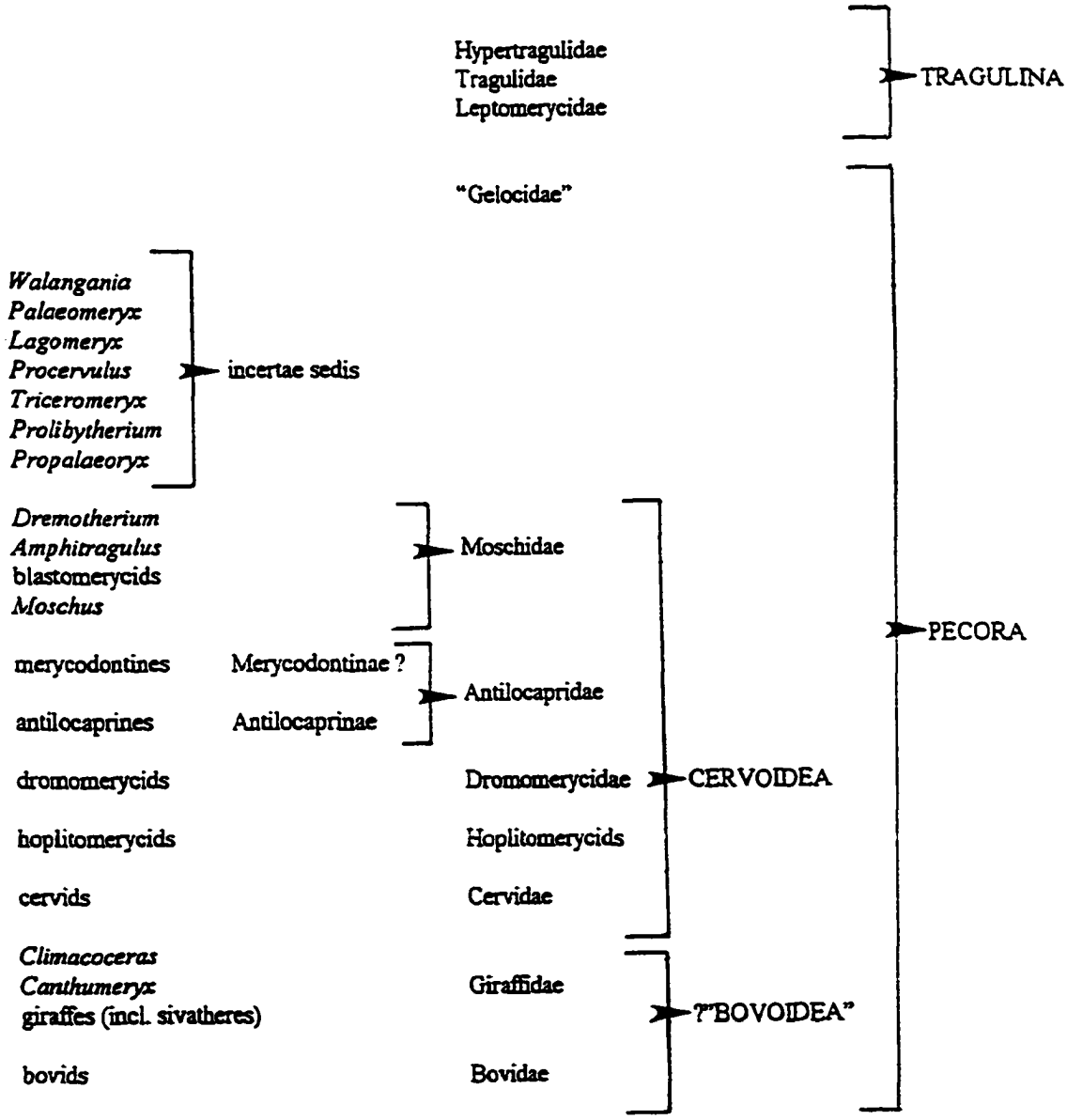

Fig. 2-2. Classification of the Ruminantia. Modified from Scott and Janis 1987.

Although those features alone are not sufficient evidence to include the Antilocaprinae within the Cervoidea, when considering the related Merycodontinae, the antilocaprids seem to align more closely with the cervids than the bovids (Scott and Janis 1987).

Most Pecoran evolution occurred in the Old World, and North America experienced a pecoran radiation and diversification during the Miocene with the arrival of the hornless Blastomerycinae and the horned Merycodontinae and Dromomerycidae (Tedford et al. 1987; Janis et al. 1998). True cervids were absent from North America until the Pliocene, and bovids were an even more recent immigration arriving during the Pleistocene (Janis et al. 1998). Although other artiodactyls have been present in North America since the Eocene, the sudden arrival of horned cervoids with advanced pecoran features such as selenodont cheek teeth, elongated fused metapodials, and a parallel-sided astragalus would seem to support migration (Janis et al. 1998).

Antilocapridae — The Antilocapridae is a unique North American family of pecoran artiodactyls, currently divided into two sub-families, the Merycodontinae and the Antilocaprinae. The Merycodontinae first appeared in the North American fossil record during the late Arikareean mammal age of the late early Miocene, approximately 21 million years ago with the appearance of *Paracosoryx* (Tedford et al. 1987; Scott and Janis 1987). The merycodonts evolved and diversified during the Hemingfordian, Barstovian and Clarendonian mammal ages (19-9 Ma), and were eventually reduced to three genera, becoming extinct by the late Clarandonian (9 Ma) (Webb 1973; Tedford et al. 1987). The first antilocaprine *Plioceros* appeared during the late Clarendonian (9 Ma), followed shortly thereafter by the more derived *Ceratomeryx* and *Sphenophalos* during the

early Hemphillian (9-8 Ma) (Webb 1973; Tedford et al.1987). The antilocaprines experienced a greater diversification than did the earlier merycodonts, with 13 genera spanning the period from the late Clarandonian to present. All are extinct except for the living pronghorn, *Antilocapra americana*, with the genera *Capromeryx*, *Stockoceros*, and *Tetrameryx* becoming extinct at the end of the Rancholabrean (10,000 ybp) (Frick 1937; Kurtén and Anderson 1980; Janis et al. 1998).

The current view is that the Merycodontinae is in actuality a paraphyletic grouping with members allied only by generalized antilocaprid features, with those features differing somewhat from the later antilocaprines (Ahern 1988; Janis et al. 1998). Merycodontine features include horn shafts that are round in cross-section, supraorbital horns present presumably in males only, the presence of one or more "burrs" at the base of the horns and two or more tines present distally, hypsodont dentition, and elongated metapodials (Janis et al. 1998). The genotypic species, *Merycodus necatus* Leidy, identified from fragmentary teeth, was classified as an antilocaprid on the basis of significant hypsodonty which contrasted to the brachydont dentition of contemporary Miocene cervids (Frick 1937). A revised classification by McKenna and Bell (1997) renames Merycodontinae (Matthew 1904), as Cosorycinae, following Cope (1887). While this may be a valid choice of the sub-family name, this dissertation will use the former term, as it has a much longer history in the literature.

The merycodonts are characterized by small body size, very hypsodont dentition, and supra-orbital, non-deciduous "pseudo antlers", some with cervid-like burrs (Fig.2-3) at the base or mid-shaft at the pedicel (Janis and Scott 1987; Bubenik 1990). The "burrs"

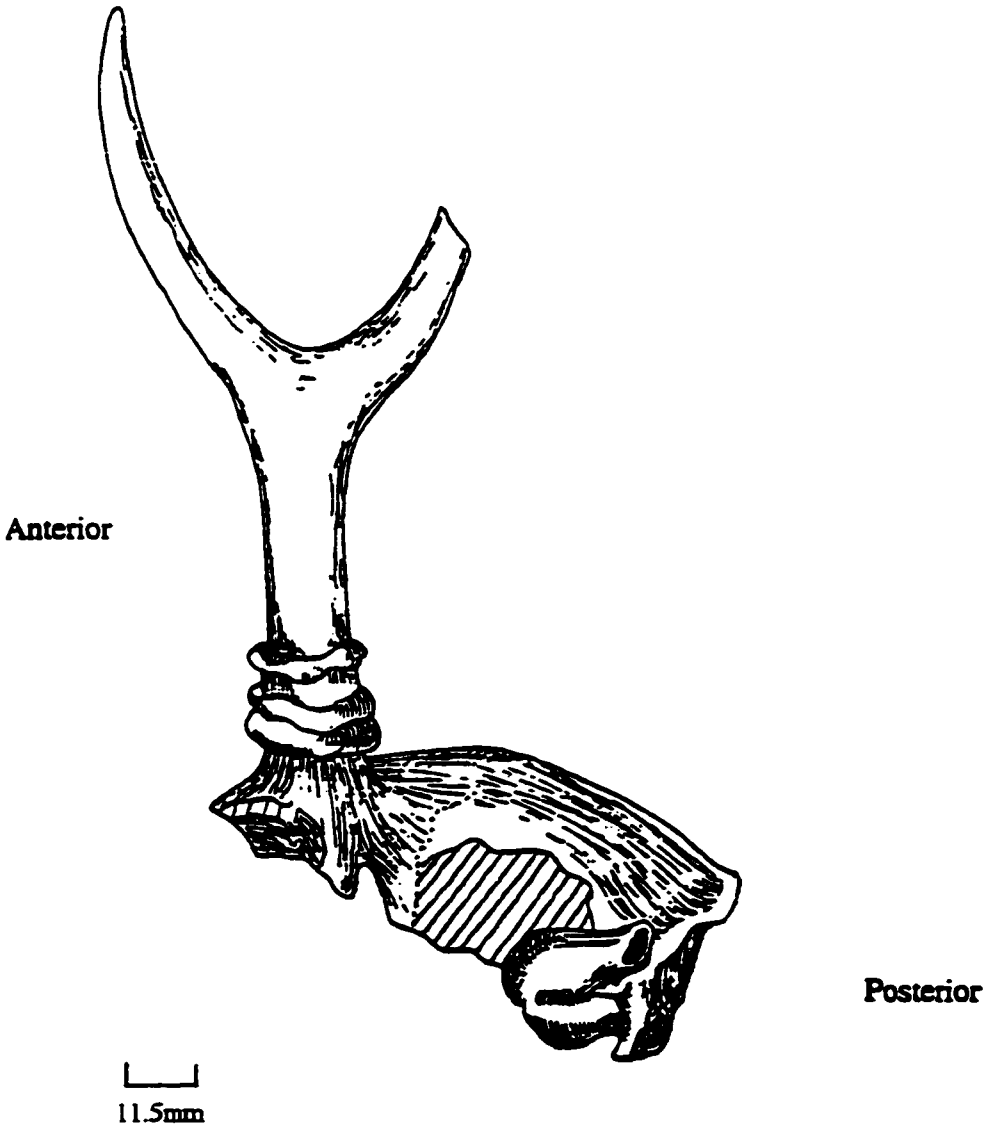

Fig. 2-3. *Cosoryx* showing the merycodontine "pseudo antlers" with burrs. Modified from Frick (1937).

are unlike cervid burrs in that they are not thought to have been shed annually with the rest of the antler as in true cervids. The surface above the burr on the merycodontine antler is covered with shallow sulci, reminiscent of the vascularization present on cervid antlers. The sulci seem to indicate that the appendage was covered by skin (Webb 1973; Janis and Scott 1987). The current consensus is that the merycodont cranial appendage grew to full size covered by a layer of skin which was then shed, leaving the exposed bony core (Furlong 1927; Voorhies 1969; Janis et al.1998). Multiple burrs most likely represent successive years of bone deposition and thickening of the diameter of the horn with the shedding of accompanying layers of skin (Voorhies 1969). In contrast, antilocaprine horn morphology consists of a bony horn core covered by a keratinous sheath, and no burr is formed.

The merycodonts have been allied with the Antilocaprinae because of the supraorbital position of the horn cores, significant elongation of the metapodials, hypsodont dentition and other osteological features (Janis and Scott 1987). All these are generalized features that may be found in other groups inhabiting open plains environments. Janis and Scott (1987) suggest that these characters have evolved numerous times in ungulates and should not be considered indicators of taxonomic relationships. If one accepts the apparent paraphyly of the merycodonts, as well as the obvious difference between merycodontine and antilocaprine cranial appendages, it may be that the two groups are unrelated (Janis and Scott 1987).

The larger and later occurring antilocaprines share all of the generalized antilocaprid features with the merycodontines, but in addition possess supraorbital bony

horn-cores that are smooth without burrs and may be forked or spiraled. Many species show medial-lateral flattening of the horn cores (Fig.2-4A) (Frick 1937). The modern antilocaprid *Antilocapra americana* Ord, has a smooth bony horn-core covered by a keratinous sheath that is shed annually (Fig.2-4B). As with both cervids and bovids, the "pronghorns" are located on the frontal bone.

In bovids, horn-cores develop from the *os cornu*, or horn bud, a collection of tissues which includes connective and dermal tissues superficial to the frontal bone periosteum (Dove 1935; Janis and Scott 1987). After approximately 3-4 weeks, the first recognizable keratin sheath appears at the horn-core tip and grows downward towards the base. The sheath is non-deciduous but may be subject to occasional flaking and renewal in some species of bovids (O'Gara and Matson 1975; Janis and Scott 1987). In cervids, antlers develop directly from the frontal bone periosteum, without involvement of connective and dermal tissues (Goss 1983).

The cellular origin of pronghorn horn-cores has not yet been determined, and thus any affiliation with either cervoids or bovoids must be made on the basis of other characters (Janis and Scott 1987). The modern pronghorn sheath is deciduous, and therefore the cranial appendage is not considered a true horn, but rather something unique among ruminants (Cope 1887; Bubenik 1990; Janis et al. 1998). The presence of smooth horn-cores in other species of antilocaprines, such as *Sphenophalos* imply the presence of keratinous sheaths, although it is impossible to know if they were deciduous (Webb 1973). *A. americana* is sexually dimorphic in the possession of horn-cores, with females having horn-cores considerably smaller than the males (Skinner 1942; O'Gara 1978).

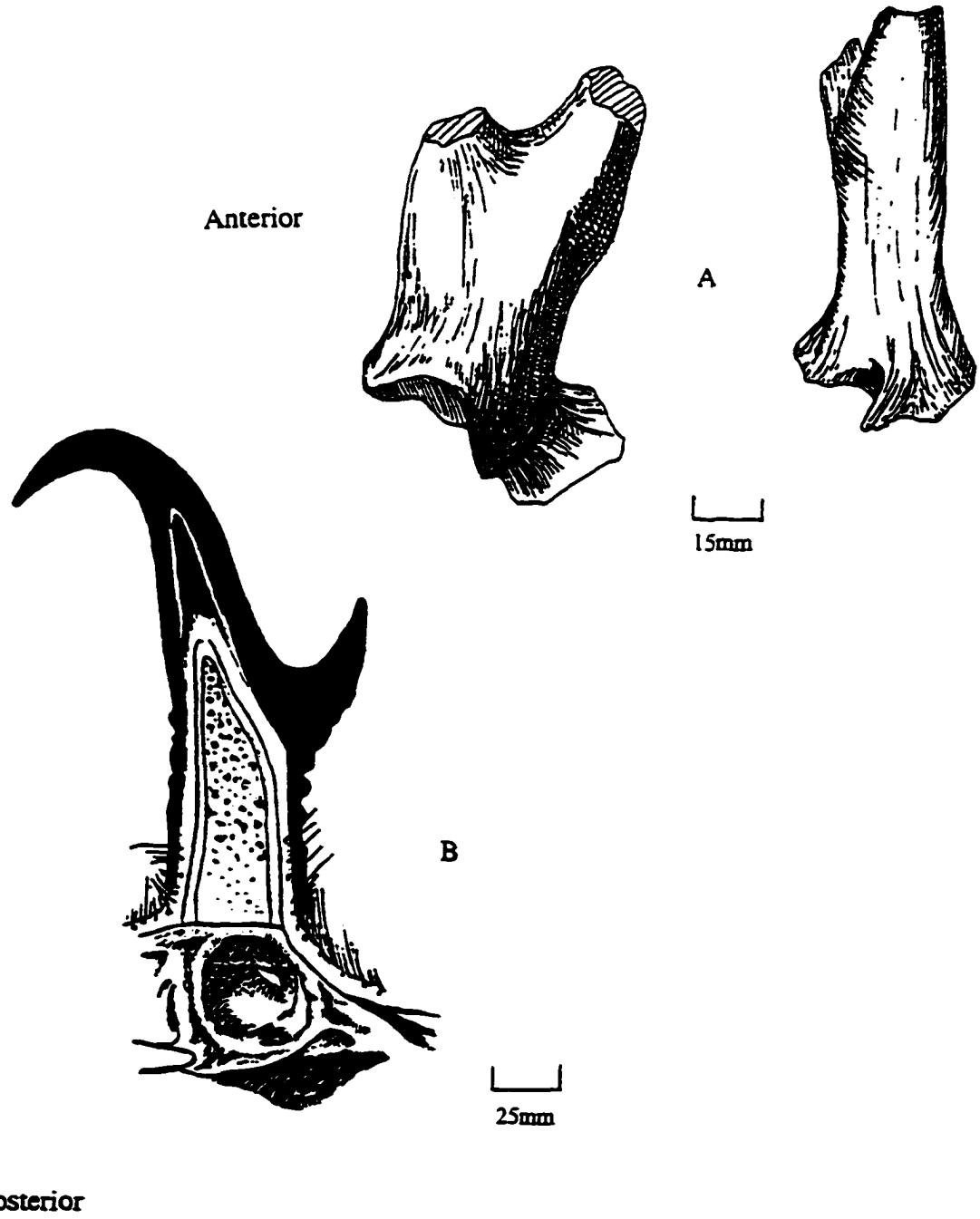

Fig. 2-4A. Horn-core of *Plioceros* F:AM 31682 showing antero-posterior flattening. Modified from Frick 1937.
Fig. 2-4B. Sagittal section of horn-core and sheath of *Antilocapra americana*. Modified from Bubenik 1990.

Capromeryx — Of the antilocaprines, the Plio-Pleistocene genus *Capromeryx* is of particular interest because of its widespread geographical and temporal distribution. There are currently five recognized species within *Capromeryx* (Kurtén and Anderson 1980). Another species, *C. gidleyi* from Curtis Flats, Benson, Arizona was named by Frick (1937). The specimen consists of the posterior tine of a left horn-core. All species have horn-cores with two tines that arise vertically from the frontal bone. *C. tauntonensis* is the largest member of the genus; *C. arizonensis* is slightly smaller and is a contemporary of the former for at least several thousand years. *C. furcifer* is a tiny antilocaprid from the late Irvingtonian of Nebraska (0.5 Ma). *C. minor* and *C. mexicanus* are both very small species that were described from the Rancholabrean of California and Mexico. Although the genus was widespread throughout North America, most records come from the state of Washington, the central and southern United States and northern and central Mexico. There was a dwarfing trend within *Capromeryx* over time, with later species being as much as 50% smaller in body size than earlier species (Morgan and Morgan 1995). This occurred during a period when many other mammalian families were experiencing increases in body size (Kurtén and Anderson 1980; Janis et al. 1998). Although an extensive history of *Capromeryx* is provided by Morgan and Morgan (1995), the primary focus of that paper was to describe the newly discovered species, *C. tauntonensis*, and not to redefine the genus. A brief review will follow here.

The mid-Blancan *C. tauntonensis* from the Taunton site in Washington was described recently (Morgan and Morgan 1995). Paleomagnetic studies conducted close to the Taunton site in 1979 indicate a reversed polarity interval, most likely the Kaena

subchron of the normal Gauss Chron (Packer and Johnston 1979). This evidence suggests an age of 3.02-3.09 Ma. (Berggren et al. 1995), indicating a mid-Blancan North American Land Mammal (NALMA) age for this species (Packer and Johnson 1979; Morgan and Morgan 1995).

The mid-Blancan to early Irvingtonian (2.66-1.5 Ma) *C. arizonensis* was first identified from Dry Mountain, Graham County, Arizona, and is the mid-sized member of the genus (Skinner 1942). The most significant amount of material is from the Inglis 1A and Santa Fe 1B faunas of Florida (Webb 1974). Slightly larger than all other species except *C. tauntonensis*, *C. arizonensis* has been estimated to weigh approximately 17 kilograms (Scott 1983). Skinner (1942) also recognizes a subspecies, *C. arizonensis schultzi*, with the type being a crushed partial cranium with both horn cores. The subspecies was named because of the geographic locale and presumed minor size differences in the horn cores (Skinner 1942). The Santa Fe 1B Florida material is mid-Blancan in age (2.5 Ma), and is 600 Ka younger than the Taunton material (3.1 Ma).

Lindsey and Tessman (1974) place the age of the Benson l.f. just below the Mammoth reversed subchron of the Gauss chron, at approximately 3.21 Ma. Therefore, the type specimen of *C. gidleyi* is actually >200 Ka older than the Taunton site, making *C. gidleyi* the oldest member of *Capromeryx*.

The type of *C. furcifer* is from the late Irvingtonian (0.5 Ma) Hay Springs locality in Nebraska (Matthew 1902). The age of *C. furcifer* was questioned by Hesse (1935) and again by Stirton (1938) when both Pliocene and Pleistocene vertebrates were noted to occur at Hay Springs. These authors suggested that *C. furcifer* may have actually been

from the Pliocene deposits. Hibbard and Taylor (1960) stated that enough evidence had accumulated over the years to securely place the type of *C. furcifer* within the Pleistocene deposits. This assumption was partly based upon the presence of *Microtus pennsylvanicus*, a vole known to occur in North America no earlier than the late Irvingtonian (650-400 Ka) (Hibbard and Taylor 1960). Recently however, the ability to differentiate among species of *Microtus* has been questioned, and it may not be possible to identify *M. pennsylvanicus* from its teeth (Repenning, pers. comm). It is therefore unclear as to which species of *Microtus* is actually present at Hay Springs, although the age of the site has been verified by the presence of other fauna known to be late Irvingtonian, such as *Smilodon fatalis* (Lundelius et al. 1987; Repenning pers.comm.). There are two late Rancholabrean (40,000-10,000 ybp) species; *C. mexicanus* from Tequixquiac, Mexico (Furlong 1925), and *C. minor* from Rancho La Brea (Taylor 1911). The site at El Tajo de Tequixquiac consists of Pleistocene beds located within a quarry, and is approximately 30 miles north of Mexico City. The site is securely dated as being Rancholabrean in age due to the associated fauna which includes *Bison* and *Canis dirus* (Furlong 1925). Rancho La Brea is the site of the well known "tar pits" in Los Angeles, and is the site for which the Land Mammal Age is named. The Rancholabrean starts at approximately 0.4- 0.25 Ma, and is characterized by the presence of *Bison*.

The taxonomy of *Capromeryx* is redundant and a revision is in order. Of the six named species, the three latest, *C. furcifer*, *C. minor*, and *C. mexicanus* appear to be similar enough to one another to warrant only one species name. There is also a size and temporal overlap among *C. tauntonensis*, *C. arizonensis*, and *C. gidleyi*. An analysis of

horn-cores and three molar teeth (M2, m1, and m2) of each of the named species was undertaken in an attempt to clarify phylogenetic relationships within the genus.

METHODS AND MATERIALS

Fossil Material

The amount of available material of *Capromeryx* varied from species to species. A very large sample of *C. arizonensis* was available from sites in Florida. However, there were only a few specimens of *C. mexicanus* available for study here in the United States, with the bulk of the material housed in Mexico. The holotype of *C. mexicanus* from the University of California Museum of Paleontology is fairly complete except for the mandible, with almost an entire cranium and most of the postcrania present. Two horn-cores and three mandibles were also available for *C. mexicanus* from other institutions. There was a paucity of material for *C. tauntonensis*, which was represented only by the type cranium, several teeth and one very worn metatarsal which were not found in association. *C. minor* from Rancho La Brea and McKittrick in California was relatively well represented with 38 teeth from 12 individuals and four horn-cores available. Much of the *C. minor* material at Rancho la Brea was not included, as many were immature specimens, evidenced by either the presence of deciduous teeth or unfused postcranial epiphyses. The availability of specimens of *C. furcifer* was also a problem, but there were 29 teeth from 11 adult individuals and six horn-cores for comparison. Only a photograph of the type specimen of *C. gidleyi*, a left posterior horn-core, was available.

Estimates of body mass — All measurements were taken with a Mitutoyo digital calipers and are in millimeters. Length, and width measurements were taken of m1, m2, and M2 at the occlusal surface. The lengths of these teeth have been shown to provide the best estimates of mass in artiodactyls (Damuth 1990; Janis 1990). Lengths of m1, m2, and M2 were $\log_{10}$ transformed and entered into least squares regression equations taken from Damuth (1990). It was necessary to use published regression equations, as my data did not include a sample of teeth of modern pecorans, other than those of *A. americana*, which would not have provided the necessary variation for the development of predictive equations. Damuth's equations were based upon a large sample of modern selenodont artiodactyls, which closely approximated the pecoran sample used in Chapter III. Damuth's regressions give results in millimeters and grams, and as my postcranial equations for *Capromeryx* provided results in millimeters and kilograms, a conversion was necessary for comparison, by dividing grams by 1000 to report the predicted masses in kilograms. Occlusal surface areas (length x width) were not used, as the r^2 reported for regressions for areas was less than .90 (Damuth 1990).

Means for the length of each of the three molars for each species was obtained and used for comparison among species. Body mass estimates obtained from the teeth were compared to postcranial body mass estimates that were obtained in Chapter III. Morgan and Morgan (1995) used the length of m3 to estimate mass in *C. tauntonensis*. This tooth measurement is not the best estimator of mass, and the associated problems will be discussed later (Janis 1990). Measurements of m3 of the other species were taken for comparison, but no mass estimates were attempted with this tooth.

Horn-core Measurements — Measurements were taken of horn-cores in order to test for similarities among the species of *Capromeryx*. Antero-posterior and medio-lateral measurements of both the anterior and posterior tines were taken at the notch. The greatest length of each tine was measured from the notch to the tip (Fig.2-5). In many instances, the tips of the horn-cores were broken or worn, so measurements of many of the lengths are inaccurate. Horn-core lengths were not used as criteria in taxonomic revisions.

Institutional Abbreviations — **AMNH**, American Museum of Natural History, New York; **F:AM**, Frick Collection of the American Museum of Natural History, New York; **LACM**, Natural History Museum of Los Angeles County; **MSU**, Midwestern State University, Wichita Falls, Texas; **SDSM**, South Dakota School of Mines, Museum of Geology, Rapid City; **TMM**, Texas Memorial Museum, University of Texas at Austin; **UAHMP**, Universidad Autónoma del Estrado de Hidalgo, Museo de Paleontología, Pachuga, Mexico; **UCMP**, University of California Museum of Paleontology, Berkeley; **UF**, University of Florida, Florida Museum of Natural History, Gainesville; **UM**, University of Michigan Museum of Paleontology, Ann Arbor; **UNSM**, University of Nebraska State Museum, Lincoln; **UTEP**, University of Texas at El Paso.

SYSTEMATIC PALEONTOLOGY

Order Artiodactyla Owen, 1848

Antilocapridae Gray, 1866

Antilocaprinae Gray, 1866

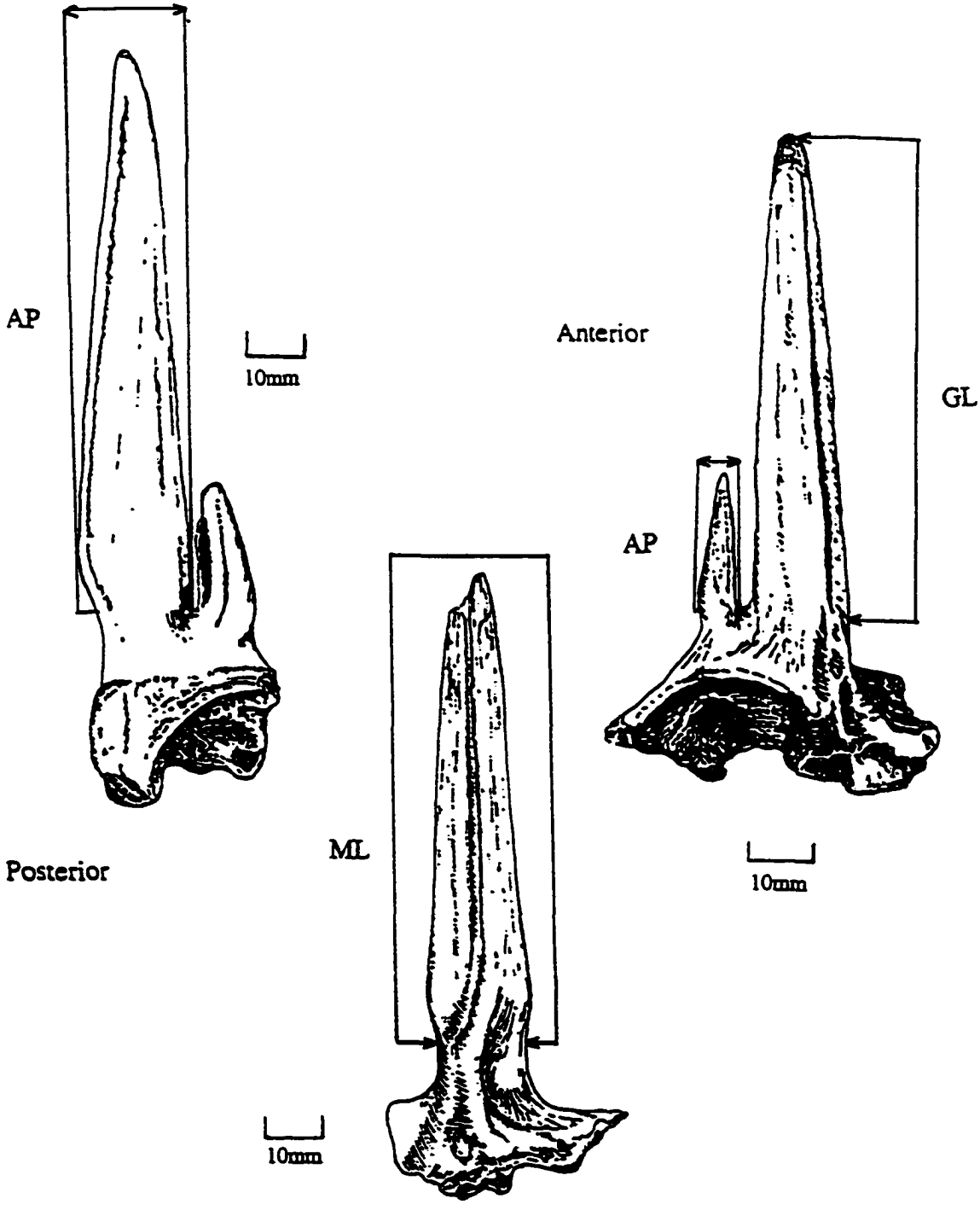

Fig. 2-5. Measurements of the Capromeryx horn-core. AP = antero-posterior, ML = medio-lateral, GL = greatest length measured from the notch.

Capromeryx Matthew, 1902

Breameryx Furlong, 1946

Diagnosis — Small antilocaprines present in North America from the mid-Blancan (3.1 Ma) to the late Rancholabrean (10K-40K ybp). Horn-cores are bifurcate and arise vertically from the frontal bone. Anterior tine is smaller than posterior tine. There are two distinct forms within the genus; species with anterior tine approximately two thirds the size of posterior, and those with anterior tine only one quarter the size of posterior. Horn-cores are positioned directly over orbit in earlier species, moving slightly posterior in later species. Horn-cores exhibit considerable individual variation, similar to that observed in *Antilocapra* (Skinner 1942). Rear tine is deeply grooved postero-laterally, and anterior tine is deeply grooved posteriorly. The grooves indicate the location of the main blood supply to the horn-cores and sheaths, the cornual artery. There is a deep pit just below the junction of the two tines on the frontal. A prominent parasagittal crest is present along the temporal-parietal suture. Orbit is prominent with well developed rims, and there is a single elongate frontal foramen. Diastema and premolar row are shorter than in *Antilocapra*, and the overall jaw is shortened. Teeth are hypsodont and conservative in morphology, and essentially indistinguishable from the teeth of other antilocaprids. The dental formula is 0/3, 0/0, 3/3, 3/3 = 30. There is a deep anterior lingual inflection on the occlusal surfaces of p3 and p4, with a variable deep to shallow posterior lingual inflection. With wear in p4, there is a tendency towards metaconid-entoconid closure. The m3 has a variable inflation of the basal portion of the third lobe, and a variable posterior heel on M3. Except for the small size, the postcrania are typical of the family.

Capromeryx furcifer Matthew, 1902

Capromeryx (?) *minor* Taylor, 1911: p.192

Capromeryx minor Chandler, 1916: p.111

Capromeryx mexicanus Furlong, 1925: p.145

Capromeryx minimus Meade, 1942: p.89

Holotype — AMNH 2771, left partial ramus, p2-m3.

Type Locality — Hay Springs, Nebraska, Pleistocene beds.

Referred Specimens — LACM 12523, left partial ramus dp3-dp4; LACM 12817, right partial ramus dp3-m1; LACM 21445, partial cranium ; LACM 49, right horn-core; LACM 20036, right partial ramus p2-m2; UCMP 26648, skull and large portion of skeleton; UCMP 26649, portion of skull and limb elements (immature); WTM No.18, partial left ramus p3-m3; WTM No. 21, incomplete ramus, dp2-m1; WTM Nos. 19 and 20, two left horn-cores.

Revised Diagnosis — Very small (10 kg) Pleistocene antilocaprine with the horn-core consisting of two tines rising vertically from a single base and the anterior tine significantly smaller than posterior. Horn-core is slightly flattened medio-laterally, and the horn-core base is constricted antero-posteriorly. The anterior tine is deeply grooved posteriorly and the rear tine is deeply grooved postero-laterally as is typical of the genus. The junction of anterior and posterior tines of horn-core is situated slightly posteriorly over orbit. The posterior tine is cylindrical in cross-section with a flattened anterior face, and the anterior tine is triangular in cross-section with a flattened posterior face. There is variable anterior curvature of the horn-core, and a variable area of expansion above horn-core base

(Fig. 2-6). Dentition is hypsodont, p3 and p4 with deep anterior lingual inflection and variable deep to shallow posterior lingual inflection, m3 with variable inflation of the basal portion of the third lobe, and variable posterior heel on M3.

Comparisons and relationships

Capromeryx furcifer — The genotypic species *C. furcifer*, was first described by Matthew (1902) from the Pleistocene deposits at Hay Springs, Nebraska. The type specimen is a partial left ramus with complete dentition p2-m3, figured in a later paper (Matthew 1904). Matthew comments on the degree of hypsodonty as being comparable to the modern *A. americana*, but that the premolar pattern is more "primitive", like that of *Merycodus* (Matthew 1904). Matthew mentions the lack of a "deuteroconid", now known as the paraconid. Janis and Lister (1985) identified five different types of p4 premolar patterns within pecoran artiodactyls. They state that the anterior portion of the lower fourth premolar is highly variable even on an individual level, and that the p4 should not be used in isolation to assign a single specimen to a particular lineage (Janis and Lister 1985). Therefore, the apparent lack of a paraconid in the type of *C. furcifer* is probably due to individual variation.

The type ramus is that of an adult, with the occlusal surfaces of the premolars in particular showing extreme wear, obscuring diagnostic details that were later elucidated in other specimens, such as the configuration of the p4. Matthew (1902) assigned *C. furcifer* to the Merycodontinae, primarily due to similarities in size. Two left horn-cores were found at the Hay Springs locality in 1929-1930. Frick (1937) describes the posterior tine

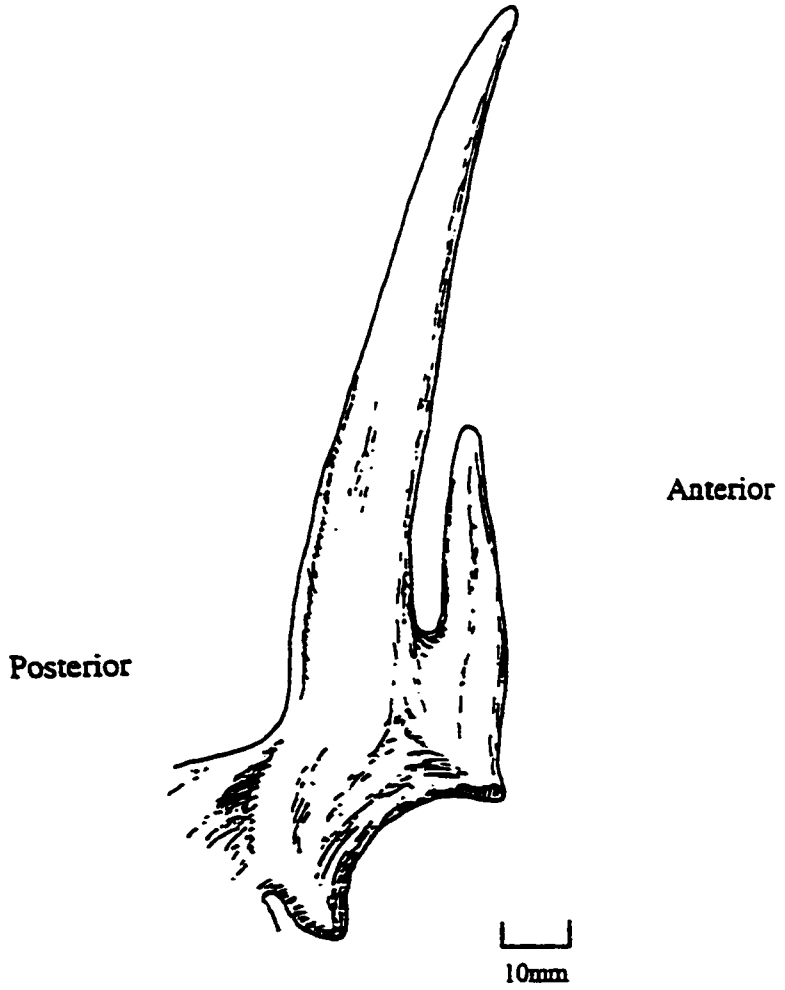

Fig. 2-6. Right horn-core (holotype) of *Capromeryx mexicanus* sensu Furlong 1925. From the El Tajo de Tequixquiac site, Mexico. Modified from Furlong 1925.

as being flattened anteriorly , with a deep groove on the posterior side. The anterior tine is "rudimentary", and both tines curve forward slightly (Frick 1937). More recent discoveries of horn-cores of the species do not curve forward, suggesting that individual variation is a factor. Horn-core variation among modern *Antilocapra* was first documented in the literature by Skinner (1942), and the amount of variation is striking.

***Capromeryx minor* sensu Taylor 1911** — *C. minor* was first described from Rancho La Brea in Los Angeles, and was identified from three juvenile rami, several metapodials, two phalanges, and one astragalus found in association (Taylor 1911). Taylor's discussion revolves around a comparison with *Antilocapra* and other antilocaprines, with only a brief mention of the type of *C. furcifer* that had been identified nine years before by Matthew (1902). Why the Rancho La Brea specimen was not referred to *C. furcifer* is puzzling, but may have been due to the fact that the age of the Rancho la Brea specimens were so much younger than those from Hay Springs.

Chandler (1916) described more fossil material of *C. minor* that had been recovered from the tar pits in the intervening years since Taylor first named the species. More postcranial material was discovered, but more importantly, adult dentition and a horn-core were now available. Chandler described a prominent orbit, a single frontal foramen, a shallow depression or pit on the frontal below the junction of the tines, the anterior tine being much smaller than the posterior, with both tines arising from a common base that is approximately 15 mm high measured from the top of the orbit. The posterior tine is described as being more or less cylindrical in shape, 65 mm in height, with an anteriorly flattened face (Chandler 1916). The anterior tine is much shorter, triangular in

cross-section, and has a posteriorly flattened face. Furlong (1930) described *C. minor* from the McKittrick, California asphalt on the basis of upper and lower molars. Late Rancholabrean in age, *C. minor* is an extremely small antilocaprid, virtually indistinguishable in size and morphology to both *C. furcifer* and *C. mexicanus*.

C. mexicanus sensu Furlong 1925 — The most complete specimen of the genus, *C. mexicanus*, is from El Tajo de Tequixquiac, Mexico and consists of the skull and most of the skeleton of an adult individual, and a partial skull and skeleton of a juvenile (Furlong 1925). *Capromeryx mexicana* is now recognized as *Capromeryx mexicanus*, resolving a gender problem between the genus and species which was rectified by Morgan and Morgan (1995). There is little difference between this species and *C. minor*, either morphologically or temporally, and Hibbard and Taylor (1960) commented that it was likely that they were the same species. Why the two were not synonymized at the time is unclear. The horn-core of the type (UCMP 26648) is described as being very similar to that of *C. minor*, but that the anterior tine is slightly more robust (Furlong 1925). It would appear that individual variation in horn-core morphology was not accounted for and resulted in the naming of a new species. Figs. 2-7A, 2-7B, and 2-7C show the considerable similarities among the horn-cores of the three Rancholabrean species. Indeed, individual variation could easily account for the minor differences.

***Capromeryx minimus* sensu Meade 1942** — *Capromeryx minimus* was described from the Slaton l.f., Lubbock Co., Texas. The horn-cores are quite small, precipitating the naming of a new species despite apparent similarities to *C. minor*. Meade discusses individual variation between the two horn-cores, but does not carry that discussion any

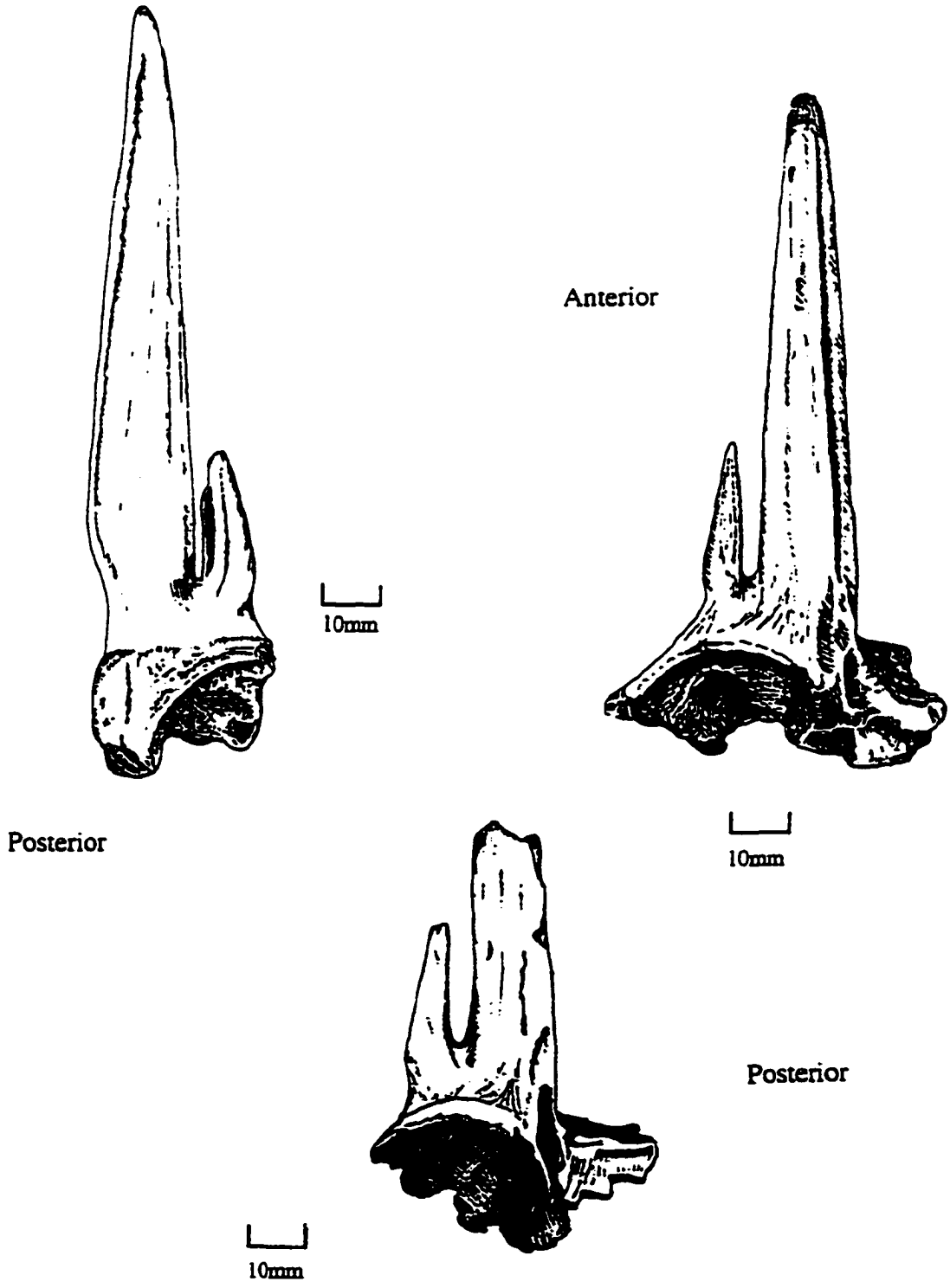

Fig. 2-7A. Horn-core of *Capromeryx furcifer* UNSM 5438.
Fig. 2-7B. Horn-core of *Capromeryx minor* sensu Taylor 1911 LACM Z8523.
Fig. 2-7C. Horn-core of *Capromeryx mexicanus* sensu Skinner 1942 MU 9934.

farther so as to incorporate the specimens into existing species of *Capromeryx*. Small differences between dental features on the type mandible and dental features of *C. minor* can again be dismissed as individual variation. The length of m3 is mentioned as being longer and narrower than that of *C. minor*, but it is now known that the length of m3 increases with age (Janis 1990). Similarly, Meade placed considerable emphasis on the configuration of the p4, stating that there were two lingual inflections present in the specimen, whereas in *C. minor*, there was only one. Janis and Lister (1985) comment on the considerable variability of the p4 form in the cervoid and bovid lineages even within single populations, and caution against the use of this character when assigning an isolated specimen to a particular lineage. Hibbard and Taylor (1960) referred *C. minimus* to *C. furcifer* on the basis of individual variation due to sexual and age differences. The specimen was referred to *C. furcifer* and not *C. minor* due to the age of the Slaton l.f., which is late Irvingtonian (0.45 Ma).

Capromeryx gidleyi Frick, 1937

Capromeryx arizonensis Skinner, 1942: p. 216

Capromeryx arizonensis schultzi Skinner, 1942: p. 219

Holotype — F:AM 23324, partial left horn-core, posterior tine only.

Referred Specimens — F:AM 42878, portions of a crushed cranium and left horn-cores; UNSM 5439, crushed cranium with two horn-cores; F:AM 117078, left ramus fragment p2-m3.

Type Locality — Curtis Flats, Benson, Arizona.

Revised Diagnosis — Medium sized mid-Blancan to early Irvingtonian (3.21-1.5 Ma) species estimated to weigh approximately 17 kg (Janis 1990). The Benson, Arizona locality is mid-Blancan in age (3.21 Ma), with a paleomagnetic date just below the Mammoth reversed subchron of the Gauss normal chron (3.16 Ma). This makes the type locality for *C. gidleyi* slightly older than the Taunton site, posing an interesting situation. It may be that *C. gidleyi* and *C. tauntonensis* are the same species, and that the type of *C. tauntonensis* is the cranium of a very large male. The holotype of *C. gidleyi* is a left posterior tine only, but both the age, size, and configuration of the tine suggest that it is synonymous with *C. arizonensis*. *C. gidleyi* was named in 1937, and I accept this name as the senior synonym according to the International Code of Zoological Nomenclature, Rules of Chapter V, Article 23, Law of Priority, which states that it is mandatory that the prior name be used for a species International Code of Zoological Nomenclature (ICZN 1961). Although the holotype of *C. gidleyi* was not figured by Frick (1937), the inclusion of an illustration with the description of a new taxon is a recommendation only in Appendix E: General Recommendations, paragraph 17 of the ICZN. The general recommendations do not have the force of rules, and are not mandatory. I refer the types of *C. arizonensis* and *C. arizonensis schultzi* to *C. gidleyi* on the basis of the age of the type Benson site (3.21Ma), the physical appearance of the tine, and the fact that *C. gidleyi* is the senior synonym. The status of the relationship of *C. gidleyi* and *C. tauntonensis* remains unresolved at this time.

The horn-core of this species is bifurcate and arises vertically from the frontal with the base situated directly over the center to slightly posteriorly over the orbit. The anterior

prong is approximately two thirds of this species is as large as the posterior (Fig.2-8). The posterior prong is cylindrical in shape with a deep postero-lateral groove and a flattened anterior face. The anterior prong is also cylindrical in shape, with a postero-lateral groove and a flattened posterior face. The horn-core is slightly flattened medio-laterally, and the amount of antero-posterior constriction varies from slight to none. Many specimens exhibit a slightly roughened area at the base of each prong which would seem to indicate the presence of separate sheaths on each prong (Skinner 1942). The p4 has deep anterior and posterior lingual inflections that bracket a mid-lingual rib, and with wear, there is a tendency for metaconid-entoconid closure as in the other species of *Capromeryx*. Other cheek teeth and postcrania are as described for the genus.

Capromeryx tauntonensis Morgan and Morgan, 1995

Holotype —UWBM 78964, fragmentary cranium without maxilla with right horn-core base, bullar and palatal features partially intact.

Referred specimens — TMM 41068-85, right horn-core from Cita Canyon, Randall Co., Texas, mid-Blancan (2.5-2.7 Ma).

Type Locality — Mid-Blancan Taunton locality, Adams County, Washington.

Revised Diagnosis — This is the largest species of *Capromeryx*. Horn-core is situated directly over the orbit. Only the horn-core base is preserved in the holotype (Fig.2-9). The anterior tine is severely damaged anteriorly, but from the medio-lateral basilar dimensions, it is obvious that the anterior tine is nearly as large as the posterior, similar to the condition found in *C. gidleyi*. The posterior tine is cylindrical in shape with a flattened

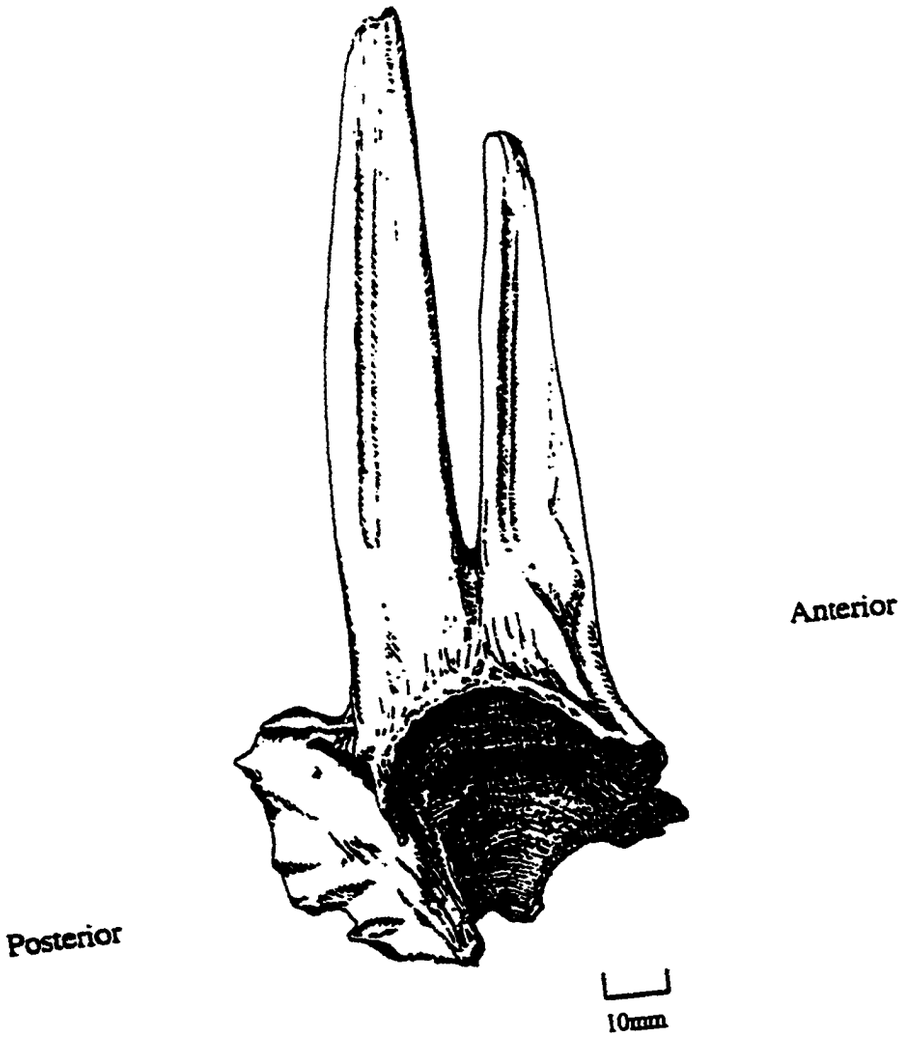

Fig. 2-8. Right horn-core of *Capromeryx arizonensis* sensu Skinner 1942, UF 115962.

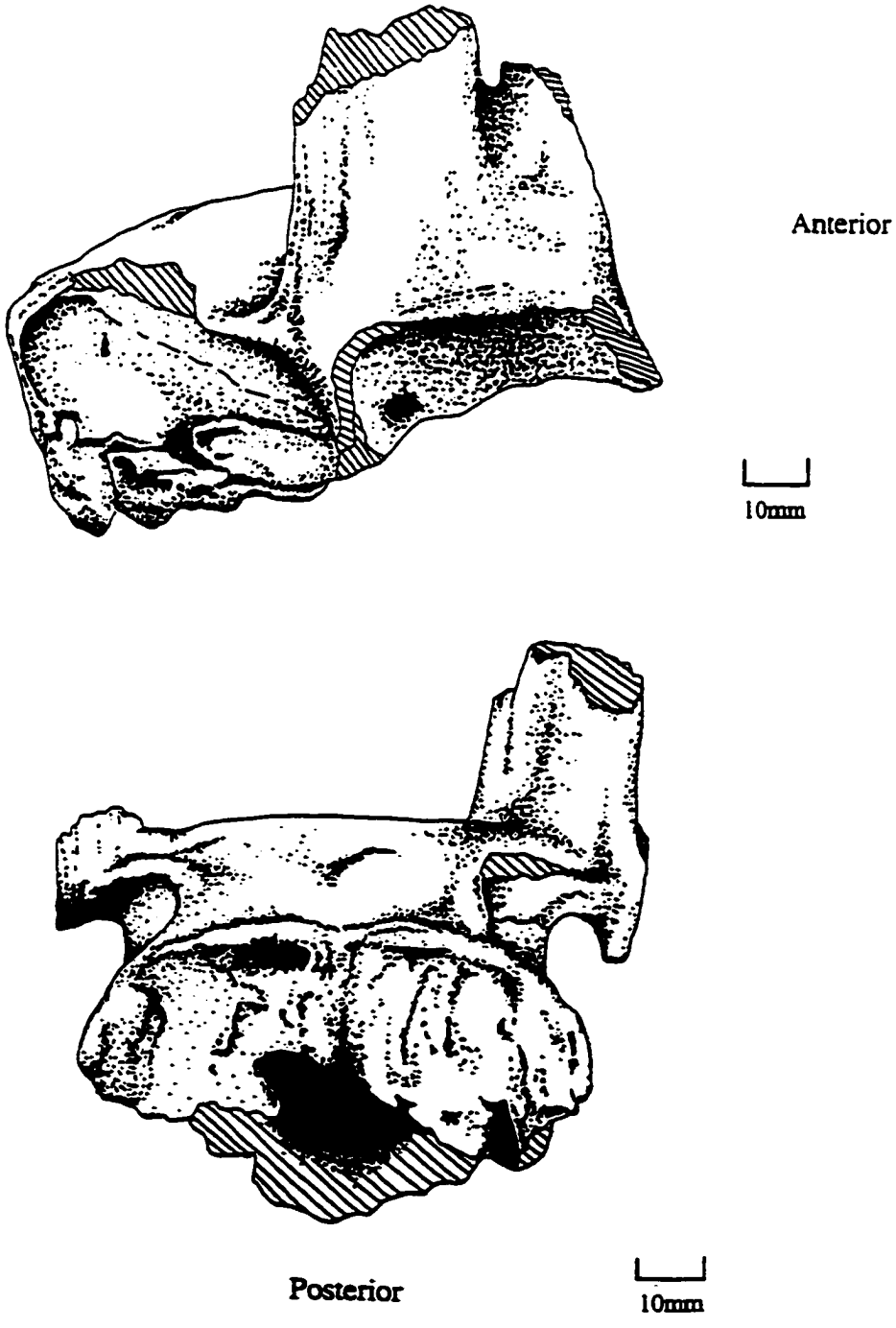

Fig. 2-9. Type cranium of *Capromeryx tauntonensis*. UWBM 78964. Modified from Morgan and Morgan (1995).

anterior face. There is not enough of either tine preserved to ascertain the position of the dorso-ventral grooves. There is a deep pit present just below the junction of the two tines on the frontal, as is present in other species of *Capromeryx*. There is evidence of the parasagittal crest that is typical of the genus present along the temporal parietal suture, but significant weathering of the type has smoothed distinguishing features, making recognition of fine features somewhat problematic. Neither the teeth nor the single metatarsal were found in association with the type cranium. The metatarsal exhibits signs of extreme weathering. Dentition is unremarkable and typical of the genus.

Comparisons and relationships — *C. tauntonensis* is the largest member of the genus, with a body mass estimated to be approximately 40 kilograms (Morgan and Morgan 1995). In their analysis, Morgan and Morgan (1995) used the length of the lower m3 to obtain this mass estimate. However, the length of this molar has been found to vary considerably with feeding strategies, and intermediate feeders, or those ungulates that combine grazing and browsing (such as antilocaprids), and omnivores all have significantly longer m3's than would be expected from their body masses (Janis 1990). Therefore, any estimate of mass using m3 would tend to overestimate the body mass of any ungulate utilizing an intermediate feeding strategy, including *C. tauntonensis*.

C. gidleyi and *C. tauntonensis* appear to be closely related, with *C. furcifer* being a later and more diminutive species The deep posterior lingual inflection of p4 mentioned in the diagnosis of *C. tauntonensis* (Fig. 2-10A), was also found in one specimen of *C. gidleyi*, UF 54670 (Fig. 2-10B). One illustration in Frick (1937) identified as *C. furcifer* (F:AM 31749) from the *Stegomastodon* Quarry (Sand Draw l.f) of Brown

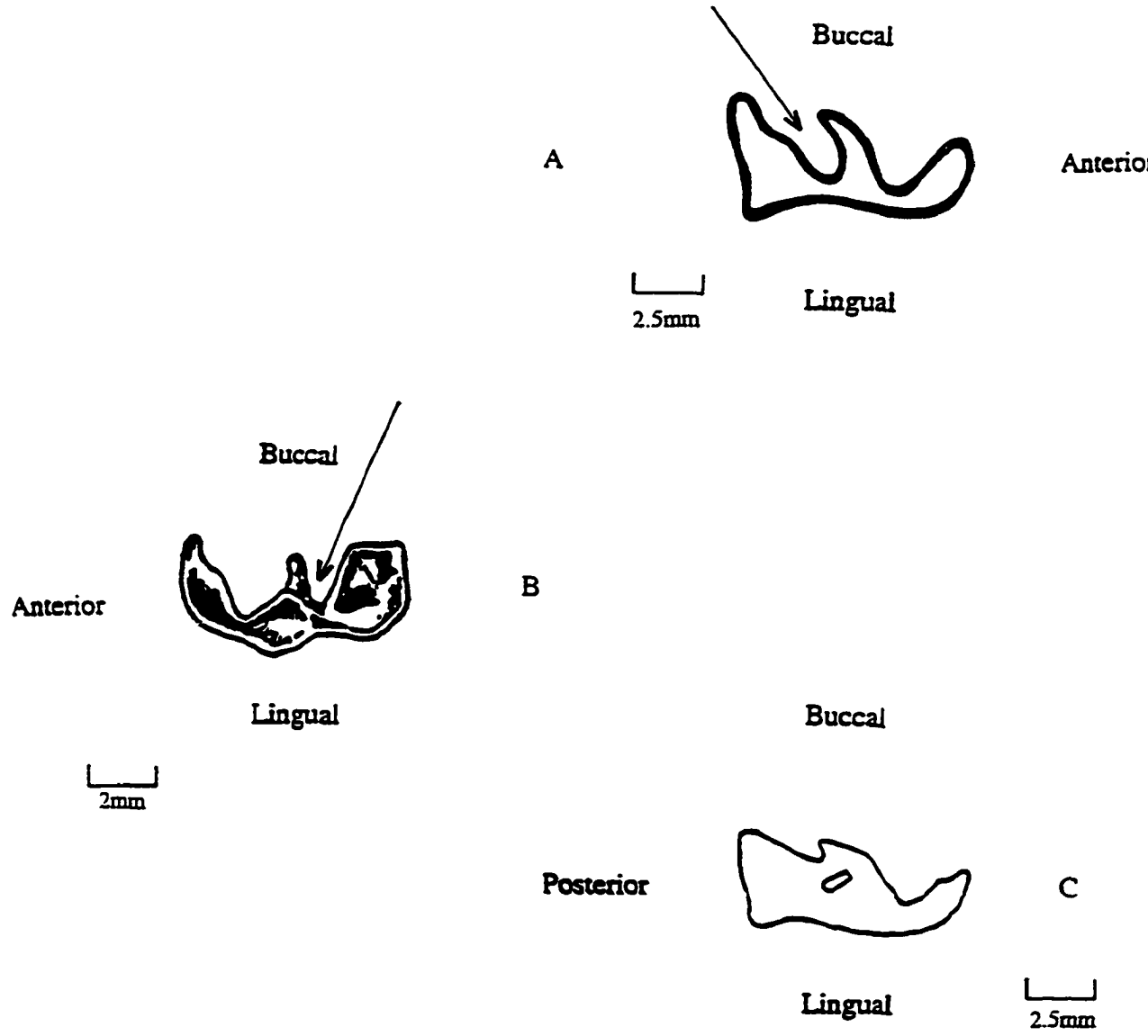

Fig. 2-10A. *Capromeryx tauntonensis* right p4; UWBM 78979. Modified from Morgan and Morgan (1995). Arrow points to posterior lingual inflection.
Fig. 2-10B. *Capromeryx arizonensis* sensu Taylor 1942, left p4; UF 54670. Arrow points to posterior lingual inflection.
Fig. 2-10C. *Capromeryx tauntonensis* right p4; UWBM 78993, showing the metaconid/entoconid closure typical of specimens with wear. Modified from Morgan and Morgan (1995).

County, Nebraska, was referred to *C. tauntonensis* by Morgan and Morgan (1995) on the basis of a deep posterior lingual inflection of the p4 and the mid-Blancan age of the Sand Draw l.f. The posterior lingual inflection is found in other specimens of p4's as well, showing the wear reduction of the posterior inflection due to progressive metaconid-entoconid closure. (*C. arizonensis* sensu Skinner 1942 UF 18267; *C. furcifer* UM 37169; *C. mexicanus* sensu Furlong 1925 DPs/n). This appears to be a generic rather than a species specific character (Fig.2-10C). The M3 posterior external heel is a variable character that is present not only in *Capromeryx*, but in several other members of the family, such as *Stockoceros* (F:AM 42545) and *Osbornoceros* (F:AM 32983). Neither the presence of an M3 posterior heel nor a pronounced posterior lingual inflection of p4 should be considered diagnostic.

RESULTS

Results are reported for molar lengths and antero-posterior (AP) and medio-lateral (ML) measurements of the horn-cores of the various species of *Capromeryx*. Only the length of the posterior horn-core of the type of *C. gidleyi* is available. Despite the earlier synonymy of *C. minor* and *C. mexicanus* with *C. furcifer*, and that of *C. arizonensis* with *C. gidleyi*, the original names will be maintained for clarity for the analysis. Measurements of both teeth and horn-cores support the synonymy and are of interest.

Upper molar (M2) length — There were no specimens of *C. mexicanus* sensu Furlong 1925 available, one of *C. furcifer*, four of *C. arizonensis* sensu Skinner 1942; seven of *C. minor* sensu Taylor 1911, and six of *C. tauntonensis*.

M2 lengths for *C. arizonensis* ranged from 10.54-11.04 mm. The tooth length for *C. furcifer* was 9.72. For *C. minor*, the range was 9.36-10.78 mm. The size range for *C. tauntonensis* was between 11.86-12.95 mm. Mean lengths for each species are as follows: *C. arizonensis*, 10.79 mm; *C. furcifer*, 9.72 mm; *C. minor*, 10.19 mm; *C. tauntonensis*, 12.50 mm.

Figure 2-11 shows the regression line of M2 length in mm plotted against the estimated body mass in kg for the various species of *Capromeryx*. Specimens of *C. arizonensis* tend to cluster in the middle of the graph, with *C. furcifer/C. minor* tending to cluster towards the bottom of the graph, indicating a smaller body mass, although there is some overlap with *C. arizonensis*. *C. tauntonensis* is larger, but the estimated mass for this species is 20-29 kg, below the 40 kg estimate made by Morgan and Morgan (1995).

Lower molar (m_1) length — A much larger sample size was available for this tooth, the only species that was under represented was *C. mexicanus* with only three specimens. The rest of the species provided larger sample sizes: *C. arizonensis*, 11; *C. furcifer*, six; *C. minor*, 13; and *C. tauntonensis*, six. Of the three tooth variables used to predict body mass, the length of m_1 is considered the least accurate, and better mass estimates are obtained from second molar lengths (upper and lower) in ungulates (Janis 1990).

Ranges for lengths for this tooth are as follows: *C. arizonensis*, 7.94-10.28 mm; *C. furcifer*, 7.19-9.3 mm; *C. minor*, 6.45-9.53 mm; *C. tauntonensis*, 9.59-10.64 mm; and *C. mexicanus*, 7.13-7.26 mm. Mean tooth lengths: *C. arizonensis*, 9.28 mm; *C. furcifer*, 8.3 mm; *C. minor*, 8.18 mm; *C. tauntonensis*, 10.17 mm; *C. mexicanus*, 7.2 mm.

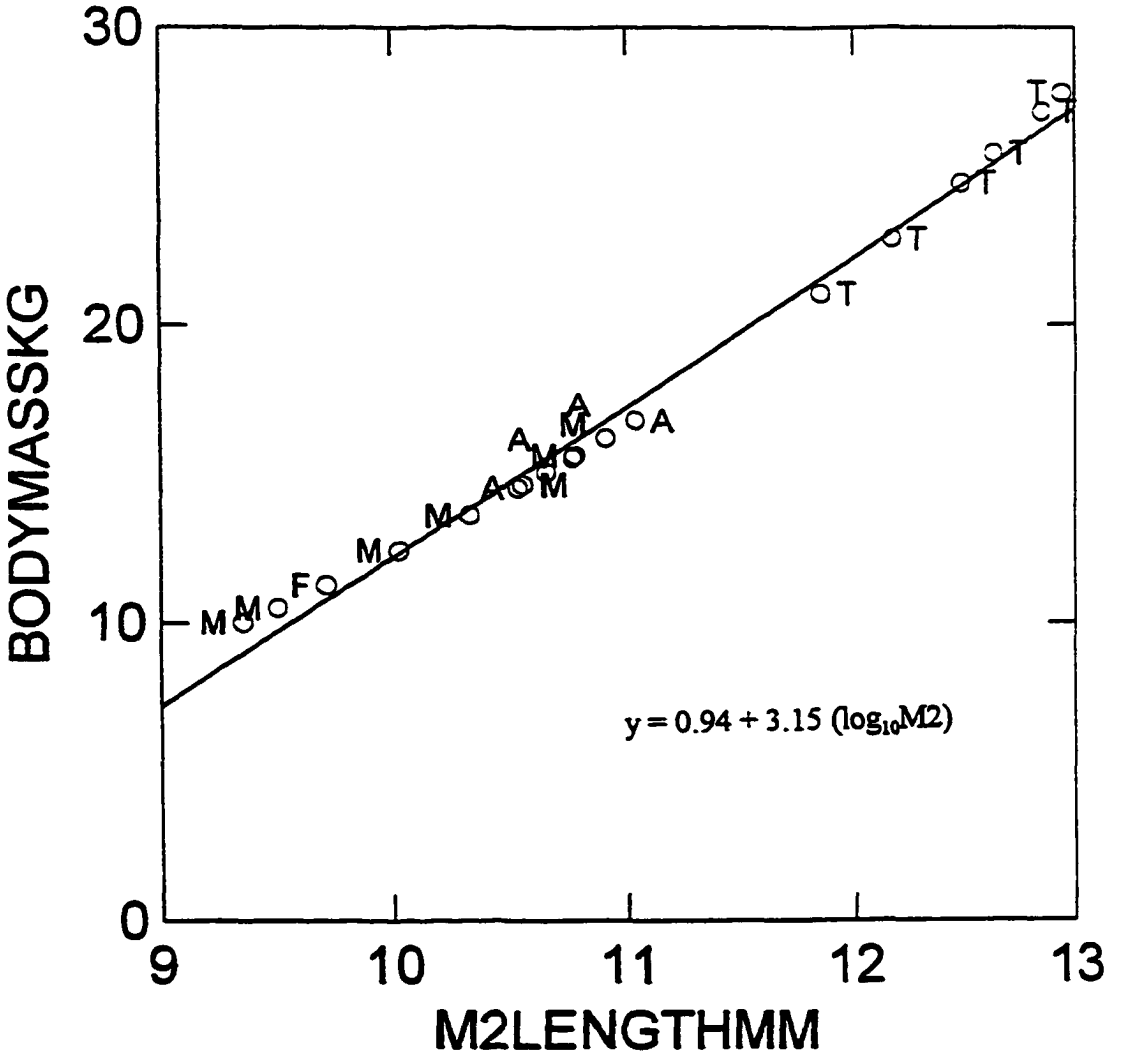

Fig. 2-11. Least squares regression of body mass (kg) on upper M2 length (L) in (mm). M = *C. minor*; A = *C. arizonensis*; F = *C. furcifer*; T = *C. tauntonensis*. Data points are from this research; regression equation is from Damuth (1990).

Fig. 2-12 shows more overlap in the middle range of the regression line, with a particularly interesting overlap of *C. arizonensis* and *C. tauntonensis* at the upper end.

Lower molar (m2) length — Both Janis (1990) and Damuth (1990) show that the length of this tooth provides the best estimates of body mass for ruminant selenodont artiodactyls. For m2, there were 14 specimens of *C. arizonensis*, 7 of *C. furcifer*, 15 of *C. minor*, and two of *C. mexicanus*. Ranges for tooth lengths were the following: *C. arizonensis*, 9.48-12.01 mm; *C. furcifer*, 8.95-11.55 mm; *C. minor*, 8.07-11.15 mm; *C. tauntonensis*, 11.29-13.14; and *C. mexicanus*, 9.29-9.36 mm. Means for each species were: *C. arizonensis*, 10.84 mm; *C. furcifer*, 9.94 mm; *C. minor*, 9.90 mm; *C. tauntonensis*, 12.3 mm; and *C. mexicanus*, 9.33 mm. Fig. 2-13 again shows considerable overlap of species in the mid-range of the regression line. The mass for the largest specimen of *C. tauntonensis* is estimated at approximately 32 kg.

Horn-cores — Measurements of the horn-cores were taken at the notch, and included antero-posterior, medio-lateral, and greatest length of the horn-cores (Fig. 2-5). Lengths are inaccurate in most of the sample, due to breakage of the tips, and these are not reported. A mean of each measurement was calculated for each species due to the differences in sample sizes. *C. arizonensis* was represented by the greatest number of individuals (n= 38), while *C. tauntonensis* was represented only by only two individuals, the type specimen, and the referred horn-core from Cita Canyon, TMM 41068-85. Horn-core sizes follow species, with *C. furcifer* (including *C. minor* and *C. mexicanus*) having the smallest horn-cores, *C. arizonensis* being mid-sized, and *C. tauntonensis* (n=1) having the largest horn-core.

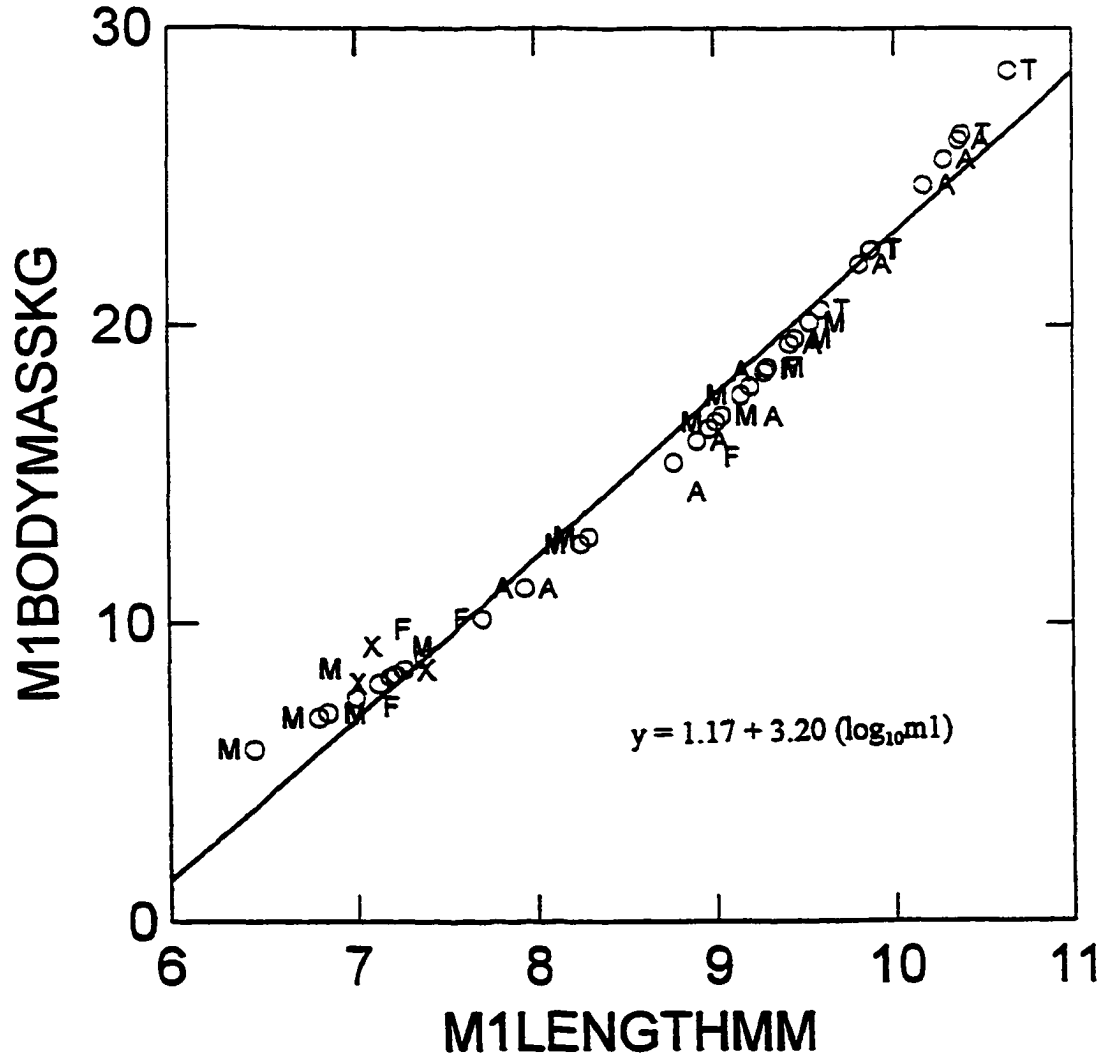

Fig. 2-12. Least squares regression of body mass (kg) on lower m_1 length (L) in (mm). M = *C. minor*; A = *C. arizonensis*; F = *C. furcifer*; T = *C. tauntonensis*. Data points are from this research; regression equation is from Damuth (1990).

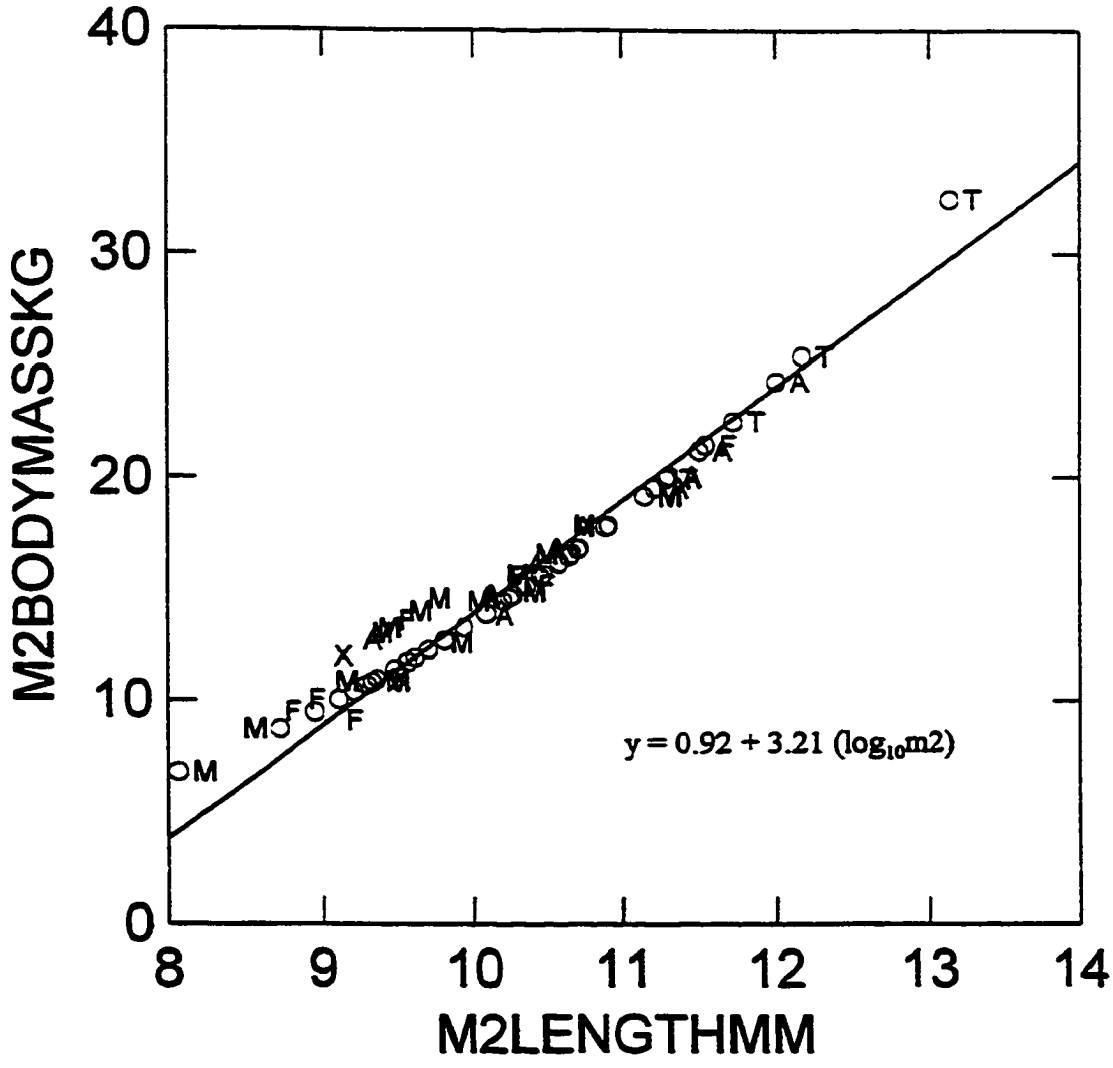

Fig. 2-13. Least squares regression of body mass (kg) on lower m_2 length (L) in (mm). M = *C. minor*; A = *C. arizonensis*; F = *C. furcifer*; T = *C. tauntonensis*. Data points are from this research; regression equation is from Damuth (1990).

DISCUSSION

Mean body mass estimates for tooth measurements for all of the species were remarkably consistent with those obtained for postcranial elements in Chapter III. Table 2-1 summarizes the mean values for each species for each tooth length as well as the mean body mass estimate for postcrania, which includes all of the postcrania combined with the exception of one. Values for the lengths of the metapodials were not included in the postcranial mean, as they have been found to correlate more closely with habitat than mass, and typically considerably overestimate body mass (Scott 1985).

In examining the regression graphs (Figs. 2-11, 2-12, and 2-13) it appears that a quadratic equation would better fit the data (Fig. 2-14). The problem with this is that a quadratic is more likely a reflection of the variation among the specimens that were measured, and is not a true indicator of general relationships, which is really what needs to be addressed (Damuth pers. comm.). Since tooth size reflects metabolism, which when log transformed scales linearly with body mass in large samples of mammals (Calder 1984), then it is likely that the observed quadratic relationship is merely an artifact of the specimens and the sample size. The linear equation, although it does not exactly fit the data at hand, is considerably more useful for estimating relationships between teeth and mass in a variety of species of that size (10-30 kg), than is a more complicated quadratic equation that is limited to a small data set (Damuth, pers.comm.).

The species concept — The definition of a species has changed considerably over the last 200 years. Perhaps the first one to formally address the species concept was

Table 2-1. Mean Body Mass Estimates for Teeth and Postcrania

Species	Variable	Estimated Body Mass (kg)
C. tauntonensis	Mean postcranial	21
	M2	25
	m1	24
	m2	25
	Mean all variables	**24**
C. arizonensis sensu Skinner 1942	Mean postcranial	17
	M2	16
	m1	17
	m2	18
	Mean all variables	**17**
C. furcifer	Mean postcranial	13
	M2	11
	m1	15
	m2	14
	Mean all variables	**13**
C. minor sensu Taylor 1911	Mean postcranial	12
	M2	13
	m1	13
	m2	13
	Mean all variables	**13**
C. mexicanus sensu Furlong 1925	Mean postcranial (n=1)	10
	M2 (n=0)	N/A
	m1 (n=3)	8
	m2 (n=2)	11
	Mean all variables	**10**

Note: As *C. minor* and *C. mexicanus* have been synonymized with *C. furcifer*, the mean value for that species may be calculated as (13+13+10)/2 = 12 kg. *C. gidleyi* is the senior synonym for *C. arizonensis*. Species means are as follows:
C. tauntonensis: 24 kg *C. gidleyi*: 17 kg *C. furcifer*: 12 kg

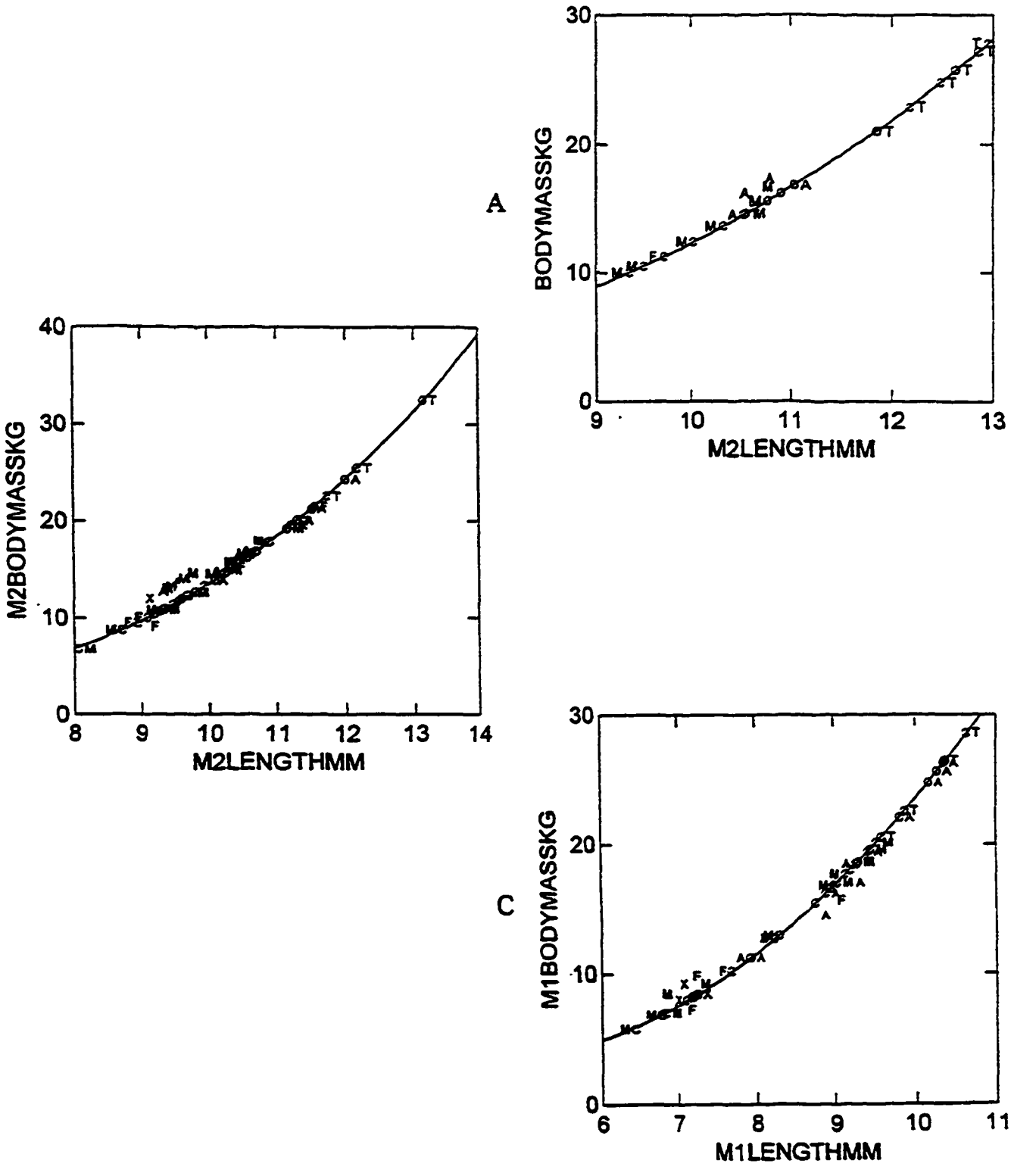

Fig. 2-14. Summary of quadratic plots for M2 (A); m1 (B) and m2 (C); body mass estimates (kg) against molar lengths (mm), showing the best fit line for the data set used in this research. M = *C. minor*; A = *C. arizonensis*; F = *C. furcifer*; T = *C. tauntonensis*.

Linneaus, whose Systema Naturae was published in 1758. He developed the system of zoological nomenclature, and applied it to groups of plants and animals with common structural characteristics, which he called species. Linneaus considered all species to be products of divine creation. This was the inception of the morphospecies concept, or species established by morphological similarity alone without regard to variability within natural populations. This concept continued well into the mid-1900's, until Mayr (1942) first attacked morphospecies as ignoring reproductive isolation. Mayr (1942, p.120) developed the biological species concept, which defines a species as the following: "Species are groups of actually or potentially interbreeding natural populations which are reproductively isolated from other such groups". There were many criticisms of this definition as well, primarily due to the fact that it excluded uniparental or temporally sequential species (Simpson 1961). In an attempt to deal with the problems encountered by paleontologists, Simpson (1961, p.153) proposed the following definition: "An evolutionary species is a lineage (an ancestor-descendant sequence of populations), evolving separately from others and with its own unitary evolutionary role and tendencies." Later definitions included niche (Mayr 1982), mate recognition (Paterson 1978), and phylogeny based upon molecular evidence (Cracraft 1983).

The argument as to how one defines a species continues, and differs considerably according to the scientific discipline. An ecologist may be more comfortable with the biological species concept because it deals with the reality of reproductive isolation. A paleontologist on the other hand, must of necessity deal with morphospecies, since other evidence cannot be gleaned from the fossil record. An operational definition preferred by

many cladists is that of a minimal monophyletic group (a group of species that includes an ancestral species and all of its known descendants), defined by one or more autapomorphies (advanced or derived characteristics unique to a specific taxon) which are usually morphologically recognized character states (Schoch 1986). While the cladistic definition sounds more complicated, it too is essentially reliant upon morphology (character states) when dealing with fossil animals. Although there have been recent advances in the retrieval of DNA from fossils, but it would appear that the refinement of this methodology is still a number of years away, leaving the profession at present with the morphospecies concept as the best method for classifying species (Kring et al. 1997; Kelman and Kelman 1999).

The species of *Capromeryx* in this dissertation were redefined using morphological characters as a basis. Hence, all of the species of *Capromeryx* should be considered as morphospecies. It is not possible to establish closer relationships at this time, particularly among a group as morphologically conservative as the ruminants. The fact that the type of *C. furcifer* and the latest representatives of the species, *C. minor* sensu Taylor 1911 and *C. mexicanus* sensu Skinner 1942 are separated by a span of 0.4-0.5 Ma is not of a particular concern, as it is known that the average species longevity of Cenozoic mammals is two to three million years, with the duration of genera close to eight million years (Romer 1966; Kurtén and Anderson 1980; Raup 1991).

Parameters relating to sample size and recognition of *Capromeryx*

Dental and postcranial characters — Because of the conservative nature of both

teeth and postcrania in ruminant pecoran artiodactyls, it is difficult to separate species, genera, and sometimes families just with a cursory glance. Antilocaprids have high crowned (hypsodont) dentition, whereas a number of other families (cervids, moschids, and giraffids) have low to moderately crowned (brachydont) dentition (Janis and Scott 1987). If presented with a tooth exhibiting hypsodont features, one might suspect it was an antilocaprid. If however, the tooth was brachydont, then one would be forced to rely on more detailed dental features. For example, the presence of an internal cingulum on the upper molars is considered a primitive trait characteristic of the Tragulidae (Janis and Scott 1987). While absent in all living ruminant families, the internal cingulum does appear in some of the more derived species of extinct ruminants, such as *Palaeomeryx* and the cervid *Dicrocerus* (Janis and Scott 1987). Once generic relationships have been established, tooth size, and particularly length, can be of considerable use in distinguishing among species. *Capromeryx* is an excellent example of this situation, where the tooth morphology within the genus is virtually indistinguishable among species. The size differences separates species of *Capromeryx* with minimal overlap, except for the mid-range of sizes where there is some overlap, perhaps due to sexual dimorphism.

Postcranial characters can also present difficulties due to the necessity of looking for very subtle differences among families where size or shape of certain surfaces may be the only thing that separates groups. One example that remains critical to North American archaeologists is the problem of trying to differentiate between *Bos* and *Bison* postcrania. Balkwill and Cumbaa (1992) discuss numerous very subtle postcranial differences between *Bos* and *Bison* without taking into account individual variation among

adults of the two species. The assumption is made that if an osteological character is identifiable in some large percentage of either *Bison* or *Bos*, then it is a valid character and may be used without question for one or the other species. The osteological characters as defined by them are helpful, but should be used with caution and only in conjunction with other information derived from a particular archaeological site.

Horn-core morphology remains one of the most reliable methods for separating ruminant species, because even though there may be considerable individual variation in the shape of the cranial appendages, the basic morphology remains consistent among species. An antilocaprid pronghorn is distinct from the antlers of a deer, while postcranial characters are considerably more problematic.

Cladistic analysis — I considered a cladistic analysis using the computer program PAUP (Phylogenetic Analysis Using Parsimony) (Swofford 1984), but rejected it due to problems that are well known when attempting to separate taxa at the species level. A major issue is that of characters that may vary even from individual to individual within a single species. Even at the family level, there may be characters that exhibit enough variability as to render them worthless in a cladistic analysis. For example, bovids are considered to have a single lacrimal orifice, whereas cervids typically have two such orifices. On the basis of having a single lacrimal orifice, *Antilocapra* was linked with the Bovidae (O'Gara and Matsen 1975). Subsequent studies however, have shown that this character is variable among individuals in the species, and that 80% of a large sample of *Antilocapra* examined by Scott and Janis (1987) actually had double lacrimal orifices, which would seem to indicate cervid affinities. Thus, use of the number of lacrimal

orifices would not be a good character to use in a cladistic analysis. The situation at the species level is even worse, as exemplified by the minute differences in horn-core morphology among the species of *Capromeryx*. *C. mexicanus* sensu Furlong 1925 was identified as a different species than that of *C. minor* sensu Taylor 1911 largely on the basis of the horn-cores slanting forwards, a trait now known to subject to individual variation as was so well documented by Skinner (1942) for the modern *A. americana*.

There are numerous cases of both cranial and postcranial characters varying within single species of many different taxa. The identification of microtines from teeth may be problematic. *Microtus pennsylvanicus* has long been identified on the basis of an idiosyncracy of M2. The typical microtine M2 has four alternating triangles on the occlusal surface. It has been known for at least 50 years that *M. pennsylvanicus* had an extra area on the M2 known as the fifth dental field; not an entire extra triangle, but a small rounded structure where the fifth triangle would be (Bell and Repenning in review). Microtine teeth identified from numerous paleontological sites that had this feature on M2 were automatically identified as *M. pennsylvanicus*. Recently, a study examining the M2's of different species of *Microtus* revealed the presence of the fifth dental field on at least a few individuals of almost every living species (Bell and Repenning, in review). Therefore, the usefulness of this character for identification to the species level in *Microtus* is questionable due to the overlap of the character among species.

Similarly, many dental characters are highly variable within *Capromeryx* at the individual level, such as the inflation of the base of the posterior lobe of m3, and the posterior lingual inflection on p4 (Frick 1937; Morgan and Morgan 1995). PAUP is a

very useful tool when attempting to discern phylogenetic relationships at the family level or higher where there is less character overlap, but is not as useful at the level of the species where individual variation can significantly affect the results.

Differential survivorship — There were many fewer specimens of upper molars of *Capromeryx* available for study than there were lower molars. The reason for this is partly due to the paucity of crania in the fossil record because of postmortem differential survivorship of body parts. Differential survivorship is due to a number of different processes, including the degree of carnivore ravaging, depositional habitat such as swamp versus savanna, and density mediated attrition (Berensmeyer 1983; Lyman 1994). Density studies on bones from several species of mammals have been performed using photon densitometry, and a direct correlation has been found between the denseness of a particular skeletal part and the likelihood of preservation in the fossil record (Lyman 1984; Kreutzer 1992). Individual teeth, the mandible, distal ends of long bones and the carpals and tarsals are very dense and are therefore more common. The cranium, on the other hand, is not very dense relative to other elements, so the likelihood of finding an entire cranium is much less than that of finding a mandible. While there is no difference in the density of upper versus lower teeth, the cranium is less likely to be preserved intact than is the mandible, and upper teeth are more common as isolated finds (Lyman 1994). The results for the more numerous lower molars were very comparable to those for the upper molars, so the lack of a statistically significant sample of M2 for this research appears not to be a problem in this instance.

Sexual dimorphism — Modern pronghorn males are approximately 10% to 15% larger than the females. The horn-cores of male pronghorns, however, are considerably larger than the female horn-core, which in some individuals has been reduced to a mere bud on the frontal bone. There is also some evidence of sexual dimorphism in *Capromeryx*. Because of the large sample size of *C. arizonensis* sensu Skinner 1942, differences in the overall size of horn-cores among individuals was apparent. Four specimens in particular are suggestive of the presence of dimorphism in this species. UF 115962 and UF 115963 are two very large horn-cores that are essentially intact except for perhaps a few millimeters in length. UF 10808 (right and left) are much smaller, and are also virtually intact. The measurements are reported on Table 2-3. Antero-posterior and medio-lateral measurements showed less variation than did the length of the horn-cores that were intact and could be measured. The smaller horn-cores were approximately two-thirds the size of the larger specimens. It is of course possible that the smaller horn-cores represented young males, but the sheer numbers of available specimens from Florida, including at least four almost complete adult crania with fused sutures, make it highly unlikely that there are not at least some females in the sample. There were also differences in the size of many of the adult postcrania with fused epiphyses, with many being smaller and more gracile than others possibility due to sexual dimorphism in this species.

Measurements of teeth (M2, m1, and m2) show an overlap of species in the mid-range of sizes, with some specimens of *C. arizonensis* sensu Skinner 1942 being smaller than the larger specimens of *C. furcifer*. It may be that the smaller individuals of *C. arizonensis* are females. Size differences are much less noticeable in *C. furcifer*, and it

Table 2-2. Summary of Horn-core Measurements by Species

Species	Ant. AP	Ant. ML	Post. AP	Post ML	Total HC AP
C. furcifer	6	7	14	13	23
C. minor	5	7	12	13	20
C. mexicanus	6	6	12	11	22
C. arizonensis	13	12	16	15	32
C. tauntonensis	---	16	26	20	---

Number of Specimens of horn-cores

C. *furcifer*: 6

C. minor sensu Taylor 1911: 2

C. mexicanus sensu Furlong 1925: 3

C. arizonensis sensu Skinner 1942: 38

C. tauntonensis: 2

Key:

AP = antero-posterior measurement at notch
ML = medio-lateral measurment at notch
Ant. = Measurements of anterior tine
Post. = Measurements of posterior tine

Note: All units are in mm

may well be that there was little or no sexual dimorphism in this species. It is beyond the scope of this dissertation to deal in depth with the issue of sexual dimorphism in *Capromeryx*. The large sample from the Inglis 1A fauna in Florida suggests that at least *C. arizonensis* may have exhibited at least slight sexual dimorphism, comparable to the modern *A. americana*.

***C. tauntonensis* as a valid species** — It is unfortunate that only one cranium has been collected thus far of *C. tauntonensis*, as it is morphologically so similar to *C. arizonensis* that were it smaller, it would probably would have been considered to be conspecific. The primary criteria used by Morgan and Morgan (1995) to define *C. tauntonensis* were size, unconstricted horn-core base, lack of a posterior heel on M3, and a deep posterior lingual inflection on p4. All of these features are present in at least a few individual specimens of *C. arizonensis*.

Examples of horn-cores with unconstricted bases are present in *C. arizonensis* from the Inglis 1A fauna (UF 115962, UF 115963). One p4 with the identical anterior and posterior lingual inflections noted for *C. tauntonensis* was identified (UF 54670). Upper M3's lacking a posterior heel were also present in the sample (UF 52745, UF 179271). The age of the two species is very comparable, with *C. tauntonensis* present during the mid-Blancan (3.1 Ma), and *C. arizonensis* present from the mid-Blancan in Nebraska (3.21Ma) to the early Irvingtonian in Florida (1.5 Ma). The type of *C. gidleyi* from the Benson l.f. of Arizona is actually older than the type of *C. tauntonensis*. While the cranium of the type *C. tauntonensis* is larger overall than the four nearly intact crania from the Inglis 1A site (UF 18256, UF 67822, UF 67823, UF 115960), the size difference is not

enough to preclude the possibility that *C. tauntonensis* is merely a very large male *C. arizonensis* sensu Skinner 1942.

Body mass estimates for *C. tauntonensis* using teeth and the two available postcranial elements (humerus and metatarsal) were consistent and suggest a body mass of 24 kg, not the 40 kg (85% of the modern pronghorn) as indicated by Morgan and Morgan (1995). Their estimates were made using m3, which is not the best tooth to use to estimate body mass (see previous discussion). Although 24 kg is still larger than the estimated 17 kg for *C. arizonensis*, the difference is not so significant that one can dismiss the possibility that they are one species. Given the information at hand, the naming of a new species, *C. tauntonensis* by Morgan and Morgan (1995) remains valid; the issue of conspecificity with *C. arizonensis* must await the discovery of further specimens.

CONCLUSIONS

The antilocaprid genus *Capromeryx* consists of three species, spanning approximately 3 million years from the mid-Blancan to the late Rancholabrean, when the genus became extinct. *Capromeryx* was wide ranging geographically, and is found throughout North America with the exception of Canada, with concentrations in Washington state, California, Kansas, Florida, and Mexico. The genus experienced a mild dwarfing trend over time, from approximately 24 kg to 10 kg by the late Rancholabrean. Body mass estimates using tooth regressions for selenodont ruminants developed by Damuth (1990) were remarkably consistent with the results obtained for postcrania. This fact is of particular interest, because this suggests that accurate estimates of body mass

can be obtained with either teeth or postcrania, in the event that both types of specimens are not available. The later occurring *C. furcifer* was not only a smaller species, but the horn-core morphology was dissimilar from the earlier occurring two species in that the anterior tine was reduced significantly to only one quarter the size of the posterior.

C. minor sensu Taylor 1911, *C. mexicanus* sensu Furlong 1925, and *C. furcifer* exhibit only very minor morphological differences that may be explained by individual variation, and are placed together in one species, with *C. furcifer* (Matthew 1902) having priority. *C. gidleyi* and *C. tauntonensis* remain separate species, but with some reservations. With the exception of size, all of the characters used to define *C. tauntonensis* as delineated by Morgan and Morgan (1995) are present in some or all of the other species of *Capromeryx*. *C. tauntonensis* appears to be most closely related to *C. gidleyi* both temporally and in the configuration of the horn-cores. There is a distinct possibility that the type cranium of *C. tauntonensis* represents a very large male *C. gidleyi*, but a more definitive diagnosis must await the discovery of additional specimens of *C. tauntonensis*.

REFERENCES

Ahern, M. E. 1988. Systematics and evolution of the Antilocapridae. Journal of Vertebrate Paleontology 8 (suppl. to no.3), p.8A.

Balkwill, D. M. and S. L. Cumbaa. 1992. A Guide to the Identification of Postcranial Bones of *Bos taurus* and *Bison bison*. Canadian Museum of Nature Syllogeus No. 71, Ottawa, 277 pp.

Bell, C. J. and C. A. Repenning. Ms. in review. Observations on dental variation in *Microtus* from the type Cudahy fauna, Meade County, Kansas, and implications for Irvingtonian microtine rodent biochronology. Journal of Vertebrate Paleontology.

Berensmeyer, A. K. 1983. Patterns of natural bone distribution on recent land surfaces: implications for archaeological site formation; pp. 93-106 *in* J. Clutton-Brock and C. Grigson (eds.), Animals and Archaeology: 1. Hunters and Their Prey. British Archaeological Reports International Series 163.

Berggren, W. A., F .J. Hilgren, C. G. Langerieis, D. V. Kent, J. D. Obradovich, I. Raffi, M. E. Raymo, and N. J. Shackleton. 1995. Late Neogene chronology: New perspectives in high-resolution stratigraphy. Geological Society Bulletin 107(11):1272-1287.

Bubenik, A. B. 1990. Epigenetical, morphological, physiological, and behavioral aspects of evolution of horns, pronghorns, and antlers; pp.3-113 *in* G. A. Bubenik and A. B. Bubenik (eds.), Horns, Pronghorns, and Antlers. Springer-Verlag, New York.

Calder, W. A. 1984. Size, Function, and Life History. Dover Publications Inc., New York, 431 pp.

Carroll, R. L. 1988. Vertebrate Paleontology and Evolution. W.H. Freeman and Company, New York, 698 pp.

Chandler, A. C. 1916. Notes on *Capromeryx* material from the Pleistocene of Rancho La Brea. University of California Publications; Bulletin of the Department of Geology 9(10):111-120.

Colbert, E. H. 1941. The osteology and relationships of *Archaeomeryx*, an ancestral ruminant. American Museum Novitiates 1135:1-24.

Cope, E. D. 1887. The classification and phylogeny of the Artiodactyla. Proceedings of the American Philosophical Society 24:377-400.

Cracraft, M. 1983. Species concepts and speciation analysis. Current Ornithology 1:159-187.

Damuth, J. 1990. Problems in estimating body masses of archaic ungulates using dental measurements; pp.229-254 *in* J. Damuth and B. J. MacFadden (eds.), Body Size in Mammalian Paleobiology: Estimation and Biological Implications. Cambridge University Press, Cambridge.

Demment, M. W. and P. J. Van Soest. 1985. A nutritional hypothesis for body size patterns of ruminant and nonruminant herbivores. American Naturalist 125:641-672.

Dove, W. F. 1935. The physiology of horn growth: a study of the morphogenesis, interaction of tissues, and the evolutionary processes of a Mendelian recessive character by means of transplantation of tissues. Journal of Experimental Zoology 69:347-405.

Frick, C. 1937. Horned Ruminants of North America. Bulletin of the American Museum of Natural History 69:1-699.

Furlong, E. L. 1925. Notes on the occurrence of mammalian remains in the Pleistocene of Mexico, with a description of a new species, *Capromeryx mexicana*. University of California Publications in Geological Sciences 15:137-152.

Furlong, E. L. 1927. The occurrence and phylogenetic status of Merycodus from the Mohave Desert Tertiary. University of California Publications, Department of Geological Sciences, 17:145-186.

Furlong, E. L. 1930. *Capromeryx minor* Taylor from the McKittrick Pleistocene, California. Carnegie Institute Washington Publication 404:49-53.

Gazin, C. L. 1955. A review of the upper Eocene Artiodactyla of North America. Smithsonian Miscellaneous Collections. 128(8):1-96.

Goss, R. J. 1983. Deer antlers: Regeneration, Function, and Evolution. Academic Press, New York, 316 pp.

Guthrie, R. D. 1984. Mosaics, alleolchemics, and nutrients: An ecological theory of Late Pleistocene megafaunal extinctions; pp. 259-298 *in* P. S. Martin and R. G. Klein (eds.), Quaternary Extinctions: A Prehistoric Revolution. 2nd. ed. The University of Arizona Press, Tucson.

Hesse, C. J. 1935. New evidence on the ancestry of *Antilocapra americana*. Journal of Mammalogy 16:307-315.

Hibbard, C. W. and D. W. Taylor. 1960. Two late Pleistocene faunas from southwestern Kansas. Contributions, Museum of Paleontology, University of Michigan 16:1-223.

Janis, C. M. 1976. The evolutionary strategy of the Equidae and the origins of rumen and cecal digestion. Evolution 30:757-774.

Janis, C. M. 1990. Correlation of cranial and dental variables with body size in ungulates and macropodoids; pp.255-300 *in* J. Damuth and B. J. MacFadden (eds.), Body Size in Mammalian Paleobiology: Estimation and Biological Implications. Cambridge University Press, Cambridge.

Janis, C. M. and A. Lister. 1985. The morphology of the lower fourth premolar as a taxonomic character in the Ruminantia (Mammalia:Artiodactyla), and the systematic position of *Triceromeryx*. Journal of Paleontology 59(2):405-410.

Janis, C. M. and K. M. Scott. 1987. The interrelationships of higher ruminant families with special emphasis on the members of the Cervoidea. American Museum Novitiates 2893:1-85.

Janis, C. M., E. Manning, and M. E. Ahern. 1998. Antilocapridae; pp. 491-507 *in* C. M Janis, K. M. Scott, and L. L. Jacobs (eds.), Evolution of Tertiary Mammals of North America. Volume I: Terrestrial Carnivores, Ungulates, and Ungulatelike Mammals. Cambridge University Press, New York.

Kelman, L. M. and Z. Kelman. 1999. The use of ancient DNA in paleontological studies. Journal of Vertebrate Paleontology 19(1):8-20.

Kleiber, M. 1961. The Fire of Life. John Wiley, New York. 453 pp.

Kreutzer, L. A. 1992. Bison and deer bone mineral densities: comparisons and implications for the interpretation of archaeological faunas. Journal of Archaeological Science 19:271-294.

Krings, M., A. Stone, and S. Paabo. 1997. Neandertal DNA sequences and the origin of modern humans. Cell 90(1):19.

Krishtalka, L. and R. K. Stucky. 1986. Early Eocene artiodactyls from the San Juan Basin, New Mexico, and the Piceance Basin, Colorado; *in* K. M. Flanagan and J. A. Lilligraven (eds.), Vertebrates, Phylogeny, and Philosophy. Contributions to Geology, the University of Wyoming, Special Paper 3.

Kurtén, B., and E. Anderson. 1980. Pleistocene Mammals of North America. Colombia University Press, New York, 442 pp.

Leinders, J. M. M. and E. Heintz. 1980. The configuration of the lacrimal orifice in pecorans and tragulids (Artiodactyla:Mammalia) and its significance for the distinction between Bovidae and Cervidae. Beaufortia 30:155-160.

Lindsey, E. H. and N. T. Tessman. 1974. Cenozoic vertebrate localities and faunas in Arizona. Journal of the Arizona Academy of Science 9:3-24.

Lundelius, E. L., T. Downs, E. H. Lindsay, H. A. Semken, R. J. Zakrzewski, C. S. Churcher, C. R. Harington, G. E. Schultz, and S. D. Webb. 1987. The North American Quaternary Sequence; pp.211-235 *in* M.O. Woodburne (ed.), Cenozoic Mammals of North America: Geochronology and Biostratigraphy. University of California Press, Berkeley.

Lyman, R. L. 1984. Bone density and differential survivorship of fossil classes. Journal of Anthropological Archaeology 3:259-299.

Lyman, R. L. 1994. Vertebrate Taphonomy. Cambridge University Press, Cambridge, 524 pp.

MacFadden, B. J. 1992. Fossil Horses: Systematics, Paleobiology, and Evolution of the Family Equidae. Cambridge University Press, Cambridge, 369 pp.

Matthew, W. D. 1902. List of the Pleistocene fauna from Hay Springs, Nebraska. Bulletin of the American Museum of Natural History 16:317-322.

Matthew, W. D. 1904. A complete skeleton of *Merycodus*. Bulletin of the American Museum of Natural History 20:101-129.

Mayr, E. 1942. Systematics and Origins of Species. Columbia University Press, New York, 334 pp.

Mayr, E. 1982. The Growth of Biological Thought: Diversity, Evolution, and Inheritance. Harvard University Press, Cambridge, 974 pp.

McKenna, M. and S. K. Bell. 1997. Classification of Mammals Above the Species Level. Colombia University Press, New York, 631 pp.

Meade, G. E. 1942. A new species of *Capromeryx* from the Pleistocene of west Texas. Bulletin of the Texas Archaeological and Paleontological Society. 14:88-96.

Morgan, J. K. and N. H. Morgan. 1995. A new species of *Capromeryx* (Mammalia:Artiodactyla) from the Taunton local fauna of Washington, and the correlation with other Blancan faunas of Washington and Idaho. Journal of Vertebrate Paleontology 15(1):160-170.

Nowak, R. M. 1991. Order Artiodactyla; pp. 1334-1499 *in* R. M. Nowak (ed.), Walker's Mammals of the World. Vol. II. 5th. ed. The Johns Hopkins University Press, Baltimore.

O'Gara, B. W. 1978. *Antilocapra americana*. Mammalian Species No. 90:1-7.

O'Gara, B. W. and G. Matson. 1975. Growth and casting of horns by pronghorns and exfoliation of horns by bovids. Journal of Mammalogy 56(4):829-846.

Owen-Smith, R. N. 1988. Megaherbivores: The Influence of Very Large Body Size on Ecology. Cambridge University Press, Cambridge, 369 pp.

Packer, D. R. and J .M. Johnston. 1979. A preliminary investigation of the magnetostratigraphy of the Ringold Formation. Woodward-Clyde Consultants Report RHO-BWI-C-42, San Francisco.

Paterson, H.E.H. 1978. More evidence against speciation by reinforcement. South African Journal of Science 74:369-371.

Raup, D. M. 1991. Extinction: Bad Genes or Bad Luck? W.W. Norton and Company, New York, 210 pp.

Romer, A. S. 1966. Vertebrate Paleontology. University of Chicago Press, 468 pp.

Rose, K. D. 1982. Skeleton of *Diacodexis*, oldest known artiodactyl. Science 216:621-623.

Schmidt-Nielsen, K. 1990. Animal Physiology: Adaptation and Environment. 4th.ed. Cambridge University Press, Cambridge, 602 pp.

Schoch, R. M. 1986. Phylogeny Reconstruction in Paleontology. Van Nostrand Reinhold Company, New York, 351 pp.

Scott, K. M. 1983. Prediction of body weight in fossil Artiodactyla. Zoological Journal of the Linnean Society 77:199-215.

Scott, K. M. 1985. Allometric trends and locomotor adaptations in the Bovidae. Bulletin of the American Museum of Natural History 179(2):197-288.

Scott, K. M. and C. M. Janis. 1987. Phylogenetic relationships of the Cervidae, and the case for a superfamily "Cervoidea"; pp. 3-20 *in* C.M. Wemmer (ed.), Biology and Management of the Cervidae. Smithsonian Institution Press, Washington.

Simpson, G. G. 1945. Principles of classification and a classification of mammals. Bulletin of the American Museum of Natural History 85:1-350.

Simpson, G. G. 1961. Principles of Animal Taxonomy: The Species and Lower Categories. Colombia University Press, New York, 247 pp.

Skinner, M. F. 1942. The fauna of Papago Springs Cave, Arizona and a study of Stockoceros; with three new antilocaprines from Nebraska and Arizona. Bulletin of the American Museum of Natural History 80:143-220.

Stirton, R. A. 1938. Notes on some Late Tertiary and Pleistocene antilocaprids. Journal of Mammalogy 19:366-370.

Stirton, R. A. 1944. Comments on the relationships of the Palaeomerycidae. American Journal of Science 242:633-655.

Swofford, D. L. 1984. Phylogenetic analysis using parsimony (PAUP), version 3.1. Illinois Natural History Survey, Champaign-Urbana.

Taylor, W. P. 1911. A new antelope from the Pleistocene of Rancho la Brea. University of California Publications, Bulletin of the Department of Geology 6:191-197.

Tedford, R. H., M. F. Skinner, R. W. Fields, J. M. Rensberger, D. P. Whisler, T. Galusha, B. E. Taylor, J. R. Macdonald and S. D. Webb. Faunal succession and biochronology of the Arikareean through Hemphillian interval (Late Oligocene through earliest Pliocene epochs) in North America; pp.153-210 *in* M.O. Woodburne (ed.), Cenozoic Mammals of North America: Geochronology and Biostratigraphy. University of California Press, Los Angeles.

Vaughn, T. A. 1986. Mammalogy. 3rd. Ed. Saunders College Publishing, Philadelphia, 576 pp.

Voorhies, M. R. 1969. Taphonomy and population dynamics of an early Pliocene vertebrate fauna, Knox County, Nebraska. Contributions to Geology, the University of Wyoming, Special Paper 1:1-69.

Webb, S. D. 1973. Pliocene pronghorns of Florida. Journal of Mammalogy 54(1):203-221.

Webb, S. D. 1974. Chronology of Florida Pleistocene mammals; pp.5-31 *in* S. D. Webb (ed.), Pleistocene Mammals of Florida. University of Florida Press, Gainesville.

Webb, S. D. and B. E. Taylor. 1980. The phylogeny of hornless ruminants and a description of the cranium of *Archaeomeryx*. Bulletin of the American Museum of Natural History 167:121-157.

CHAPTER III: MULTIVARIATE MORPHOMETRIC ANALYSES OF SKELETAL VARIABLES IN MODERN AND FOSSIL PECORANS

INTRODUCTION

The reconstruction of body size in fossil mammals is of interest to paleontologists because of ecological and physiological variables that correlate directly to size (Calder 1996; Eisenberg 1981; Damuth 1981; McNab 1990). Ecological variables include population density (Brown and Maurer 1989), home range size (Damuth 1981), competitive displacement (MacArthur 1972; Jarman 1974; Boyce 1979; Belovsky 1984; Maiorana 1990), climatic and environmental change over time (Guthrie 1984; Graham 1985), vegetation patterns affecting animal distributions (Graham and Lundelius 1984; Demment and Van Soest 1985; Wiens 1989), and social behavior and its effects on the horns and antlers of ungulates (Gould 1973; Bubenik 1990). Physiological variables correlated to body size include diet (Demment and Van Soest 1985), metabolism (Kleiber 1932), temperature regulation (Wunder 1984), small mammal energetics (Wunder 1992), water balance (Calder and Braun 1983), and mass specific oxygen consumption (Wunder et al. 1977).

Because fossils do not display behavior or allow us to measure physiological variables, all of this information must, of necessity, be derived from living animals of similar phylogeny, size and morphological features. Body mass predictions using

osteological variables from modern mammals can be of use to paleontologists attempting to reconstruct the masses and hence the ecological and physiological traits of extinct species. Studies using teeth and long bone lengths have met with some success, but are influenced by both of these variables as being correlated to factors other than body mass, such as diet and habitat (Scott 1983; Creighton 1980; Gingerich 1990).

Measurements providing reasonable estimates of body mass include cortical cross-sectional area of long bones, diameters of long bone shafts, and diameters of articular surface areas (Scott 1979; Ruff 1981; Scott 1985). Cortical bone refers to the dense, compact outer layer of bone, and the usage of the term is more common in the human anatomy literature than in the zoological literature where it is referred to as compact or dense bone. It is used here since the methodology for determination of the cross-sectional area of cortical bone was developed by physical anthropologists.

Cortical cross-sectional areas of long bones have been shown to provide the most accurate estimates of body mass. However, obtaining the data for fossils usually involves obtaining biplanar radiographs, since the actual cutting of bones is usually not possible in museum collections (Ruff 1981; 1990; Biknevicius et al.1993; Churchill 1994). Radiographs are taken at a point along the length of the shaft, usually at the midpoint of the length of the bone, unless there is a specific anatomical feature to be avoided which would effect the results. An asymmetrical cross-section involving for example, the deltoid crest of the humerus, would provide an erroneously high cortical cross-sectional area. The deltoid crest is very large in some fossorial and aquatic species, so radiographs are typically taken at 35 percent of the length of the shaft from the distal end in order to

obtain an accurate estimate of the true cortical area of the diaphysis. Although estimates of the lengths of long bones can be made from partial shafts in known taxa, it is preferable to have whole bones available for study (Bicknevicius et al.1993; Churchill 1994).

Although whole bones can be found in the paleontological record, fragments are much more common. It would be useful to have available other measures that could be taken directly from fragmentary remains of elements such as the articulations of distal long bones. Due to the high density of these elements, differential preservation makes them relatively common in the fossil record, and therefore a potential source of valuable information (Brain 1969; Lyman 1984).

The intent of this study is the development of postcranial osteological parameters that can be used to predict body mass in extant pecoran artiodactyls, with subsequent use of these variables to predict body mass in an extinct genus of antilocaprids (*Capromeryx*). Representatives of three families of pecorans were used in the study, Cervidae, Bovidae, and Antilocapridae, represented by the only living species, *Antilocapra americana*. The other members of the Pecora with comparable postcranial morphology, moshids and giraffids, were not included due to the lack of available specimens. A number of long bones, carpals and tarsals of bovids, cervids and *Antilocapra* were measured, and the articulations modeled on volumes and surface areas of various geometric shapes.

Mechanical Properties of Bone

Bone is considered a biphasic composite material, and is made up of dense, mineralized hydroxyapatite, $Ca_{10}(PO_4)_6(OH)_2$, which is embedded throughout the matrix

by the protein collagen (Nordin and Frankel 1980). In mammals there are three types of bone matrix, each defined by the pattern of the collagen and osteocytes within the bone structure. The first is called woven bone, which is laid down quickly and consists of fine fibrils of collagen oriented in a random fashion (Wainwright et al. 1976; Currey 1984). The second type, or lamellar bone, is characterized by collagen and associated minerals laid down in sheets, or lamellae, with the collagen fibrils oriented in one plane within the matrix (Wainwright et al. 1976; Currey 1984). The third type is called parallel-fibered bone, has a matrix structure between the first two types and is more highly calcified than either woven or lamellar bone (Currey 1984). All three types of bone present in different combinations make up different bone tissue, depending upon the age of the animal, the presence of fractures, and the growth needs of the animal. This dissimilar structure of bone in the longitudinal and transverse directions gives considerable strength and stiffness, while at the same time allowing for a certain amount of plasticity.

Abbreviations Used

F = force (Newton) L = length in mm σ = stress (force per unit area)
M = mass (kg) m = meter V = velocity in meter per second (m s^{-1})
h = height in mm kg = kilogram D = diameter in mm r = radius in mm

a = acceleration (m s^{-2}) or meter per second squared
N = Newton (one Newton = m kg s^{-2}) or kg per meter per second squared

Mechanical loading — Load as defined here, is considered to be any force applied to a solid object such as a bone. Force (or load) is measured as mass times acceleration, or F = Ma. In SI units (Système Internationale), mass is measured as kilograms (kg) and acceleration is measured as meters per second-squared (m s^{-2}) (Pennycuick 1992).

Velocity (in seconds) measures how fast an object's position is changing so that if it is at position X1 initially, and then at position X2 at t time later, the average velocity may be expressed as (X2-X1)/t, measured in this instance as meters per second. Acceleration measures how fast the velocity of an object is changing, so at initial velocity V1, after a time t, it has a velocity of V2, then the average acceleration is (V2-V1)/t. This may also be expressed as meters per second squared (m s^{-2}). The unit of force of one newton (N), when applied to a mass of 1 kg, will cause it to accelerate at one meter per second squared (1 m s^{-2}) (Pennycuick 1992).

Load causes a deformation, or a change in the dimensions of the structure of the bone, which can be plotted on a load-deformation curve (Fig.3-1). Axial loading refers to a force, either compressive or tensile, that occurs in an orientation parallel to the long axis of the bone. Because axial loads are parallel, the force is distributed evenly over a cross-sectional area causing less stress per unit area (Nordin and Frankel 1980).

When placed under loads along different axes, mammalian bone exhibits different mechanical properties depending upon the direction of the loads (Nordin and Frankel 1980). This property is called anisotropy, and accounts for variations in strength and stiffness in bone caused by the different type of bone tissues present in any one bone (Nordin and Frankel 1980). Long bones have been modeled on hollow cylinders or beams

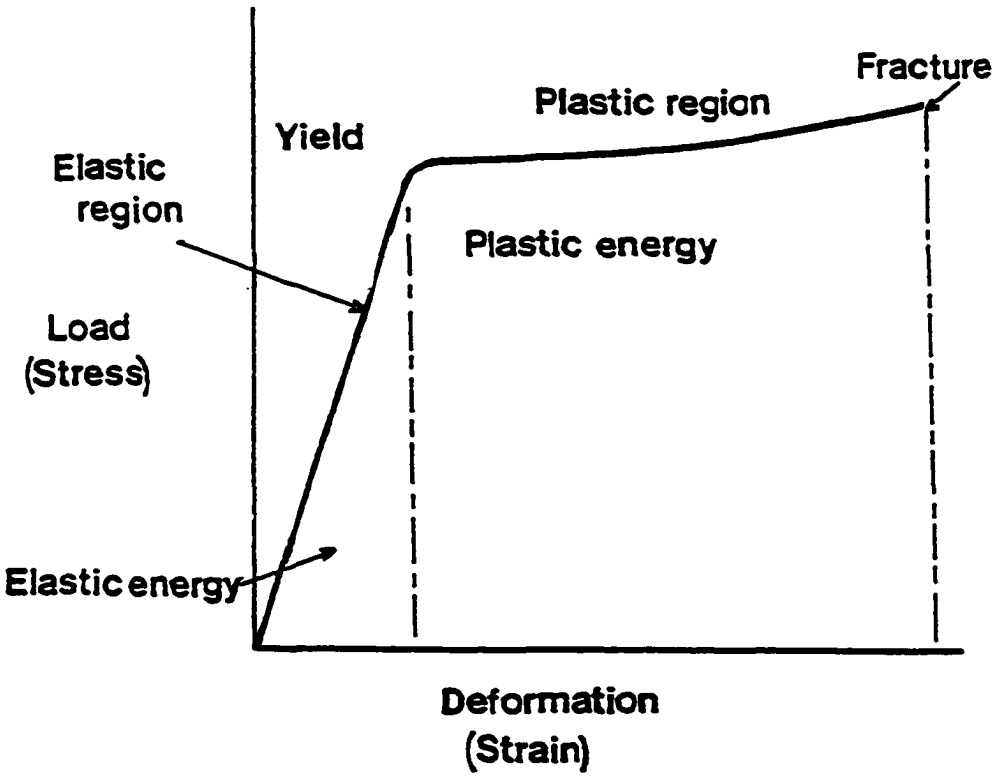

Fig. 3-1. Load-deformation curve. Modified from Nordin and Frankel (1980).

in several previous studies. This method has proven to be useful in explaining the different forces acting upon a long bone (Nordin and Frankel 1980; Hildebrand 1988; Biknevicius et al.1993; Churchill 1994).

There are different types of forces that can act upon a long bone, either individually or in conjunction with other forces. In order to remain in equilibrium, an animal standing still is acted upon simultaneously by two forces; the vertical force of its own mass downward due to gravity, and the equal upward vertical force of the ground which produces a mechanical loading on the skeleton (Hildebrand 1988; Ruff 1990). In this instance only, the mechanical loading may be expressed in mass units, whereas any other force must be expressed in force units such as Newtons (Pennycuick 1992). Compression is a force that is directed towards an object. Tension is a force that is directed away from an object, causing a pulling effect (Fig.2A).

Compression and tension can occur together, and if the load is not perpendicular to the end of the cylinder, bending occurs (Hildebrand 1988). A bending load causes an object to bend around an axis (Fig 2B). In the case of a loaded beam, one side becomes convex and experiences tension, and the other side becomes concave and experiences compression (Ruff 1981).

Stress (σ) is the force per unit area that develops in response to an externally applied load on an object, and is measured in Newtons per centimeter squared (N/cm^2) (Nordin and Frankel 1980). Strain is the deformation caused by stress, and is measured by the percentage of change in the dimensions of the object experiencing the load (Nordin and Frankel 1980). A stress-strain curve is a load-deformation curve that measures the

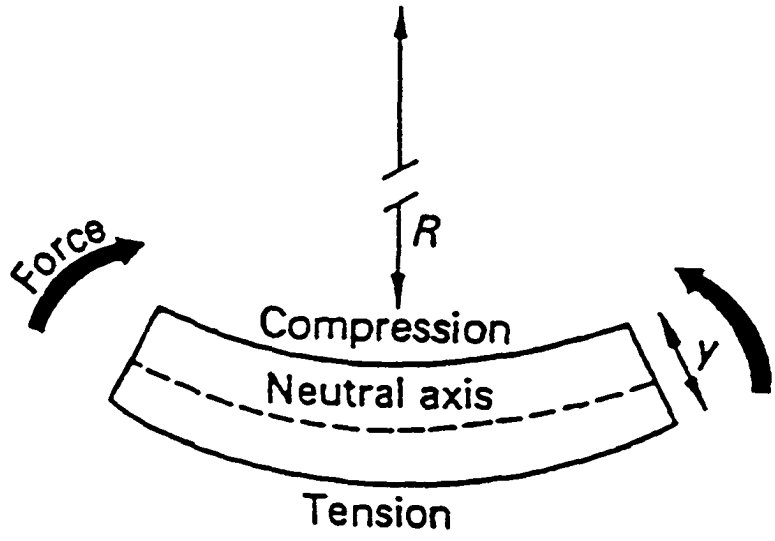

A

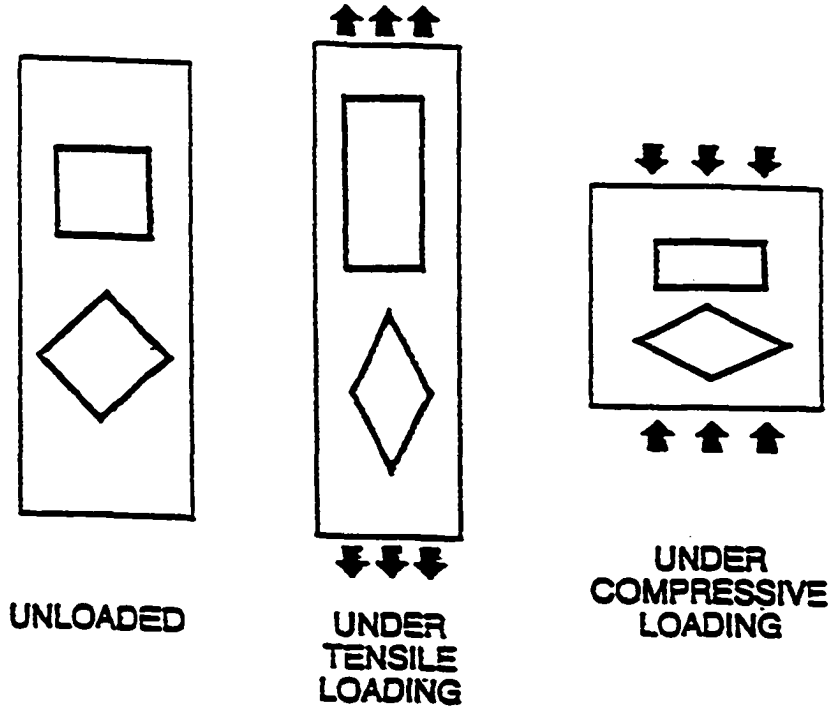

B

Fig. 3-2A. Bending forces in a loaded beam.
Fig. 3-2B. Compression and tension in a loaded beam.
Reproduced with permission from Edward Arnold Ltd.

force per unit area on a plane surface (or cross-sectional area) within the structure of the object (Nordin and Frankel 1980). Because of the precision of the units used to measure stress and strain, it is possible to obtain information from bone fragments as well as whole bones (Nordin and Frankel 1980).

Stiffness and bending refer to the property of a material known as elasticity, which describes the tendency of a material to return to its original shape after the removal of a load (Hildebrand 1988). If the stiffness of an object, such as a column, is insufficient to resist bending, the object buckles (elastic buckling) and fails to return to its original shape, causing a fracture (Timoshenko and Gere 1972; Schmidt-Nielsen 1984)).

Robusticity is a term that is used frequently in the physical anthropology literature, and has specific meaning. In essence, robusticity refers to the strengthening or buttressing of a skeletal element in response to higher mechanical loadings (Ruff et al. 1993). This strengthening is accomplished by addition of bone tissue, and results in an increased diaphyseal external circumference (or breadth) relative to the length of the bone (Ruff et al. 1993). Robusticity typically refers to long bones, but the term also has been used to describe the relative size of articulations, cortical thickness, and muscle attachments (Ruff et al. 1993). Most of the literature on bone biomechanics deals with stresses and strains applied to bones during locomotion (Gregory 1912; Howell 1944; Wainwright et al. 1976; Nordin and Frankel 1980; Biewener 1983; Currey 1984). Cross-sectional properties of mid-diaphyses of long bones have been found to provide the best estimates of body mass, because they reflect mechanical loading of the mass of the animal that is placed upon the skeleton (Biewener 1982; Biknevicius et al. 1993).

Articulations may also be viewed as having cross-sectional properties. Pecoran artiodactyls have a range of limb motion that is limited primarily to the parasagittal plane. As a group, the Pecora are structurally homogeneous. The size of articulations should scale isometrically within the group and correlate directly to body mass as a surface area with an exponent of 0.67 ($A \propto M^{0.67}$). Although primates are also structurally similar, some functional differences such as brachiation and obligate bipedalism separate them from other groups, and hence the cross-sectional scaling factors in primates may not conform exactly to isometry but will rather reflect unusual mechanical loadings (Godfrey et al. 1991).

Cross-sectional properties of bone — Applying engineering beam theory, resistance to bending is a function of the cross-sectional area of the beam (Nordin and Frankel 1980). Looking at a cross-section of a beam during bending, there is a point where compressive and tensile forces meet and essentially cancel each other out. This line is called the neutral axis, and runs the length of the object. "I" is the area moment of inertia, or second moment area, which is the, measure of resistance to bending in one plane. I_x is the measure of antero-posterior bending stress, and I_y is the measure of medio-lateral bending stress. In long bone cross sections, antero-posterior and medio-lateral directions rarely correspond to the axes of maximum and minimum second moments of area due to the irregular shape of the bones, and the actual I_{min} and I_{max} must be calculated (Fig.3-3) (Ruff 1981).

When twisting (torsion) of a beam is involved, there is no neutral axis, but rather a neutral point or centroid where opposing forces meet and cancel each other out. The

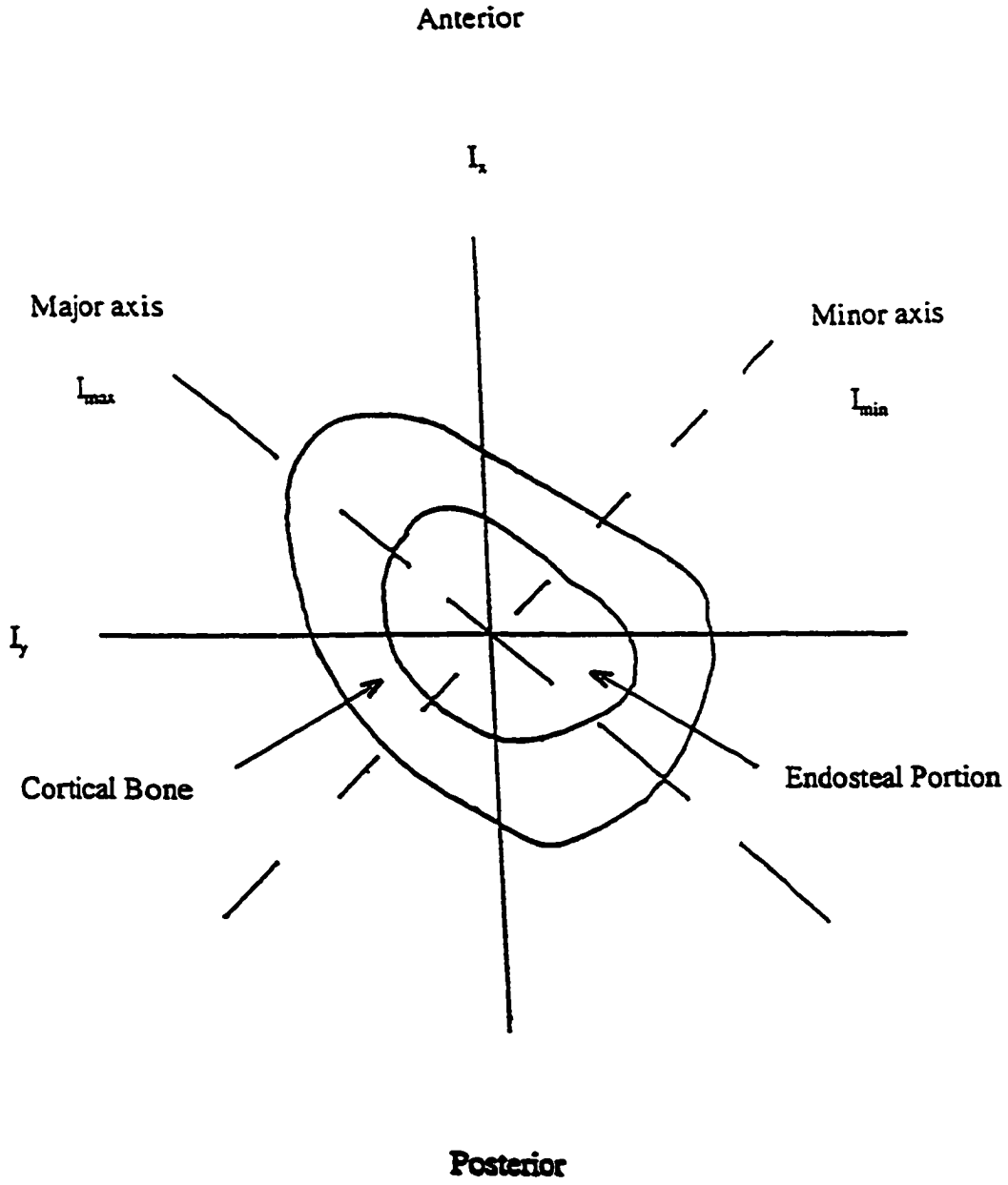

Fig. 3-3. Cross-section of a long bone with major axes and second moments of area. I_x = Antero-posterior bending stress; I_y = Medio-lateral bending stress; I_{max} = Major axis; I_{min} = Minor axis. The endosteal portion is subtracted out when using beam theory adapted for bone, leaving only the cortical bone for consideration.

resistance to torsional motion is called "J" and is merely the sum of $I_x + I_y$. J is also a general measure of resistance to bending stress as well as to torsion (Churchill 1994). Both I and J increase with area and distance from the neutral axis, so there is more stress towards the periphery of a bone where the structurally stronger compact cortical bone is located. The actual calculation of I and J are performed using engineering beam formulae adapted for bone, allowing for the endosteal portion of the bone to be subtracted out from the area, leaving only the cortical area for consideration (Fresia et al. 1990; Biknevicius 1993).

The principles underlying the mechanics of cross-sectional geometry of bone and body mass explains why articulations and diameters proved to be such good predictors of mass in pecorans. There are other theories involving skeletal proportions and body mass which are related, but do not take into account the effect the forces of locomotion have upon the shape of various surfaces.

Similarity Theories

Skeletal mass in mammals has been shown by Prange et al. (1979) to increase with body mass at an exponent of 1.09, exhibiting a slight positive allometry. An isometric increase in skeletal mass would exhibit an exponent of 1.0. Articular surface areas of long bones modeled as cross-sectional areas ($A \propto M^{0.67}$) also increase approximately isometrically. The most notable exceptions are among the primates where examples of both negative and positive allometry in the hip joint have been demonstrated (Jungers 1990). Quadrupedal species tend to have smaller femoral heads than would be expected

from isometry, and both *Pongo* and humans have larger femoral heads than would be expected, probably related to range of motion in *Pongo*, and increased limb loading due to bipedalism in humans (Jungers 1988). In groups with more consistent range of motion and limb loadings such as ungulates, articulations should conform more closely to isometry. The volume of a joint includes the mass of bone within the articulation which more directly reflects the mass of an animal whereas the surface area is more reflective of range of motion and locomotion (Jungers 1988; Ruff 1988).

Geometric, elastic and static stress slopes are different for almost all proportions, and are reported differently depending upon whether mass is modeled as the dependent or independent variable in the regression equation (McMahon 1975; Alexander 1977; Ruff 1990).

Geometric similarity — The assumption that all animal growth is isometric, and that large animals are merely proportional enlargements of small animals is the principle of geometric similarity. The principle states that as some length (L) increases, then other properties such as surface area (S), diameters (D), and mass (M) change in proportion to the length, so that $M \propto L^3$, $S \propto L^2$, $L \propto M^{1/3}$, $D \propto L^{1/3}$, and $S \propto M^{2/3}$ (Hildebrand 1988). The idea of geometric similarity first arose over 2000 years ago, and can be explained by an example of Euclidean geometry, where two triangles are considered similar if their corresponding sides are proportional in a constant ratio, and the corresponding angles are equal (Schmidt-Nielsen 1984). This principle can be applied to any geometric shape, including those with volumes. Similar geometric shapes that are proportional as defined above are said to exhibit isometry. In isometric shapes with volume, the surface area

increases as the square of the linear dimensions, and the volume increases as the cube. It has long been noted that as animals increase in size, the thickness of the limbs increases (Galileo 1637). Since the compressive strength of bone is a function of the material composing the bone matrix, the only way to increase the strength of the bone is to increase the dimensions, especially the diameter (Schmidt-Nielsen 1984). If a long bone were to increase geometrically in size, then the bone should increase in relation to mass as the product of the cross sectional area times the length. The volume may be calculated by using the formula for the volume of a cylinder, or $\pi r^2 h$, where r^2 is the radius of the cross-sectional area, and h is the height of the cylinder. The slope of the regression line for the volume or mass of the mammalian skeleton versus body mass adhering to geometric similarity should be 1.0 (Schmidt-Nielsen 1984).

Prange et al. (1979) established the slope of this regression to be 1.09, indicating an allometric relationship. That study used dried skeletal mass from museum collections for the source of data collection. When fresh unscraped bone mass was used, the slope of the regression scaled at 0.96, taking into account moisture and organic material that is a normal component of living bone. Fresh bone adheres to geometric similarity (Calder 1996). Geometric similarity is observed within phyletic lines as long as only moderate size differences are observed (Hildebrand 1988). Alexander et al. (1979), found the dimensions of the limb bones of mammals over a wide range of size scale close to geometric similarity. However, as an organism becomes much larger, certain structural changes must occur to allow for increased limb loading and metabolic requirements that cannot be explained by isometric proportions alone.

Allometry — Allometry refers to the principle whereby many ecological, physiological, and morphological variables in animals are correlated with the size of the animal, but that the quantitative correlation is not the same for all organs and all functions (Calder 1996). These variables may scale above or below the ($\log_{10}$) slope of the regression line of increase of body mass. The allometric equation describes these scaling relationships:

$$Y = aM^b$$

or

$$\log Y = \log a + b \log M$$

where Y is any variable correlated with mass, a is a constant, M is body mass, and b is the scaling factor or the slope of the regression equation used to describe the relationship. By using the allometric equation, log transformed, a plot of a biological variable versus body mass is nearly a straight line (Kleiber 1932). This is an extremely useful concept in that it implies that there are other morphological and physiological factors at work in relation to metabolism other than just body mass.

Elastic similarity — McMahon (1973) argued that animals cannot increase in size geometrically because the cross-sectional area of their limbs would only increase as the square whereas the volume would increase as the cube, rendering the limbs too slender to support the mass. He initially looked at trees and the limbs of generalized mammals, modeled as cylinders. Applying engineering beam theory to an axially loaded cylinder, the cylinder would fail if the compressive strength were great enough, but would fail sooner if it was very slender, because of elastic buckling, involving a small lateral displacement

(Nordin and Frankel 1980). Instead, he proposed that animals increased in size by obeying a principle which he called elastic similarity, which predicted that limb lengths and diameters would increase allometrically with consistent exponents. McMahon (1973) predicted that body lengths would be proportional to mass ($L \propto M^{0.25}$), diameters proportional to mass ($D \propto M^{0.375}$), and lengths to diameters ($L \propto D^{0.67}$). McMahon (1975) tested his theory on a group of ungulates, measuring the proportion of lengths to diameters of long bones. The length to diameter correlation of bovids agreed well with his elastic similarity theory (0.63), but other groups exhibited differing exponents; cervids (0.79), suids (0.54), and perissodactyls (0.60), suggesting a more limited applicability of this principle.

McMahon's theory was tested by Alexander (1977) who looked at seven species of African antelopes of varying size. He found that while most of the exponents agreed well with elastic similarity, some of the exponents derived for the hindlimb were significantly different. Alexander attributed this to the stress of locomotion in the hindlimb, which he hypothesized as being independent of body mass. In a subsequent study, Alexander et al. (1979) measured the leg bones of 37 species of terrestrial mammals from the size of shrews to elephants. In this study, it was found that except for the bovids, the exponents of lengths and diameters were ($L \propto M^{0.35}$) and ($D \propto M^{0.36}$) respectively, correlating more closely to isometry with an exponent of 0.33. Bovids were the only group conforming to elastic similarity, and may be considered somewhat idiosyncratic due

to the apparent correlation of limb length and habitat that is not as apparent in many other taxa (Alexander et al. 1979; Scott 1979).

Static stress similarity — It has been recognized that if the limbs of animals are geometrically similar, they will increase in size so that the lengths are directly proportional to the diameters ($L \propto D$) (Thompson 1917). If this were true, then the peak stresses within the bones, measured as the ability to withstand compressive stress in a cross sectional plane, should also increase with increasing size (Biewener 1983). Elastic similarity suggests that mammalian limbs would become distorted, more robust, and essentially out of proportion, as the animals increased in size ($L \propto D^{0.67}$) (McMahon 1973). Alexander et al. (1979) showed however, that in mammals over a large size range, limb proportions ($L \propto D$) increased at a rate close to geometric similarity ($L \propto M^{0.97}$).

The force acting through a cross-sectional area of bone is defined as stress (σ) being equal to force (F) divided by the cross-sectional area (A), or ($\sigma = F/A$). Upon actually testing bone stress in animals ranging in size from a chipmunk to a horse, Biewener (1989) found the peak bone stress (maximum without fracture) is independent of size, and allows for a two to four fold safety factor. The reason for this lower peak bone stress is related to two factors, having to do with limb posture as well as with limb robustness in larger animals. Limb muscles propel and support an animal by exerting torque around the joints of the limbs (Biewener 1989). The force necessary for the muscles to exert depends upon the "ground reaction force", which is essentially the force exerted upward by the ground against a mass (Biewener 1989).

The weight of an object refers to the gravitational force exerted on it by the earth, w = mg; and is measured in Newtons. The mass of an object is a constant, and is measured in kg. The mass of an object would be the same whether it was on the surface of the earth, or at zero gravity in space (ISO 1993). The ground reaction force is the force exerted by the ground on an animal. When the animal is at rest, the ground reaction force (GRF) equals the weight of the animal (GRF + weight = 0). If an animal begins to move, it exerts an additional force on the ground, and vice versa. If the animal has an acceleration a and mass M, then GRF = M (g + a) where g = the acceleration of gravity, or approximately 9.81 N kg^{-1}. GRF, g and a are all vectors, where Mg is the weight of the animal, or the vertical component of GRF, and Ma is the horizontal force. The total GRF is the sum of the two vectors Ma and Mg (Biewener 1989; Pennycuick 1992).

Small animals run in a crouched posture, which effectively decreases the amount of muscle force necessary to counteract the ground, because the entire mass of the animal is no longer placed upon each joint, but is also shared by the muscles. Animals up to approximately 300 kg maintain a lower bone stress by adjusting their posture as they run. In mammals over 300 kg, limbs become more nearly vertical in order to support the mass of the animal. As it is no longer possible in large forms to achieve postural changes in order to decrease bone stress, limbs typically become more robust as size increases, as in the ceratomorphs (rhinos, tapirs), scaling would be expected from stress similarity as ($L \propto D^{0.5}$) (Biewener 1989; Bertram and Biewener 1990).

Stress similarity states there are two different mechanisms by which animals maintain a safety range for the stress placed upon the cross-sectional area of bone. First,

small animals up to approximately 300 kg maintain a more crouched position during locomotion, effectively decreasing the ground reaction force placed upon a joint. Second, in large animals greater than 300 kg, the limb bones increase in diameter and robusticity beyond what one would expect from geometric similarity, but less than that predicted for elastic similarity.

MATERIALS AND METHODS

Body Masses

Twenty-six species of bovids, cervids, and the one modern antilocaprid *Antilocapra americana*, were used as the modern sample. *A. americana* is represented by the greatest number of individuals (n=65). Modern specimen numbers and sexes are listed in Appendix I. The fossil sample consisted of five species of *Capromeryx*, an extinct genus of antilocaprids that was present in North America between the mid-Blancan (ca.3.1 Ma.) and the late Rancholabrean (40,000-10,000 Ka). The fossils were borrowed from a number of institutions, and the specimen numbers are listed in Appendix II.

Modern adult specimens were used, as indicated by fusion of the long bone epiphyses, the only exception being the musk-ox, for which only a sub-adult was available. The musk-ox was included because there were very few specimens available >200 kg. Zoo specimens were not used unless it was the only representative of that species such as the musk-ox and both axis deer. Captive animals not from a zoo, but rather a game ranch and farm situation respectively, include the fallow deer and the domestic sheep.

Predictive least squares regression equations were developed using the modern sample. The preferred method of estimating mammalian body mass is to have available a large sample of wildshot individuals of a species taken from a wide geographic range, and then take the mean of the sum of the individual masses (Scott 1990). Unfortunately, this is the ideal situation, and is rarely encountered in museum collections. Individual body masses are occasionally available in museums for small mammals, but only rarely for large specimens due to the difficulties presented in weighing a large animal in the field. Masses are available in the literature, but there is a bias present in favor of big game species, particularly those from Africa. Masses are often taken from hunting records which record trophy animals, usually the largest males, which skews the masses upward by at least 10%-15% (Best et al. 1962; Scott 1990; Runestad 1994). Walker's Mammals of the World (Nowak 1991) includes ranges of masses for entire families, but there may be a huge difference in masses within a single family. For example, for the Cervidae, the range is 7-825 kilograms, making any estimation of masses for an individual species impossible from that particular source. Body masses for this research were derived primarily from published data of other researchers including Alexander (1977), Scott (1979), Gingerich (1990), Janis (1990), Nowak (1991), and Silva and Downing (1995). Specimens were separated by sex when possible, and respective mass estimates for each sex were used when available. When the sex was unknown, a mean of the male and female mass was used for the individual. Zoo animals were avoided if possible, as they tend to be heavier than wildshot individuals, are subject to skeletal deformations due to dietary stress and

inactivity, and are not representative of species in the wild (Scott 1990). A list of modern specimens and catalog numbers is included in Appendix I.

Measurements

Measures used in this research include lengths, widths, articular surface areas and volumes of articulations of the astragalus, calcaneum, cubonavicular, femur, humerus, magnum, metacarpal, metatarsal, radius, scapula, tibia and ulna. Both right and left sides were measured, and a mean of the two was used in the final calculations. In animals with only a right or a left element available, the measurements from that side were used in the calculations. Measurements were made using Mitytoyo digital calipers, accurate to .01 mm. Two sizes of calipers were used, and in the event of an element longer than 300 mm, a metal ruler at room temperature was used. Both proximal and distal leg bones were included, as well as one carpal and three tarsal bones. The magnum was chosen because of the relatively flat shape and the medial position of the bone in the carpal assembly. The cubonavicular occupies a position in the tarsal assembly which would be subjected to axial loadings. The calcaneum and astragalus were used due to the prevalence of these elements in the fossil record and the potential usefulness in studies of body mass.

Statistical Analyses

All analyses were performed using $\log_{10}$ transformed arithmetic means of each parameter for each individual species. All statistical calculations were made using the

software package SYSTAT 7.0 (SPSS 1997). Least squares regressions were calculated for each variable for each element, with $\log_{10}$ transformed body mass as the dependent variable. Least squares regression remains the most appropriate method when the goal of the study is to develop "predictive" allometric equations (Sokel and Rohlf 1981). Least squares regression assumes that all of the error is in the y axis (the dependent variable) and that the independent variable on the x axis is without error (Kleinbaum et al. 1988). The reason that all data points do not all fit onto the line is due primarily to both measurement error and real biological variation. A line is then fit through the cloud of data points so as to minimize the sum of squares of the vertical line segments which run from the regression line either up or down to each data point along the x axis (Hofman 1988; Kleinbaum et al. 1988). Because only one axis is considered to have error, this makes the least squares method the most the preferred method when prediction is the goal of the study.

Variables were log transformed for several reasons. First, transformation of the allometric equation $y = ax^b$ to $\log y = \log a + b \log x$ results in a linear relationship which is easier to interpret and lends itself better to statistical manipulation (Smith 1984). Second, even when untransformed data are normally distributed and linear, a logarithmic transformation provides a means of reducing statistical problems related to outliers (Smith 1984). Third, in instances where the data distribution is heteroscedastic (increasing or unequal variances), log transformation renders the data more nearly Gaussian, or homoscedastic (Smith 1993). Fourth, in situations where there is a large difference in the values of the variables of interest, such as in the almost hundred fold difference in body

mass between the smallest and largest pecoran artiodactyl, log transforming the data provides a way of examining proportional changes in size by providing a regression slope unaffected by the units of measurement and is scale independent, thus reducing perceptual bias in data analysis (Calder 1996; Smith 1984).

One problem with log transformation is that there is bias present when the data are detransformed for comparison with original data. There is no bias present unless the predicted values are detransformed (Smith 1993). The nature of this bias becomes apparent when the mean of the log transformed data is taken for purposes of calculation and then detransformed to estimate the mean of the original arithmetic units (Smith 1993). Detransformation produces a geometric rather than arithmetic mean because adding logarithms is the same as multiplying arithmetic equivalents. The arithmetic mean is calculated by taking the sum of the values of the data set and dividing by the sample size ($\sum x/n$). The geometric mean (GM) is calculated by multiplying ($\sqrt[n]{x_1 \cdot x_2 \cdot x_3 \ldots x_n}$). For a given x value, the allometric equation produces a single value of y, which upon detransformation, is in actuality the geometric mean of that y value. The geometric mean is always less than the arithmetic mean, so detransformed predictive values will underestimate the y, or parameter of interest (Smith 1993).

So that detransformed values have meaning and are accurate, it is necessary to apply a correction factor to the detransformed data (Smith 1993). There are several correction factors that are available, but one of the easiest to use is the ratio estimator (Snowdon 1991). The ratio estimator is the mean of the observed y values divided by the mean of the detransformed predicted values, or for purposes of this study, the mean of the

original observed body masses divided by the detransformed predicted body masses for each variable of interest (Snowdon 1991). One number results and is then multiplied by each of the detransformed y values, producing corrected detransformed y values.

Subsequent analyses used both forward and backwards stepwise multiple regressions with the alpha level set at .05. The correlation coefficient (r) was used to determine strength of the association between the dependent variable body mass, and the independent variable. The percent standard error of the estimate (%SEE) and percent prediction error (%PE) were calculated in order to evaluate the predictive power of the independent variable (Smith 1981; 1984; Damuth 1990).

The correlation coefficient may be misleading in interspecific studies when used exclusively as the measure of the strength of the relationship in question (Smith 1984). The correlation is affected by the range of values for the dependent and independent variables, as well as by the slope of the regression line (Smith 1984). In studies such as mine, where there may be greater than a one hundred fold difference in body mass among species, the wide range of values can skew the correlation coefficient upward, presenting the researcher with an erroneously high r value (Smith 1984).

Due to the problems in using the correlation coefficient by itself, other measures have been determined to provide confirmation of the relatedness of the dependent to the independent variable. The percent prediction error (%PE) is an indicator of the percent difference between the actual mass (or the species mean mass), and that predicted by the regression equation. The mean of the absolute value of the %PE provided an index of predictive accuracy for each regression, and was then compared among regressions for

each element to see which variable for the element provided the best predictor of mass (Van Valkenburgh 1990). The formula for %PE is the following:

$$\%PE = 100 \times (\text{observed} - \text{predicted}) / \text{predicted}$$

The percent standard error of the estimate (%SEE) reflects the ability of the independent variable to predict the dependent variable. The %SEE is defined as:

$$\%SEE = \text{antilog}\,(2 + \log_{10} SEE) - 100$$

The amount in excess of 100 is the standard error in percent (Smith 1984). Assuming a normal distribution, a %SEE of 40 would indicate that 68% of cases (one standard deviation) would be within +/- 40% of predicted values (Smith 1984).

RESULTS

Estimation of Mass Using Modern Sample

Regression equations for prediction of body mass were developed using least squares regressions on $\log_{10}$ transformed mean body masses for each modern species. Lengths, diameters, and volumes were modeled as the independent variables with body mass as the dependent variable of interest. A simple linear regression was run for each variable for each element. Although this is somewhat of an unusual procedure, in that multiple regressions are usually preferred, these simple regressions were performed as the desired end result was the prediction of body mass using individual elements. The regression then was used to predict $\log_{10}$ body mass, and the predicted masses were detransformed and corrected using the ratio estimator as discussed on p. 93. Table 3.1

Table 3-1. Definitions of Variables and Formulae for Volumes and Surface Areas of Geometric Shapes

Variable	Description	Formulae
Astragalus		
AS1:	Greatest length of the astragalus.	
AS2:	Greatest width of the astragalus measured at midsection including the projection on the medial side.	
AS3:	Volume of the distal articular surface, modeled on an hyperboloid of revolution. Q is the radius.	$V = \Pi h/3\ (2a^2+Q^2)$
AS4:	Surface area of the anterior articular surface area modeled on a rectangle.	$A = ab$
Calcaneum		
CL1:	Greatest length of the calcaneum, measured from the calcanean tuberosity to the most distal portion of the tarsal.	
CL2:	Greatest width of the sustentaculum.	
CL3:	Surface area of the proximal end of the calcaneum modeled on a rectangle.	$A = ab$
CL4:	Combined surface areas of the distal calcaneum modeled on the sum of an equilateral triangle plus a rectangle.	$A = (a^2\sqrt{3})/4) + ab$
Cubonavicular		
CU1:	Surface area of the distal articular surface modeled on a circle.	$A = \Pi r^2$
Femur		
FM1:	Greatest length of the femur from the greater trochanter to the most distal portion of the lateral side of the patellar articular surface.	
FM2:	Anterior-posterior diameter of the shaft at 50% of the length of the femur.	

FM3:	Volume of the femoral head, modeled on a spherical segment (Q is the radius).	$V = 1/6\ \Pi h(3Q^2 + h^2)$
FM4:	Surface area of the femoral head, modeled on a spherical segment; A_c is the surface areaof the curved portion.	$A_c = 2\Pi rh$

Humerus

HM1:	Greatest length of the humerus from the greater tubercle to the most distal portion of the lateral epicondyle.	
HM2:	Anterior-posterior diameter of the humerus at the 50% level of the shaft.	
HM3:	Volume of the distal articular surface area of the humerus (trochlea + capitulum)modeled on an hyperboloid of revolution.	$V= \Pi h/3(2a^2 + Q^2)$
HM4:	Volume of the distal articular surface area of the humerus (trochlea + capitulum) modeled on an obliquely ut right circular cylinder. S_1 is the length of the longer side, and S_2 is the length of the shorter side.	$V = \Pi r^2/2(S_1 + S_2)$
HM5:	Volume of the distal articular surface area of the humerus (trochlea + capitulum)modeled on the frustrum of right circular cone. R_2 is the smallerof the two radii.	$V = h\{(r_1)^2+(r_1r_2)+(r_2)^2\}$

Magnum

MN1:	Volume of the proximal surface modeled on the spherical segment of two bases.	$V = 1/6\Pi h\{(3Q_1)^2 + (3Q_2)^2 + h^2\}$

Metacarpal

MC1:	Greatest length of the metacarpal measured from the carpal articular surface to the most distal sagittal ridge	
MC2:	Proximal surface area modelled on a trapezium	$A = (a+c)/2*h$
MC3:	Volume of the distal articular surface area (medial and lateral condyles and the intertrochlear incisure) modeled on a barrel	$V = 1/3\Pi h(2R^2 + r^2)$

Metatarsal

MT1:	Greatest length of the metatarsal measured from the tarsal articular surface to the sagittal ridge	
MT2:	Proximal surface area modelled on a circle	$A = \Pi r^2$
MT3:	Volume of the distal articular surface area (medial and lateral condyles and the intertrochlear incisure) modeled on a barrel	$V = 1/3\Pi h(2R^2 + r^2)$

Radius

RD1:	Greatest length of the radius from the highest point of the proximal articular surface area to the styloid process	
RD2:	Area of the proximal articular fovea of the radius modeled on a rectangle	$A = ab$

Scapula

SC1:	Surface area of the glenoid fossa modeled on a circle	$A = \Pi r^2$

Tibia

TA1:	Greatest length of the tibia measured from the intercondylar eminence to the medial malleolus	
TA2:	Distal breadth of the tibia measured medial-laterally	
TA3:	Surface area of the lateral condyle (rectangle) plus the surface area of the medial condyle (trapezium)	$A = ab + (a+c)/2*h$
TA4:	Surface area of the lateral condyle (rectangle) plus the surface area of the medial condyle (rectangle)	$A = ab + ab$
TA5:	Surface area of the distal articular surface modeled on a trapezium	$A = (a+c)/2*h$

Ulna

UL1:	Length of the olecranon from the anconeal process to the olecranon tuberosity	
UL2:	Surface area of the trochlear notch modeled on a trapezium	$A = (a+c)/2*h$

includes definitions of variables and formulae for volumes and surface areas of geometric shapes. These regressions were then used on the fossil sample to predict body mass in the extinct species. Original body masses and predicted body masses for each species for each variable may be found in Table 3-2. The %PE and %SEE were then calculated. The summary of predictive equations and prediction errors are found in Table 3-3. Multiple forwards and backwards stepwise regressions were run for all variables for each element ($\alpha = .05$) in order to ascertain which of the variables should be included in the final model as the best predictors of body mass in modern pecorans. Of the two stepwise procedures, the forward stepwise estimation is superior in that it examines the contribution of each variable to the model before inclusion in the model by examining the partial correlation coefficient (Hair et al.1995). Backwards elimination is more of a trial and error procedure that involves the initial computation of a regression equation that includes all of the variables, and then goes back and deletes variables that do not add significantly to the model.

Scapula

Surface area of the glenoid fossa — Because the scapula of ungulates is oriented against the side and not the back of the thorax, and is unencumbered by a clavicle, it essentially becomes an extension of the forelimb, with the glenoid fossa subjected to similar loadings as the rest of the bones of the forelimb when the animal is standing at rest (Fig.3-4). The surface area of the glenoid fossa (SC1) was modeled as an ellipse (Fig.3-5). The regression of $\log_{10}$ body mass against $\log_{10}$ area yielded a slope of 1.642

Table 3-2. Mean body masses
and predicted masses for each variable for modern species

See Table 3-1 (p.96-98) for definitions of variable abbr. "X" is mean mass for species

Element/Species	Common name	X Mass (kg)	Variables				
Scapula			SC1				
Dama dama	Fallow Deer	44	55				
Axis axis	Axis Deer	47	50				
Cervus elaphus	Elk	325	366				
Odocoileus hemionus	Mule Deer	68	69				
Odocoileus virginianus	White-tailed Deer	87	74				
Alces alces	Moose	525	475				
Antilocapra americana	Pronghorn	48	80				
Tragelaphus strepsiceros	Greater Kudu	215	152				
Taurotragus derbianus	Giant Eland	500	431				
Bison bison	American Bison	658	641				
Kobus ellipsiprymnus	Common Waterbuck	227	318				
Oryx gazella	Gemsbok	168	155				
Alcelapus buselaphus	Hartebeest	135	150				
Connochaetes taurinus	Blue Wildebeest	205	222				
Oreotragus oreotragus	Klipspringer	13.5	10				
Aepyceros melampus	Impala	53	89				
Litocranius walleri	Gerenuk	35	45				
Gazella thomsoni	Thomson's Gazelle	23	21				
Gazella granti	Grant's Gazelle	63	64				
Oreamnos americanus	Mountain Goat	90	105				
Ovibos moschatus	Muskox	282	223				
Ovis aries	Domestic Sheep	80	97				
Ovis canadensis	Bighorn Sheep	90	84				
Humerus			HM1	HM2	HM3	HM4	HM5
Dama dama	Fallow Deer	44	42	41	51	50	52
Axis axis	Axis Deer	47	39	46	43	35	37
Cervus elaphus	Elk	344	501	415	427	359	353
Odocoileus hemionus	Mule Deer	74	116	84	91	81	82
Odocoileus virginianus	White-tailed Deer	87	99	65	93	81	84
Alces alces	Moose	544	656	395	554	393	421
Rangifer tarandus	Caribou	81	151	89	96	90	88
Antilocapra americana	Pronghorn	48	72	61	57	60	61
Tragelaphus strepsiceros	Greater Kudu	215	169	187	217	238	236
Taurotragus derbianus	Giant Eland	500	315	307	405	468	505
Bison bison	American Bison	658	420	665	560	505	476
Kobus ellipsiprymnus	Common Waterbuck	227	254	340	274	304	306
Oryx gazella	Gemsbok	168	126	192	157	210	208
Alcelaphus buselaphus	Hartebeest	135	108	136	127	154	147
Connochaetes taurinus	Blue Wildebeest	205	145	200	192	244	234
Oreotragus oreotragus	Klipspringer	13.5	.	.	13	10	10
Aepyceros melampus	Impala	53	60	82	61	78	76
Litocranius walleri	Gerenuk	35	47	28	44	51	50
Gazella thomsoni	Thomson's Gazelle	23	21	27	20	25	24
Gazella granti	Grant's Gazelle	63	48	58	65	68	66
Oreamnos americanus	Mountain Goat	90	165	155	99	126	119
Ovibos moschatus	Muskox	282	175	190	297	280	283
Ovis aries	Domestic Sheep	80	98	65	80	95	91
Ovis canadensis	Bighorn Sheep	79	95	96	70	85	84

Table 3-2. Mean body masses
and predicted masses for each variable for modern species

Radius			RD1	RD2
Axis axis	Axis Deer	47	31	38
Cervus elaphus	Elk	344	450	335
Odocoileus hemionus	Mule Deer	74	118	79
Odocoileus virginianus	White-tailed Deer	87	110	76
Alces alces	Moose	544	729	429
Rangifer tarandus	Caribou	81	163	124
Antilocapra americana	Pronghorn	48	79	59
Tragelaphus strepsiceros	Greater Kudu	215	218	214
Taurotragus derbianus	Giant Eland	500	255	467
Bison bison	American Bison	658	308	631
Kobus ellipsiprymnus	Common Waterbuck	227	208	279
Oryx gazella	Gemsbok	160	202	189
Connochaetes taurinus	Blue Wildebeest	205	273	215
Oreotragus oreotragus	Klipspringer	13.5	11	13
Aepyceros melampus	Impala	53	94	57
Litocranius walleri	Gerenuk	35	103	44
Gazella thomsoni	Thomson's Gazelle	23	30	18
Gazella granti	Grant's Gazelle	63	86	64
Oreamnos americanus	Mountain Goat	90	116	106
Ovibos moschatus	Muskox	282	131	298
Ovis aries	Domestic Sheep	80	96	96
Ovis canadensis	Bighorn Sheep	81	98	78
Ulna			**UL1**	**UL2**
Dama dama	Fallow Deer	44	37	44
Axis axis	Axis Deer	47	36	40
Cervus elaphus	Elk	344	338	313
Odocoileus heminous	Mule Deer	74	90	85
Odocoileus virginianus	White-tailed Deer	87	101	66
Alces alces	Moose	544	388	436
Rangifer tarandus	Caribou	81	116	116
Antilocapra americana	Pronghorn	48	60	59
Tragelaphus strepsiceros	Greater Kudu	215	152	212
Taurotragus derbianus	Giant Eland	500	405	671
Bison bison	American Bison	658	712	519
Kobus ellipsiprymnus	Common Waterbuck	227	245	296
Oryx gazella	Gemsbok	168	221	139
Alcelaphus buselaphus	Hartebeest	135	137	114
Connochaetes taurinus	Blue Wildebeest	205	290	193
Oreotragus oreotragus	Klipspringer	13.5	12	21
Aepyceros melampus	Impala	53	70	77
Litocranius walleri	Gerenuk	35	36	39
Gazella thomsoni	Thomson's Gazelle	23	25	14
Gazella granti	Grant's Gazelle	63	60	65
Oreamnos americanus	Mountain Goat	90	110	137
Ovibos mosachatus	Muskox	282	224	246
Ovis aries	Domestic Sheep	80	100	86
Ovis canadensis	Bighorn	84	101	87
Ovis dalli	Dall's Sheep	70	102	89

Table 3-2. Mean body masses
and predicted masses for each variable for modern species

Metacarpal			**MC1**	**MC2**	**MC3**
Dama dama	Fallow Deer	44	100	42	36
Axis axis	Axis Deer	47	83	34	30
Cervus elaphus	Elk	344	325	339	384
Odocoileus heminous	Mule Deer	74	164	82	80
Odocoileus virginianus	White-tailed Deer	87	168	73	75
Alces alces	Moose	550	355	484	545
Rangifer tarandus	Caribou	81	137	115	109
Antilocapra americana	Pronghorn	48	161	56	59
Taurotragus derbianus	Giant Eland	500	222	407	380
Bison bison	American Bison	616	142	576	526
Kobus ellipsiprymnus	Common Waterbuck	227	216	260	258
Oryx gazella	Gemsbok	168	180	164	155
Alcelaphus buselaphus	Hartebeest	135	210	161	160
Connochaetes taurinus	Blue Wildebeest	205	175	203	216
Oreotragus oreotragus	Klipspringer	13.5	40	14	16
Aepyceros melampus	Impala	53	184	63	69
Litocranius walleri	Gerenuk	35	257	44	45
Gazella thomsoni	Thomson's Gazelle	23	112	21	22
Gazella granti	Grant's Gazelle	63	202	58	65
Oreamnos americanus	Mountain Goat	90	53	120	101
Ovibos mosachatus	Muskox	282	86	349	344
Ovis aries	Domestic Sheep	80	96	87	77
Ovis canadensis	Bighorn	82	125	82	82
Ovis dalli	Dall's Sheep	70	124	80	81

Magnum			**MN1**
Dama dama	Fallow Deer	44	40
Axis axis	Axis deer	47	36
Cervus elaphus	Elk	344	343
Odocoileus heminous	Mule Deer	74	73
Odocoileus virginianus	White-tailed Deer	87	79
Alces alces	Moose	550	561
Rangifer tarandus	Caribou	81	101
Antilocapra americana	Pronghorn	48	55
Taurotragus derbianus	Giant Eland	500	443
Bison bison	American Bison	658	519
Kobus ellipsiprymnus	Common Waterbuck	227	316
Oryx gazella	Gemsbok	168	152
Alcelaphus buselaphus	Hartebeest	135	161
Connochaetes taurinus	Blue Wildebeest	205	233
Oreotragus oreotragus	Klipspringer	13.5	16
Aepyceros melampus	Impala	53	68
Litocranius walleri	Gerenuk	35	43
Gazella thomsoni	Thomson's Gazelle	23	21
Gazella granti	Grant's Gazelle	63	54
Oreamnos americanus	Mountain Goat	90	116
Ovibos mosachatus	Muskox	282	294
Ovis canadensis	Bighorn	82	82
Ovis dalli	Dall's Sheep	70	75

Table 3-2. Mean body masses
and predicted masses for each variable for modern species

Femur			FM1	FM2	FM3	FM4	
Dama dama	Fallow Deer	44	42	51	61	61	
Axis axis	Axis deer	47	40	45	33	33	
Cervus elaphus	Elk	344	514	366	330	335	
Odocoileus heminous	Mule Deer	74	112	74	88	88	
Odocoileus virginianus	White-tailed Deer	87	107	65	80	79	
Alces alces	Moose	544	639	575	385	391	
Rangifer tarandus	Caribou	81	125	96	100	100	
Antilocapra americana	Pronghorn	48	61	49	45	44	
Taurotragus derbianus	Giant Eland	500	384	415	443	442	
Bison bison	American Bison	658	433	526	681	680	
Kobus ellipsiprymnus	Common Waterbuck	227	324	314	301	297	
Oryx gazella	Gemsbok	168	176	211	225	223	
Alcelaphus buselaphus	Hartebeest	135	121	132	158	155	
Connochaetes taurinus	Blue Wildebeest	205	163	200	257	254	
Oreotragus oreotragus	Klipspringer	13.5	13	15	15	15	
Aepyceros melampus	Impala	53	71	66	71	70	
Litocranius walleri	Gerenuk	35	46	38	42	41	
Gazella thomsoni	Thomson's Gazelle	23	22	22	25	25	
Gazella granti	Grant's Gazelle	63	59	50	57	56	
Oreamnos americanus	Mountain Goat	90	108	132	98	100	
Ovibos mosachatus	Muskox	282	148	278	250	253	
Ovis aries	Domestic Sheep	80	74	86	76	77	
Ovis canadensis	Bighorn	79	95	72	57	57	

Tibia			TA1	TA2	TA3	TA4	TA5
Dama dama	Fallow Deer	44	43	46	52	51	46
Axis axis	Axis deer	47	36	48	47	48	46
Cervus elaphus	Elk	344	532	453	375	376	427
Odocoileus heminous	Mule Deer	74	184	89	84	85	87
Odocoileus virginianus	White-tailed Deer	87	185	90	84	83	94
Alces alces	Moose	544	651	540	505	496	526
Rangifer tarandus	Caribou	81	203	114	108	109	117
Antilocapra americana	Pronghorn	48	74	54	49	48	51
Taurotragus derbianus	Giant Eland	500	253	388	380	376	446
Bison bison	American Bison	658	282	560	546	544	497
Kobus ellipsiprymnus	Common Waterbuck	227	243	307	336	345	294
Oryx gazella	Gemsbok	168	140	167	212	215	189
Alcelaphus buselaphus	Hartebeest	135	129	152	175	176	136
Connochaetes taurinus	Blue Wildebeest	205	168	202	247	251	204
Oreotragus oreotragus	Klipspringer	13.5	16	14	11	11	13
Aepyceros melampus	Impala	53	91	72	71	71	74
Litocranius walleri	Gerenuk	35	73	43	46	47	45
Gazella thomsoni	Thomson's Gazelle	23	36	20	23	23	20
Gazella granti	Grant's Gazelle	63	89	50	60	60	52
Oreamnos americanus	Mountain Goat	90	103	95	118	117	98
Ovibos mosachatus	Muskox	282	92	244	202	197	269
Ovis aries	Domestic Sheep	80	93	70	68	69	79
Ovis canadensis	Bighorn	84	166	64	82	82	70

Table 3-2. Mean body masses
and predicted masses for each variable for modern species

Metatarsal			MT1	MT2	MT3
Dama dama	Fallow Deer	44	98	39	36
Axis axis	Axis deer	47	77	42	31
Cervus elaphus	Elk	344	338	399	384
Odocoileus heminous	Mule Deer	74	241	80	94
Odocoileus virginianus	White-tailed Deer	87	223	90	87
Alces alces	Moose	544	405	500	654
Rangifer tarandus	Caribou	81	239	99	119
Antilocapra americana	Pronghorn	48	138	56	55
Taurotragus derbianus	Giant Eland	500	215	497	383
Bison bison	American Bison	616	168	447	489
Kobus ellipsiprymnus	Common Waterbuck	227	171	308	284
Oryx gazella	Gemsbok	168	159	159	142
Alcelaphus buselaphus	Hartebeest	135	165	136	133
Connochaetes taurinus	Blue Wildebeest	205	159	222	186
Oreotragus oreotragus	Klipspringer	13.5	35	13	16
Aepyceros melampus	Impala	53	163	72	71
Litocranius walleri	Gerenuk	35	173	53	50
Gazella thomsoni	Thomson's Gazelle	23	93	21	22
Gazella granti	Grant's Gazelle	63	175	71	64
Oreamnos americanus	Mountain Goat	90	51	109	93
Ovibos mosachatus	Muskox	282	76	258	287
Ovis aries	Domestic Sheep	80	84	71	75
Ovis canadensis	Bighorn	84	116	68	75
Ovis dalli	Dall's Sheep	70	119	67	77

Astragalus			AS1	AS2	AS3	AS4
Dama dama	Fallow Deer	44	39	45	44	41
Axis axis	Axis deer	47	46	44	39	39
Cervus elaphus	Elk	508	475	400	456	378
Odocoileus heminous	Mule Deer	74	93	100	104	94
Odocoileus virginianus	White-tailed Deer	87	103	108	112	99
Alces alces	Moose	550	605	616	570	560
Rangifer tarandus	Caribou	81	134	118	132	121
Antilocapra americana	Pronghorn	48	56	52	58	59
Taurotragus derbianus	Giant Eland	500	518	470	491	502
Bison bison	American Bison	658	566	621	541	554
Kobus ellipsiprymnus	Common Waterbuck	227	315	292	326	349
Oryx gazella	Gemsbok	168	165	143	167	180
Alcelaphus buselaphus	Hartebeest	135	126	129	140	148
Connochaetes taurinus	Blue Wildebeest	205	181	190	202	212
Oreotragus oreotragus	Klipspringer	13.5	14	14	19	15
Aepyceros melampus	Impala	53	69	59	66	67
Litocranius walleri	Gerenuk	35	47	38	37	46
Gazella thomsoni	Thomson's Gazelle	23	21	19	17	19
Gazella granti	Grant's Gazelle	63	62	53	62	60
Oreamnos americanus	Mountain Goat	90	81	119	89	97
Ovibos mosachatus	Muskox	282	205	265	240	268
Ovis aries	Domestic Sheep	80	68	79	79	84
Ovis canadensis	Bighorn	84	72	75	70	69
Ovis dalli	Dall's Sheep	70	64	73	65	65

Table 3-2. Mean body masses
and predicted masses for each variable for modern species

Calcaneum			CL1	CL2	CL3	CL4
Dama dama	Fallow Deer	44	44	44	43	46
Axis axis	Axis deer	47	39	37	49	36
Cervus elaphus	Elk	344	416	409	400	374
Odocoileus heminous	Mule Deer	74	120	82	87	85
Odocoileus virginianus	White-tailed Deer	87	118	96	97	99
Alces alces	Moose	550	604	540	462	521
Rangifer tarandus	Caribou	81	124	126	118	127
Antilocapra americana	Pronghorn	48	53	56	49	49
Taurotragus derbianus	Giant Eland	500	425	437	390	484
Bison bison	American Bison	616	554	521	543	553
Kobus ellipsiprymnus	Common Waterbuck	227	269	265	377	238
Oryx gazella	Gemsbok	168	153	176	166	184
Alcelaphus buselaphus	Hartebeest	135	133	160	179	141
Connochaetes taurinus	Blue Wildebeest	205	165	203	191	201
Oreotragus oreotragus	Klipspringer	13.5	13	13	12	16
Aepyceros melampus	Impala	53	79	86	73	65
Litocranius walleri	Gerenuk	35	53	51	51	44
Gazella thomsoni	Thomson's Gazelle	23	23	21	22	20
Gazella granti	Grant's Gazelle	63	72	78	62	58
Oreamnos americanus	Mountain Goat	90	71	77	96	94
Ovibos mosachatus	Muskox	282	184	233	241	278
Ovis aries	Domestic Sheep	80	71	64	67	66
Ovis canadensis	Bighorn	84	71	70	73	72
Ovis dalli	Dall's Sheep	70	65	73	67	66

Cubonavicular			CN1
Axis axis	Axis deer	47	34
Cervus elaphus	Elk	344	347
Odocoileus heminous	Mule Deer	74	84
Odocoileus virginianus	White-tailed Deer	87	84
Alces alces	Moose	550	505
Rangifer tarandus	Caribou	81	95
Antilocapra americana	Pronghorn	48	50
Taurotragus derbianus	Giant Eland	500	488
Bison bison	American Bison	699	637
Kobus ellipsiprymnus	Common Waterbuck	227	290
Oryx gazella	Gemsbok	168	168
Alcelaphus buselaphus	Hartebeest	135	150
Connochaetes taurinus	Blue Wildebeest	205	217
Oreotragus oreotragus	Klipspringer	13.5	13
Aepyceros melampus	Impala	53	79
Litocranius walleri	Gerenuk	35	56
Gazella thomsoni	Thomson's Gazelle	23	24
Gazella granti	Grant's Gazelle	63	72
Oreamnos americanus	Mountain Goat	90	99
Ovibos mosachatus	Muskox	282	215
Ovis aries	Domestic Sheep	80	74
Ovis canadensis	Bighorn	84	68
Ovis dalli	Dall's Sheep	70	67

Table 3-3. Summary of componants of regression equations predicting body mass and errors

Element	Variable	YIntercept	R^2	r	%SEE	%PE	Slope	Shape
Scapula	Glenoid	-2.964	0.951	**0.975**	26.183	17.121	**1.639**	Area
Humerus	GL	-5.172	0.869	**0.932**	40.929	29.257	**3.066**	Length
	50AP	-1.788	0.921	**0.96**	30.617	21.022	**1.289**	Area
	Volume 1	-2.527	0.983	**0.991**	14.288	11.217	**0.947**	Volume
	Volume 2	-1.897	0.961	**0.98**	22.744	17.203	**0.915**	Volume
	Volume 3	-2.043	0.964	**0.982**	21.339	15.586	**0.914**	Volume
Radius	GL	-5.802	0.799	**0.894**	61.065	40.611	**3.283**	Length
	Area	-2.142	0.976	**0.988**	18.032	13.074	**1.362**	Area
Ulna	UlOle	-3.095	0.95	**0.975**	25.314	19.653	**2.844**	Length
	TrNotch	-1.897	0.939	**0.969**	28.529	20.815	**1.355**	Area
Metacarpal	GL	-2.132	0.272	**0.522**	139.332	70.459	**1.792**	Length
	PrSArea	-2.337	0.973	**0.986**	18.304	13.992	**1.495**	Area
	DsVolume	-2.25	0.966	**0.983**	20.504	15.738	**1.028**	Volume
Magnum Carpal	Volume	-1.857	0.975	**0.987**	18.032	13.178	**0.991**	Volume
Femur	GL	-6.544	0.926	**0.962**	33.045	23.499	**3.514**	Length
	50AP	-2.04	0.972	**0.986**	19.124	14.21	**1.427**	Area
	VolFmHd	-2.381	0.96	**0.98**	23.311	18.128	**1.021**	Volume
	SAFmHd	-3.3	0.962	**0.981**	22.462	17.726	**1.537**	Area
Tibia	GL	-7.057	0.722	**0.85**	73.78	46.071	**3.636**	Length
	DsBd	-2.89	0.968	**0.984**	20.504	14.136	**3.063**	Diameter
	PrSaQ	-2.988	0.962	**0.981**	22.744	16.042	**1.513**	Area
	PrSaR	-3.028	0.958	**0.979**	23.88	16.655	**1.509**	Area
	DsTibia	-2.704	0.973	**0.986**	18.85	13.642	**1.561**	Area
Metatarsal	GL	-2.415	0.328	**0.573**	129.087	67.548	**1.877**	Length
	PrSArea	-2.708	0.97	**0.985**	19.124	13.902	**1.606**	Area
	DsVolume	-2.58	0.959	**0.979**	22.744	16.11	**1.106**	Volume
Astragalus	GL	-3.222	0.965	**0.982**	21.899	14.522	**3.181**	Length
	GW	-2.629	0.974	**0.987**	18.304	12.714	**3.182**	Diameter
	Volume	-2.588	0.961	**0.98**	23.027	14.151	**1.07**	Area
	Area	-2.472	0.967	**0.983**	21.06	14.358	**1.63**	Volume
Calcaneum	GL	-4.66	0.942	**0.971**	27.938	18.779	**3.375**	Length
	Sus	-2.904	0.959	**0.979**	23.027	14.743	**3.185**	Diameter
	PrSArea	-2.159	0.959	**0.979**	23.027	14.158	**1.529**	Area
	DsSArea	-2.602	0.976	**0.988**	17.22	10.943	**1.574**	Area
Cubonavicular	Area	-2.606	0.967	**0.983**	20.504	13.702	**1.551**	Area

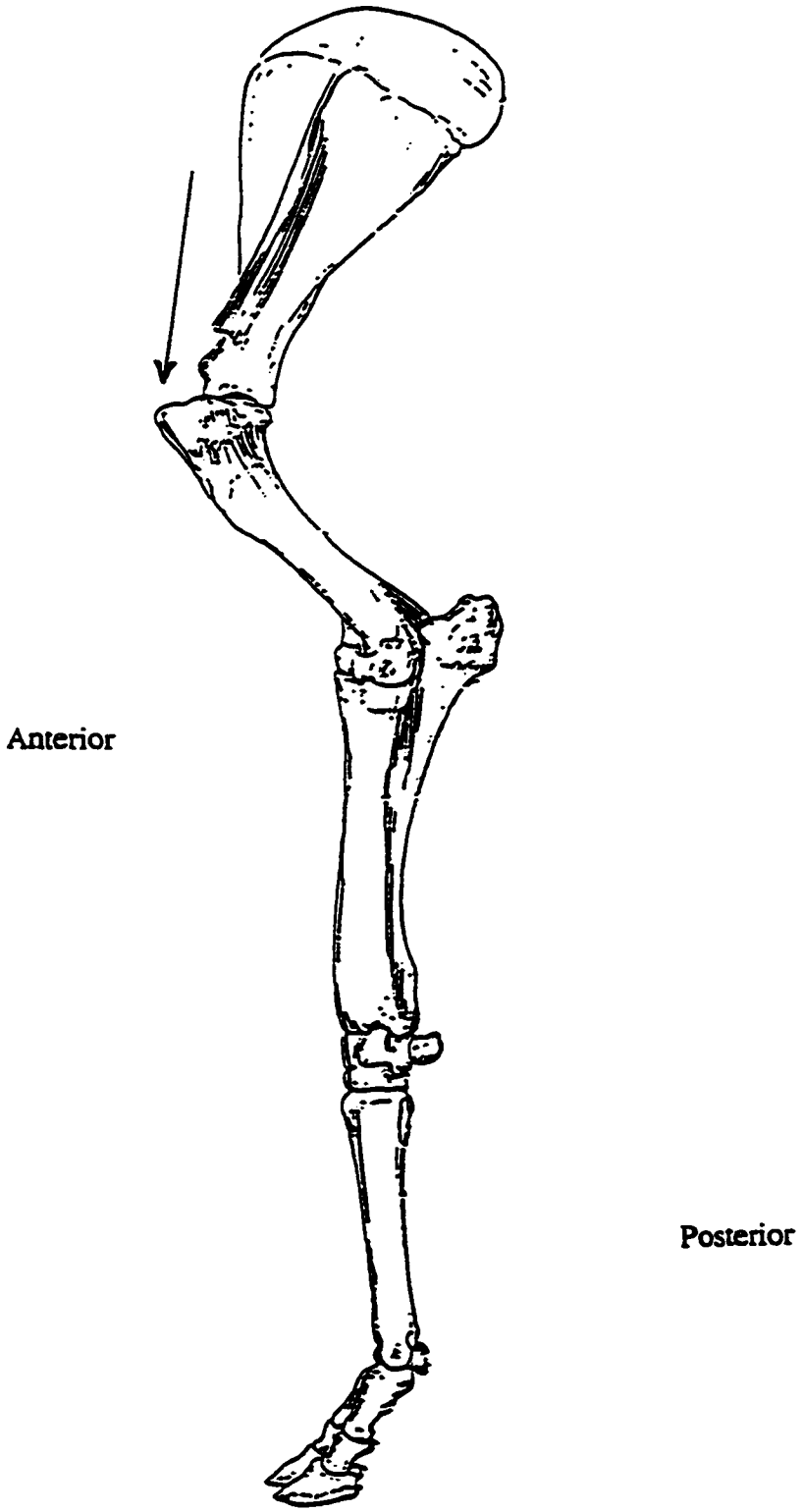

Fig. 3-4. Ungulate forelimb showing scapular near vertical orientation.

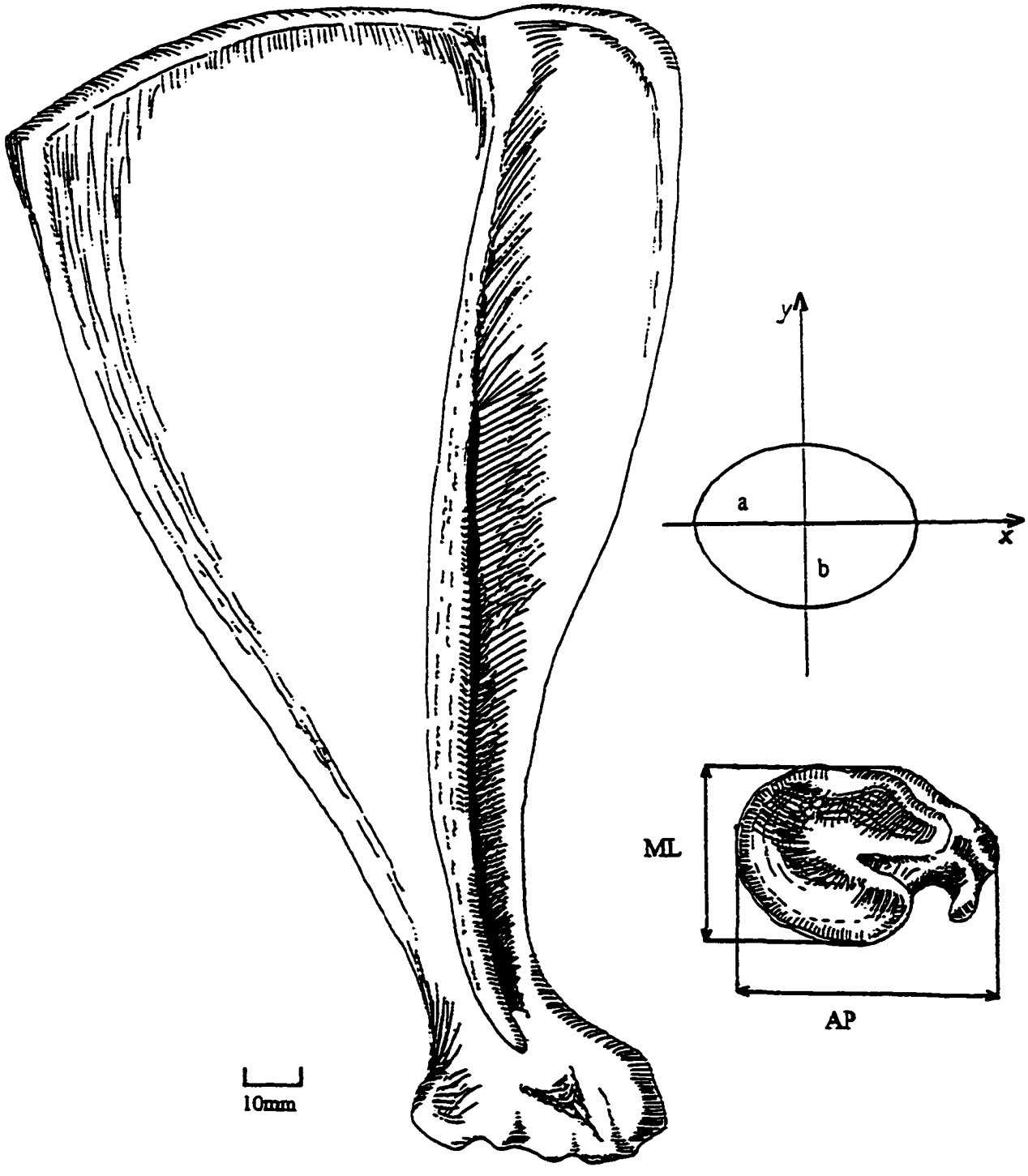

Fig 3-5. Measurements of the scapula in mm. ML = medio-lateral; AP = antero-posterior; a = radius of AP measurement; b = radius of ML measurement; area of ellipse (glenoid fossa) = πab. Ellipse reproduced with permission of Academic Press.

and a correlation coefficient (r) of .972 (Fig.3-6). The %PE of 18 and the %SEE 28, indicating good prediction of mass from this variable. The slope conforms to none of the similarity principles; geometric (1.5), elastic (1.33), or static stress (1.25), and reveals a positive allometry, indicating that the glenoid fossa is larger than would be expected from the models (Table 3-2).

Humerus

Greatest length of the humerus — A number of useful variables were identified for the humerus (Fig.3-7). Using a simple linear regression, length (HM1) yielded an r of .932 with a %PE of 30 and a %SEE of 41. The %PE and %SEE are higher for this variable than for any of the other humeral variables, indicating length may not be the best predictor of body mass. The slope was 3.066, indicating that humeral length conforms closely to the slope for geometric similarity of 3.0 (Fig.3-8A), which would seem to agree with the findings of Alexander et al. (1979) who suggested that limb lengths increase isometrically in size. The slope, however, is the "best fit' line, and closer examination of the results reveals that there may be a number of other factors at work.

Cross-sectional area of the mid-diaphysis — The cross-sectional area of the shaft (HM2), obtained from the squared diameter, also proved to be a reasonable predictor of mass, with an r of .960 and a %PE of 21 and %SEE of 31. Results of the multiple stepwise regression excluded the cross sectional area in the final model, in favor of the volume 1 of the distal articular surface (HM3). The regression produced a slope of 1.289 (Fig.8B) which conforms closely to the predicted slope of 1.25 for static stress similarity

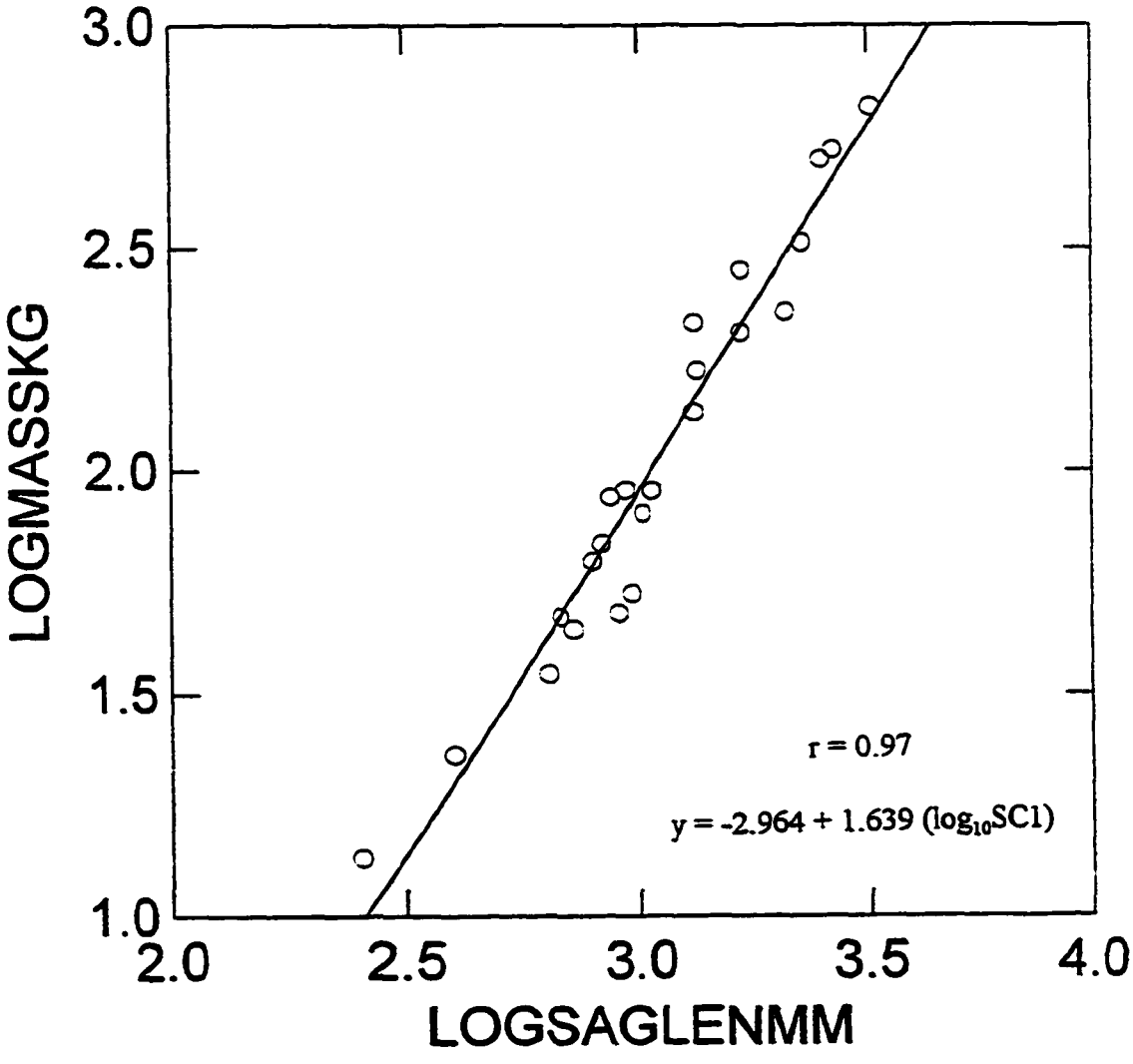

Fig. 3-6. Log_{10} body mass plotted against log_{10} surface area glenoid fossa (mm^2). SC1 = Surface area of the glenoid modeled on a circle.

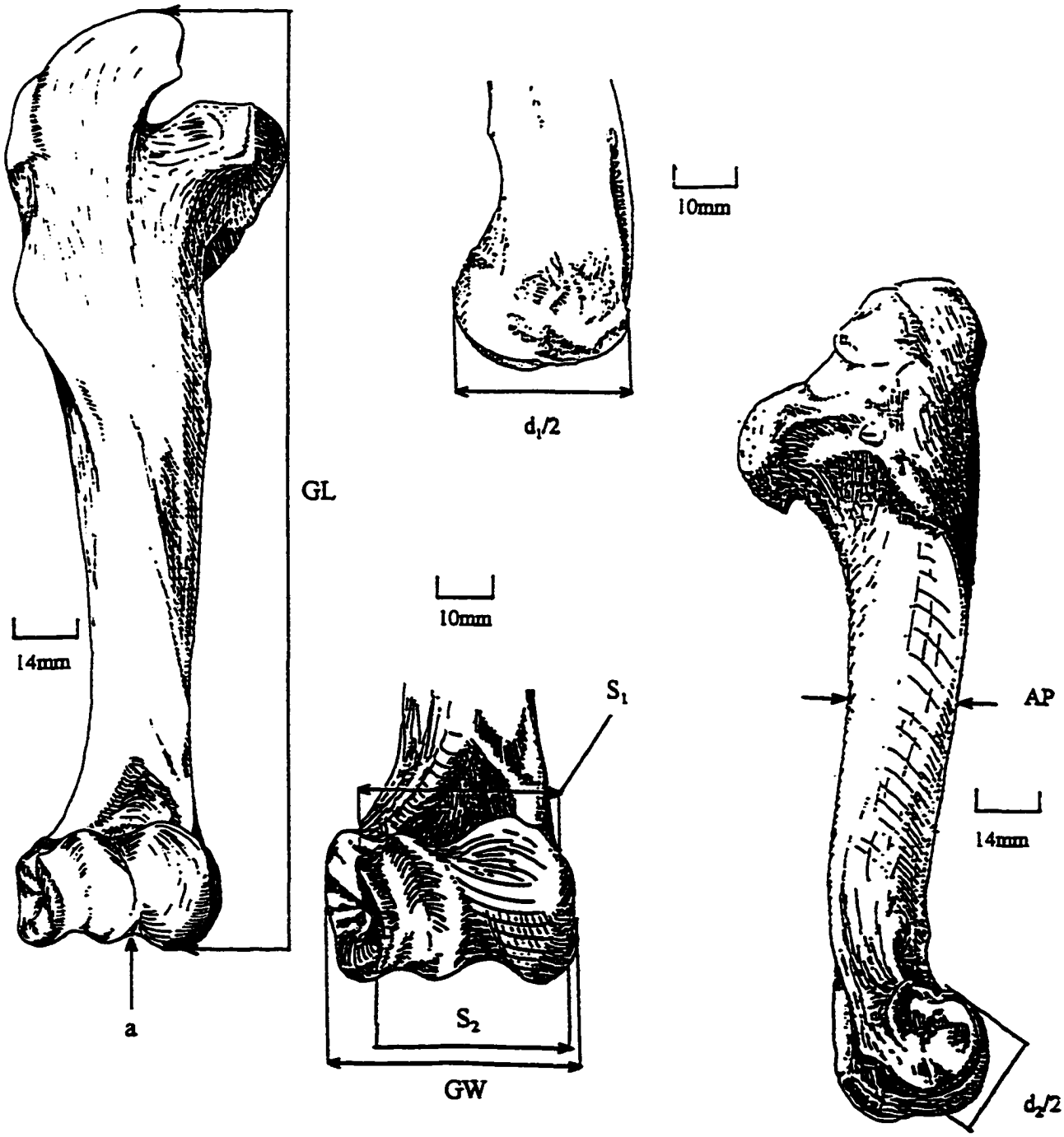

Fig. 3-7. Measurements of the humerus in mm. GL = greatest length, AP = antero-posterior measurement at mid-shaft; $d_1/2 = r_1$ is the AP measurement of medial trochlea; $d_2/2 = r_2$ or Q is the measurement of the lateral trochlea; S_1 = dorsal side distance from trochlea to capitulum; S_2 = ventral side distance from trochlea to capitulum; GW = distance from capitulum to medial epicondyle; h = distance from lateral to medial epicondyle; a = least diameter humeral condyle.

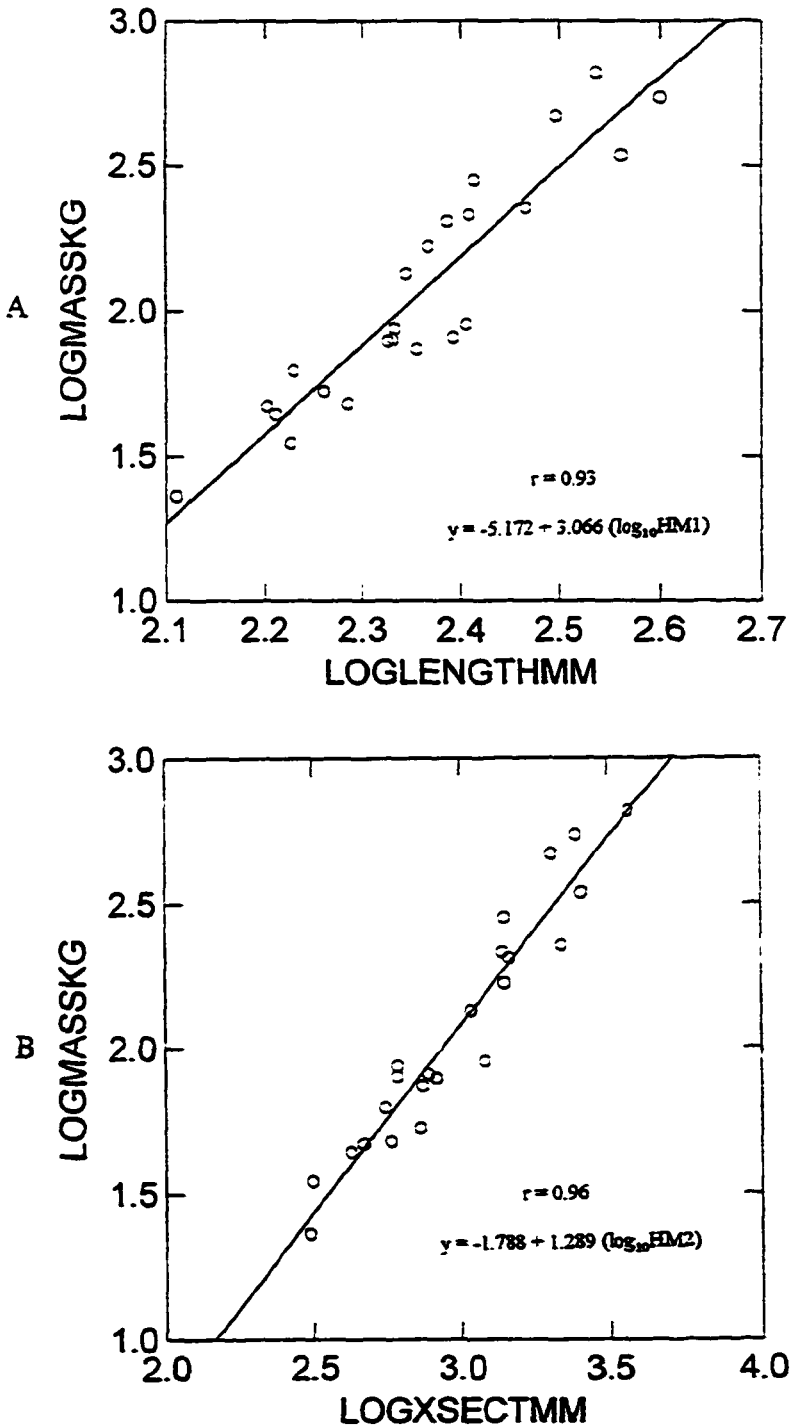

Fig.8A. Log_{10} mass in kg plotted against log_{10} length of the humerus in mm (HM1).
Fig.8B. Log_{10} mass in kg plotted against log_{10} cross-sectional area of the humerus at midshaft (HM2) in mm^2.

(Biewener 1989). The slope implies that some of the larger pecorans have humeri that are thinner than would be expected from isometry, while some of the smaller forms have thicker humeri.

Volume 1 of the distal articulation — This variable (HM3) was modeled on an hyperboloid of revolution of one sheet (Fig.3-9A). HM3 was by far the best predictor of body mass of all of the variables of the humerus, was tightly correlated to mass with an $r = .992$. Results of the multiple stepwise regression left HM3 alone in the final model. The regression slope was 0.947, indicating that the volume of the articulation of the distal humerus scales proportionally to body mass, close to the expected slope of 1.0 (Fig.10A). The %PE was 13 and the %SEE 14, indicating a relatively small error and very good predictability of the regression equation. This variable appears to be an excellent predictor of the volume of bone mass contained within the articulation.

Volume 2 of the distal articulation — The second volume (HM4) was modeled on an obliquely cut right circular cylinder (Fig.9-B). The regression slope for this model is 0.915 (Fig.10B). While the slope is also close to 1.0, it is less than of HM3, and indicates a slight negative allometry. Here, $r = .980$, the %PE was 19 and the %SEE 23, implying this is also a good predictor of mass when used by itself. Most of the body mass estimates were within a reasonable range of approximately 10%-15%. The masses of the two largest species however, *Alces alces* and *Bison bison*, were underestimated by 25%.

Volume 3 of the distal articulation — The final geometric shape used to model the volume of the distal humerus (HM5) was that of a frustrum of a right circular cone (Fig.9-C). For this shape, %PE was 17, %SEE 21, the correlation coefficient was .982.

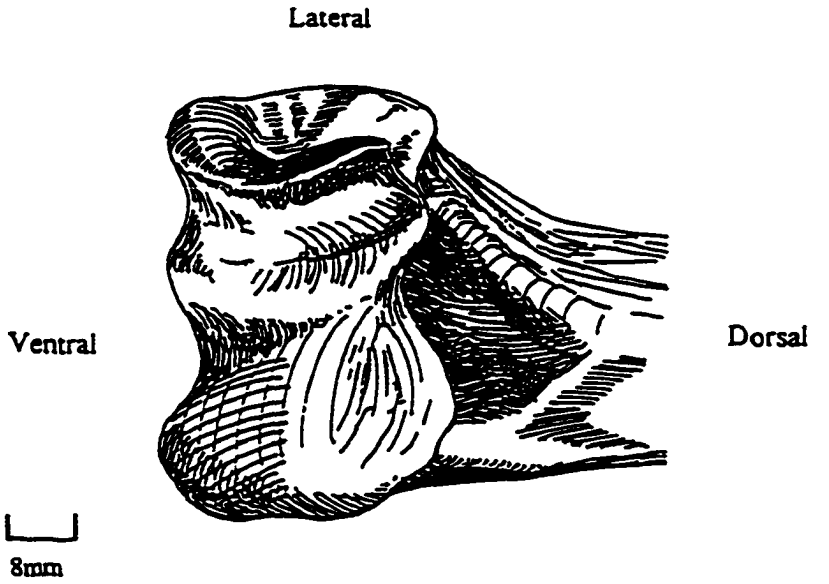

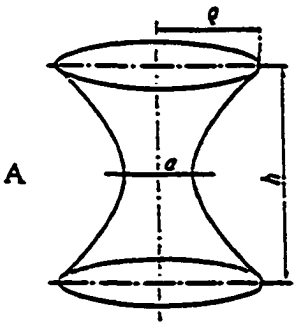

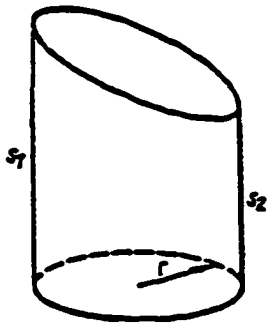

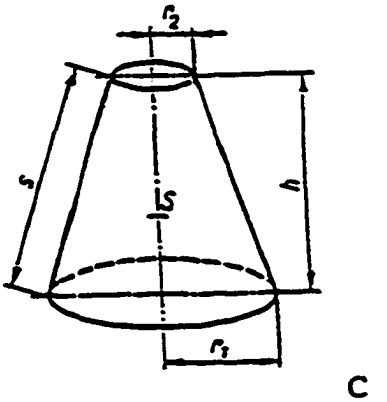

Fig. 3-9A. Hyperboloid of revolution; distal humerus.
Fig. 3-9B. Obliquely cut right circular cylinder; distal humerus.
Fig. 3-9C. Frustrum of a right circular cone; distal humerus.
Figures reproduced with permission from Academic Press.

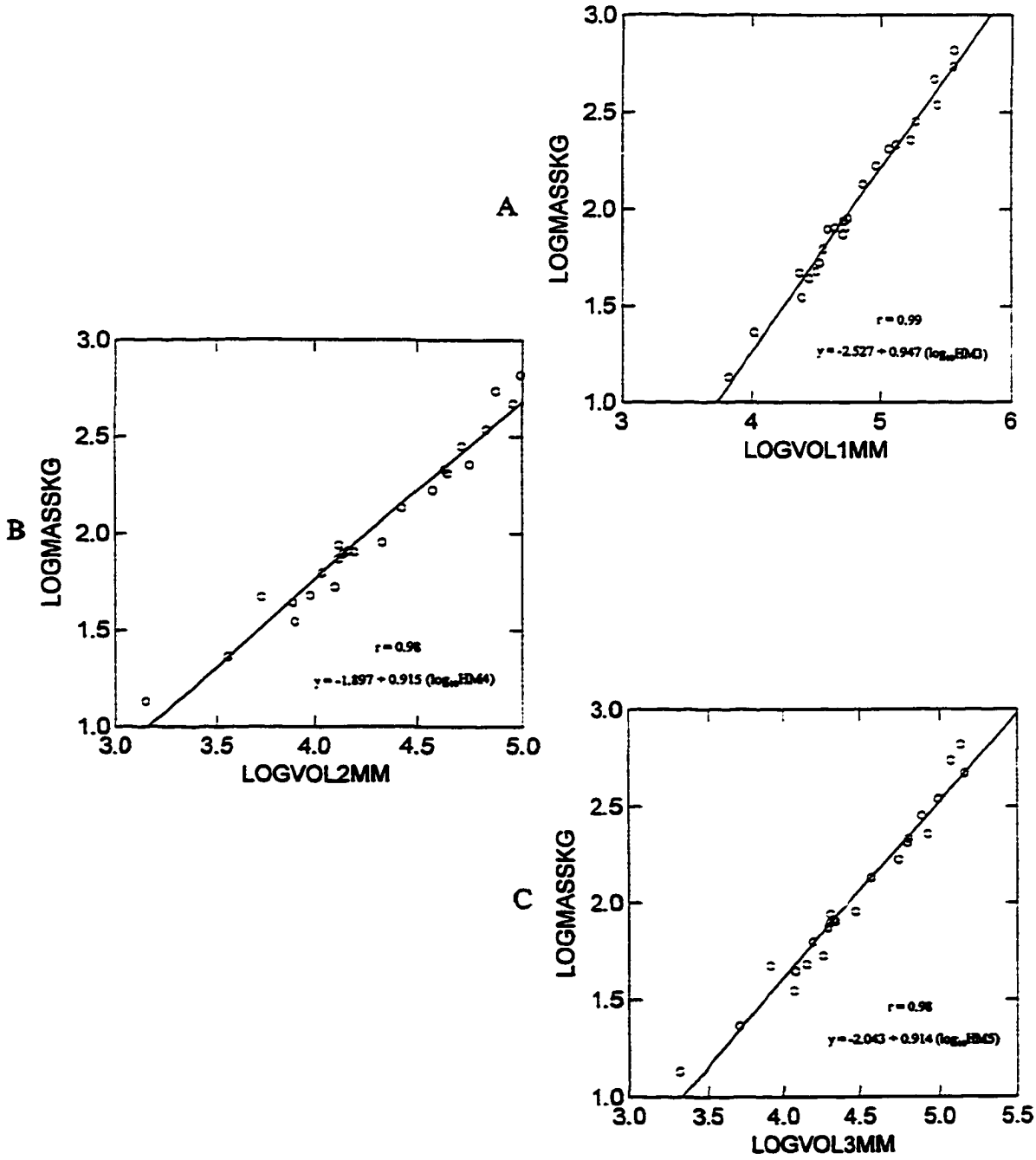

Fig. 3-10A. Log_{10} body mass (kg) against log_{10} HM3 = Hyperboloid of revolution.
Fig. 3-10B. Log_{10} body mass (kg) against log_{10} HM4 = Oblique right circular cylinder.
Fig. 3-10C. Log_{10} body mass (kg) against log_{10} HM5 = Frustrum of a right circular cone.

As with HM4, used by itself, this is a good predictor of body mass. The regression slope is 0.914 (Fig.10C), again scaling fairly close to isometry, but not as close as volume 1 (HM3). This variable was also left out of the final model generated by multiple stepwise regression, but only because volume 1 (HM3) showed such a high correlation to mass. Once again, the masses of the two largest species, moose (*Alces alces*) and bison (*Bison bison*), are underestimated by 20%-25%.

All of the humeral variables correlate highly to body mass, with correlation coefficients (r) ranging between .932-.992. Based upon the correlation coefficient, the %PE and the %SEE, or the volume of the distal humerus articulation based on the hyperboloid of revolution (HM3) is the best predictor of body mass. The other variables in descending order of importance are the volume of the distal humerus based on a right circular cone (HM5), the volume based on a right circular cylinder (HM4), the diaphyseal cross sectional area (HM2), and lastly the length of the humerus (HM1). In the event of a fragmentary humerus, any one of these variables can be used to predict body mass with a reasonable degree of accuracy.

Radius

Greatest length of the radius — Based upon the %PE (41) and the %SEE (61), the length of the radius (RD1) is not a good predictor of mass (Table 3-3). The r was .894 and the slope of the regression was 3.283 and conforms to none of the similarity models (Fig.12A).

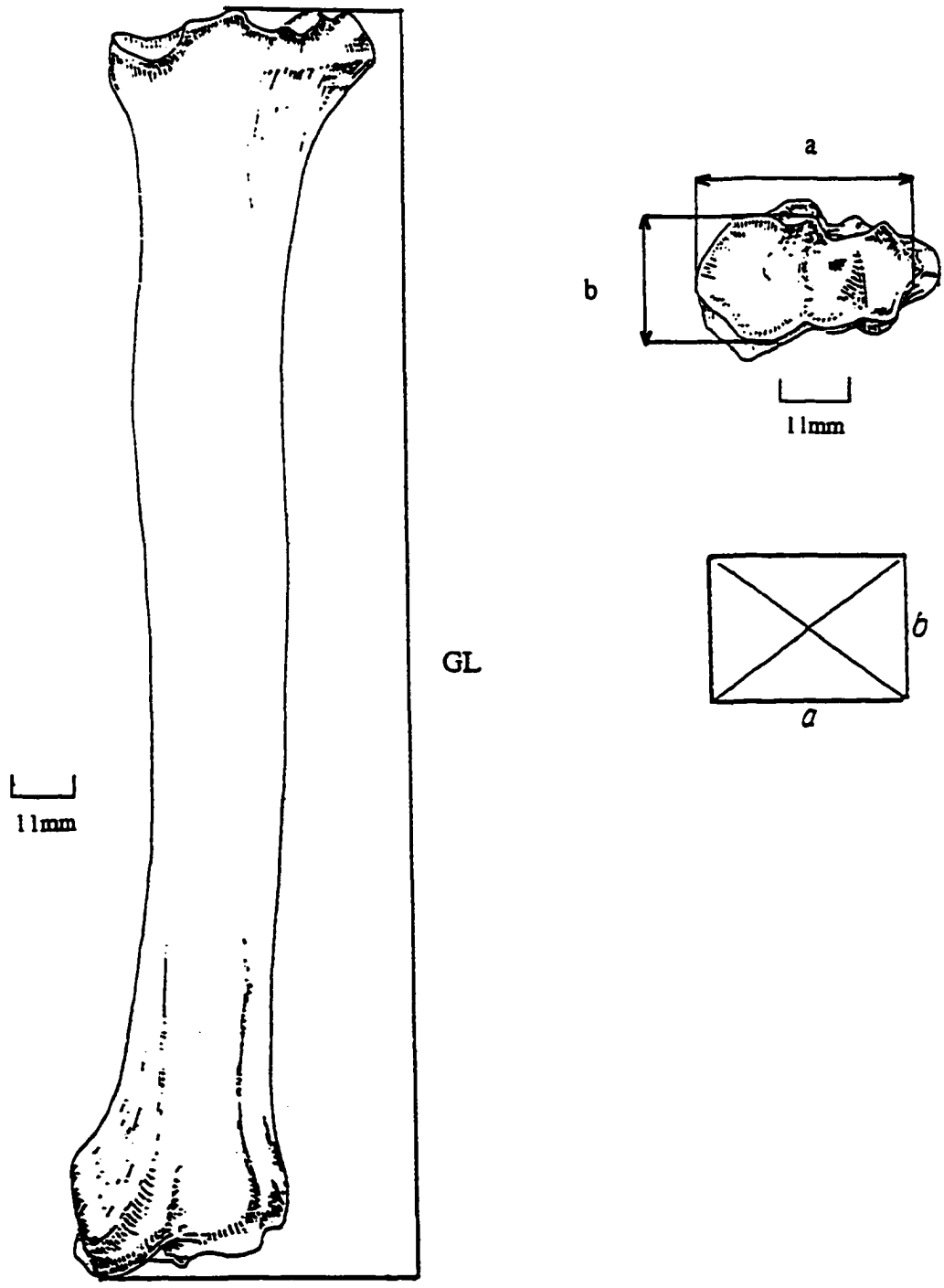

Fig. 3-11. Surface area of the proximal radius articulation. GL = greatest length, a = medio-lateral measurement; b = antero-posterior measurement. Rectangle reproduced with permission from Academic Press.

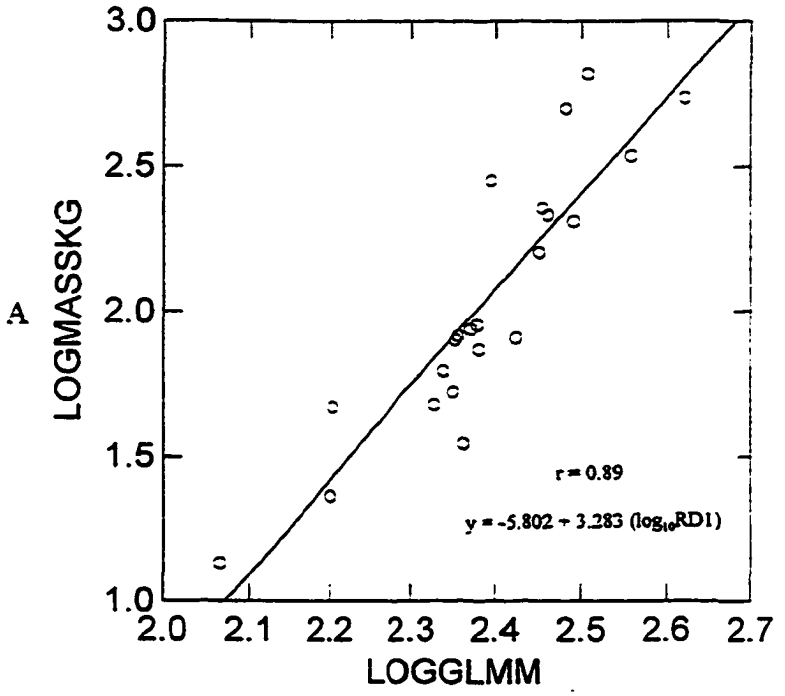

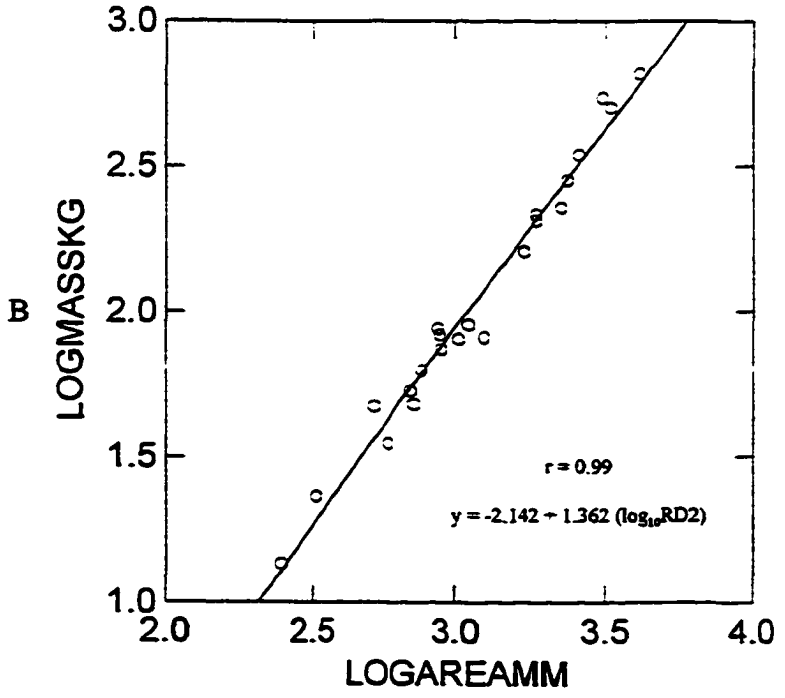

Fig. 12A. Log_{10} mass in kg plotted against log_{10} greatest length of the radius (RD1) mm.
Fig. 12B. Log_{10} mass in kg plotted against log_{10} surface area of proximal radius (RD2) in mm^2.

Surface area of the proximal articulation — This articulation was modeled on a rectangle (Fig.3-11) and showed an extremely tight correlation to body mass (r = .988). The %PE was 13, and the %SEE 18 and is thus a very good predictor of mass in pecorans. The stepwise regression kept this variable (RD2) in the model and rejected greatest length of the radius as an inadequate predictor of mass. The regression slope of 1.362 implies a scaling that corresponds to McMahon's elastic similarity principle (Fig.12B.).

For the radius, the proximal articular surface area is a much better predictor of mass than is the length of the radius. The masses of the three largest bovids are again underestimated in mass, but only by about 15%. The body mass estimation for the pronghorn is within 5% of the observed mass.

Ulna

Length of the olecranon — The length of the olecranon (UL1) was measured from the anconeal process to the top of the olecranon tuberosity (Fig.3-13). The regression slope of this variable is 2.844, which is less than the 3.0 one would expect for geometric similarity (Fig.14A). Upon regressing olecranon length on body mass, the resultant regression slope is 0.334, which correlates to geometric similarity (0.33). The correlation to body mass was high (r = 0.975), and the %PE of 20 and %SEE of 25 indicates that olecranon length is a good predictor of mass. The largest species were overestimated in mass by 10%-20%. The mass of the caribou was overestimated by 25%.

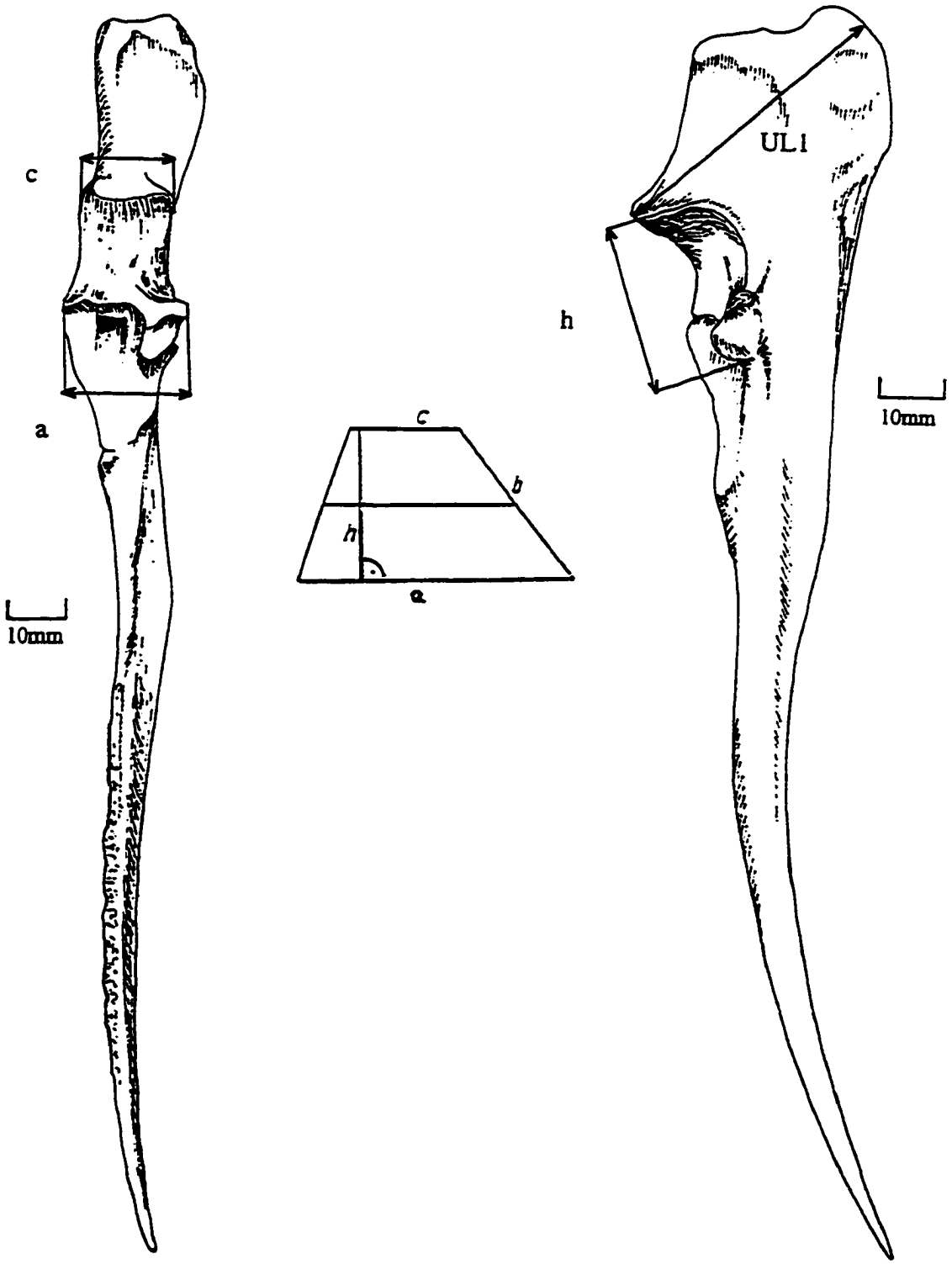

Fig. 3-13. Measurements of the ulna. UL1 = length of the olecranon from anconeal process to olecranon tuberosity; h = height of trochlear notch from coronoid process to anconeal process; c = least width of trochlear notch; a = greatest width of trochlear notch. Trapezoid reproduced with permission from Academic Press.

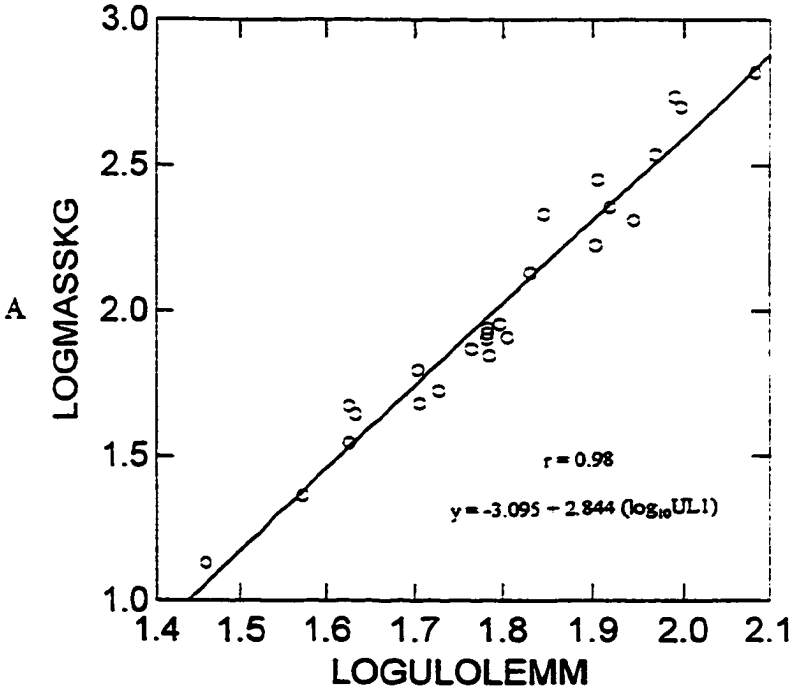

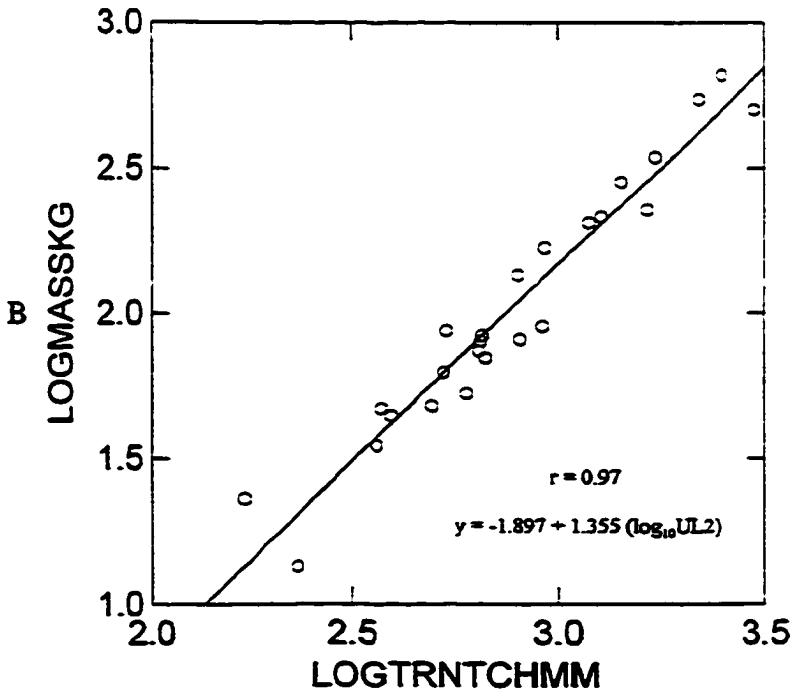

Fig. 14A. Log_{10} mass in kg plotted against log_{10} length of the olecranon (UL1) (mm).
Fig. 14B. Log_{10} mass in kg plotted against log_{10} surface area trochlear notch (UL2)(mm^2).

Area of the trochlear notch — The area of the trochlear notch (UL2) was modeled on a trapezium (Fig.3-13) and the regression of body mass on this variable produced an r of 0.969. The slope of the regression line was 1.355, and corresponded closely to the slope predicted by elastic similarity (Fig.14B). The %PE was 21, and the %SEE 29, indicating that this variable as well as the length of the olecranon is a very good predictor of mass. Stepwise regression included the area of the trochlear notch (mm^2) as well as that of the length of the olecranon in the final model.

Masses of the largest species were again either overestimated or underestimated by 10%-20%. The mass of the caribou was again overestimated by 25%, and this seems to indicate an increased robusticity of the limbs for this species.

Magnum

Volume of the magnum — The volume of this element was modeled on a spherical segment of two bases (Fig.3-15). The slope of the regression was 0.991, or essentially the slope of 1.0 expected for all of the similarity models (Fig.3-16). The volume of the carpal (MN1) shows a very tight correlation to body mass (0.987). The %PE was 13, and the %SEE 18, suggesting extremely good predictability and accuracy from this element. Once again, the masses of two of the largest bovids, bison and eland, were underestimated by 20%. Most of the other weight estimates were within 10% of the observed weights. Since carpals and tarsals are often preserved in the fossil record due to the dense nature of these elements, it is encouraging to find such a high correlation to body mass (Kreutzer 1992).

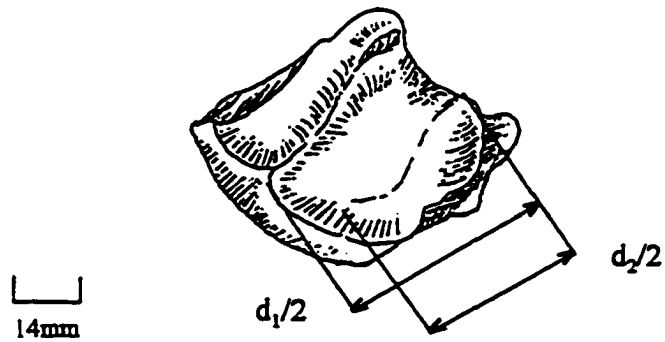

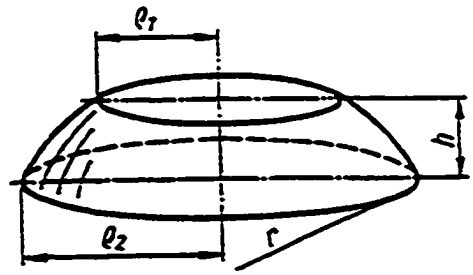

Fig. 3-15. Measurements of the magnum. $Q_1 = d_1/2$; $Q_2 = d_2/2$; h = height of magnum measured dorso-ventrally.

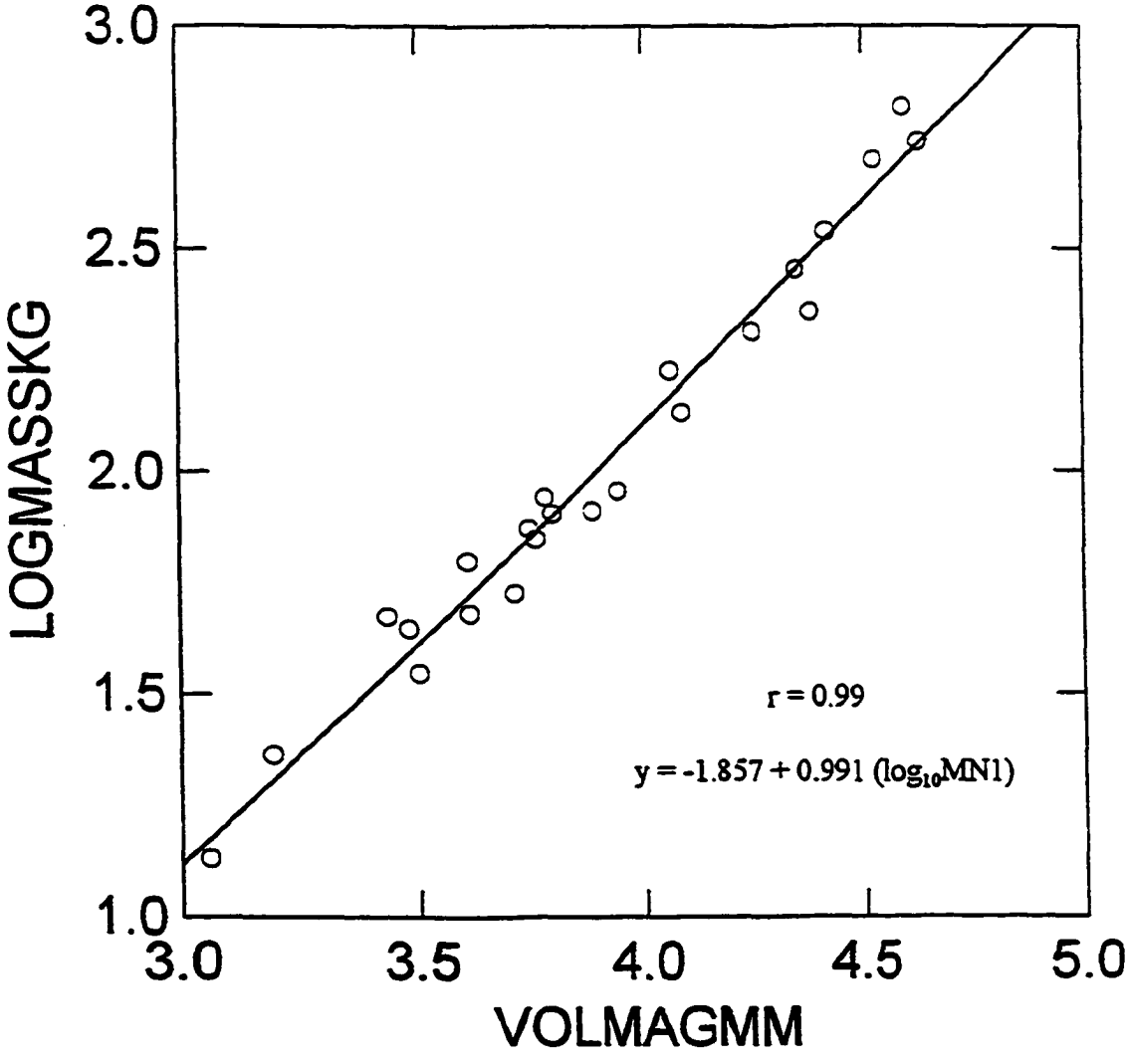

Fig. 3-16. Log_{10} body mass (kg) plotted against log_{10} volume of the magnum (MN1) in mm^3.

Metacarpal

Greatest length of the metacarpal — Several studies have shown that the length of the metacarpal (Fig.3-17A) is a poor predictor of mass in pecorans (Alexander et al. 1979; Scott 1985; Gingerich 1990). This is presumably due to the fact that metapodials increase or decrease in length with locomotory or habitat adaptations, and is more highly correlated to those parameters than to mass. The results of this study confirm the previous findings. The regression of body mass to length (MC1) produced a slope of 1.792. In looking at the plot of the regression, the slope cannot be interpreted as being meaningful. (Fig.3-18A). The length of the metacarpal appears to be largely uncorrelated to mass, with a number of large species having shorter metacarpals than would be expected from the mass, and a number of smaller species having longer elements than would be expected from the mass. The correlation coefficient of 0.522 was the lowest of all of the variables tested. Similarly, the %PE of 70 and the %SEE of 139 indicate both poor accuracy and predictability.

Carpal articular surface — The proximal articular surface of the metacarpal (MC2) was modeled on a trapezium (Fig.3-17B). The regression against body mass yielded a slope of 1.495, which indicates that the surface area increases isometrically, despite the fact that the length of the metacarpal is idiosyncratic (Fig.3-18B). This variable underestimates the weights of the largest pecorans by only 15%, coinciding with low predictions of masses in species by other variables. The mass of the caribou is overestimated by about 20%. The correlation coefficient was 0.986, the %PE 14, and the %SEE 18. Multiple stepwise regression kept this variable as the only one in the final

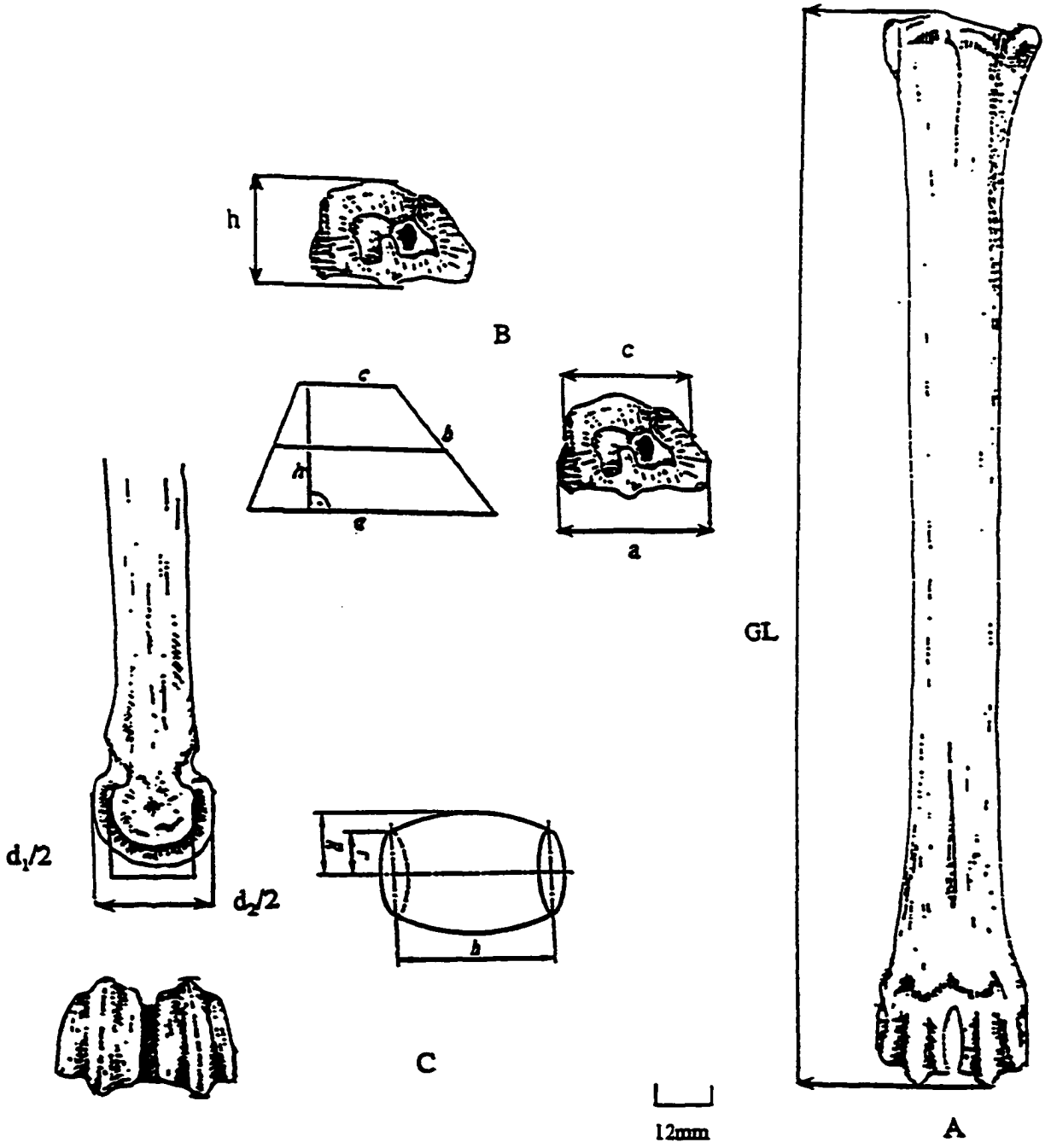

Fig. 3-17A. Greatest length of the metacarpal.
Fig. 3-17B. Proximal surface area of the metacarpal modeled on a trapezium; h = antero-posterior height of articulation; c = least medio-lateral width of articulation; a = greatest medio-lateral width of articulation.
Fig. 3-17C. Distal articulation of metacarpal modeled on a barrel; h = medio-lateral width of articulation; $r = d_1/2$; $R = d_2/2$. Figures of barrel and trapezium with permission from Academic Press.

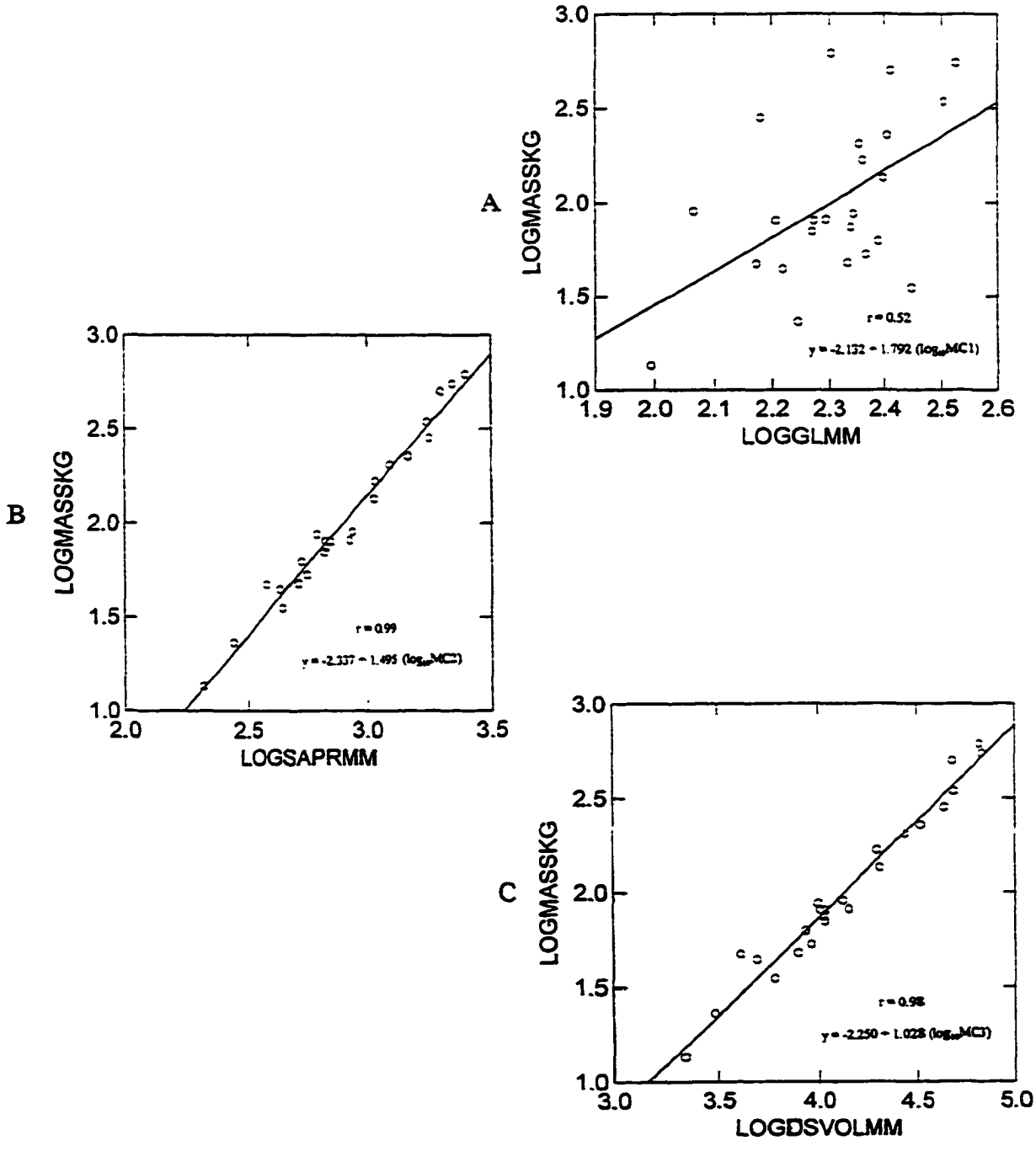

Fig. 3-18A. Log_{10} body mass (kg) plotted against log_{10} metacarpal length (MC1) (mm).
Fig. 3-18B. Log_{10} body mass (kg) plotted against log_{10} proximal area (MC2) (mm^2).
Fig. 3-18C. Log_{10} body mass (kg) plotted against log_{10} distal volume (MC3) (mm^3).

model, although by itself, the volume of the distal articulation is also a good predictor of mass.

Volume of the distal articulation — This variable (MC3), modeled the distal articular surface area of the metacarpal on the volume of a barrel (Fig.3-17C). The slope of the regression line was 1.028, very close to the slope of 1.0 that would be predicted by isometry. This regression produced a very tight correlation of volume of the articulation to mass with an $r = 0.983$ (Fig.3-18C). The %PE was 16, and the %SEE 21, implying that this variable is almost as good a predictor of mass as is MC2.

Interestingly, the volume of this articular surface predicted the mass of the largest cervid, the moose (*Alces alces*) within 1%. The mass of the two largest bovids, *Bison* and the eland (*Taurotragus derbianus*) were once again underestimated by 15%-20%. It may be there are fewer osteological characters available that can accurately estimate body mass in large bovids, due to skeletal modifications that have been made in order to accommodate the increased mass within this family. *Rangifer* is again an outlier, with the mass overestimated by 25%. The volume of this articulation adheres to geometric similarity, and in the case of fragmentary remains, should prove to be an excellent predictor of body mass.

Femur

Length of the femur — The regression slope for the length of the femur (FM1) is 3.514, which conforms to neither geometric (3.0) nor elastic similarity (4.0) (Fig.3-20A).

The correlation coefficient for this variable is 0.962, with the %PE 24 and the %SEE 33. Three large bovids, bison, eland and musk-ox, fall above the regression line, indicating shorter and more robust femurs than would be expected from their mass. When the limb proportions are examined, however, the length of the femur (Fig.3-19), is greater than of the tibia in all three cases, again showing the "force-directed" changes noted by Scott (1979) for large bovids.

Cross sectional area of the midshaft of the femur — This variable is the best predictor of body mass using both the correlation coefficient (0.986) and %PE (14) and %SEE (19). The slope of the regression is 1.427, which is actually somewhat closer to the slope for elastic similarity (Fig.3-20B). Stepwise regressions included only the cross sectional area of the midshaft (FM2) in the final model. However, all of the other variables correlate tightly to mass, and this particular measure necessitates an entire femur to take an accurate measurement, rendering it somewhat less useful than the other variables. Mass predictions for the entire size range are much more accurate for this variable than for length, and should be used preferentially when possible. *Ovibos moschatus* and *Bison bison* were again underestimated in mass by slightly less than 20%. Other mass estimates are considerably more accurate.

Volume of the femoral head — This variable (FM3) is modeled on a spherical segment (Fig.3-19). This variable proved to be a very good predictor of mass, in all but some of the largest species, with the %PE 18, and the %SEE 23. The volume of the femoral head shows a tight correlation to body mass, with $r = 0.98$. The slope of the regression was 1.021 (Fig.3-21A) scaling very close to the predicted 1.00.

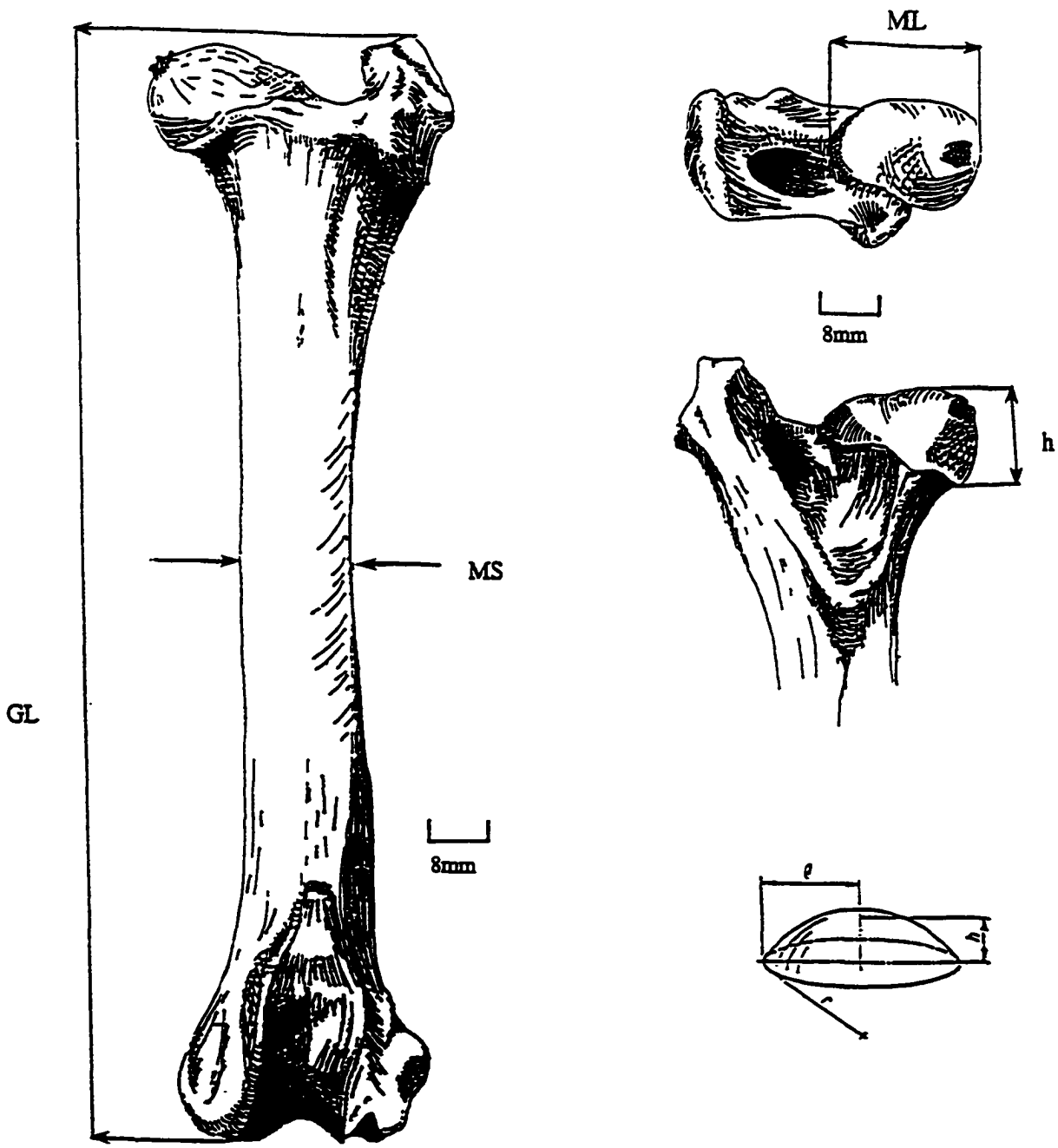

Fig. 3-19. Measurements of the femur. GL = greatest length; MS = medio-lateral mid-shaft measurement; h = height of the femoral head; ML = medio-lateral measurement of femoral head; Q = ML/2. Figure of spherical segment with permission.

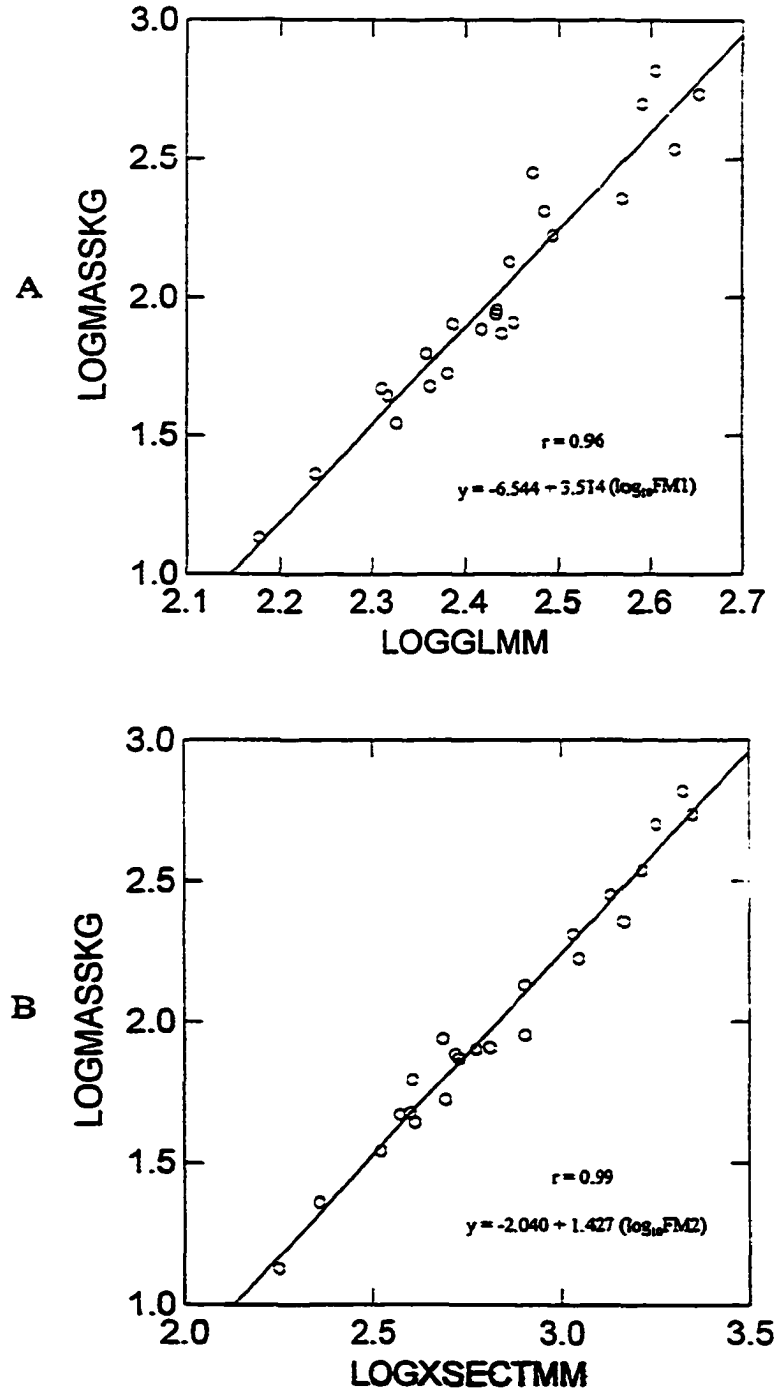

Fig. 3-20A. Log_{10} body mass plotted against log_{10} greatest length of femur (FM1) in mm.
Fig. 3-20B. Log_{10} body mass plotted against log_{10} cross-sectional area (FM2) in mm^2.

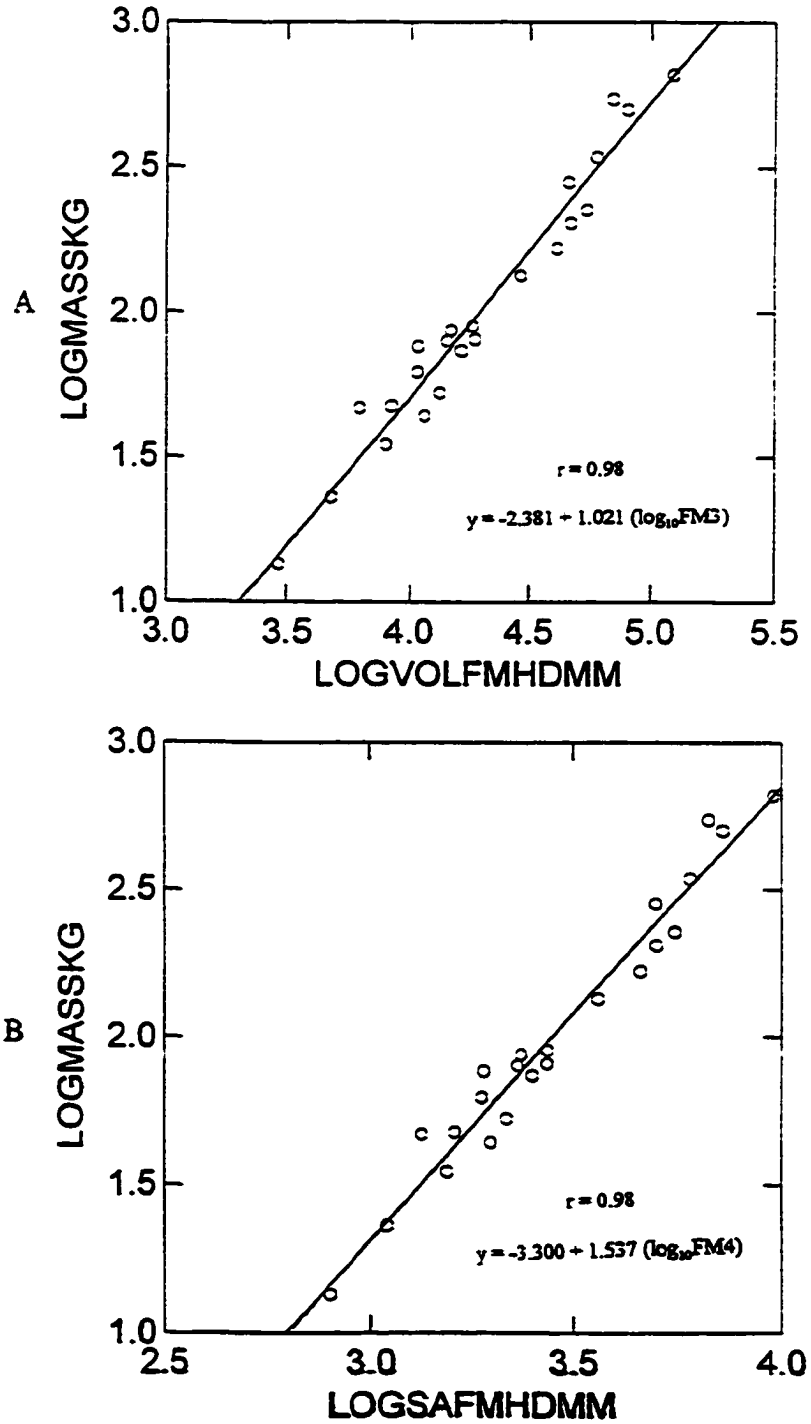

Fig. 3-21A. Log_{10} body mass (kg) plotted against log_{10} femoral head volume (FM3) mm^3.
Fig. 3-21B. Log_{10} body mass (kg) plotted against log_{10} surface area femoral head (FM4) in mm^2.

Surface area of the femoral head — The surface area of the femoral head (FM4) was also modeled on a spherical segment, using the formula for the area of the curved portion (Fig.3-19). This variable correlates tightly to mass, with an r of 0.981. The %PE was 18, and the %SEE 22 indicating that this variable is a very good predictor of the dependent variable of body mass, comparable to the volume of the femoral head. The slope of the regression is 1.537, which coincides with geometric similarity (Fig.3-21B). Although the surface area was left out in the final stepwise regression model, the femoral head is frequently preserved in the fossil record, and by itself is an excellent predictor of mass.

Tibia

Greatest length of the tibia — The length of the tibia (TA1) is not as good a predictor of body mass as are the other variables for this element. The correlation coefficient is 0.85, and the slope of the regression is 3.636 which lies between exponents for similarity models (Fig.3-23A). The %PE is 46, and the %SEE is 74, which implies that this variable is not a good predictor of mass. Although the cluster around the regression line is not that tight, the three largest bovids, musk-ox, bison and eland, all are extreme outliers with much shorter tibiae than expected from observed body mass.

Distal breadth of the tibia — The breadth of the distal tibia (TA2) is a good predictor of body mass in modern pecorans (Fig.3-22). The correlation coefficient was 0.984, and the slope of the regression 3.063, very close to that predicted by isometry (Fig.3-23B). The %PE was 14, and the %SEE 21, indicating good predictability for this variable. While the stepwise regression eliminated the distal breadth in the final model, by

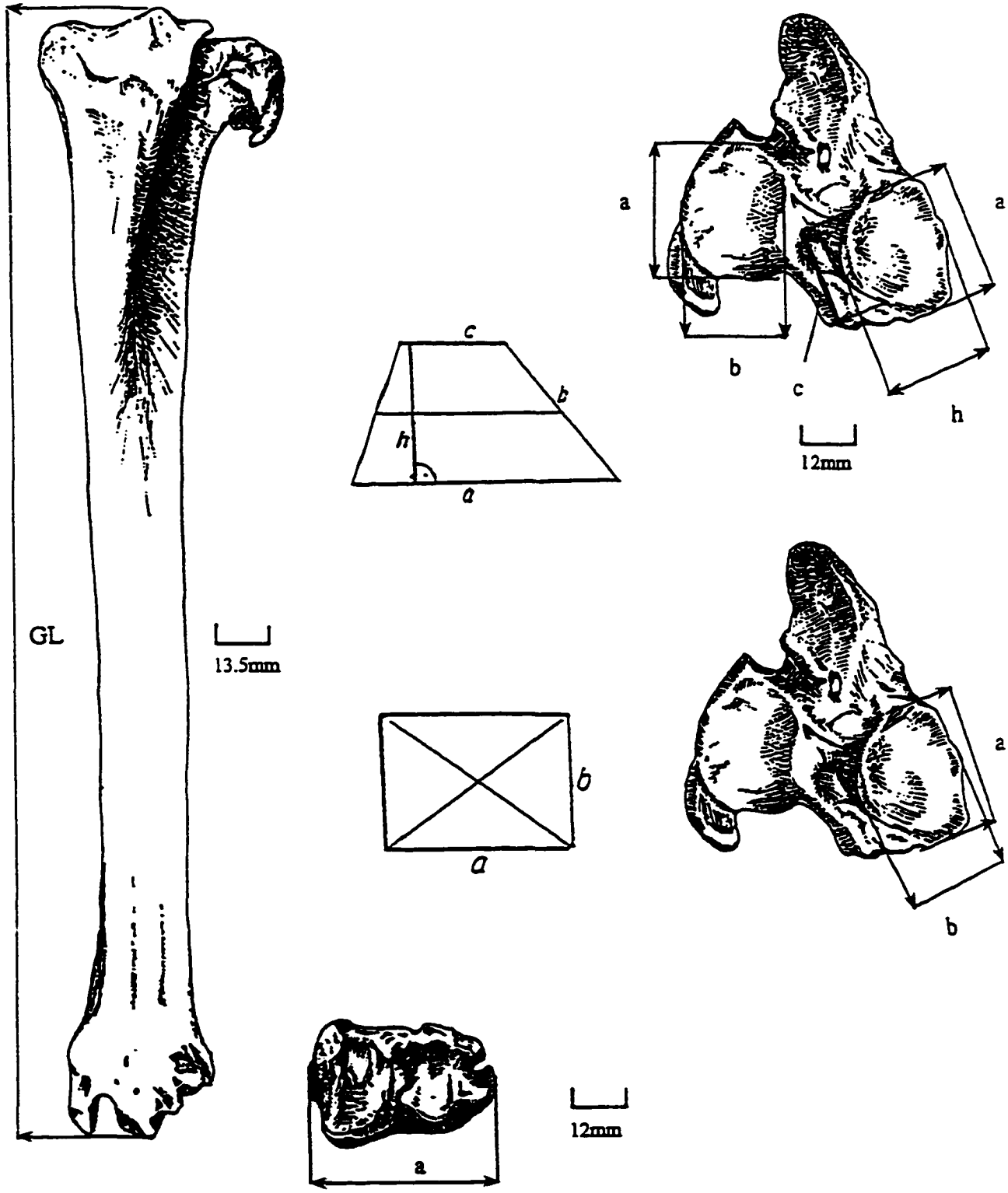

Fig. 3-22. Measurements of the tibia. GL = greatest length; a = antero-posterior lateral and medial condyles proximal tibia and medio-lateral distal tibia; b = medio-lateral medial condyle proximal tibia and antero-posterior distal tibia; c = least antero-posterior distance medial proximal condyle; h = medio- lateral medial proximal condyle. Trapezium and rectangle reproduced with permission of Academic Press.

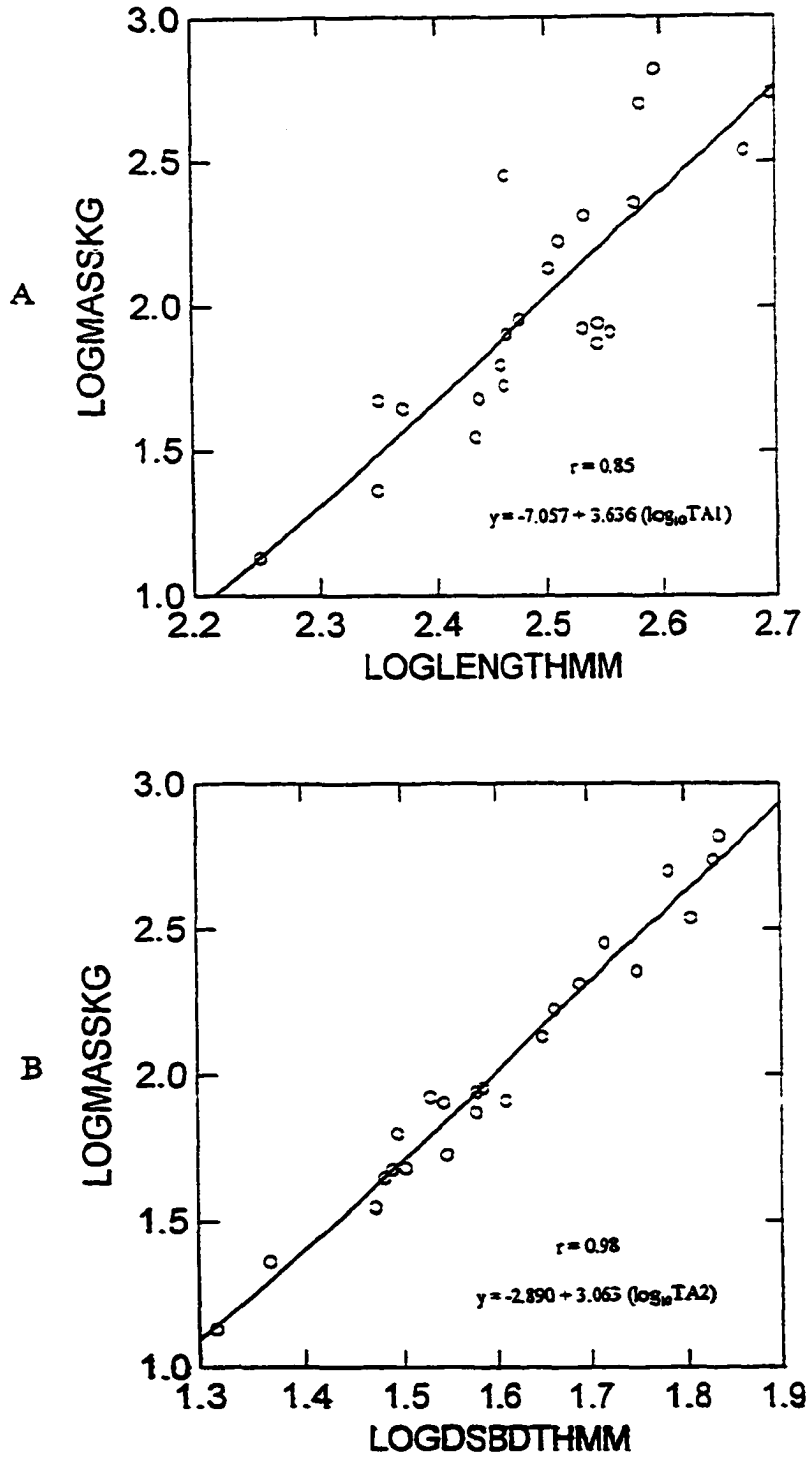

Fig. 3-23A. Log_{10} body mass plotted against log_{10} length of the tibia (TA1) in mm.
Fig. 3-23B. Log_{10} body mass plotted against log_{10} distal breadth of the tibia (TA2) in mm.

itself it is an extremely good predictor of mass. All predicted masses are within 10%-15% of the observed, except for that of the moose, which was underestimated by 25%.

Surface area of the proximal articular surface (medial condyle as a trapezium) — The lateral condyle was modeled on a rectangle. The medial condyle is more variable in shape, and was modeled on both a quadrilateral (trapezium) in this case (Fig.3-22), and on a rectangle for the next variable. The areas for the rectangle and the trapezium were added together to obtain an articular surface area (TA3) for the proximal tibia. Both models proved equally as good for predicting mass. When the medial condyle was modeled on a trapezium, as in this variable, the r = 0.981, with a %PE of 16 and a %SEE of 23. The regression slope was 1.513, and corresponded to geometric similarity (Fig.3-24A). The mass of the four largest species were underestimated by only 10%-15%, making this an exceptionally good variable with which to estimate mass across a wide range of sizes.

Surface area of the proximal tibia (medial condyle as a rectangle) — The lateral condyle was modeled on a rectangle. The medial condyle was modeled on a rectangle as well, and the areas of both shapes added together to obtain an area (TA4) for the proximal tibia articulation (Fig.3-22). This variable was a good predictor of mass, with a correlation coefficient of 0.979, a %PE of 17, and a %SEE of 24. The regression slope was 1.509, very close to that predicted by isometry (Fig.3-24B). Mass estimations for the largest species were low by 20%-25%, indicating the medial condyle of the tibial plateau is better modeled as a trapezium rather than a rectangle.

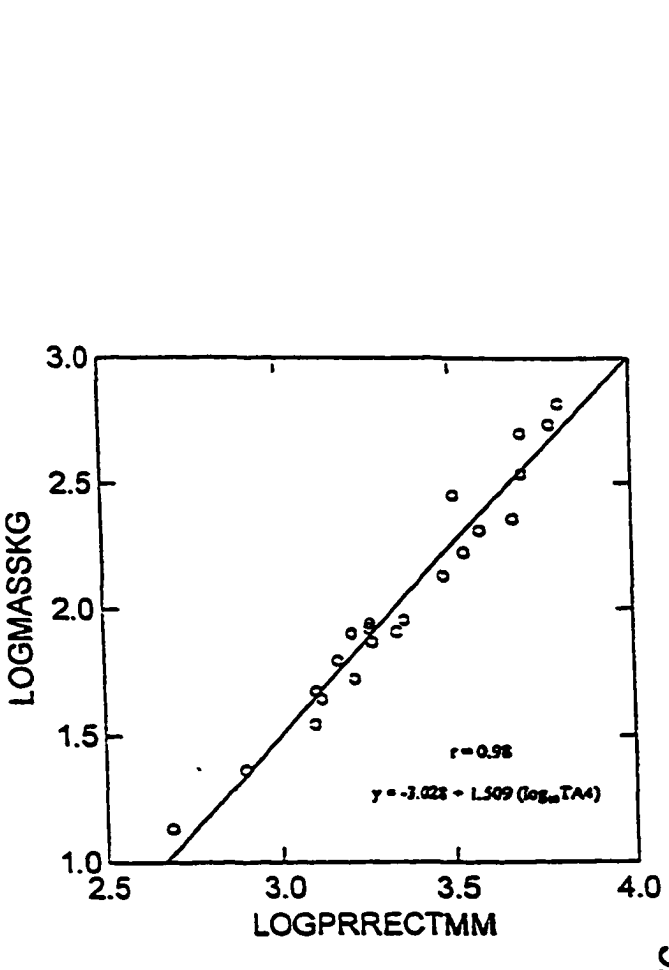

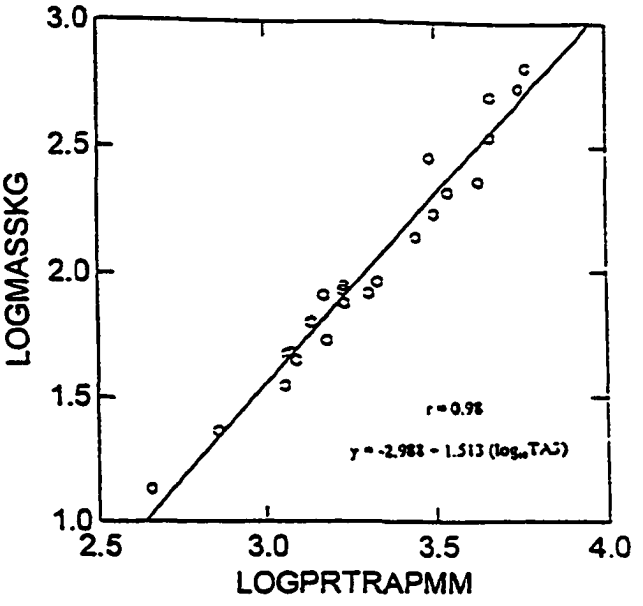

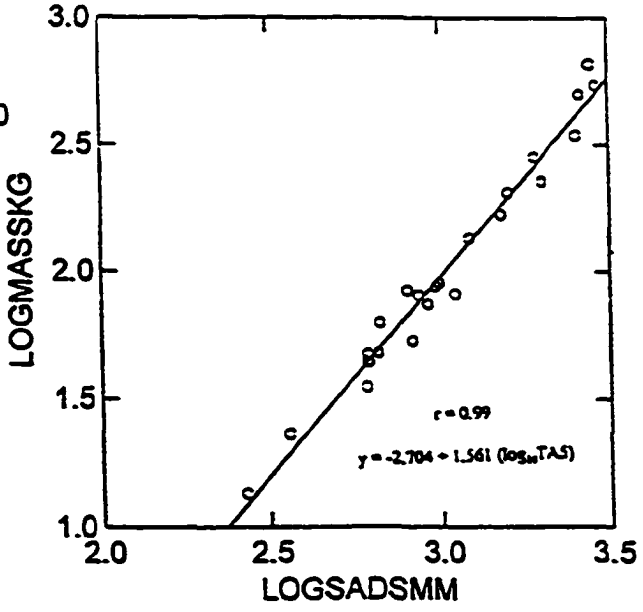

Fig. 3-24A. Log_{10} body mass (kg) plotted against surface area medial condyle tibia (TA3) as a trapezium (mm^2).
Fig. 3-24B. Log_{10} body mass (kg) plotted against surface area medial condyle of tibia (TA4) as a rectangle (mm^2).
Fig. 3-24C. Log_{10} body mass (kg) plotted against surface area distal tibia (TA5) (mm^2).

Surface area of the distal tibia — This articulation (TA5) was modeled on a trapezium (Fig.3-22). Once again, this variable proved to be a good predictor of body mass. The correlation coefficient was 0.986, the %PE was 14, and the %SEE 19. This variable showed the tightest correlation to mass of all of the tibial variables, and was the only one left in the stepwise model. The regression slope was 1.561, correlating well to geometric similarity (Fig.3-24C). Three of the largest species were either overestimated (elk) or underestimated (bison and eland) by approximately 20%. Nonetheless, for most species, this is an excellent predictor of body mass.

Astragalus

Greatest length of the astragalus — Measured from the top of the trochlea to the base of the distal articular surface (Fig.3-25), the length of the astragalus (AS1) is an extremely good predictor of body mass, as are all the other variables for the astragalus. The correlation coefficient for the length was 0.982, the %PE was 15, and the %SEE 22, indicating good predictive accuracy. The slope of the regression was 3.181, which was fairly close to geometric similarity (Fig.3-26A). This variable was left out of the stepwise multiple regression, although by itself is a good predictor of mass.

The masses of most species fell within 10%-25% of observed mean weights. The most interesting finding is that of the caribou (*Rangifer tarandus*), with the mass estimate falling 40% above the observed.

Greatest width of the astragalus — The width of the astragalus (AS2) (Fig.3-25) proved to be the best predictor of mass, and was the only variable left in the multiple

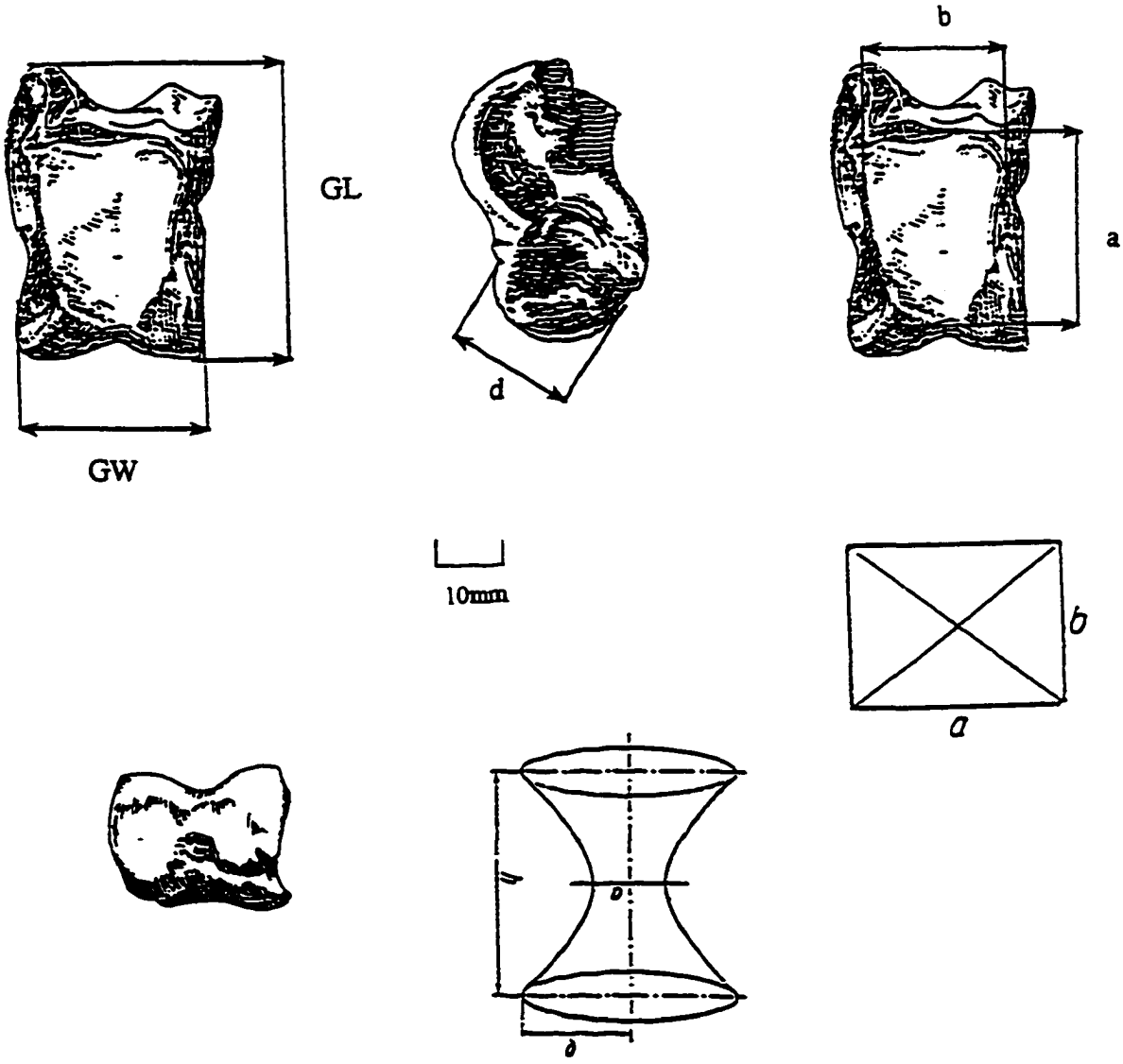

Fig. 3-25. Measurements of the astragalus. GL = greatest length; GW = greatest width; a = greatest length of posterior articular surface; b = greatest width of posterior articular surface; d = diameter of lateral side of distal articulation.

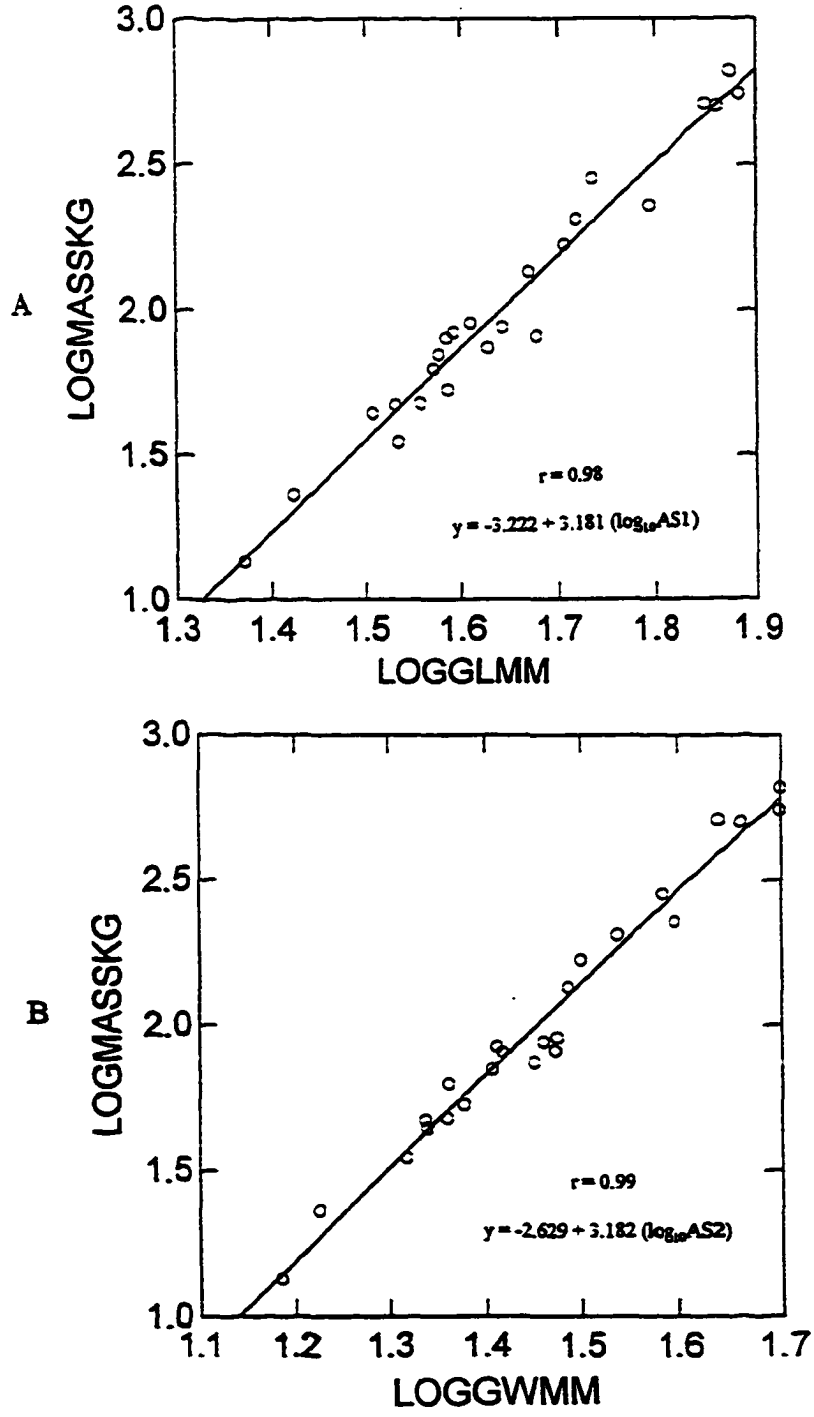

Fig. 3-26A. Log_{10} body mass plotted against log_{10} length astragalus (AS1) (mm).
Fig. 3-26B. Log_{10} body mass plotted against log_{10} width astragalus (AS2) (mm).

stepwise regression. The %PE was 13, the %SEE was 18, and the correlation coefficient was 0.987, indicating good correlation and predictive accuracy. The slope of the regression line was 3.128, thereby adhering to the expectation of geometric similarity (Fig.3-26B).

Volume of the distal articulation — This variable was modeled on the volume of an hyperboloid of revolution of one sheet (Fig.3-25). The volume (AS3) was tightly correlated with body mass (r = 0.978). This variable showed good predictive accuracy, with a %PE of 14, and a %SEE of 23. The regression slope was 1.070, close to the 1.0 predicted by all of the similarity principles (Fig.3-27A). Although the volume of the distal articulation was left out of the final model developed by stepwise regression, by itself, it is an excellent predictor of mass. The mass of the caribou was again overestimated by 40%.

Surface area of the posterior articulation — This variable was modeled on a rectangle (Fig.3-25), and showed a high degree of correlation to body mass, with an r of 0.983. The %PE and %SEE were 14 and 21 respectively, and indicated good predictability of this variable. The slope of the regression was 1.630, somewhat above the expectation for geometric similarity (Fig.3-27B).

Calcaneum

Greatest length of the calcaneum — The length (CL1) was measured from the calcanean tuberosity to the most distal portion of the bone. Of the four variables tested for the calcaneum, the length had the lowest r value, which was still very high at 0.971. The %PE was 19, and the %SEE 28, indicating reasonable predictive accuracy. The

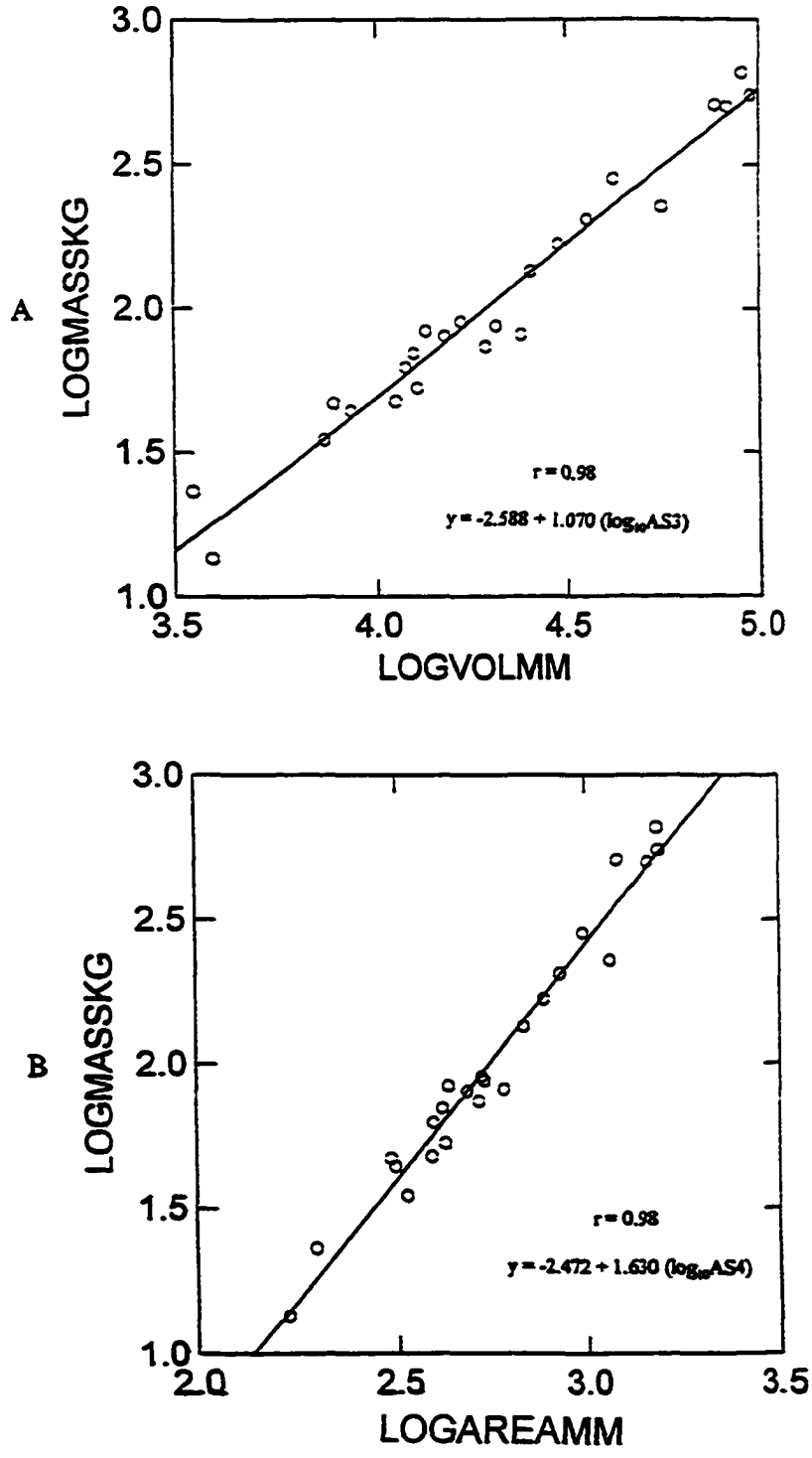

Fig. 3-27A. Log_{10} mass plotted against log_{10} volume distal astragalus (AS3) (mm^3).
Fig. 3-27B. Log_{10} mass plotted against log_{10} surface area posterior surface (AS4) (mm^2).

slope of the regression showed a slight positive allometry at 3.375, scaling above 3.0 as would be expected for geometric similarity, but below the elastic slope of 4.0 (Fig.3-29A). This variable was not included in the final stepwise model.

Width of the sustentaculum — The greatest width (CL2) across the sustentaculum tali (Fig.3-28) correlated highly with body mass with an r = 0.979. The slope of the regression line was 3.185, scaling more closely to geometric similarity than did the length of the bone (Fig.3-29B). This variable was an extremely good predictor of mass, with a %PE of 15, and a %SEE of 23. This is a valuable measurement, as often the only part of the calcaneum left in the fossil record is the distal portion with the sustentaculum intact.

The masses of the three largest bovids were underestimated by about 15%. The mass of the caribou was overestimated by 35%, suggesting a locomotory adaptation, perhaps related to long migrations.

Surface area of the calcaneal tuberosity — This area was modeled on a rectangle (Fig.3-28). The predictive accuracy for this variable (CL3) is virtually identical to the sustentacular width. The correlation coefficient was 0.979, the %PE 14, and the %SEE 23, making this another excellent predictor of body mass. The regression slope was 1.529, coinciding with the expected slope of 1.5 for geometric similarity (Fig.3-30A).

Surface area of the distal articulation — The distal articular surface of the calcaneum (CL4) is a combination of two different surfaces at right angles to one another. The first set of surfaces is oriented vertically, and articulates with the lateral astragalus, the proximal lateral surface of the cubonavicular, and the lateral malleolus. The second set of surfaces is oriented at right angles to the first, and articulates with the posterior astragalus.

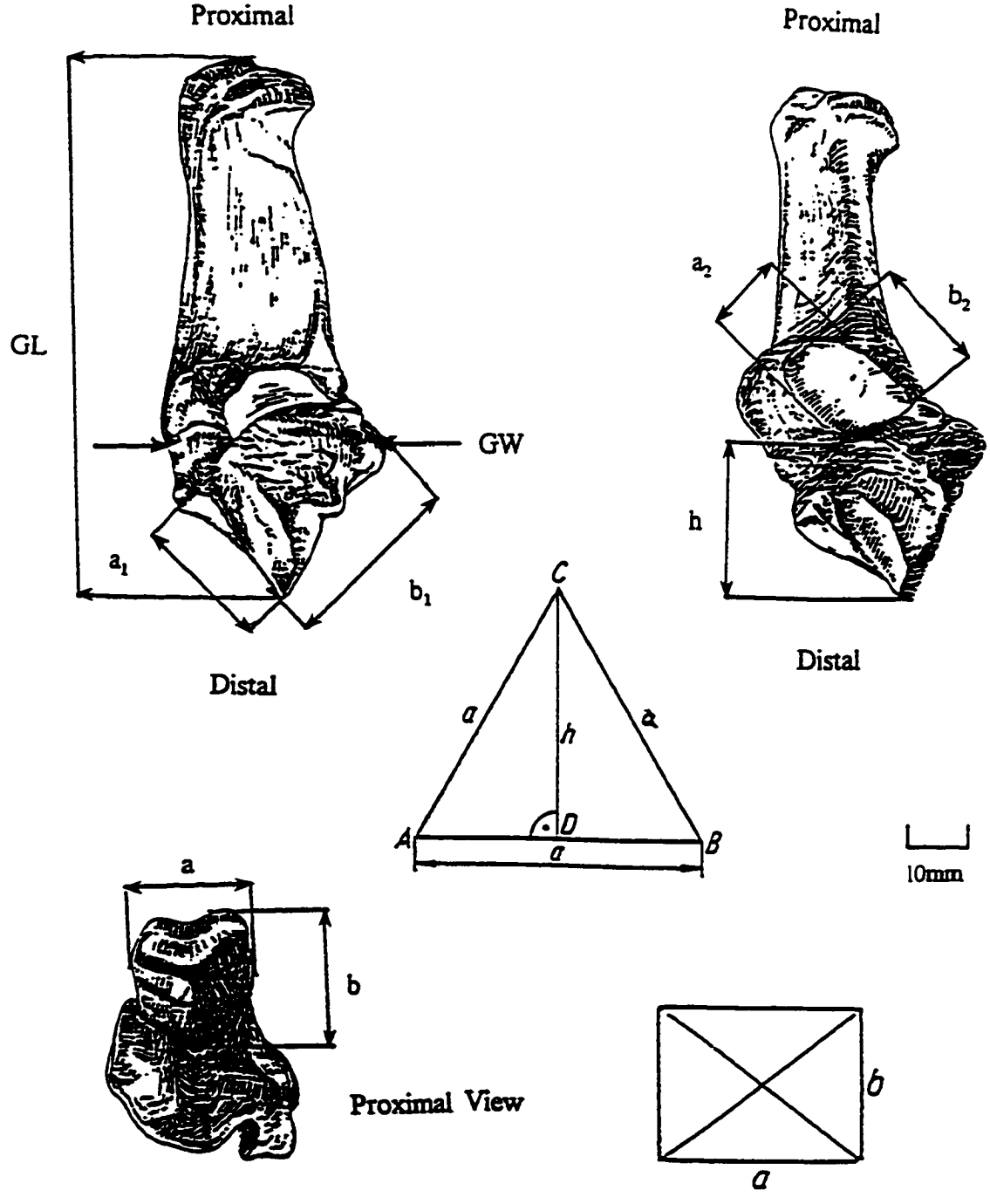

Fig. 3-28. Measurements of the calcaneum. GL = greatest length; GW = greatest width of sustentaculum; Proximal end: a = medio-lateral measurement of calcaneal tuberosity; b = antero-posterior measurement of calcaneal tuberosity. Distal end: a_1 = length of cubonavicular articular surface; b_1 = length of anterior articular surface; a_2 = width of astragalus articular surface; b_2 = length of astragalus articular surface. Equilateral triangle and rectangle reproduced with permission Academic Press.

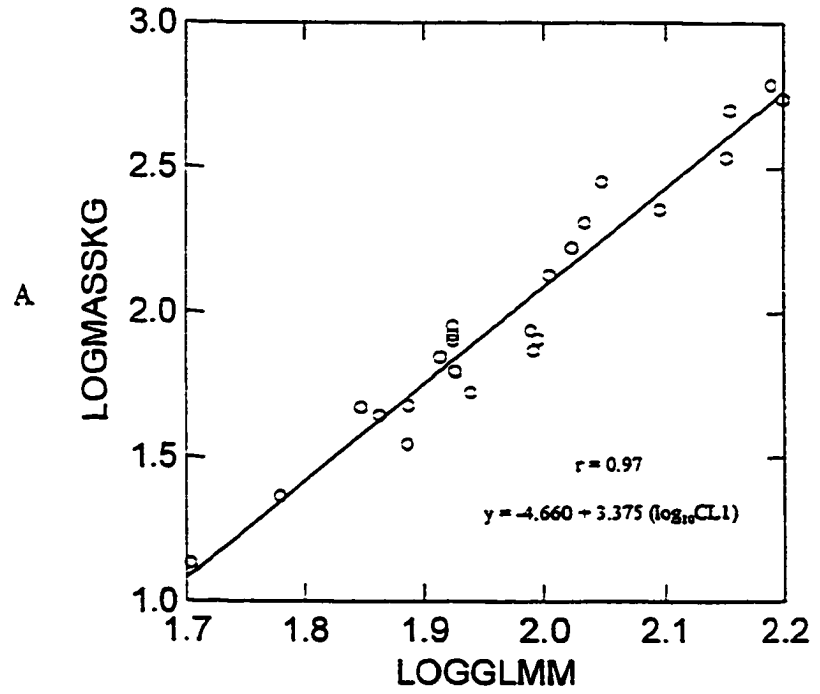

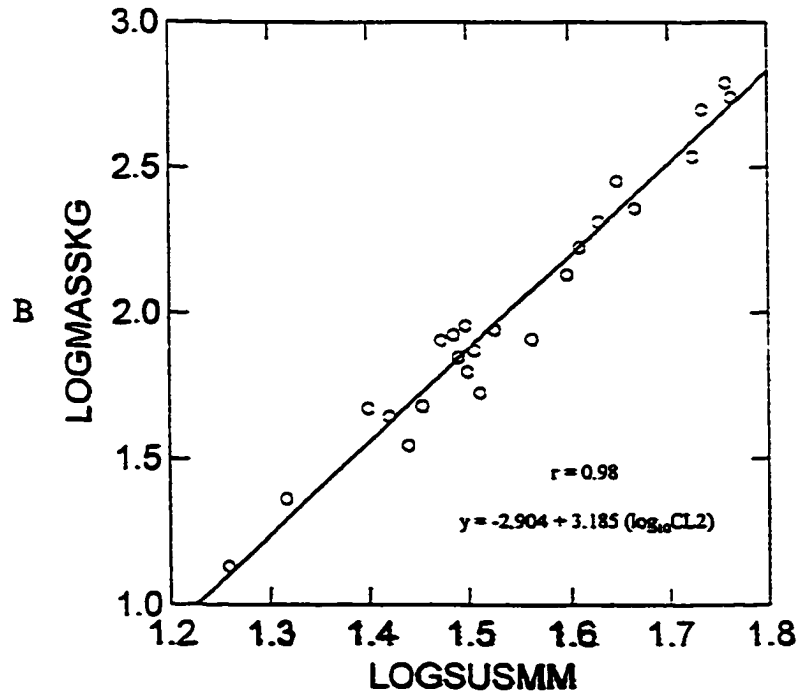

Fig. 3-29A. Log_{10} body mass plotted against log_{10} length of calcaneum (CL1) (mm).
Fig. 3-29B. Log_{10} body mass plotted against log_{10} width sustentaculum (CL2) (mm).

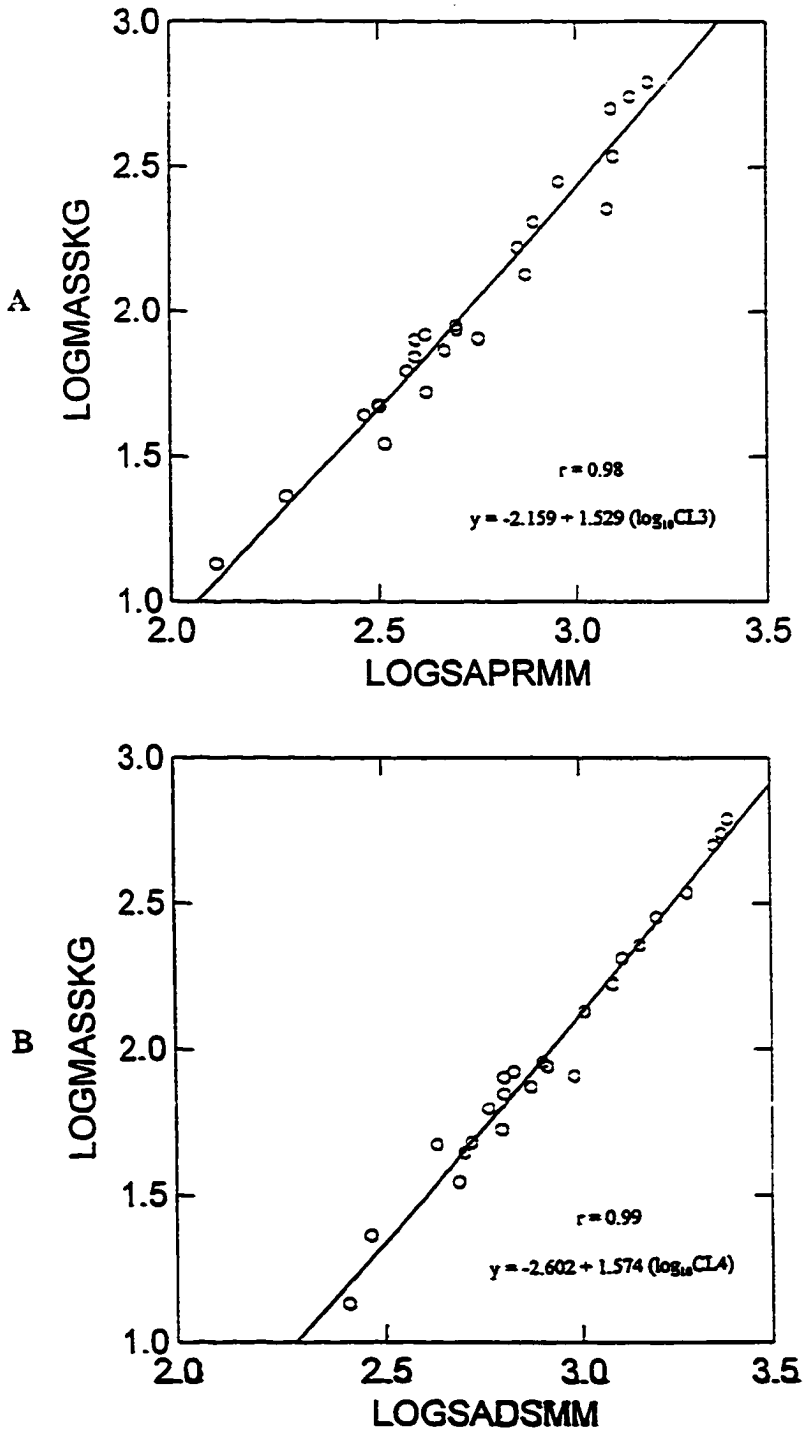

Fig. 3-30A. Log_{10} body mass plotted against area proximal calcaneum (CL3) (mm^2).
Fig. 3-30B. Log_{10} body mass plotted against area distal calcaneum (CL4) (mm^2).

The combined surface was modeled on an equilateral triangle for the lateral surface, and a rectangle for the ventral portion (Fig.3-28). The areas of the triangle and rectangle were then summed to obtain a total distal surface area. This variable was the best predictor of body mass for the calcaneum, with an r of .988, a %PE of 11, and a %SEE of 17. The regression slope was 1.574, again very close to geometric similarity (Fig.3-30B). This variable was the only one retained in the final model developed by the stepwise regression process. Most species showed mass estimates within 10% of the observed, the only exception being that of the caribou, which again was overestimated by almost 40%.

Cubonavicular

Ventral surface of the tarsal — The ventral surface of the cubonavicular (CU1) was chosen as the dorsal surface would have been redundant as the concave image of the distal astragalus. This surface was modeled on a circle (Fig.3-31), and showed an extremely high correlation to mass, with an r of 0.983. The %PE was 14, and the %SEE 21, indicating a good predictive accuracy for this variable. The slope of the regression was 1.551, close to geometric similarity (Fig.3-32).

Metatarsal

Greatest length of the Metatarsal — Like the metacarpal, the metatarsal length (Fig.3-33) shows a very poor correlation to body mass (r = 0.573). The regression slope is 1.877 (Fig.3-34A), the %PE 68, and the %SEE 129. This variable (MT1) was not part of the final stepwise model. The lengths of the metapodials of most artiodactyls have

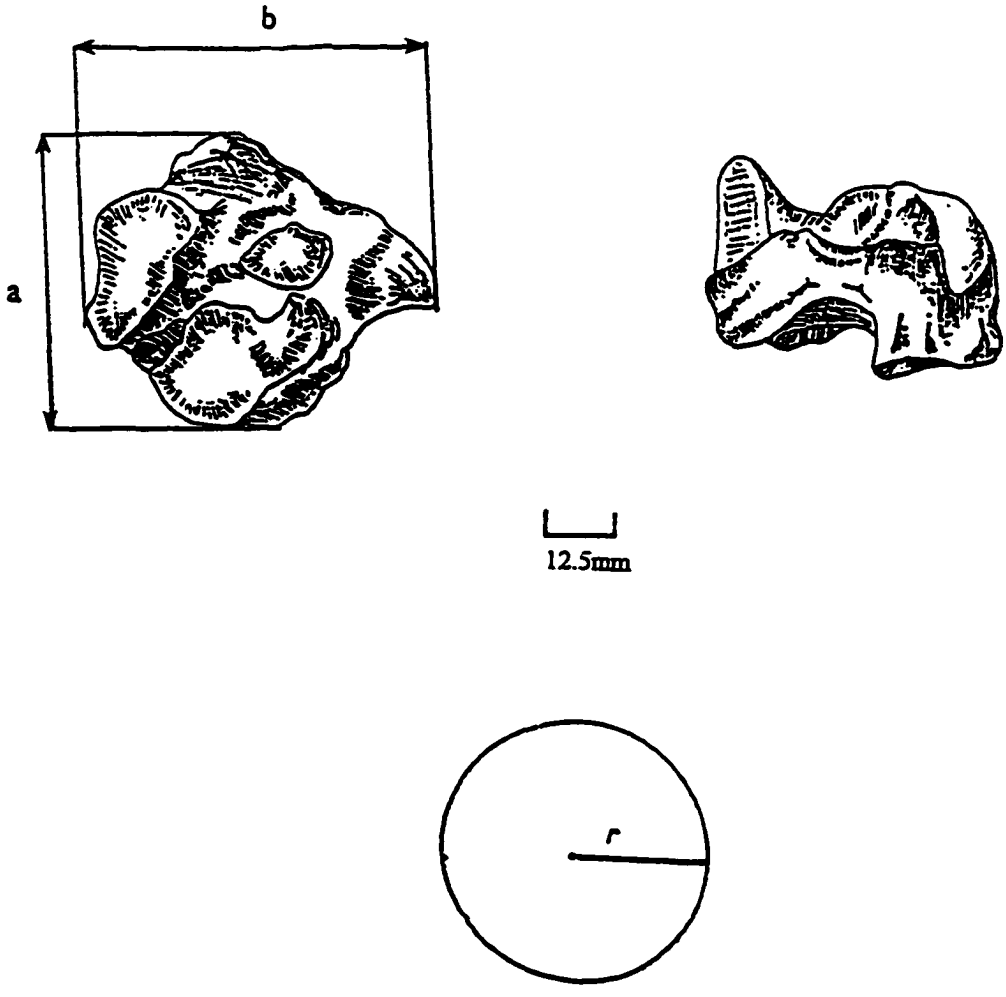

Fig. 3-31. Measurements of the cubonavicular. a = antero-posterior measurement of ventral side; b = medio-lateral measurement of ventral side. a+b/2 = r or the radius.

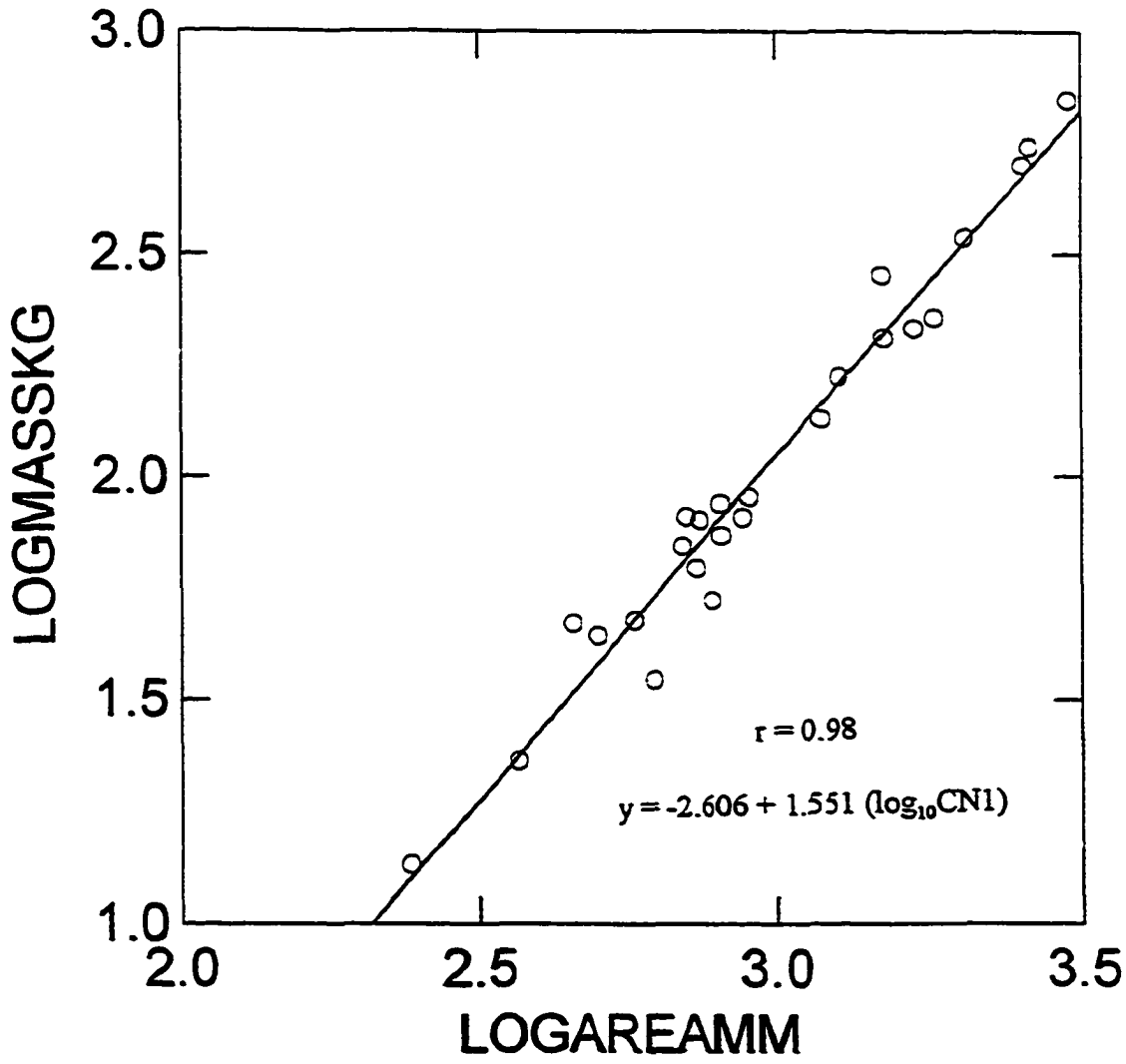

Fig. 3-32. Log_{10} body mass plotted against log_{10} ventral surface area cubonavicular (CN1) (mm^2).

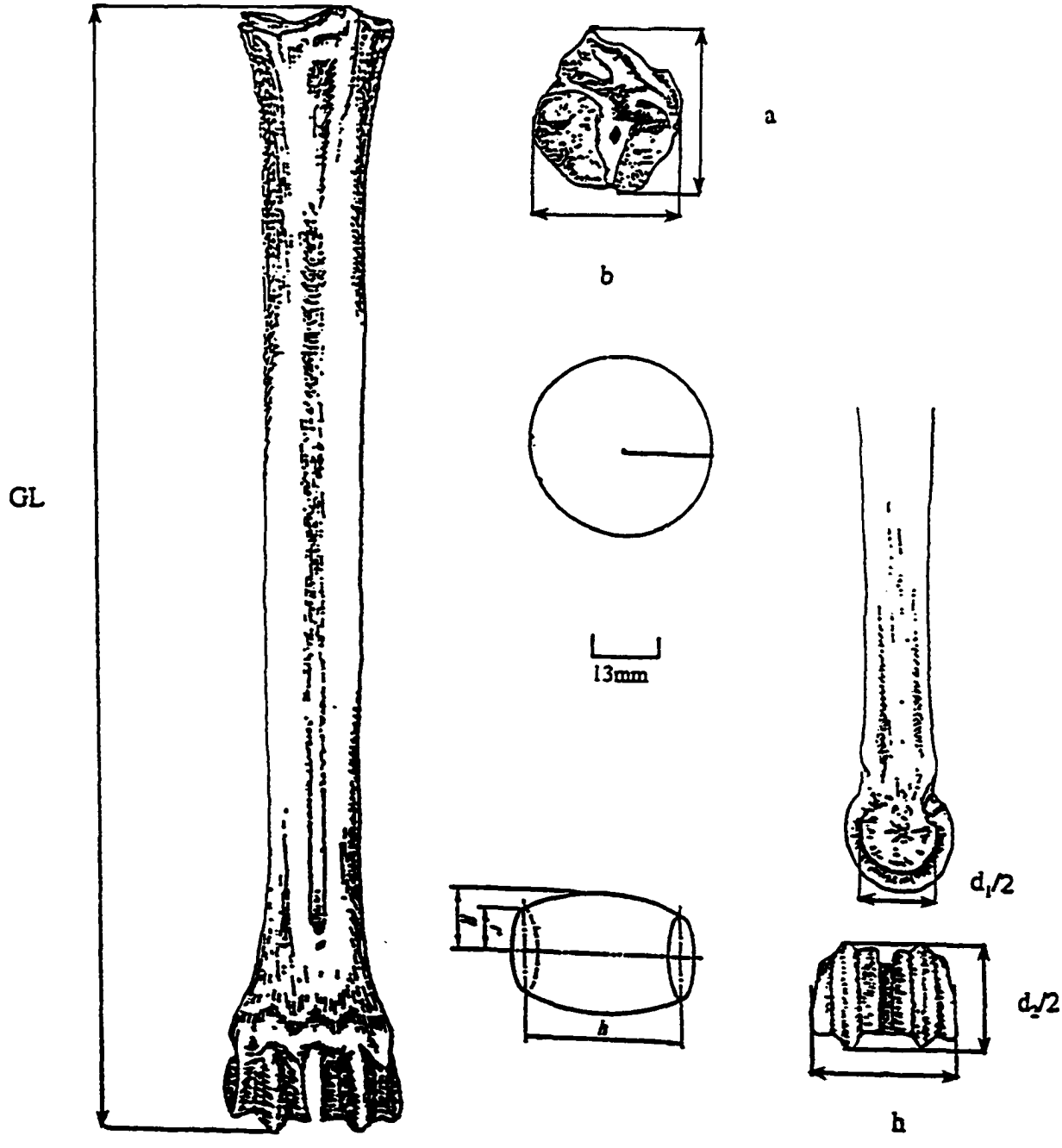

Fig. 3-33. Measurements of the metatarsal. GL = greatest length; a = antero-posterior measurement of proximal metatarsal; b = medio-lateral measurement of proximal metatarsal; $r = d_1/2$; $R = d_2/2$; h = distal breadth of metatarsal. Figure of barrel with permission of Academic Press.

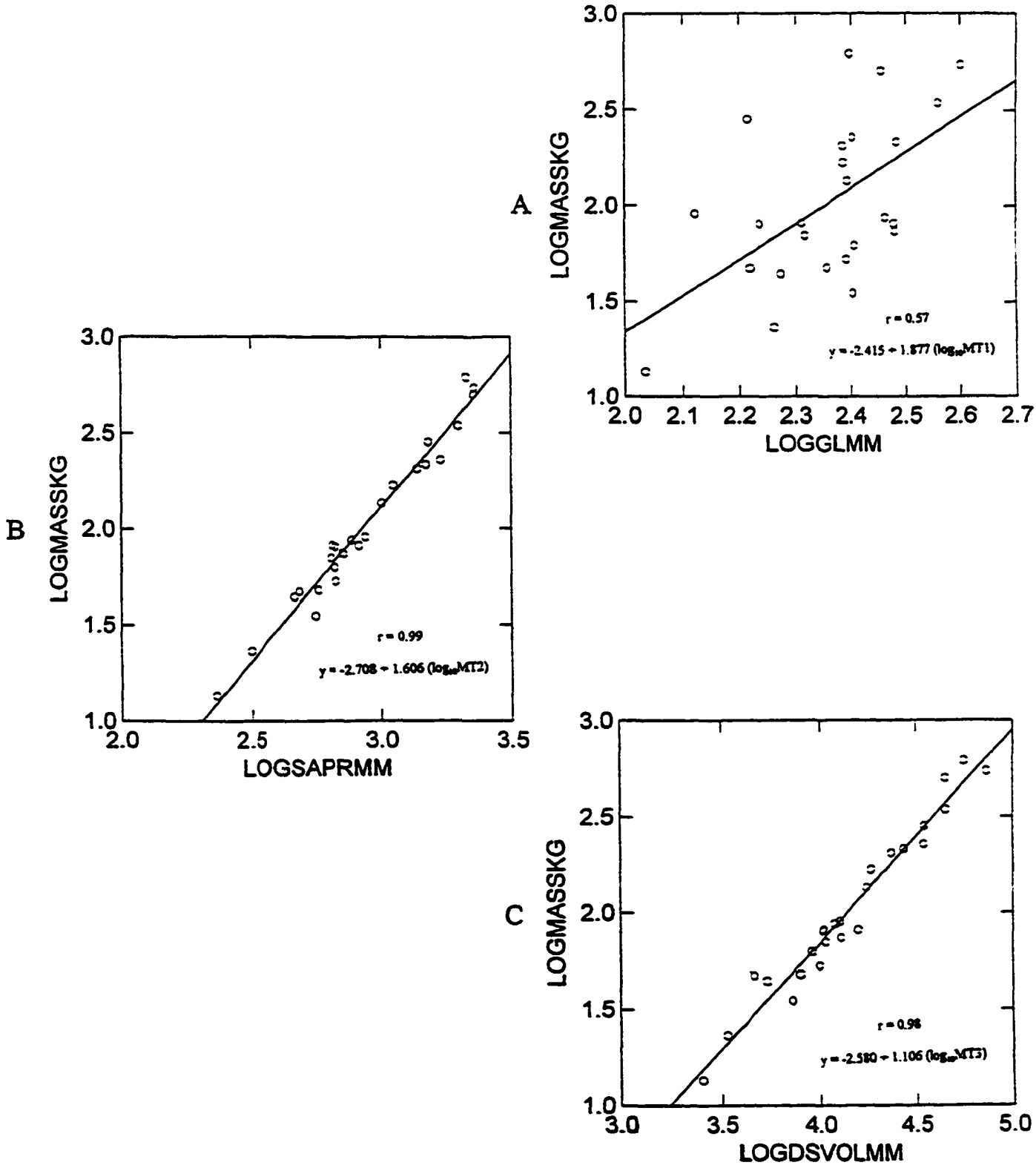

Fig. 3-34A. Log_{10} body mass plotted against log_{10} metatarsal length (MT1) (mm).
Fig. 3-34B. Log_{10} body mass plotted against log_{10} proximal surface (MT2) (mm^2).
Fig. 3-34C. Log_{10} body mass plotted against log_{10} distal articulation (MT3) (mm^3).

been shown to correlate with habitat and not mass, which explains the scatter around the regression line (Scott 1982).

Tarsal articular surface — The proximal surface area of the metatarsal (MT2) was modeled on a circle (Fig.3-33). This variable shows a tight correlation to body mass, with an r = 0.985, a %PE of 14, and a %SEE of 19. The slope of the regression is 1.606, above what would be expected for geometric similarity (Fig.3-34B).

Volume of the distal articulation — This articulation (MT3) was modeled on a barrel, as was the distal metacarpal (Fig.3-33). This variable is also an extremely good predictor of body mass, with an r = 0.979, a %PE of 16, and a %SEE of 23. The slope of the regression is 1.106, again implying that the metatarsal is somewhat thinner in the larger pecorans than would be expected from any of the similarity principles (Fig.3-34C). Results for the large species were mixed, with the mass of the bison and eland underestimated by approximately 20%-25%, and the mass of the moose overestimated by around 15%. This variable was also left out of the final model produced by the stepwise regression, although by itself, is an excellent predictor of body mass, with the exception of a few of the largest species.

Fossil Sample

In order to test the usefulness of the predictive regression equations developed for the modern sample for a paleontological sample, it was necessary to choose a group of fossil pecoran artiodactyls, preferably with extant relatives. There were four genera of late Rancholabrean (10,000-40,000 ybp) antilocaprids present in North America before the end

of the last glaciation. Only the modern *Antilocapra* survived the extinction event. Because there were other genera alive so recently that were so closely related to *A. americana*, I decided to choose one group on which to test the body mass estimators developed for the modern sample of pecorans.

Capromeryx is an extinct genus of antilocaprids consisting of six species that spanned a temporal period from approximately 3.21 mya (Benson l.f.) to the late Rancholabrean approximately 10,000-40,000 ybp (Mexico and La Brea). As with all other antilocaprids, they were endemic to North America. The family consists of two subfamilies, the Merycodontinae and the Antilocaprinae. Antilocaprines first appeared during the late Miocene, and possibly evolved from the merycodontines, which may have been Eurasian immigrants (Scott and Janis 1987). *Capromeryx* is characterized by having vertically oriented double horn cores. The anterior horn core is always smaller than the posterior. The five species included in this study of postcrania are *Capromeryx arizonensis* sensu Skinner 1942; *Capromeryx furcifer*, *Capromeryx mexicanus* sensu Furlong 1925; *Capromeryx minor* sensu Taylor 1911; and *Capromeryx tauntonensis*. *C. minor* and *C. mexicanus* were synonomized with *C. furcifer* in Chapter II, and *C. arizonensis* is now the junior synonym of *C. gidleyi* according to the ICZN rules of nomenclature as indicated in Chapter II. For the purposes of this study however, the six original species will stay separated in order to avoid confusion, as the postcranial measurements support the synonymy.

C. tauntonensis is the largest member of the genus, and is mid-Blancan in age (ca.3.1 mya) (Morgan and Morgan 1995). *C. arizonensis* is the mid-sized species of the

five, and is present from the mid-Blancan to early Irvingtonian (3.21-1.5 Ma). The type of *C. gidleyi* is from the Benson l.f. in Arizona, and is the oldest representative of the genus at 3.21 Ma.. The holotype of *C. gidleyi* is a partial horn-core, and cannot be used in the following analysis of postcrania. In both *C. tauntonensis* and *C. arizonensis*, the anterior horn-core is almost as large as the posterior, in contrast to the other three species which are small and have horn core configurations with the anterior horn-core being significantly smaller than the posterior. Fossil locations and ages are indicated in Table 3-4.

Because fossils are usually not found in the form of entire skeletons, not all elements were available for all of the species of *Capromeryx*. Good samples do exist for *C. arizonensis* from the Inglis 1A site in Florida, and for *C. minor* from Rancho la Brea, but the other members of the genus are not as well represented. Nonetheless, there was sufficient material present to provide mass estimates for five of the species, using regression equations developed for the modern sample. Regressions developed for the modern sample were run on $\log_{10}$ transformed fossil postcranial raw data, as there were not enough individuals present to obtain means for each species. Body mass predictions are shown in Table 3-5.

DISCUSSION

General comments about predictors

Scapula — The regression slope for the glenoid fossa (1.642) conformed to none of the similarity theories. While these theories provide general guidelines in predicting how

Table 3-4. Fossil Localities

Species	Locality	Age	
Capromeryx arizonensis	Inglis 1A, Florida	early Irvingtonian	1.5 mya
	Santa Fe 1A, Florida	mid-Blancan	2.5 mya
	Santa Fe 4A, Florida	mid-Blancan	2.5 mya
	Santa Fe 8, Florida	mid-Blancan	2.5 mya
	Santa Fe River 1B, Florida	mid-Blancan	2.5 mya
	Santa Fe River 4B, Florida	mid-Blancan	2.5 mya
	Curtis Ranch, Arizona	early Irvingtonian	1.88 mya
	Broadwater A, Nebraska	mid-Blancan	2.8 mya
Capromeryx minor	La Brea, California	late Rancholabrean	10K-40K ybp
	McKittrick, California	late Rancholabrean	10K-40K ybp
	Pendejo Cave	late Rancholabrean	10K-40K ybp
Capromeryx furcifer	Hay Springs, Nebraska	late Irvingtonian	0.4-0.5 mya
	Rushville, Nebraska	late Irvingtonian	0.4-0.5 mya
	Butler Spring, Kansas	early Rancholabrean	0.35-0.4 mya
	Slaton Quarry, Texas	late Irvingtonian	0.4-0.5 mya
	Gordon Quarry, Nebraska	late Irvingtonian;	0.4-0.5 mya
	Cragin Quarry, Kansas	mid-Rancholabrean;	0.2-0.3 mya
Capromeryx mexicanus	Cedazo, Mexico	late Rancholabrean	10K-40K ybp
	Tequixquiae, Mexico	mid-Rancholabrean	200K ybp
	Rancho la Brisca, Mexico	late Rancholabrean	10K-40K ybp
	Hidalgo, Mexico	late Rancholabrean	10K-40K ybp
	Hueyahaco, Mexico	late Rancholabrean	10K-40K ybp
Capromeryx tauntonensis	Taunton, Washington	mid-Blancan	3.1 mya
	Cita Canyon, Texas	mid Blancan	2.5-2.7 mya
Capromeryx gidleyi	Curtis Flats, Benson AZ	mid-Blancan	3.21 mya
Capromeryx sp.	Dark Canyon Cave, Texas	late Rancholabrean	10K-40K ybp
	Pendejo Cave, Arizona	late Rancholabrean	10K-40K ybp
	Animal Fair, Texas	late Rancholabrean	10K-40K ybp
	Underwood #3, Texas	late Rancholabrean	10K-40K ybp

Table 3-5. Mean Body Mass Predictions for Fossil Capromeryx in Kilograms

Element	Variable	C.arizonensis	C.furcifer	C.mexicanus	C.minor	C.tauntonensis	%SEE
Scapula	SC1	15 (n=37)	.	.	9 (n=5)	.	+/-26
Humerus	HM1	19 (n=3)		10 (n=1)	12 (n=1)		
	HM3	16 (n=40)	14 (n=4)	10 (n=1)	11 (n=10)	22 (n=1)	+/-14
	HM4	18 (n=40)	16 (n=4)	10 (n=1)	12 (n=10)	21 (n=1)	+/-23
	HM5	17 (n=40)	16 (n=4)	11 (n=1)	12 (n=10)	20 (n=1)	+/-21
Radius	RD1	22 (n=10)	.	.	15 (n=1)	.	+/-61
	RD2	15 (n=47)	.	11 (n=2)	10 (n=2)	.	+/-18
Ulna	UL1	17 (n=15)	.	.	14 (n=1)	.	+/-25
	UL2	14 (n=16)	.	.	10 (n=1)	.	+/-29
Metacarpal	MC1	91 (n=11)	.	.	72 (n=4)	.	+/-139
	MC2	29 (n=17)	.	15 (n=1)	17 (n=13)	.	+/-18
	MC3	14 (n=20)	11 (n=1)	16 (n=1)	11 (n=8)	.	+/-21
Magnum	MN1	17 (n=11)	.	8 (n=1)	9 n=1)	.	+/-18
Femur	FM1	18 (n=11)	.	.	.	.	+/-33
	FM2	16 (n=10)	.	.	.	.	+/-19
	FM3	15 (n=27)	.	.	9 (n=1)	.	+/-23
	FM4	15 (n=27)	.	.	9 (n=1)	.	+/-23
Tibia	TA1	24 (n=20)	.	.	.	.	+/-74
	TA3	13 (n=36)	.	.	.	.	+/-21
	TA4	13 (n=36)	14 (n=2)	.	.	.	+/-23
	TA5	26 (n=43)	23 (n=2)	16 n=1)	19 n=1)	.	+/-24
Metatarsal	MT1	75 (n=16)	51 (n=1)	48 (n=1)	69 (n=2)	102 (n=1)	+/-129
	MT2	15 (n=32)	8 (n=1)	9 (n=1)	10 (n=8)	21 (n=1)	+/-19
	MT3	14 (n=21)	.	8 (n=1)	12 (n=2)	19 (n=1)	+/-23
Astragalus	AS1	16 (n=33)	15 (n=2)	7 (n=1)	11 (n=8)	.	+/-22
	AS2	14 (n=33)	12 (n=2)	6 (n=1)	8 (n=9)	.	+/-18
	AS3	16 (n=33)	13 (n=2)	7 (n=1)	11 (n=8)	.	+/-23
	AS4	16 (n=33)	16 (n=2)	8 (n=1)	11 (n=9	.	+/-21
Calcaneum	CL1	13 (n=20)	.	6 (n=1)	12 (n=5)	.	+/-28
	CL2	15 (n=21)	.	11 (n=1)	15 (n=5)	.	+/-23
	CL3	16 (n=16)	.	14 (n=1)	12 (n=5)	.	+/-23
	CL4	20 (n=21)	.	9 (n=1)	12 (n=5)	.	+/-17
Cubonavicular	CN1	17 (n=16)	.	8 (n=1)	12 (n=4)	.	+/-21
Species Means		17	13	10	12	21	

Note: Values for C.mexicanus are for one individual only. Lengths of metapodials not included in species mean body masses.

animals increase proportionally in size, there are other factors that may influence the shape of articulations. While some of the less cursorial species display predicted body masses that are 10%-20% less than would be expected, the more cursorial species such as the pronghorn (*A. americana*) and the impala (*A. melampus*), display predicted masses that are 45% higher than would be expected from the size of this articulation. This suggests that the surface area of the glenoid fossa in cursorial species is considerably larger than can be explained from an increase in size alone. Mode of locomotion is a possible explanation, and it may well be that the size of the glenoid fossa is related more to rotational stresses encountered during running (Hildebrand 1988).

Humerus — The length of the humerus appears to correlate more highly with habitat than with mass, with many of the species exhibiting masses that are overestimated by 15%-30%. The three largest bovids, *Ovibos moschatus* (musk-ox), *Bison bison* (American bison), and *Taurotragus derbianus* (giant eland) have masses which are underestimated by 35%-40%. This is consistent with the results of Scott (1979), who discusses "force-directed" changes in very large bovids. She noted that as large bovids increase in size, the forelimbs assume increasing importance in applying force to move the animal forward in a stride. This is the result of the increase in the sized of the head, neck, and internal organs with a subsequent shift of mass and the center of gravity forward in these animals (Scott 1979).

"Force-directed" changes result in the lengthening of the proximal segment (humerus) and the shortening of the distal segment (radius). This proportion was also documented by Osborn and Gregory (1929). Their interpretation was somewhat different,

and they suggested that these proportions are "retrogressions" from the high speed limb ratios of lighter limbed ancestral forms. In other words, while the limb proportions are still compatible with a cursorial mode of locomotion, they are not as pronounced as one would find in lighter limbed species.

The mid-shaft cross-sectional area of the humerus revealed that both the bighorn (*Ovis canadensis*) and the mountain goat (*Oreamnos americanus*) have relatively thicker humeri than expected, which may be directly correlated to climbing habits. The large pecorans exhibiting thinner humeri than expected from body mass are the moose (*Alces alces*) and the giant eland (*Taurotragus derbianus*). Scott (1987) remarks upon the fact that cervids such as the moose, are more variable in the proportions of their limb segments than are bovids, and that those proportions are likely correlated to both habitat and/or locomotion. The results for the bovid, (giant eland) are less clear, but Scott (1979) suggests that the somewhat unusual limb proportions of elands may be related to phylogeny rather than either habitat or locomotion. The volumes of the distal articulation of the humerus also underestimate the mass of both the moose and eland. There appears to be no good explanation for this other than the previously noted trend of inaccurate body mass estimates noted for large cervids and bovids.

Radius — Although the slope for the length of the radius implies that the element is longer than would be expected from isometry, the radii of three of the larger species of bovids are actually shorter than expected, and the masses underestimated by 60%. The musk-ox, giant eland, and bison appear to conform once again to the conclusions of Scott (1979) who discusses proportional changes of limb lengths with increasing body mass.

Conversely, the body mass of the moose is overestimated by 15%. While this is not especially a significant mass overestimation, the mass of the caribou (*Rangifer tarandus*) which is considerably smaller than the moose, is overestimated by 25%. This animal migrates over very long distances between summer and winter ranges, typically as much as 1000 km, but recent satellite telemetry demonstrated movements of some individuals up to 5055 km (Nowak 1991). It is possible that some skeletal adjustments, such as increased robusticity of the limbs, has been developed as an adaptation to increased mechanical stresses from long migrations over difficult terrain. The wildebeest (*Connochaetes taurinus*) also makes very long migrations, but does not encounter severe cold, boggy permafrost and other inclement conditions.

Ulna — The regression slope for the length of the olecranon was 2.844, somewhat less than would be expected for geometric similarity. Biewener (1989) predicted that animals in the size range of 55 g to 300 kg reduce bone strain by assuming more erect postures with increasing size. Therefore, one would expect the larger animals to have a longer olecranon which acts as a lever that balances the forces between the muscles and the force exerted by the ground (Biewener 1989). A long olecranon correlates with a fossorial or aquatic lifestyle, and provides greater leverage for the triceps muscle for digging or swimming (Van Valkenburgh 1984; Hildebrand 1988). It has been noted by Hildebrand (1988) that muscles can move joints through wider angles when they insert closer to joints rather than farther away. It is advantageous for cursorial species such as pecorans to have the triceps insert closer to the "elbow" joint. The obvious way to accomplish this is to shorten the length of the olecranon, so that the triceps inserts closer to the joint.

When the largest animals (>200 kg) were run separately with body mass as the dependent variable, the resultant slope was 10.624. This slope is somewhat difficult to interpret, and while it does indicate the expected positive allometry for the length of the olecranon, the extreme value is more likely due to individual variation and the small sample size of large individuals (n=20), and the fact that three species account for 14 of the individuals. It suggests a trend of increasing length of the olecranon with increasing body mass independent of cursorial considerations, but a more detailed study with a much larger sample size of animals would be needed for a definitive conclusion.

Metacarpal — It has been found that the length of the metacarpal is a poor predictor of mass due to the fact that it is more highly correlated to habitat than to body mass (Scott 1979; 1990; Gingerich 1990). For example, species that are climbers such as the klipspringer (*Oreotragus oreotragus*), mountain goat (*Oreamnos americanus*), and the bighorn sheep (*Ovis canadensis*) all exhibit short metapodials relative to the total length of the forelimb. The shortening of the metapodials may be an adaptation to increased stresses encountered while moving over uneven terrain (Sondaar 1977; Scott 1979).

Femur — In the case of the large cervids, elk (*Cervus elaphus*) and moose (*Alces alces*), both have proximal limb bones shorter than the distal. The extreme length of the femur in both species causes the mass estimates for this predictor to be skewed upwards for 15% in the moose, and 30% in the elk. Femur length appears to be a good predictor of mass in small to medium sized pecorans, but loses accuracy above 200 kg.

The shape of a partial sphere chosen as a model for the femoral head of primates was deemed inappropriate for pecorans. In primates, the femoral head is spherical in

shape. In pecorans, the medio-lateral diameter of the femoral head is elongated for movement primarily confined to the parasagittal plane. The shape of the spherical segment chosen as a model more closely approximated the shape of the more elongate pecoran femoral head. The mass estimates for some of the larger species are low for both the femoral head volume and surface area. Unlike some of the other variables, however, there seems to be no consistent correlation with family or habitat. The mass of the bison is predicted within 4%, whereas the mass of the moose is underestimated by 30%.

Tibia — The parameters for the tibia were generally proven to provide good estimates of mass, the only exception being length. Results for the length of the tibia agree with Scott (1979) who discusses adaptations of very large bovids to stresses placed upon the skeleton just from mass alone. The caribou was again an outlier, with the body mass overestimated by 25%.

Astragalus — This variable proved to be a very good estimator of mass overall, with the only major exceptions being the elk (>25%), and the caribou (>30%). The consistent overestimation of the mass of the caribou by a number of estimators is interesting, and really warrants further study, although that is beyond the scope of this dissertation.

Calcaneum — An unexpected result was that the length of the calcaneum appears to separate out the cervids from the bovids. The mass of the cervids was consistently overestimated, whereas the mass of the bovids was underestimated. This trend was not confined to large species, and the body mass of the mule deer (*Odocoileus heminous*) was overestimated by 40%. The reason for this is most likely a phylogenetic phenomenon. The calcanean tuberosity serves as the site of attachment for the calcanean

tendon which then attaches to the gastrocnemius muscle of the tibia, one of the major locomotory muscles (Pasquini and Spurgeon 1989). The tuberosity serves as a lever arm and correlates well with body mass.

Cubonavicular — Body mass estimations for this variable were close to observed, with 10% or less variation in all species but the gerenuk (*Litocranius walleri*), which showed and overestimation of 40%. This antelope has a rather unique adaptation of standing on its hindlimbs to browse, bracing itself against a tree in order to reach new growth (Nowak 1991). This behavior places increased loading upon the hindlimbs and may account for the body mass overestimation. This trend was also observed in other elements of the hindlimb for this species, but not as to such an extent as with the cubonavicular.

Metatarsal — The regression slope for the tarsal articular surface was positively allometric at 1.606, above the 1.5 expected for geometric similarity. This implies that some of the larger pecorans have slightly thinner cross sectional areas of the proximal metatarsal than would be expected from their mass. This variable was generally a good predictor of mass, with the exception of the bison. The mass of the bison was underestimated by 30%. The bison is an extreme example of forward shifted weight. The cross-sectional area of the proximal metacarpal predicted the mass of *Bison* within 5%. The metatarsal, on the other hand, is not subjected to as much axial loading as is the metacarpal, and does not need to be so robust.

Modern Sample

With the exception of the length of the metapodials, all of the skeletal variables in this study can be used to predict body mass with a reasonable degree of accuracy in the three families of modern pecorans examined. Very large species tend to be more problematic, and when at all possible, the volume of the distal humerus (HM3) should be used preferentially, due to the accuracy across a wide range of body sizes. Lengths of long bones tend to be less accurate than diameters or cross-sectional areas, and the lengths of the distal elements (radius and tibia) are less accurate than the proximal elements (humerus and femur).

The best mass estimates come from surface areas and volumes of articulations. Dimensions of carpals and tarsals also produced excellent correlations to body mass. Particular skeletal variables were chosen because it was felt that they all reflected some sort of mechanical loading related to body mass of the animal. Many of these variables have cross-sectional properties which are known to produce good correlations to mass (Runestad et al. 1992; Biknevicius 1993).

Three similarity theories were considered when evaluating the results; geometric, elastic, and static stress. While many of the variables correlated to one or more of these principles, often the slope of the regression could not be explained by similarity theories alone. The fact that the sample is composed of cervids, bovids, and *Antilocapra* likely affected the slopes, as bovids and cervids tend to scale differently. Bovids are the only taxon that adhere to the elastic similarity principle (McMahon 1977; Scott 1979).

Alexander et al. (1979) found that most species increased in size by scaling geometrically. Basically, it appears that mass increases in pecorans, and probably in most other taxa as well, are much more complicated than can be explained just by using proportional increases described by scaling exponents. The issue of which similarity theory best predicts scaling in mammals continues to be discussed in the literature. This may not have an easily solvable solution, and the continued focusing on simple scaling relationships as explanations for skeletal proportions is diverting attention from the more complicated issues at hand, such as the role of habitat and locomotion within each species. In a recent study relating body length to mass, Silva (1998) separated terrestrial, marine and volant species and concluded that the geometric similarity hypothesis fits better with most taxonomic orders. Orders that varied from the expectations of geometric similarity were discussed as exceptions, possibly due to phylogenetic influences on morphology (Silva 1998).

Elastic similarity models long bones on hollow symmetrical cylinders without regard to the different shapes of the long bones. Nonetheless, by applying engineering beam theory, McMahon (1973) addressed both compressive and bending loads that affect a bone during locomotion. Biewener (1989) took this concept further and examined peak stresses in bone cross-sections during strenuous activity. In addition to bending, he included the affects of torque and concluded that below about 300 kg, animals shift posture rather than change the shape of long bones in order to keep peak locomotor stresses at a safe level during locomotion. Above 300 kg, an upright posture is adopted, and the bones become more robust in order to deal with peak stresses. This implies that

cross-sectional properties of small and large mammals would scale differently because of the different strategies used to deal with peak locomotory stresses.

The stress similarity principle is appealing in that it deals with actual mechanical stresses placed on bones by looking at cross-sectional properties and allowing for shape changes. Despite this, it is not possible to explain scaling relationships using stress similarity alone. Scott (1979) discusses habitat differences and varying limb proportions among bovid species, which appears to have considerable validity. It appears that differences in scaling among orders of mammals, or even among species within the same order can be best accounted for by examining a variety of factors, including habitat, diet, mode of locomotion and phylogeny. It seems unwise to continue to attempt to try to find an easy explanation in the guise of generalized similarity theories to account for scaling differences for skeletal proportions, when in reality the explanation is rather complicated. While some general trends may be observed within some taxa, there are always individual species that do not fit the proposed mold, presumably due to morphological differences that can only be attributed to factors other than simple scaling relationships.

The other issue at hand is whether or not certain osteological variables may be used to accurately predict body mass. The answer to this appears to be yes, but that all variables do not predict mass for each species equally as well. Many of the mass predictions for larger pecorans change considerably from variable to variable. This suggests that shape changes in the limbs, as suggested by static stress similarity, may be a factor. In addition, Scott's (1979) hypothesis that a shifting of mass forward in large bovids accounts for changes in limb proportions appears to be a factor. The masses of

smaller species were more consistently predicted, with exceptions occurring among extremely cursorial species such as the pronghorn (*Antilocapra americana*) and the impala (*Aepyceros melampus*) . Another species that consistently varied from the expected mass was the caribou (*Rangifer tarandus*). The apparent robustness of the limbs for this animal may be related to an adaptation to increased stresses placed on bones due to migrations over boggy terrain in the spring, and through snow late in the season.

There are a number of variables that can be reliably used to predict body mass in pecoran artiodactyls. Of the 35 variables and 12 elements examined in the study, only four produced a correlation coefficient of less than 0.930. These were all lengths, including the radius length (0.894), metacarpal length (0.522), tibia length (0.850), and metatarsal length (0.573). Of these four, only the metapodial lengths were uncorrelated to mass and seem to be more indicative of habitat. The variables producing the best correlation coefficients as well as the best predictive accuracy can be found on Table 3-6.

With the exception of the cross-sectional area of the femur at midshaft, all of these variables can be used on fragmentary remains. Some caution should be used with the following variables when attempting to predict mass in large bovids: RD2, MC2, MN1, and TA5. All of these tend to underestimate the mass by 15%-20%. The mass of the caribou is greatly overestimated with the following variables: MC2, TA5, AS2, and CL4. Most of the body mass predictions for *Antilocapra* were within 10% of expected, the only exception being the glenoid fossa of the scapula. No adjustments to mass predictions are made for the fossil sample of *Capromeryx*, except for use of the ratio correction factor for $\log_{10}$ detransformations (Smith 1993).

Table 3-6. Osteological Variables Providing Best Estimations of Mass

Variable	Definition	r	%PE	%SEE
HM3	Volume of the distal humerus modeled on an hyperboloid of revolution (mm^3)	0.991	13	14
RD2	Area of proximal radius modeled on a rectangle (mm^2)	0.988	13	18
MC2	Area of the carpal articular surface of the metacaparpal modeled on a rectangle (mm^2)	0.986	14	18
MN1	Volume of proximal surface of magnum modeled on a spherical segment (mm^3)	.0987	13	18
FM2	Cross-sectional area of femur at mid-shaft (mm^2)	.0986	14	19
TA5	Area of the distal articular surface of tibia modeled on a trapezium (mm^2)	0.986	14	19
MT2	Proximal surface area of metatarsal modeled on a circle	0.985	14	19
AS2	Greatest width of the astragalus	0.987	14	18
CL4	Combined surface areas of distal calcaneum modeled on a rectangle plus an equilateral triangle (mm^2)	0.988	14	21

Fossil Sample

With the exception of the length of the metapodials, the mass estimates for each of the fossil species of *Capromeryx* were within two or three kilograms of one another. The metapodials produced estimates that were almost ten times those of the other variables. This result agrees with the modern sample which indicated that metapodial length may be more highly correlated with habitat than with mass. The other two variables that produced mass estimates that were five to six kilograms heavier than other estimates were those for the radius length and the tibia length. Femoral length was available for *C. arizonensis* only, and produced a mass estimation of 18 kg., which coincided with the estimates produced by other variables. Similarly, the length of the humerus was available for *C. arizonensis*, and one humerus was available for *C. minor*. Estimated body mass for these two species using humeral length was 19 kg. and 12 kilograms respectively. These mass estimates coincide with the results of other variables. These results also agree with the modern sample, and indicate that the proximal limb bones are more highly correlated to body mass than are the distal limb bones.

***Capromeryx arizonensis* sensu Skinner 1942** — Using all of the variables except distal limb lengths, the mean predicted body mass for this species is 16.5 kg., rounded to 17 kg. This agrees well with the results obtained by Scott (1983) who estimated the mass of this species at 15.5-18.9 kg. with a mean of 16.9 kg. Interestingly, many of the postcrania identified only to genus from Texas fall within the mass range of *C. arizonensis* (13-19 kg.). Most of these sites, however, including Dark Canyon Cave, Pendejo Cave, Animal Fair and Underwood #3, date from the late Wisconsin (10,000-40,000 ybp) which

is much too late for this species. Although the Texas specimens are compatible in size with *C. arizonensis*, without accompanying horn cores it is difficult to evaluate the significance, and it is more likely that the specimens represent a larger morph of *C. minor* found in Texas during the late Wisconsin, rather than an extremely late occurrence of *C. arizonensis*.

Capromeryx furcifer — The mean estimated mass for this species is 13.2 kg., rounded to 13 kg. While many of the variables were not available for *C. furcifer* due to lack of material, some of the better variables were available, including HM3, TA5, MT2, and AS2, suggesting that the mass estimate is accurate.

***Capromeryx mexicanus* sensu Furlong 1925** — Mass estimates for this species were based upon rather scant fossil material, often with only one available element for examination. Nonetheless, with the estimates combined, the mean for this species was 10 kg. Many of the best variables were available, including HM3, RD2, MN1, and AS2. *C. mexicanus* is essentially the same size as *C. minor*, and this mass estimate appears to be fairly accurate.

***Capromeryx minor* sensu Taylor 1911** — The mean mass for this species is 11.6 kg., rounded to 12 kg. This estimate is derived from a number of variables, although much of the material from Rancho La Brea was from sub-adults and could not be used in the final analysis. HM3, one of the most accurate predictor of mass, estimated the mass at 11 kg.

Capromeryx tauntonensis — The predicted mass of *C. tauntonensis* for all variables is less than that obtained from antero-posterior measurements of m3's obtained by Morgan and Morgan (1995). They estimated the mass of the species at approximately 85% of the

modern *A. americana*, which would infer a mass of approximately 40 kg. Janis (1990) showed that for ungulates, the length of m3 had a poorer correlation to body mass than did the lengths of m1, m2, and M2. She also commented that for intermediate feeders such as the Pronghorn (and presumably *Capromeryx*) which utilize both grazing and browsing strategies, the length of m3 is longer than that of other feeding types such as pure grazers or browsers. By using the length of m3, Morgan and Morgan (1995) may have somewhat overestimated the mass of *C. tauntonensis*. While the type skull of the species is obviously larger than that of *C. arizonensis* by direct comparison, it is also smaller overall than that of *A. americana*.

CONCLUSIONS

Estimators used for predicting body mass in modern pecorans appear to work well for the fossil sample of *Capromeryx*. Mass estimates supported the changes in phylogeny in Chapter II, with the mean masses for *C. furcifer*, *C. mexicanus* sensu Furlong 1925, and *C. minor* sensu Taylor 1911 being 13 kg, 10 kg, and 12 kg respectively. *C. gidleyi* (*C. arizonensis* sensu Skinner 1942) was reported to have a mean body mass of 17 kg, which agreed with the results from Scott 1990. The status of *C. tauntonensis*, while remaining the largest at 21 kg, is still uncertain. When more specimens are discovered, the possibility exists that it will need to be synonymized with C. gidleyi, since the 21 kg estimate is based upon eight teeth, one humerus and one metatarsal.

REFERENCES

Alexander. R. McN. 1977. Allometry of the limbs of antelopes (Bovidae). Journal of Zoology, London 183:125-146.

Alexander, R. McN., A. S. Jayes, G. M. O. Maloiy, and E. M. Wathuta. 1979. Allometry of the limb bones of mammals from shrews (*Sorex*) to elephant (*Loxodonta*). Journal of the Zoological Society of London 189:305-314.

Belovsky, G. E. 1984. Moose and snowshoe hare competition and a mechanistic explanation from foraging theory. Oecologia 61:150-159.

Bertram, J. E. A. and A. A. Biewener. Differential scaling of the long bones in the terrestrial carnivora and other mammals. Journal of Morphology 204:157-169.

Best, G. A., F. Edmond-Blanc, and R. C. Whitting. 1962. Rowland Ward's Records of Big Game, Rowland Ward, London, pp. 453

Biknevicius, A. R. 1993. Biomechanical scaling of limb bones and differential limb use in caviomorph rodents. Journal of Mammalogy 74(1):95-107.

Biknevicius, A. R., D. A. McFarlane, and R. D. E. MacPhee. 1993. Body size in *Amblyrhiza inundata* (Rodentia: Caviomorpha), an extinct megafaunal from the Anguilla Bank, West Indies: estimates and implications. American Museum Novitiates 3079:1-25.

Biewener, A. 1982. Bone strength in small mammals and bipedal birds: do safety factors change with body size? Journal of Experimental Biology 98:289-301.

Biewener, A. 1983. Locomotory stresses in the limb bones of two small mammals: the ground squirrel and chipmunk. Journal of Experimental Biology 103:131-154.

Biewener, A. 1989. Mammalian terrestrial locomotion and size. Bioscience 39(11): 776-783.

Boyce, M. 1979. Seasonality and patterns of natural selection for life histories. The American Naturalist 114(4):569-583.

Brain, C. K. 1969. The contribution of Namib Desert Hottentots to an understanding of australopithicine bone accumulations. Scientific Papers of the Namib Desert Research Station 39:13-22.

Brown, J. H. and B. A. Maurer 1989. Macroecology: the division of food and space among species on continents. Science 243:1145-1150.

Bubenik, A. B. 1990. Epigenetical, morphological, physiological, and behavioral aspects of horns, pronghorns and antlers; pp.3-113 *in* G. A. Bubenik and A. B. Bubenik (eds.), Horns, Pronghorns, and Antlers. Springer-Verlag, New York.

Calder, W. A. III. 1996. Size, Function, and Life History. 2nd. ed. Dover Publications, Inc., Mineola, New York, 431 pp.

Calder, W. A. III. and E. J. Braun. 1983. Scaling osmotic regulation and body size in mammals and birds. American Journal of Physiology 244:R601-R606.

Churchill, S. D. 1994. Human upper body evolution in the Eurasian later Pleistocene. Ph.D. dissertation, University of New Mexico, Albuquerque, 395 pp.

Creighton, G. K. 1980. Static allometry of mammalian teeth and the correlation of tooth size and body size in contemporary mammals. Journal of Zoology, London 191:235-243.

Currey, J. 1984. The Mechanical Adaptations of Bones. Princeton University Press, Princeton 294 pp.

Damuth, J. 1981. Population density and body size in animals. Nature 290:699-700.

Damuth, J. 1990. Problems in estimating body masses of archaic ungulates using dental measurements; pp.229-254 *in* J. Damuth and B.J. MacFadden (eds.), Body Size in Mammalian Paleobiology: Estimation and Biological Implications. Cambridge University Press, Cambridge.

Demment, M. W. and P. J. Van Soest 1985. A nutritional hypothesis for body size patterns of ruminant and non ruminant herbivores. American Naturalist 125:641-672.

Eisenberg, J. F. 1981. The Mammalian Radiations. Univ. of Chicago Press, Chicago, 610 pp.

Fresia, A. E., C. B. Ruff, and C. S. Larsen. 1990. Temporal decline in bilateral asymmetry of the upper limb on the Georgia coast; pp.121-132 *in* C. S. Larsen (ed.), The Archaeology of Mission Santa Catalina de Guale: 2. Biocultural Interpretations of a Population in Transition. Anthropological Papers of the American Museum of NaturalHistory 68.

Galilei, G. 1637. Dialogues concerning two new sciences (translated by H. Crew and A. De Salvio), MacMillen, New York, 1914, 300 pp.

Godfrey, L., M. Sutherland, D. Boy, and N. Gomberg. 1991. Scaling of limb joint surface areas in anthropoid primates and other mammals. Journal of the Zoological Society of London 223:603-625.

Gould, S. J. 1973. The origin and function of "bizarre" structures: antler size and skull size in the "Irish Elk", *Megaloceros giganteus*. Evolution 28:191-220.

Gingerich, P. D. 1990. Prediction of body mass in mammalian species from long bone lengths and diameters. Contributions from the Museum of Paleontology, The University of Michigan 28(4):79-92.

Graham, R. W. 1985. Diversity and community structure of the late Pleistocene mammal fauna of North America. Acta Zoologica Fennica 170:181-192.

Graham, R. W. and E. L. Lundelius. 1984. Coevolutionary disequilibrium and Pleistocene extinctions; pp.223-249 *in* P. S. Martin and R. G. Klein (eds.), Quaternary Extinctions: A Prehistoric Revolution. University of Arizona Press, Tucson.

Gregory, W. K. 1912. Notes on the principles of quadrupedal locomotion and on the mechanism f the limbs in hoofed animals. Annals of the New York Academy of Sciences 90:217-256.

Guthrie, R. D. 1984. Mosaics, allelochemics and nutrients: An ecological theory of late Pleistocene megafaunal extinctions; pp. 259-298 *in* P. S. Martin and R. G. Klein (eds.) Quaternary Extinctions: A Prehistoric Revolution. University of Arizona Press. Tucson.

Hair, J. F., R. E. Anderson, R. L. Tatham, and W.C. Black. 1995. Multivariate Data Analysis. 4th.ed. Prentice Hall, Englewood Cliffs, New Jersey, 731 pp.

Hildebrand, M. 1988. Analysis of Vertebrate Structure. 3rd. ed. John Wiley and Sons, Inc. New York, 701 pp.

Hofman, M. A. 1988. Allometric scaling in palaeontology: a critical survey. Human Evolution 3(3):177-188.

Howell, A. B. 1944. Speed in Animals. Hafner Publishing Company, New York, 270 pp.

Janis, C. M. 1990. Correlation of cranial and dental variables with body size in ungulates and macropodoids; pp.255-299 *in* J. Damuth and B. J. MacFadden (eds.), Body Size in Mammalian Paleobiology: Estimation and Biological Implications. Cambridge University Press, Cambridge.

Jarman, P. J. 1974. The social organization of antelope in relation to their ecology. Behaviour 48:215-267.

Jungers, W. L. 1988. Relative joint size and hominoid locomotor adaptations with implications for the evolution of hominid bipedalism. Journal of Human Evolution 17:247-265.

Jungers, W. L. 1990. Scaling of postcranial joint size in hominoid primates; pp.87-95 *in* F. K. Jouffroy, M. H. Stack, and C. Niemitz (eds.), Gravity, Posture, and Locomotion in Primates. Firenze: Editrice Il Sedicesimo.

Kleiber, M. 1932. Body size and Metabolism. Hilgardia 6:315-353.

Kleinbaum, D. G., L. L. Kupper, and K. E. Muller. 1988. Applied Regression Analysis and Other Multivariable Methods. Duxbury Press, Belmont, California, 718 pp.

Kreutzer, L. A. 1992. Bison and deer bone mineral densities: comparisons and implications for the interpretation of archaeological faunas. Journal of Archaeological Science 19:271-294.

Lyman, R. L. 1984. Bone density and differential survivorship of fossil classes. Journal of Anthropological Archaeology 3:259-299.

MacArthur, R. H. 1972. Geographical Ecology: Patterns in the Distribution of Species. Harper & Row, New York,

Maiorana, V. C. 1990. Evolutionary strategies and body size in a guild of animals; pp. 69-102 *in* J. Damuth and B. J. MacFadden (eds.), Body Size in Mammalian Paleobiology: Estimation and Biological Implications. Cambridge University Press, Cambridge.

McMahon, T. 1973. Size and shape in biology. Science 179:1201-1204.

McMahon, T. 1975. Allometry and biomechanics: limb bones in adult ungulates. American Naturalist. 109(969): 547-563.

McNab, B. 1990. The physiological significance of body size; pp.11-23 *in* J. Damuth and B. J. MacFadden (eds.), Body Size in Mammalian Paleobiology: Estimation and Biological Implications. Cambridge University Press, Cambridge

Nordin, M. And V. H. Frankel. 1980. Biomechanics of whole bones and bone tissue; pp. 5-60 *in* V. H. Frankel and M. Nordin (eds.), Basic Biomechanics of the Skeletal System. Lea and Febiger, Philadelphia, 323 pp.

Nowak, R. M. 1991. Order Artiodactyla; pp 1334-1499 *in* R. Nowak (ed.), Walker's Mammals of the World. Vol II. 5th ed. The Johns Hopkins University Press, Baltimore

Osborn, H. F. and W. K. Gregory. 1929. Mechanics of locomotion in the evolution of limb structure as bearing on the form and habits of the titanotheres and the related odd-toed ungulates; pp. 727-756 *in* The Titanotheres of Ancient Wyoming, Dakota and Nebraska. U.S. Geological Survey Monograph 55(2).

Pasquini, C. and T. Spurgeon. 1992. Anatomy of Domestic Animals: Systematic and Regional Approach. 5th. ed. Sudz Publishing, Pilot Point, Texas, 641 pp.

Pennycuick, C. J. 1992. Newton Rules Biology: A Physical Approach to Biological Problems. Oxford University Press, Oxford, 111 pp.

Prange, H. D., J. F. Anderson, and H. Rahn. 1979. Scaling of skeletal mass to body mass in birds and mammals. American Naturalist 113:103-122.

Ruff, C. B. 1981. Structural changes in the lower limb bones with aging at the Pecos Pueblo, Ph.D. dissertation, University of Pennsylvania, 492 pp.

Ruff, C. B. 1988. Hindlimb articular surface allometry in Hominoidea and *Macaca*, with comparisons to diaphyseal scaling. Journal of Human Evolution 17:687-714.

Ruff, C. B. 1990. Body mass and hindlimb cross-sectional and articular dimensions in anthropoid primates pp. 119-150 *in* J. Damuth and B. J. MacFadden (eds.) Body Size in Mammalian Paleobiology: Estimation and Biological Implications. Cambridge University Press, Cambridge

Ruff, C. B., E. Trinkhaus, A. Walker, and C. S. Larsen. 1993. Postcranial robusticity in *Homo*, I: Temporal trends and mechanical interpretation. American Journal of Physical Anthropology 91:21-53.

Runestad, J. A. 1994. Humeral and femoral diaphyseal cross-sectional geometry and articular dimensions in prosimii and platyrrhini (Primates) with application for reconstruction of body mass and locomotor behavior in the Adapidae (Primates: Eocene). Ph.D. dissertation, The Johns Hopkins University, Baltimore, 443 pp.

Runestad, J. A., C. B. Ruff, J. C. Nieh, R. W. Thorinton, Jr. and M. F. Teaford. 1993. Radiographic estimation of long bone cross-sectional geometric properties. American Journal of Physical Anthropology 90:207-213.

Schmidt-Nielsen, K. 1984. Scaling: Why is Animal Size so Important? Cambridge University Press, Cambridge, 241 pp.

Scott, K. M. 1979. Adaptation and allometry in bovid postcranial proportions. Ph.D. dissertation, Yale University, 493 pp.

Scott, K. M. 1983. Prediction of body weight of fossil Artiodactyla. Zoological Journal of the Linnean Society 77:199-215.

Scott, K. M. 1985. Allometric trends and locomotor adaptations in the bovidae. Bulletin of the American Museum of Natural History, Vol. 179(2):197-288.

Scott, K. M. 1990. Postcranial dimensions of ungulates as predictors of body mass; pp.301-336 *in* J. Damuth and B.J. MacFadden (eds.), Body Size in Mammalian Paleobiology: Estimation and Biological Implications. Cambridge University Press, Cambridge.

Silva, M. and J. A. Downing. 1995. Handbook of Mammalian Body Masses. CRC Press, Boca Raton, 361 pp.

Silva, M. 1998. Allometric scaling of body length: elastic or geometric similarity in mammalian design. Journal of Mammalogy 79(1):20-32.

Sokel, R. R. and F. J. Rohlf. 1981. Biometry: the principles and practice of statistics in biological research. 2nd. ed. W.H. Freeman and Company, New York, 859 pp.

Sondaar, P. Y. 1977. Insularity and its effect on mammal evolution; pp. *in* M. Hecht (ed.), Major Problems in Vertebrate Evolution. Plenum Press, New York.

Smith, R. J. 1981. Interpretation of correlations in intraspecific and interspecific allometry. Growth 45:291-297.

Smith, R. J. 1984. Allometric scaling in comparative biology: problems of concept and method. American Journal of Physiology 246:R152-R160.

Smith, R. J. 1993. Logarithmic transformation bias in allometry. American Journal of Physical Anthropology 90:215-228.

Snowdon, P. 1991. A ratio estimator for bias correction in logarithmic regressions. Canadian Journal of Forestry Research 21:720-724.

Stahl, W. R. 1967. Scaling of respiratory variables in mammals. Journal of Applied Physiology 22:453-460.

Thompson, D'A. W. 1917. On Growth and Form (rpt. 1942). Cambridge University Press, Cambridge, pp. 22-77.

Timoshenko, S. P. and J. M. Gere. 1972. Mechanics of Materials. D. Van Nostrand Company, New York, 423 pp.

Van Valkenburgh, B. 1984. A Morphological Analysis of Ecological Separation Within Past and Present Predator Guilds. Ph.D. dissertation, The Johns Hopkins University, Baltimore, 286 pp.

Van Valkenburgh, B. 1990. Skeletal and dental predictors of body mass in carnivores; pp. 181-206 *in* J. Damuth and B. J. MacFadden (eds.), Body Size in Mammalian Paleobiology: Estimation and Biological Implications. Cambridge University Press, Cambridge.

Wainwright, S. A., W. D. Biggs, J. D. Currey, and J. M. Gosline. 1976. Mechanical Design in Organisms. John Wiley and Sons, New York, pp. 423

Wilkinson, L. 1997. SYSTAT for Windows. SPSS, Chicago.

Wiens, J. A. 1989. The Ecology of Bird Communties, Volume 1: Foundations and Patterns. Cambridge University Press, Cambridge, 539 pp.

Wunder, B. A. 1984. Strategies for, and environmental cueing mechanisms of, seasonal changes in thermoregulatory parameters of small mammals; pp. 165-172 *in* J. Merritt (ed.), Winter Ecology of Small Mammals. Special Publication of the Carnegie Museum of Natural History 10, Pittsburgh.

Wunder, B. A. 1992. Morphophysiological indicators of energy state of small mammals; pp.81-104 *in* T. E. Tomasi and T. H. Horton (eds.), Mammalian Energetics: Interdisciplinary Views of Metabolism and Reproduction. Comstock Publishing Associates, Ithaca, New York.

Wunder, B. A., D. S. Dobkin, and R. D. Gettinger. 1977. Shifts of thermogenesis in the Prairie Vole (*Microtus ochrogaster*): strategies for survival in a seasonal environment. Oecologia 29:11-26.

Appendix I: Modern Specimens

Species	Common Name	Institution	Specimen #	Sex
Dama dama	Fallow Deer	KU	109504	F
Cervus axis	Axis Deer	KU	140302	F
Cervus axis	Axis Deer	KU	140303	F
Cervus elaphus	Elk	KU	14662	F
Cervus elaphus	Elk	KU	2390	M
Cervus elaphus	Elk	KU	14666	M
Cervus elaphus	Elk	KU	2397	M
Odocoileus hemionus	Mule Deer	KU	9327	M
Odocoileus hemionus	Mule Deer	KU	9328	F
Odocoileus hemionus	Mule Deer	KU	2319	M
Odocoileus hemionus	Mule Deer	KU	143916	F
Odocoileus virginianus	White-tailed Deer	KU	152886	M
Odocoileus virginianus	White-tailed Deer	KU	152887	M
Alces alces	Moose	KU	2425	.
Alces alces	Moose	KU	2444	M
Alces alces	Moose	KU	2467	F
Alces alces	Moose	KU	2419	M
Rangifer tarandus	Caribou	KU	2258	F
Rangifer tarandus	Caribou	KU	2228	F
Antilocapra americana	Pronghorn	USNM	13980	M
Antilocapra americana	Pronghorn	USNM	12726	M
Antilocapra americana	Pronghorn	USNM	22387	M
Antilocapra americana	Pronghorn	USNM	22659	F
Antilocapra americana	Pronghorn	USNM	49688	M
Antilocapra americana	Pronghorn	USNM	557229	M
Antilocapra americana	Pronghorn	USNM	3460	F
Antilocapra americana	Pronghorn	USNM	251131	M
Antilocapra americana	Pronghorn	USNM	22386	M
Antilocapra americana	Pronghorn	USNM	266393	M
Antilocapra americana	Pronghorn	USNM	842	F
Antilocapra americana	Pronghorn	USNM	245622	M
Antilocapra americana	Pronghorn	USNM	256452	M
Antilocapra americana	Pronghorn	USNM	256666	M
Antilocapra americana	Pronghorn	USNM	250126	M
Antilocapra americana	Pronghorn	USNM	251104	F
Antilocapra americana	Pronghorn	USNM	266158	M
Antilocapra americana	Pronghorn	USNM	266159	F
Antilocapra americana	Pronghorn	USNM	266542	F

Species	Common Name	Institution	Specimen #	Sex
Antilocapra americana	**Pronghorn**	USNM	266550	F
Antilocapra americana	**Pronghorn**	USNM	270589	F
Antilocapra americana	**Pronghorn**	USNM	270590	F
Antilocapra americana	**Pronghorn**	USNM	270591	F
Antilocapra americana	**Pronghorn**	USNM	270592	M
Antilocapra americana	**Pronghorn**	USNM	271662	M
Antilocapra americana	**Pronghorn**	USNM	271663	F
Antilocapra americana	**Pronghorn**	USNM	271664	F
Antilocapra americana	**Pronghorn**	USNM	271665	M
Antilocapra americana	**Pronghorn**	USNM	271686	M
Antilocapra americana	**Pronghorn**	USNM	271687	F
Antilocapra americana	**Pronghorn**	USNM	271866	M
Antilocapra americana	**Pronghorn**	USNM	271687	F
Antilocapra americana	**Pronghorn**	USNM	271869	F
Antilocapra americana	**Pronghorn**	USNM	271870	M
Antilocapra americana	**Pronghorn**	USNM	272094	F
Antilocapra americana	**Pronghorn**	USNM	272095	M
Antilocapra americana	**Pronghorn**	USNM	271590	F
Antilocapra americana	**Pronghorn**	USNM	272099	M
Antilocapra americana	**Pronghorn**	USNM	347891	.
Antilocapra americana	**Pronghorn**	USNM	563013	M
Antilocapra americana	**Pronghorn**	USNM	563014	F
Antilocapra americana	**Pronghorn**	USNM	563015	F
Antilocapra americana	**Pronghorn**	USNM	567240	M
Antilocapra americana	**Pronghorn**	USNM	23527	F
Antilocapra americana	**Pronghorn**	KU	12108	F
Antilocapra americana	**Pronghorn**	KU	12113	M
Antilocapra americana	**Pronghorn**	KU	144047	M
Antilocapra americana	**Pronghorn**	KU	145967	F
Antilocapra americana	**Pronghorn**	KU	145966	F
Antilocapra americana	**Pronghorn**	KU	144050	M
Antilocapra americana	**Pronghorn**	KU	146462	M
Antilocapra americana	**Pronghorn**	UW	8361B	M
Antilocapra americana	**Pronghorn**	UW	8255B	.
Antilocapra americana	**Pronghorn**	UW	8403B	M
Antilocapra americana	**Pronghorn**	UW	8409B	M
Antilocapra americana	**Pronghorn**	UW	9092B	F
Antilocapra americana	**Pronghorn**	UW	9101B	M
Antilocapra americana	**Pronghorn**	UW	9315B	M
Antilocapra americana	**Pronghorn**	UW	8262B	M
Antilocapra americana	**Pronghorn**	UW	8425B	F
Antilocapra americana	**Pronghorn**	UW	9281B	M
Antilocapra americana	**Pronghorn**	UW	9270B	F
Antilocapra americana	**Pronghorn**	UW	8263B	M
Antilocapra americana	**Pronghorn**	UW	9271B	M
Antilocapra americana	**Pronghorn**	UW	8492B	F

Species	Common Name	Institution	Specimen #	Sex
Antilocapra americana	Pronghorn	UW	9273B	F
Antilocapra americana	Pronghorn	UW	8408B	F
Tragelaphus strepsiceros	Greater Kudu	KU	EJ43	.
Taurotragus derbianus	Giant Eland	KU	DD48	F
Bison bison	American Bison	UW	9073B	F
Bison bison	American Bison	UW	9262B	F
Bison bison	American Bison	UW	8510B	M
Bison bison	American Bison	UW	8529B	M
Bison bison	American Bison	UW	8330B	M
Bison bison	American Bison	KU	8637B	F
Kobus ellipsiprymnus	Common Waterbuck	KU	DD15	M
Oryx gazella	Gemsbok	KU	CY25	.
Oryx gazella	Gemsbok	KU	835568	F
Alcelaphus buselaphus	Hartebeest	KU	ED10	.
Connochaetes taurinus	Blue Wildebeest	KU	ED27	F
Connochaetes taurinus	Blue Wildebeest	KU	DD24	.
Oreotragus oreotragus	Klipspringer	KU	DD42	M
Aepyceros melampus	Impala	KU	ED3	.
Aepyceros melampus	Impala	KU	CY33	.
Litocranius walleri	Gerenuk	KU	DL30	.
Gazella thomsoni	Thomson's Gazelle	KU	CY47	
Gazella granti	Grant's Gazelle	KU	DL23	.
Oreamnos americanus	Mountain Goat	KU	2640	M
Ovibos moschatus	Musk-ox	KU	10652	M
Ovis aries	Domestic Sheep	KU	145990	.
Ovis canadensis	Bighorn	KU	2770	M
Ovis canadensis	Bighorn	KU	1782	M
Ovis canadensis	Bighorn	KU	1781	M
Ovis canadensis	Bighorn	KU	1802	F
Ovis canadensis	Bighorn	KU	1792	M
Ovis canadensis	Bighorn	KU	1804	M
Ovis canadensis	Bighorn	KU	1808	M
Ovis canadensis	Bighorn	KU	1805	F
Ovis canadensis	Bighorn	KU	1804	M
Ovis canadensis	Bighorn	KU	1809	F
Ovis canadensis	Bighorn	KU	54861	M
Ovis canadensis	Bighorn	KU	54862	M
Ovis canadensis	Bighorn	KU	54863	M
Ovis dalli	Dall Sheep	KU	1842	M

Appendix II: Fossil Specimens

Species	Museum	Specimen #	Locale	Element
Capromeryx arizonensis	UF	45198	Inglis 1A, FL	astragalus
Capromeryx arizonensis	UF	45199	Inglis 1A, FL	astragalus
Capromeryx arizonensis	UF	45201	Inglis 1A, FL	astragalus
Capromeryx arizonensis	UF	45202	Inglis 1A, FL	astragalus
Capromeryx arizonensis	UF	45203	Inglis 1A, FL	astragalus
Capromeryx arizonensis	UF	45204	Inglis 1A, FL	astragalus
Capromeryx arizonensis	UF	45205	Inglis 1A, FL	astragalus
Capromeryx arizonensis	UF	45207	Inglis 1A, FL	astragalus
Capromeryx arizonensis	UF	45208	Inglis 1A, FL	astragalus
Capromeryx arizonensis	UF	45209	Inglis 1A, FL	astragalus
Capromeryx arizonensis	UF	45210	Inglis 1A, FL	astragalus
Capromeryx arizonensis	UF	45211	Inglis 1A, FL	astragalus
Capromeryx arizonensis	UF	45212	Inglis 1A, FL	astragalus
Capromeryx arizonensis	UF	45214	Inglis 1A, FL	astragalus
Capromeryx arizonensis	UF	45215	Inglis 1A, FL	astragalus
Capromeryx arizonensis	UF	45706	Inglis 1A, FL	astragalus
Capromeryx arizonensis	UF	57822	Inglis 1A, FL	astragalus
Capromeryx arizonensis	UF	57823	Inglis 1A, FL	astragalus
Capromeryx arizonensis	UF	57824	Inglis 1A, FL	astragalus
Capromeryx arizonensis	UF	57825	Inglis 1A, FL	astragalus
Capromeryx arizonensis	UF	57826	Inglis 1A, FL	astragalus
Capromeryx arizonensis	UF	57827	Inglis 1A, FL	astragalus
Capromeryx arizonensis	UF	57828	Inglis 1A, FL	astragalus
Capromeryx arizonensis	UF	57829	Inglis 1A, FL	astragalus
Capromeryx arizonensis	UF	57830	Inglis 1A, FL	astragalus
Capromeryx arizonensis	UF	57831	Inglis 1A, FL	astragalus
Capromeryx arizonensis	UF	57832	Inglis 1A, FL	astragalus
Capromeryx arizonensis	UF	57834	Inglis 1A, FL	astragalus
Capromeryx arizonensis	UF	57835	Inglis 1A, FL	astragalus
Capromeryx arizonensis	UF	57836	Inglis 1A, FL	astragalus
Capromeryx arizonensis	UF	57837	Inglis 1A, FL	astragalus
Capromeryx arizonensis	UF	14266	Santa Fe River 8, FL	calcaneum
Capromeryx arizonensis	UF	45216	Inglis 1A, FL	calcaneum
Capromeryx arizonensis	UF	45217	Inglis 1A, FL	calcaneum
Capromeryx arizonensis	UF	45218	Inglis 1A, FL	calcaneum
Capromeryx arizonensis	UF	45220	Inglis 1A, FL	calcaneum
Capromeryx arizonensis	UF	45221	Inglis 1A, FL	calcaneum
Capromeryx arizonensis	UF	45222	Inglis 1A, FL	calcaneum

Species	Museum	Specimen #	Locale	Element
Capromeryx arizonensis	UF	45224	Inglis 1A, FL	calcaneum
Capromeryx arizonensis	UF	45226	Inglis 1A, FL	calcaneum
Capromeryx arizonensis	UF	45227	Inglis 1A, FL	calcaneum
Capromeryx arizonensis	UF	57839	Inglis 1A, FL	calcaneum
Capromeryx arizonensis	UF	57841	Inglis 1A, FL	calcaneum
Capromeryx arizonensis	UF	57842	Inglis 1A, FL	calcaneum
Capromeryx arizonensis	UF	57843	Inglis 1A, FL	calcaneum
Capromeryx arizonensis	UF	57846	Inglis 1A, FL	calcaneum
Capromeryx arizonensis	UF	57847	Inglis 1A, FL	calcaneum
Capromeryx arizonensis	UF	57848	Inglis 1A, FL	calcaneum
Capromeryx arizonensis	UF	57849	Inglis 1A, FL	calcaneum
Capromeryx arizonensis	UF	57850	Inglis 1A, FL	calcaneum
Capromeryx arizonensis	UF	57851	Inglis 1A, FL	calcaneum
Capromeryx arizonensis	UF	43245	Inglis 1A, FL	cubonavicular
Capromeryx arizonensis	UF	45230	Inglis 1A, FL	cubonavicular
Capromeryx arizonensis	UF	45231	Inglis 1A, FL	cubonavicular
Capromeryx arizonensis	UF	45232	Inglis 1A, FL	cubonavicular
Capromeryx arizonensis	UF	45233	Inglis 1A, FL	cubonavicular
Capromeryx arizonensis	UF	45234	Inglis 1A, FL	cubonavicular
Capromeryx arizonensis	UF	45235	Inglis 1A, FL	cubonavicular
Capromeryx arizonensis	UF	45237	Inglis 1A, FL	cubonavicular
Capromeryx arizonensis	UF	45238	Inglis 1A, FL	cubonavicular
Capromeryx arizonensis	UF	45239	Inglis 1A, FL	cubonavicular
Capromeryx arizonensis	UF	45240	Inglis 1A, FL	cubonavicular
Capromeryx arizonensis	UF	45241	Inglis 1A, FL	cubonavicular
Capromeryx arizonensis	UF	45242	Inglis 1A, FL	cubonavicular
Capromeryx arizonensis	UF	45243	Inglis 1A, FL	cubonavicular
Capromeryx arizonensis	UF	45246	Inglis 1A, FL	cubonavicular
Capromeryx arizonensis	UF	4521	Inglis 1A, FL	femur
Capromeryx arizonensis	UF	7336	Inglis 1A, FL	femur
Capromeryx arizonensis	UF	7358	Inglis 1A, FL	femur
Capromeryx arizonensis	UF	24339	Santa Fe River 4A, FL	femur
Capromeryx arizonensis	UF	24343	Santa Fe River 4A, FL	femur
Capromeryx arizonensis	UF	45161	Inglis 1A, FL	femur
Capromeryx arizonensis	UF	45162	Inglis 1A, FL	femur
Capromeryx arizonensis	UF	45163	Inglis 1A, FL	femur
Capromeryx arizonensis	UF	45164	Inglis 1A, FL	femur
Capromeryx arizonensis	UF	45165	Inglis 1A, FL	femur
Capromeryx arizonensis	UF	45170	Inglis 1A, FL	femur
Capromeryx arizonensis	UF	45173	Inglis 1A, FL	femur
Capromeryx arizonensis	UF	45174	Inglis 1A, FL	femur
Capromeryx arizonensis	UF	51778	Inglis 1A, FL	femur
Capromeryx arizonensis	UF	57779	Inglis 1A, FL	femur
Capromeryx arizonensis	UF	57780	Inglis 1A, FL	femur
Capromeryx arizonensis	UF	57785	Inglis 1A, FL	femur
Capromeryx arizonensis	UF	57786	Inglis 1A, FL	femur

Species	Museum	Specimen #	Locale	Element
Capromeryx arizonensis	UF	57787	Inglis 1A, FL	femur
Capromeryx arizonensis	UF	57788	Inglis 1A, FL	femur
Capromeryx arizonensis	UF	57789	Inglis 1A, FL	femur
Capromeryx arizonensis	UF	57790	Inglis 1A, FL	femur
Capromeryx arizonensis	UF	57794	Inglis 1A, FL	femur
Capromeryx arizonensis	UF	57795	Inglis 1A, FL	femur
Capromeryx arizonensis	UF	57796	Inglis 1A, FL	femur
Capromeryx arizonensis	UF	57802	Inglis 1A, FL	femur
Capromeryx arizonensis	UF	8909	Santa Fe River 1, FL	humerus
Capromeryx arizonensis	UF	10798	Santa Fe River 1, FL	humerus
Capromeryx arizonensis	UF	11859	Santa Fe River 1, FL	humerus
Capromeryx arizonensis	UF	18273	Inglis 1A, FL	humerus
Capromeryx arizonensis	UF	24312	Santa Fe River 4A, FL	humerus
Capromeryx arizonensis	UF	24319	Santa Fe River 4A, FL	humerus
Capromeryx arizonensis	UF	45179	Inglis 1A, FL	humerus
Capromeryx arizonensis	UF	45181	Inglis 1A, FL	humerus
Capromeryx arizonensis	UF	45184	Inglis 1A, FL	humerus
Capromeryx arizonensis	UF	45185	Inglis 1A, FL	humerus
Capromeryx arizonensis	UF	45186	Inglis 1A, FL	humerus
Capromeryx arizonensis	UF	45190	Inglis 1A, FL	humerus
Capromeryx arizonensis	UF	45192	Inglis 1A, FL	humerus
Capromeryx arizonensis	UF	45194	Inglis 1A, FL	humerus
Capromeryx arizonensis	UF	45195	Inglis 1A, FL	humerus
Capromeryx arizonensis	UF	57098	Inglis 1A, FL	humerus
Capromeryx arizonensis	UF	57099	Inglis 1A, FL	humerus
Capromeryx arizonensis	UF	57752	Inglis 1A, FL	humerus
Capromeryx arizonensis	UF	57753	Inglis 1A, FL	humerus
Capromeryx arizonensis	UF	57754	Inglis 1A, FL	humerus
Capromeryx arizonensis	UF	57756	Inglis 1A, FL	humerus
Capromeryx arizonensis	UF	57757	Inglis 1A, FL	humerus
Capromeryx arizonensis	UF	57758	Inglis 1A, FL	humerus
Capromeryx arizonensis	UF	57759	Inglis 1A, FL	humerus
Capromeryx arizonensis	UF	57760	Inglis 1A, FL	humerus
Capromeryx arizonensis	UF	57761	Inglis 1A, FL	humerus
Capromeryx arizonensis	UF	57766	Inglis 1A, FL	humerus
Capromeryx arizonensis	UF	57768	Inglis 1A, FL	humerus
Capromeryx arizonensis	UF	57769	Inglis 1A, FL	humerus
Capromeryx arizonensis	UF	57770	Inglis 1A, FL	humerus
Capromeryx arizonensis	UF	57771	Inglis 1A, FL	humerus
Capromeryx arizonensis	UF	57773	Inglis 1A, FL	humerus
Capromeryx arizonensis	UF	57774	Inglis 1A, FL	humerus
Capromeryx arizonensis	UF	57775	Inglis 1A, FL	humerus
Capromeryx arizonensis	UF	57777	Inglis 1A, FL	humerus
Capromeryx arizonensis	UF	57812	Inglis 1A, FL	humerus
Capromeryx arizonensis	UF	57814	Inglis 1A, FL	humerus
Capromeryx arizonensis	UF	57816	Inglis 1A, FL	humerus

Species	Museum	Specimen #	Locale	Element
Capromeryx arizonensis	UF	57818	Inglis 1A, FL	humerus
Capromeryx arizonensis	UF	10814	Santa Fe River 1B, FL	m1
Capromeryx arizonensis	UF	18267	Inglis 1A, FL	m1
Capromeryx arizonensis	UF	45269	Inglis 1A, FL	m1
Capromeryx arizonensis	UF	7334	Inglis 1A, FL	m1/m2
Capromeryx arizonensis	UF	10810	Santa Fe River 1B, FL	m1/m2
Capromeryx arizonensis	UF	18267	Inglis 1A, FL	m1/m2
Capromeryx arizonensis	UF	18267	Inglis 1A, FL	m1/m2
Capromeryx arizonensis	UF	67812	Inglis 1A, FL	m1/m2
Capromeryx arizonensis	UF	11953	Santa Fe River 1B, FL	m2
Capromeryx arizonensis	UF	18267	Inglis 1A, FL	m2
Capromeryx arizonensis	UF	18270	Inglis 1A, FL	m2
Capromeryx arizonensis	UF	54655	Inglis 1A, FL	m2
Capromeryx arizonensis	UF	54656	Inglis 1A, FL	m2
Capromeryx arizonensis	UF	54664	Inglis 1A, FL	m2
Capromeryx arizonensis	UF	54665	Inglis 1A, FL	m2
Capromeryx arizonensis	UF	179278	Inglis 1A, FL	m2
Capromeryx arizonensis	UF	18261	Inglis 1A, FL	M2
Capromeryx arizonensis	UF	45265	Inglis 1A, FL	M2
Capromeryx arizonensis	UF	179269	Inglis 1A, FL	M2
Capromeryx arizonensis	UF	165815	Inglis 1A, FL	magnum
Capromeryx arizonensis	UF	165816	Inglis 1A, FL	magnum
Capromeryx arizonensis	UF	165817	Inglis 1A, FL	magnum
Capromeryx arizonensis	UF	165818	Inglis 1A, FL	magnum
Capromeryx arizonensis	UF	165819	Inglis 1A, FL	magnum
Capromeryx arizonensis	UF	165820	Inglis 1A, FL	magnum
Capromeryx arizonensis	UF	165821	Inglis 1A, FL	magnum
Capromeryx arizonensis	UF	165822	Inglis 1A, FL	magnum
Capromeryx arizonensis	UF	165823	Inglis 1A, FL	magnum
Capromeryx arizonensis	UF	165824	Inglis 1A, FL	magnum
Capromeryx arizonensis	UF	165825	Inglis 1A, FL	magnum
Capromeryx arizonensis	UF	5136	Santa Fe River 1, FL	metacarpal
Capromeryx arizonensis	UF	7342	Santa Fe River 1, FL	metacarpal
Capromeryx arizonensis	UF	7352	Santa Fe River 1, FL	metacarpal
Capromeryx arizonensis	UF	7353	Santa Fe River 1, FL	metacarpal
Capromeryx arizonensis	UF	7356	Santa Fe River 1, FL	metacarpal
Capromeryx arizonensis	UF	7360	Santa Fe River 1, FL	metacarpal
Capromeryx arizonensis	UF	10803	Santa Fe River 1, FL	metacarpal
Capromeryx arizonensis	UF	11851	Santa Fe River 1B, FL	metacarpal
Capromeryx arizonensis	UF	11863	Santa Fe River 1B, FL	metacarpal
Capromeryx arizonensis	UF	15108	Santa Fe River 8, FL	metacarpal
Capromeryx arizonensis	UF	18276	Inglis 1A, FL	metacarpal
Capromeryx arizonensis	UF	24327	Santa Fe River 4A, FL	metacarpal
Capromeryx arizonensis	UF	45090	Inglis 1A, FL	metacarpal
Capromeryx arizonensis	UF	45092	Inglis 1A, FL	metacarpal
Capromeryx arizonensis	UF	45108	Santa Fe River 1, FL	metacarpal

Species	Museum	Specimen #	Locale	Element
Capromeryx arizonensis	UF	55769	Inglis 1A, FL	metacarpal
Capromeryx arizonensis	UF	55770	Inglis 1A, FL	metacarpal
Capromeryx arizonensis	UF	55783	Inglis 1A, FL	metacarpal
Capromeryx arizonensis	UF	55784	Inglis 1A, FL	metacarpal
Capromeryx arizonensis	UF	55787	Inglis 1A, FL	metacarpal
Capromeryx arizonensis	UF	55791	Inglis 1A, FL	metacarpal
Capromeryx arizonensis	UF	56813	Inglis 1A, FL	metacarpal
Capromeryx arizonensis	UF	56856	Inglis 1A, FL	metacarpal
Capromeryx arizonensis	UF	56887	Inglis 1A, FL	metacarpal
Capromeryx arizonensis	UF	56896	Inglis 1A, FL	metacarpal
Capromeryx arizonensis	UF	57586	Santa Fe River 1B, FL	metacarpal
Capromeryx arizonensis	UF	7244	Santa Fe River 1B, FL	metatarsal
Capromeryx arizonensis	UF	7346	Santa Fe River 1B, FL	metatarsal
Capromeryx arizonensis	UF	10789	Santa Fe River 1B, FL	metatarsal
Capromeryx arizonensis	UF	10790	Santa Fe River 1B, FL	metatarsal
Capromeryx arizonensis	UF	10791	Santa Fe River 1B, FL	metatarsal
Capromeryx arizonensis	UF	10793	Santa Fe River 1B, FL	metatarsal
Capromeryx arizonensis	UF	10794	Santa Fe River 1B, FL	metatarsal
Capromeryx arizonensis	UF	11850	Santa Fe River 1B, FL	metatarsal
Capromeryx arizonensis	UF	11852	Santa Fe River 1B, FL	metatarsal
Capromeryx arizonensis	UF	15106	Santa Fe River 8, FL	metatarsal
Capromeryx arizonensis	UF	15108	Santa Fe River 8, FL	metatarsal
Capromeryx arizonensis	UF	16758	Santa Fe River 8, FL	metatarsal
Capromeryx arizonensis	UF	24357	Santa Fe River 4A, FL	metatarsal
Capromeryx arizonensis	UF	24358	Santa Fe River 4A, FL	metatarsal
Capromeryx arizonensis	UF	24359	Santa Fe River 4A, FL	metatarsal
Capromeryx arizonensis	UF	24362	Santa Fe River 4A, FL	metatarsal
Capromeryx arizonensis	UF	24364	Santa Fe River 4A, FL	metatarsal
Capromeryx arizonensis	UF	24365	Santa Fe River 4A, FL	metatarsal
Capromeryx arizonensis	UF	24366	Santa Fe River 4A, FL	metatarsal
Capromeryx arizonensis	UF	24367	Santa Fe River 4A, FL	metatarsal
Capromeryx arizonensis	UF	24368	Santa Fe River 4A, FL	metatarsal
Capromeryx arizonensis	UF	24369	Santa Fe River 4A, FL	metatarsal
Capromeryx arizonensis	UF	24371	Santa Fe River 4A, FL	metatarsal
Capromeryx arizonensis	UF	24372	Santa Fe River 4A, FL	metatarsal
Capromeryx arizonensis	UF	24373	Santa Fe River 4A, FL	metatarsal
Capromeryx arizonensis	UF	45095	Inglis 1A, FL	metatarsal
Capromeryx arizonensis	UF	45100	Inglis 1A, FL	metatarsal
Capromeryx arizonensis	UF	56858	Inglis 1A, FL	metatarsal
Capromeryx arizonensis	UF	56859	Inglis 1A, FL	metatarsal
Capromeryx arizonensis	UF	56860	Inglis 1A, FL	metatarsal
Capromeryx arizonensis	UF	56861	Inglis 1A, FL	metatarsal
Capromeryx arizonensis	UF	57587	Santa Fe River 1B, FL	metatarsal
Capromeryx arizonensis	UF	D135	Santa Fe River 1B, FL	metatarsal
Capromeryx arizonensis	UF	54670	Inglis 1A, FL	p4
Capromeryx arizonensis	UF	7350	Santa Fe River 5, FL	radius

Species	Museum	Specimen #	Locale	Element
Capromeryx arizonensis	UF	8914	Santa Fe River 1, FL	radius
Capromeryx arizonensis	UF	10834	Santa Fe River 1, FL	radius
Capromeryx arizonensis	UF	10835	Santa Fe River 1, FL	radius
Capromeryx arizonensis	UF	18275	Inglis 1A, FL	radius
Capromeryx arizonensis	UF	24315	Santa Fe River 4A, FL	radius
Capromeryx arizonensis	UF	24316	Santa Fe River 4A, FL	radius
Capromeryx arizonensis	UF	24317	Santa Fe River 4A, FL	radius
Capromeryx arizonensis	UF	24319	Santa Fe River 4A, FL	radius
Capromeryx arizonensis	UF	24320	Santa Fe River 4A, FL	radius
Capromeryx arizonensis	UF	24321	Santa Fe River 4A, FL	radius
Capromeryx arizonensis	UF	24323	Santa Fe River 4A, FL	radius
Capromeryx arizonensis	UF	24324	Santa Fe River 4A, FL	radius
Capromeryx arizonensis	UF	24325	Santa Fe River 4A, FL	radius
Capromeryx arizonensis	UF	24925	Santa Fe River 4A, FL	radius
Capromeryx arizonensis	UF	45103	Inglis 1A, FL	radius
Capromeryx arizonensis	UF	45104	Inglis 1A, FL	radius
Capromeryx arizonensis	UF	45105	Inglis 1A, FL	radius
Capromeryx arizonensis	UF	45109	Inglis 1A, FL	radius
Capromeryx arizonensis	UF	45110	Inglis 1A, FL	radius
Capromeryx arizonensis	UF	45111	Inglis 1A, FL	radius
Capromeryx arizonensis	UF	45112	Inglis 1A, FL	radius
Capromeryx arizonensis	UF	45113	Inglis 1A, FL	radius
Capromeryx arizonensis	UF	45117	Inglis 1A, FL	radius
Capromeryx arizonensis	UF	45118	Inglis 1A, FL	radius
Capromeryx arizonensis	UF	45119	Inglis 1A, FL	radius
Capromeryx arizonensis	UF	45121	Inglis 1A, FL	radius
Capromeryx arizonensis	UF	45124	Inglis 1A, FL	radius
Capromeryx arizonensis	UF	45125	Inglis 1A, FL	radius
Capromeryx arizonensis	UF	54687	Inglis 1A, FL	radius
Capromeryx arizonensis	UF	54688	Inglis 1A, FL	radius
Capromeryx arizonensis	UF	54689	Inglis 1A, FL	radius
Capromeryx arizonensis	UF	54690	Inglis 1A, FL	radius
Capromeryx arizonensis	UF	54691	Inglis 1A, FL	radius
Capromeryx arizonensis	UF	54692	Inglis 1A, FL	radius
Capromeryx arizonensis	UF	54696	Inglis 1A, FL	radius
Capromeryx arizonensis	UF	54697	Inglis 1A, FL	radius
Capromeryx arizonensis	UF	54698	Inglis 1A, FL	radius
Capromeryx arizonensis	UF	54963	Inglis 1A, FL	radius
Capromeryx arizonensis	UF	55758	Inglis 1A, FL	radius
Capromeryx arizonensis	UF	55759	Inglis 1A, FL	radius
Capromeryx arizonensis	UF	55763	Inglis 1A, FL	radius
Capromeryx arizonensis	UF	55765	Inglis 1A, FL	radius
Capromeryx arizonensis	UF	55766	Inglis 1A, FL	radius
Capromeryx arizonensis	UF	55767	Inglis 1A, FL	radius
Capromeryx arizonensis	UF	55768	Inglis 1A, FL	radius
Capromeryx arizonensis	UF	16760	Santa Fe River 8, FL	scapula

Species	Museum	Specimen #	Locale	Element
Capromeryx arizonensis	UF	57867	Inglis 1A, FL	scapula
Capromeryx arizonensis	UF	57868	Inglis 1A, FL	scapula
Capromeryx arizonensis	UF	57871	Inglis 1A, FL	scapula
Capromeryx arizonensis	UF	57872	Inglis 1A, FL	scapula
Capromeryx arizonensis	UF	57875	Inglis 1A, FL	scapula
Capromeryx arizonensis	UF	57877	Inglis 1A, FL	scapula
Capromeryx arizonensis	UF	57878	Inglis 1A, FL	scapula
Capromeryx arizonensis	UF	57880	Inglis 1A, FL	scapula
Capromeryx arizonensis	UF	57881	Inglis 1A, FL	scapula
Capromeryx arizonensis	UF	57884	Inglis 1A, FL	scapula
Capromeryx arizonensis	UF	57886	Inglis 1A, FL	scapula
Capromeryx arizonensis	UF	57887	Inglis 1A, FL	scapula
Capromeryx arizonensis	UF	57888	Inglis 1A, FL	scapula
Capromeryx arizonensis	UF	57889	Inglis 1A, FL	scapula
Capromeryx arizonensis	UF	57890	Inglis 1A, FL	scapula
Capromeryx arizonensis	UF	57891	Inglis 1A, FL	scapula
Capromeryx arizonensis	UF	57892	Inglis 1A, FL	scapula
Capromeryx arizonensis	UF	57893	Inglis 1A, FL	scapula
Capromeryx arizonensis	UF	57894	Inglis 1A, FL	scapula
Capromeryx arizonensis	UF	57895	Inglis 1A, FL	scapula
Capromeryx arizonensis	UF	57896	Inglis 1A, FL	scapula
Capromeryx arizonensis	UF	57897	Inglis 1A, FL	scapula
Capromeryx arizonensis	UF	57899	Inglis 1A, FL	scapula
Capromeryx arizonensis	UF	57900	Inglis 1A, FL	scapula
Capromeryx arizonensis	UF	58101	Inglis 1A, FL	scapula
Capromeryx arizonensis	UF	58103	Inglis 1A, FL	scapula
Capromeryx arizonensis	UF	58104	Inglis 1A, FL	scapula
Capromeryx arizonensis	UF	58107	Inglis 1A, FL	scapula
Capromeryx arizonensis	UF	58108	Inglis 1A, FL	scapula
Capromeryx arizonensis	UF	58109	Inglis 1A, FL	scapula
Capromeryx arizonensis	UF	58110	Inglis 1A, FL	scapula
Capromeryx arizonensis	UF	58111	Inglis 1A, FL	scapula
Capromeryx arizonensis	UF	58112	Inglis 1A, FL	scapula
Capromeryx arizonensis	UF	7335	Santa Fe River 1, FL	tibia
Capromeryx arizonensis	UF	8910	Santa Fe River 1, FL	tibia
Capromeryx arizonensis	UF	10824	Santa Fe River 1, FL	tibia
Capromeryx arizonensis	UF	16808	Santa Fe River 4A, FL	tibia
Capromeryx arizonensis	UF	24342	Santa Fe River 4A, FL	tibia
Capromeryx arizonensis	UF	24343	Santa Fe River 4A, FL	tibia
Capromeryx arizonensis	UF	24344	Santa Fe River 4A, FL	tibia
Capromeryx arizonensis	UF	24345	Santa Fe River 4A, FL	tibia
Capromeryx arizonensis	UF	24347	Santa Fe River 4A, FL	tibia
Capromeryx arizonensis	UF	24350	Santa Fe River 4A, FL	tibia
Capromeryx arizonensis	UF	24351	Santa Fe River 4A, FL	tibia
Capromeryx arizonensis	UF	24352	Santa Fe River 4A, FL	tibia
Capromeryx arizonensis	UF	45128	Inglis 1A, FL	tibia

Species	Museum	Specimen #	Locale	Element
Capromeryx arizonensis	UF	45129	Inglis 1A, FL	tibia
Capromeryx arizonensis	UF	45130	Inglis 1A, FL	tibia
Capromeryx arizonensis	UF	45132	Inglis 1A, FL	tibia
Capromeryx arizonensis	UF	45133	Inglis 1A, FL	tibia
Capromeryx arizonensis	UF	45135	Inglis 1A, FL	tibia
Capromeryx arizonensis	UF	45136	Inglis 1A, FL	tibia
Capromeryx arizonensis	UF	45138	Inglis 1A, FL	tibia
Capromeryx arizonensis	UF	45139	Inglis 1A, FL	tibia
Capromeryx arizonensis	UF	45140	Inglis 1A, FL	tibia
Capromeryx arizonensis	UF	45141	Inglis 1A, FL	tibia
Capromeryx arizonensis	UF	45143	Inglis 1A, FL	tibia
Capromeryx arizonensis	UF	45144	Inglis 1A, FL	tibia
Capromeryx arizonensis	UF	45145	Inglis 1A, FL	tibia
Capromeryx arizonensis	UF	45146	Inglis 1A, FL	tibia
Capromeryx arizonensis	UF	45147	Inglis 1A, FL	tibia
Capromeryx arizonensis	UF	45148	Inglis 1A, FL	tibia
Capromeryx arizonensis	UF	45149	Inglis 1A, FL	tibia
Capromeryx arizonensis	UF	45151	Inglis 1A, FL	tibia
Capromeryx arizonensis	UF	45152	Inglis 1A, FL	tibia
Capromeryx arizonensis	UF	45153	Inglis 1A, FL	tibia
Capromeryx arizonensis	UF	45155	Inglis 1A, FL	tibia
Capromeryx arizonensis	UF	45156	Inglis 1A, FL	tibia
Capromeryx arizonensis	UF	45158	Inglis 1A, FL	tibia
Capromeryx arizonensis	UF	45159	Inglis 1A, FL	tibia
Capromeryx arizonensis	UF	45160	Inglis 1A, FL	tibia
Capromeryx arizonensis	UF	55070	Inglis 1A, FL	tibia
Capromeryx arizonensis	UF	57062	Inglis 1A, FL	tibia
Capromeryx arizonensis	UF	57063	Inglis 1A, FL	tibia
Capromeryx arizonensis	UF	57065	Inglis 1A, FL	tibia
Capromeryx arizonensis	UF	57066	Inglis 1A, FL	tibia
Capromeryx arizonensis	UF	57071	Inglis 1A, FL	tibia
Capromeryx arizonensis	UF	57072	Inglis 1A, FL	tibia
Capromeryx arizonensis	UF	57076	Inglis 1A, FL	tibia
Capromeryx arizonensis	UF	57077	Inglis 1A, FL	tibia
Capromeryx arizonensis	UF	57078	Inglis 1A, FL	tibia
Capromeryx arizonensis	UF	57079	Inglis 1A, FL	tibia
Capromeryx arizonensis	UF	57080	Inglis 1A, FL	tibia
Capromeryx arizonensis	UF	57081	Inglis 1A, FL	tibia
Capromeryx arizonensis	UF	57082	Inglis 1A, FL	tibia
Capromeryx arizonensis	UF	57083	Inglis 1A, FL	tibia
Capromeryx arizonensis	UF	57084	Inglis 1A, FL	tibia
Capromeryx arizonensis	UF	57085	Inglis 1A, FL	tibia
Capromeryx arizonensis	UF	57086	Inglis 1A, FL	tibia
Capromeryx arizonensis	UF	57087	Inglis 1A, FL	tibia
Capromeryx arizonensis	UF	57088	Inglis 1A, FL	tibia
Capromeryx arizonensis	UF	57092	Inglis 1A, FL	tibia

Species	Museum	Specimen #	Locale	Element
Capromeryx arizonensis	UF	57095	Inglis 1A, FL	tibia
Capromeryx arizonensis	UF	57096	Inglis 1A, FL	tibia
Capromeryx arizonensis	UF	18278	Inglis 1A, FL	ulna
Capromeryx arizonensis	UF	57857	Inglis 1A, FL	ulna
Capromeryx arizonensis	UF	57858	Inglis 1A, FL	ulna
Capromeryx arizonensis	UF	57859	Inglis 1A, FL	ulna
Capromeryx arizonensis	UF	57860	Inglis 1A, FL	ulna
Capromeryx arizonensis	UF	57861	Inglis 1A, FL	ulna
Capromeryx arizonensis	UF	57863	Inglis 1A, FL	ulna
Capromeryx arizonensis	UF	58113	Inglis 1A, FL	ulna
Capromeryx arizonensis	UF	58114	Inglis 1A, FL	ulna
Capromeryx arizonensis	UF	58117	Inglis 1A, FL	ulna
Capromeryx arizonensis	UF	58119	Inglis 1A, FL	ulna
Capromeryx arizonensis	UF	58120	Inglis 1A, FL	ulna
Capromeryx arizonensis	UF	58123	Inglis 1A, FL	ulna
Capromeryx arizonensis	UF	58124	Inglis 1A, FL	ulna
Capromeryx arizonensis	UF	58126	Inglis 1A, FL	ulna
Capromeryx arizonensis	UF	58127	Inglis 1A, FL	ulna
Capromeryx arizonensis	UF	58128	Inglis 1A, FL	ulna
Capromeryx furcifer	UNSM	88631	Rushville, NE	astragalus
Capromeryx furcifer	UNSM	88632	Rushville, NE	astragalus
Capromeryx furcifer	AMNH	2777	Hay Springs, NE	humerus
Capromeryx furcifer	F:AM	25673	Hay Springs, NE	humerus
Capromeryx furcifer	UM	38634	Cragin Quarry, KS	humerus
Capromeryx furcifer	UNSM	88629	Rushville, NE	humerus
Capromeryx furcifer	UNSM	88641	Hay Springs, NE	humerus
Capromeryx furcifer	AMNH	2771	Hay Springs, NE	m1/m2
Capromeryx furcifer	KU	7418	Cragin Quarry, KS	m1/m2
Capromeryx furcifer	KU	7419	Cragin Quarry, KS	m1/m2
Capromeryx furcifer	KU	7421	Cragin Quarry, KS	m1/m2
Capromeryx furcifer	UNSM	21470	Hay Springs, NE	m1/m2
Capromeryx furcifer	KU	7420	Cragin Quarry, KS	m2
Capromeryx furcifer	UNSM	21472	Inglis 1A, FL	M2
Capromeryx furcifer	UNSM	88633	Rushville, NE	metacarpal
Capromeryx furcifer	TMM	882-341	Slaton Quarry, TX	metatarsal
Capromeryx furcifer	UM	38633	Cragin Quarry, KS	tibia
Capromeryx furcifer	TMM	882-341	Slaton Quarry, TX	tibia
Capromeryx gidleyi	F:AM	23324	Benson, AZ	horn-core
Capromeryx mexicanus	UCMP	26648	Tequixquiac, Mexico	astragalus
Capromeryx mexicanus	UCMP	26648	Tequixquiac, Mexico	calcaneum
Capromeryx mexicanus	UCMP	26648	Tequixquiac, Mexico	cubonavicular
Capromeryx mexicanus	UCMP	26648	Tequixquiac, Mexico	humerus
Capromeryx mexicanus	MSU	CF629	Cedazo, Mexico	m1

Species	Museum	Specimen #	Locale	Element
Capromeryx mexicanus	UAHMP	32	Hueyahaco, Mexico	m1/m2
Capromeryx mexicanus	UAHMP	DPs/n	Valsequillo, Mexico	m1/m2
Capromeryx mexicanus	UCMP	26648	Tequixquiac, Mexico	magnum
Capromeryx mexicanus	UCMP	26648	Tequixquiac, Mexico	metacarpal
Capromeryx mexicanus	UCMP	26648	Tequixquiac, Mexico	metatarsal
Capromeryx mexicanus	UAHMP	244	Rancho la Brisca, MX	radius
Capromeryx mexicanus	UCMP	26648	Tequixquiac, Mexico	radius
Capromeryx mexicanus	UCMP	26648	Tequixquiac, Mexico	tibia
Capromeryx minor	LACM	39730	Rancho la Brea, CA	astragalus
Capromeryx minor	LACM	48981	Rancho la Brea, CA	astragalus
Capromeryx minor	LACM	60574	Rancho la Brea, CA	astragalus
Capromeryx minor	TMM	30967-2137	Ingleside, TX	astragalus
Capromeryx minor	TMM	30967-743	Ingleside, TX	astragalus
Capromeryx minor	TMM	998-20	Scharbauer Ranch,NM	astragalus
Capromeryx minor	LACM	Z8157	Rancho la Brea, CA	astragalus
Capromeryx minor	LACM	Z8740	Rancho la Brea, CA	astragalus
Capromeryx minor	LACM	Z8744	Rancho la Brea, CA	astragalus
Capromeryx minor	TMM	31034-91	Curtis Ranch, AZ	calcaneum
Capromeryx minor	TMM	998-236	Scharbauer Ranch,NM	calcaneum
Capromeryx minor	LACM	CIT15	McKittrick, CA	calcaneum
Capromeryx minor	LACM	R25311	Rancho la Brea, CA	calcaneum
Capromeryx minor	LACM	Z8729	Rancho la Brea, CA	calcaneum
Capromeryx minor	LACM	Z8730	Rancho la Brea, CA	calcaneum
Capromeryx minor	LACM	60576	Rancho la Brea, CA	cubonavicular
Capromeryx minor	LACM	R30117	Rancho la Brea, CA	cubonavicular
Capromeryx minor	LACM	R52037	Rancho la Brea, CA	cubonavicular
Capromeryx minor	LACM	Z8745	Rancho la Brea, CA	cubonavicular
Capromeryx minor	LACM	121360	McKittrick, CA	femur
Capromeryx minor	LACM	44255	Rancho la Brea, CA	humerus
Capromeryx minor	LACM	Z8558	Rancho la Brea, CA	humerus
Capromeryx minor	LACM	Z8559	Rancho la Brea, CA	humerus
Capromeryx minor	LACM	Z8560	Rancho la Brea, CA	humerus
Capromeryx minor	LACM	Z8561	Rancho la Brea, CA	humerus
Capromeryx minor	LACM	Z8573	Rancho la Brea, CA	humerus
Capromeryx minor	LACM	Z8575	Rancho la Brea, CA	humerus
Capromeryx minor	LACM	Z8576	Rancho la Brea, CA	humerus
Capromeryx minor	UCMP	19977	Rancho la Brea, CA	m1
Capromeryx minor	LACM	60544	Rancho la Brea, CA	m1
Capromeryx minor	LACM	R18773	Rancho la Brea, CA	m1
Capromeryx minor	LACM	12674	Rancho la Brea, CA	m1/m2
Capromeryx minor	UCMP	20062	Rancho la Brea, CA	m1/m2
Capromeryx minor	LACM	60542	Rancho la Brea, CA	m1/m2
Capromeryx minor	LACM	60543	Rancho la Brea, CA	m1/m2
Capromeryx minor	LACM	1010/679	Shelter Cave, NM	m1/m2
Capromeryx minor	LACM	R52168	Rancho la Brea, CA	m1/m2

Species	Museum	Specimen #	Locale	Element
Capromeryx minor	LACM	Z8505	Rancho la Brea, CA	m1/m2
Capromeryx minor	LACM	Z8511	Rancho la Brea, CA	m1/m2
Capromeryx minor	LACM	Z8512	Rancho la Brea, CA	m1/m2
Capromeryx minor	LACM	Z8520	Rancho la Brea, CA	m1/m2
Capromeryx minor	LACM	60550	Rancho la Brea, CA	m2
Capromeryx minor	LACM	121359	Rancho la Brea, CA	m2
Capromeryx minor	LACM	CIT15	McKittrick, CA	m2
Capromeryx minor	LACM	Z8503	Rancho la Brea, CA	m2
Capromeryx minor	LACM	Z8517	Rancho la Brea, CA	m2
Capromeryx minor	LACM	60537	Rancho la Brea, CA	M2
Capromeryx minor	LACM	107249	Rancho la Brea, CA	M2
Capromeryx minor	LACM	107250	Rancho la Brea, CA	M2
Capromeryx minor	UTEP	26-9	Rm.Vanishing Floor,TX	M2
Capromeryx minor	LACM	CIT 17	McKittrick, CA	M2
Capromeryx minor	LACM	R22336	Rancho la Brea, CA	M2
Capromeryx minor	LACM	Z8526	Rancho la Brea, CA	M2
Capromeryx minor	LACM	R21035	Rancho la Brea, CA	magnum
Capromeryx minor	LACM	60561	Rancho la Brea, CA	metacarpal
Capromeryx minor	LACM	60562	Rancho la Brea, CA	metacarpal
Capromeryx minor	LACM	60563	Rancho la Brea, CA	metacarpal
Capromeryx minor	LACM	60564	Rancho la Brea, CA	metacarpal
Capromeryx minor	LACM	60567	Rancho la Brea, CA	metacarpal
Capromeryx minor	LACM	107247	Rancho la Brea, CA	metacarpal
Capromeryx minor	LACM	CIT138	McKittrick, CA	metacarpal
Capromeryx minor	LACM	R10581	Rancho la Brea, CA	metacarpal
Capromeryx minor	LACM	R16287	Rancho la Brea, CA	metacarpal
Capromeryx minor	LACM	Z158	Rancho la Brea, CA	metacarpal
Capromeryx minor	LACM	Z8657	Rancho la Brea, CA	metacarpal
Capromeryx minor	LACM	Z8658	Rancho la Brea, CA	metacarpal
Capromeryx minor	LACM	Z8659	Rancho la Brea, CA	metacarpal
Capromeryx minor	LACM	Z8668	Rancho la Brea, CA	metacarpal
Capromeryx minor	LACM	Z8670	Rancho la Brea, CA	metacarpal
Capromeryx minor	LACM	Z8672	Rancho la Brea, CA	metacarpal
Capromeryx minor	LACM	Z8686	Rancho la Brea, CA	metacarpal
Capromeryx minor	LACM	60577	Rancho la Brea, CA	metatarsal
Capromeryx minor	LACM	60593	Rancho la Brea, CA	metatarsal
Capromeryx minor	LACM	Z8692	Rancho la Brea, CA	metatarsal
Capromeryx minor	LACM	Z8693	Rancho la Brea, CA	metatarsal
Capromeryx minor	LACM	Z8695	Rancho la Brea, CA	metatarsal
Capromeryx minor	LACM	Z8698	Rancho la Brea, CA	metatarsal
Capromeryx minor	LACM	Z8701	Rancho la Brea, CA	metatarsal
Capromeryx minor	LACM	Z8706	Rancho la Brea, CA	metatarsal
Capromeryx minor	LACM	Z8709	Rancho la Brea, CA	metatarsal
Capromeryx minor	LACM	Z8710	Rancho la Brea, CA	metatarsal
Capromeryx minor	LACM	Z5889	Rancho la Brea, CA	radius
Capromeryx minor	LACM	Z8584	Rancho la Brea, CA	radius

Species	Museum	Specimen #	Locale	Element
Capromeryx minor	LACM	Z8601	Rancho la Brea, CA	radius
Capromeryx minor	LACM	66281	Rancho la Brea, CA	scapula
Capromeryx minor	LACM	Z8551	Rancho la Brea, CA	scapula
Capromeryx minor	LACM	Z8553	Rancho la Brea, CA	scapula
Capromeryx minor	LACM	Z8555	Rancho la Brea, CA	scapula
Capromeryx minor	LACM	Z8556	Rancho la Brea, CA	scapula
Capromeryx minor	LACM	60570	Rancho la Brea, CA	tibia
Capromeryx minor	LACM	60571	Rancho la Brea, CA	tibia
Capromeryx minor	LACM	60572	Rancho la Brea, CA	tibia
Capromeryx minor	LACM	107246	Rancho la Brea, CA	tibia
Capromeryx minor	LACM	R17250	Rancho la Brea, CA	tibia
Capromeryx minor	LACM	R22130	Rancho la Brea, CA	tibia
Capromeryx minor	LACM	Z8639	Rancho la Brea, CA	tibia
Capromeryx minor	LACM	Z8649	Rancho la Brea, CA	tibia
Capromeryx minor	LACM	R37112	Rancho la Brea, CA	ulna
Capromeryx sp.	UAHMP	244	Rancho la Brisca, MX	calcaneum
Capromeryx sp.	UTEP	9366-1185-17	Pendejo Cave, NM	calcaneum
Capromeryx sp.	UTEP	91-559	Jimenez Cave, TX	femur
Capromeryx sp.	TMM	40855-21	Underwood #3, TX	humerus
Capromeryx sp.	UTEP	5689-103-2	U-Bar Cave, TX	humerus
Capromeryx sp.	UTEP	9366-610-1	Pendejo Cave, NM	humerus
Capromeryx sp.	UTEP	75-11	Dark Canyon Cave,TX	metacarpal
Capromeryx sp.	UTEP	9366-449-1	Pendejo Cave, NM	metatarsal
Capromeryx sp.	UTEP	17-121	Lost Valley, TX	radius
Capromeryx sp.	UTEP	22-1649	Animal Fair, TX	scapula
Capromeryx sp.	UTEP	107-2	Sierra Dieblo Cave, TX	tibia
Capromeryx sp.	UTEP	5689-98-6	U-Bar Cave, TX	ulna
Capromeryx tauntonensis	UWBM	79006	Taunton Site, WA	humerus
Capromeryx tauntonensis	UWBM	78990	Taunton Site, WA	m1
Capromeryx tauntonensis	UWBM	78991	Taunton Site, WA	m1
Capromeryx tauntonensis	Morgan	collection	Taunton Site, WA	m1
Capromeryx tauntonensis	F:AM	31749	Taunton Site, WA	m1/m2
Capromeryx tauntonensis	UWBM	78986	Taunton Site, WA	m2
Capromeryx tauntonensis	UWBM	78987	Taunton Site, WA	m2
Capromeryx tauntonensis	UWBM	78988	Taunton Site, WA	m2
Capromeryx tauntonensis	UWBM	78989	Taunton Site, WA	m2
Capromeryx tauntonensis	UWBM	78968	Taunton Site, WA	M2
Capromeryx tauntonensis	UWBM	78969	Taunton Site, WA	M2
Capromeryx tauntonensis	UWBM	78970	Taunton Site, WA	M2
Capromeryx tauntonensis	UWBM	78971	Taunton Site, WA	M2
Capromeryx tauntonensis	UWBM	78972	Taunton Site, WA	M2
Capromeryx tauntonensis	SDSM	34418	Taunton Site, WA	metatarsal
Capromeryx tauntonensis	UWBM	79001	Taunton Site, WA	metatarsal
Capromeryx tauntonensis	UWBM	79003	Taunton Site, WA	metatarsal